Chemometric optimisation of cellulose extraction from Hemp: Removal of Synthetic Dyes from Aqueous Solutions Using Micro-Cellulose

By

Jessica Tsakani Mhlongo

Student number: 844298

BSc (Hons)

A dissertation submitted to the Faculty of Science at the University of the Witwatersrand, Johannesburg in fulfilment of the requirements for the degree of

Master of Science in Chemistry.

Supervisor: Dr Anita Etale

Co-supervisor: Dr Yannick Nuapia

Johannesburg, January 2023

DECLARATION

I, **Jessica Tsakani Mhlongo (844298),** declare that this thesis "Chemometric optimisation of cellulose extraction from Hemp: Removal of Synthetic Dyes from Aqueous Solutions Using Micro-Cellulose" is my own, unaided work. It is being submitted for the Degree of Master of Science at the University of the Witwatersrand, Johannesburg. It has not been submitted before for any degree or examination at any other University.

J.T. Mhlongo

Jessica Tsakani Mhlongo

Date: 20/01/2023

UNIVERSITY OF THE WITWATERSRAND, JOHANNESBURG

ABSTRACT

Due to increasing awareness of the environmental impacts and costs of materials used in everyday products, industries are increasingly seeking more ecologically and environmentally friendly materials that are renewable, biodegradable, economically feasible, and have lower energy demands. As a result, recent research has focused on the extraction of natural materials such as cellulose, from plants, including agricultural biomass residue. As a cellulose source, agricultural biomass presents such advantages as being low-cost, widely available, environmentally friendly, and biodegradable. This study investigated the optimisation of cellulose microfibre extraction from Hemp (*Cannabis sativa L.*) bast fibres by organic acids via response surface methodology (RSM). The goal was to determine appropriate conditions under which organic acids could be applied, in order to replace the commonly used sulphuric acid process, thus providing a greener route for cellulose extraction. Upon extraction, surface treatment by cationisation was then performed in order to demonstrate their application in the remediation of water contaminated by various synthetic dyes.

For the extraction of cellulose microfibres, hemp bast fibres were first subjected to alkali (4 wt% NaOH) and bleaching treatments using acetate buffer in aqueous chlorite. RSM was used to determine combinations of three processing conditions including acid concentration (45 – 64%), hydrolysis time (30 – 90 minutes), and temperature (45 – 65 °C), using sulfuric acid, formic acid, and maleic acid. A central composite design model with 21 experimental runs was optimised using MODDE 13.1 software. Characterisation of cellulose and cellulose microfibres included surface morphology analysis by scanning electron microscopy (SEM), functional group analysis with Fourier Transform Infrared (FTIR) spectroscopy, crystallinity degree with X-ray diffraction (XRD) analysis and thermal stability analysis with thermogravimetric analysis (TGA). SEM confirmed that hydrolysis produced cellulose microfibres of varying size and morphology. FTIR spectra showed that the main chemical structure of cellulose was not altered during the hydrolysis process. TGA also showed that microfibres with high crystallinity resulted in good thermal stability, which is a favourable property for high temperature applications. The model suitably described the data (R^2 =0.99; R^2adj = 0.96). Microfibres with an average width of 6.91 μm, degree of crystallinity range between 40% and 75% and good thermal stability were produced with acid hydrolysis processes with assisted ultrasonic treatment. The optimum degree of crystallinity 83.21% was achieved with formic acid concentration of 62 wt%, hydrolysis time of 36 minutes, and hydrolysis temperature of 47 °C as predicted by the model. The optimisation results were validated to confirm the accuracy of the model. The data suggests that formic acid can be used as an alternative to sulfuric acid for synthesis of cellulose microfibres from biodegradable hemp waste fibres.

Using hemp plant fibres as a cellulose source, cationised hemp cellulose was synthesized and applied as an adsorbent for the removal of methyl orange (MO), and sunset yellow (SY) from aqueous solutions. For cellulose extraction, the previous method was utilised. Extracted cellulose fibres were functionalised using Glycidytrimethylammonium chloride (GTMAC) to synthesize cationised cellulose (GT-cellulose). Raw plant fibre, bleached cellulose, and GT-cellulose were characterised using SEM, FTIR, XRD, and TGA techniques. SEM showed long finger-like morphologies for all fibres and displayed that cationisation did not endorse any major modifications to the size and shape of the fibres. The FTIR spectra of raw hemp fibres, bleached cellulose, and GT-cellulose displayed functional group attributed to epoxy moieties of GTMAC, confirming cationisation. The crystallinity degree (Cr*I*) of the fibres obtained from hemp bast material was 60%, which was improved following alkali and bleaching treatment extracting cellulose (Cr*I* = 73%). XRD and TGA showed GT-cellulose with lower crystallinity degree and reduced thermal stability. For synthetic dye adsorption studies, the influence of pH, dosage of adsorbent, initial dye concentration, contact time, and temperature were investigated in batch experiments using GT-cellulose as an adsorbent. From the obtained results, the equilibrium processes were best described by Langmuir isotherm model for both dyes of interest, showing a monolayer adsorption. From the kinetic experiments, the adsorption processes for MO and SY dyes followed the pseudo first-order kinetic model indicating that the overall rate of dye adsorption could be governed by one of the reactants. The thermodynamic study showed that the adsorption processes for MO and SY were both endothermic and spontaneous in nature.

Hemp bast fibres can therefore be regarded as a green and sustainable waste material for the preparation of cellulose microfibres with improved crystallinity, enhanced thermal stability and can be cationically-modified to act as an adsorbent for uptake of anionic dyes from aqueous solutions

DEDICATION

To my late grandmother SOPHIE NKHENSANI MHLONGO. Etlela hi kurhula N’wa Mhlongo.

ACKNOWLEDGEMENTS

First and foremost, I would like to thank GOD for this opportunity and journey.

I would like to sincerely thank Dr. Anita Etale and Dr. Yannick Nuapia at the University of the Witwatersrand for the supervisory role provided throughout this research. With their guidance and constructive feedback, I was able to conduct my masters research project effectively. Thank you for granting me this opportunity of growth and for your guidance, insights, advice, and encouragement throughout the seasons.

A special mention to Mbongiseni Dlamini and Kgomotso Maiphetlho thank you for your kindness, assistance, and input in throughout this journey has been highly appreciated. To all the postgraduate students from the Environmental Analytical Chemistry group, thank you for your contribution in the form of positive feedbacks during group presentations, assistance with lab equipment and a peaceful working environment. To Dr. Mxolisi Motsa and Dr. Oranso Mahlangu from the University of South Africa (UNISA), thank you for immersing contributing to the success of this dissertation. To Boitumelo Tlhaole, thank you for always pouring out positive energy since first contact in 2019.

To the Elite Master's Squad- thank you for the friendship and support always. To The Girls (UJ) thank for the emotional support during the years, since 2014 you have played such important roles individually and as a group. To Dzunisani Mbedhli, and Moditsa Cordelia Rampya, I would thank you for carrying me through my good and worst days.

To my aunt, Khanyisa Mhlongo, you have been there supporting and encouraging me from the very beginning of my tertiary studies and for that I will forever be grateful. Finally, my mother, Patricia Phamela Mhlongo, thank you so much for believing in me, you have always given me every opportunity to be great and for our endless conversations, encouragements, prayers in times of despair, and I am very grateful for you Mhana Nhunhu.

Importantly, I would like to thank National Research Funding (NRF) of South Africa and Royal society for their financial support towards my studies.

PRESENTATIONS

1. **Mhlongo, J.T.,** Nuapia, Y., and Etale. A. **'**Synthesis of cellulose nanocrystals by mineral and organic acids: the influence of acid strength, exposure duration and temperature on structure of nanocrystals' Poster presentation. 2021#RSC Poster Twitter Conference, Virtual, March 2021.
2. **Mhlongo, J.T.,** Nuapia, Y., and Etale. A. 'Optimisation of cellulose nanocrystal production using sulfuric acid and maleic acid' Poster presentation. Chemical Nanosciences and Nanotech Early Career Virtual Poster Symposium, March 2021.
3. **Mhlongo, J.T.,** Dlamini, M.L., Nuapia, Y., and Etale. A. 'Development and application of cellulosic materials for treatment of dye-contaminated water' Poster Presentation, 12th Wits Cross faculty Postgraduate Symposium 2021, Virtual, July 2021.
4. **Mhlongo, J.T.,** Dlamini, M.L., Nuapia, Y., and Etale. A. 'Adsorption of methyl orange, sunset yellow FCF, and Coomassie brilliant blue R dyes from aqueous solutions using cationised cellulose' Poster presentation. National Young Chemist's Symposium 2021, Virtual, July 2021.
5. Etale, A., Nhlane, D.S., Mosai, A. K., **Mhlongo, J.T(Presenter)**., Khan, A., Rumbold, K., and Nuapia, Y. B. 'Synthesis and application of cationised cellulose for the removal of Cr(VI) from acid mine drainage contaminated water' Oral presentation. AQUA≈360 Conference- Water for all: Emerging Issues and Innovations, Virtual, August/September 2021.
6. **Mhlongo, J.T.,** Dlamini, M.L., Nuapia, Y., and Etale. A. 'Adsorption of anionic dyes using functionalised cellulose as adsorbent' Poster presentation. 2nd Commonwealth Chemistry Posters-Building Networks to Address the Goals, Virtual, September 2021.
7. **Mhlongo, J.T.,** Nuapia, Y.B., Motsa, M.M., Mahlangu, O.T., and Etale. A. 'Green chemistry approaches for the extraction of cellulose nanofibres (CNFs): A comparison of mineral and organic acids' Oral presentation. Nanoscience's Young Researcher's Symposium (NYRS) 2020/2021, Virtual, October 2021.

PUBLICATIONS

1. **Mhlongo, J.T.,** Dlamini, M.L., Nuapia, Y., and Etale. A. (2022). Synthesis and application of cationized cellulose for adsorption of anionic dyes. *Materials Today: Proceedings*, 62(3), pp 1-8, https://doi.org/10.1016/j.matpr.2022.02.100
2. **Mhlongo, J.T.**, Nuapia, Y., Motsa, M.M., Mahlangu, O.T., and Etale. A. (2022). Green chemistry approaches for the extraction of cellulose nanofibres (CNFs): A comparison of mineral and organic acids. *Materials Today: Proceedings*, 62(1), pp 1-6, https://doi.org/10.1016/j.matpr.2022.02.088
3. **Mhlongo, J.T.**, Nuapia, Y., Tlhaole, B., Mahlangu, O.T., and Etale. A. (2022). Optimization of Hemp Bast Microfibre Acid Hydrolysis Using Response Surface Modelling. *Processes*, 10(6):1150, DOI: 10.3390/pr10061150

TABLE OF CONTENTS

LIST OF FIGURES

LIST OF TABLES

LIST OF ABBREVIATION

AC	Activated carbon
AB 24	Acid Black 24
ADI	Acceptable daily intake
ADHD	Attention deficient hypersensitivity disorder
AGU	Anhydroglucose units
AM	Acrylamide
APSP	Aminated pumpkin seed powder
AOP	Advanced oxidation processes
BBD	Box-Behnken design
BC	Bacterial cellulose
BEP	Bleached eucalyptus pulp
BET	Brunauer-Emmett-Teller
BNFC	Bacterial nanofibrillated cellulose
[Bmim]Cl	1-Butyl-3-methylimidazolium chloride
BSKP	Bleached softwood kraft pulp
CBH	Cellulogluconase
CC	Coconut coir
CCD	Central-composite design
CCR	Corncob residue
c-DAC	Cationic dialdehyde nanocellulose
CF	Coagulation/flocculation
CHPTAC	3-chloro-2-hydroxypropyltrimethylammonium chloride
CMFs	Cellulose microfibres
CNCs	Cellulose nanocrystals
CNFs	Cellulose nanofibres
CNWs	Cellulose nanowhiskers
CR	Congo Red
CRHC	Cationised rice husk cellulose
Cr*I*	Crystallinity index
CV	Coefficient of variance
DG B	Diamine green B
DP	Degree of polymerization
DPF	Date palm fibres
D-R isotherm	Dubinin-Radushkevich isotherm
DTG analysis	Derivative thermogravimetric analysis

EBSE	Eriochrome blue SE
EG	Endogluconases
EMPH	Ethylenediamine-modified peanut husk
EPTMAC	2,3-epoxypropyl trimethylammonium chloride
FA	Formic acid
FAO	Food and Agricultural Organization
FTIR	Fourier-transform infrared spectroscopy
GTMAC	Glycidyl trimethylammonium chloride
HDTMA	Hexadecyltrimethylammonium
HIUS	High intensity ultrasonication
HPH	High-pressure homogenisation
IPD	Intraparticle diffusion
JLP	Jackfruit leave powder
MA	Maleic acid
MCC	Microcrystalline cellulose
MO	Methyl orange
MMWS	Modified methanol walnut shell
NCC	Nanocellulose crystals
OPEFB	Oil palm empty fruit brunch
OPW	Orange peel waste
PAM-g-QC	Polyacrylamide grafted quatenised cellulose
PEI	Polyethyleneimine
PCC	Purified coir cellulose
PFO	Pseudo-first order
PSO	Pseudo-second order
p-TsOH	p-toluene sulfonic acid
Q-CNF	Quatenised cellulose nanofibres
RHC	Rice husk cellulose
RSM	Response surface methodology
SA	Sulfuric acid
SD	Standard deviation
SDG	Sustainable development goals
SEM	Scanning electron microscope
SMBAC	Swietenia mahagoni bark activated carbon
SY	Sunset yellow
TEM	Transmission electron microscope
TEMPO	2,2,6,6-tetramethylpiperidinyl-1-oxyl radical

TGA	Thermogravimetric analysis
T_{max}	Maximum thermal degradation temperature
T_{onset}	Thermal degradation onset temperature
UIPAC	International Union of Pure and Applied Chemistry
UV-vis	Ultraviolet visible
WHO	World Health Organization
XRD	X-ray diffraction

CHAPTER 1 INTRODUCTION

1.1 Background and motivation

According to the United Nations, in 2019 the global population was estimated to be 7.7 billion, with a projected rise to be 8.5 billion by 2030, and with this increase, the need for sustainable food sources and safe and clean drinking water will rapidly increase causing a decrease in water quality and quantity due to increase water pollution (Sharma *et al.*, 2019) (*World Population Prospects*, 2019). Water pollution is the contamination of water bodies such as groundwater, surface waters, lakes, rivers, seas, and oceans leading to poor water quality (Sharma *et al.*, 2019). Pollution leads to a significant deterioration in water quality resulting in close to 675 million people living without access to safe drinking water. This can lead to contacting sickness from waterborne diseases such as cholera, guinea worm and these mostly occur in the rural areas in underdeveloped countries (Sharma *et al.*, 2020). According to some statistics:

- Over a decade ago, it was estimated that 1.2 billion people worldwide more especially in developing countries did not have access to safe drinking water and this figure is expected to be triple by 2025 (Mukheibir, 2010)
- In 2019, 785 million people did not have access basic safe clean drinking-water service and more than 2 billion people worldwide used a drinking water source contaminated with feces (World Health Organization, 2019).
- Contaminated drinking water is estimated to cause 485 000 diarrheal deaths each year (World Health Organization, 2019).
- In least developed countries, 22% of health care facilities have no water service, 21% no sanitation service, and 22% no waste management service (World Health Organization, 2019)
- On global scale, 26.3 million people per year die from drinking water contaminated with inorganic toxic heavy metals such as arsenic, chromium, lead, and cadmium, and organics such as dyes, pesticides, and surfactants (Jain, Varshney and Srivastava, 2016).
- Due to the rapid rise in population growth, industrialization, climate change and water pollution, it is estimated that by 2050 the global population will be 9.7 billion people and over
  40% of the world's population will be living in water-stressed areas (Guppy and Anderson, 2017).

Synthetic dyes are frequently used in many industries e.g. textile, cosmetics, leather, paper dyeing, printing and colour photography, pharmaceutical, food, etc., (Hashem and El-Shishtawy, 2001)(Konicki *et al.*, 2015). When released into water systems, synthetic dyes may result in harmful

effects to humans and aquatic life such as increased heart rate, diarrhea, vomiting, shock, cyanosis, jaundice, and tissue necrosis even when present at low concentrations. Dyes can have carcinogenic and mutagenic effects in humans and animals (Mahida and Patel, 2016). They can be categorized as cationic, non-ionic, or anionic. Cationic dyes have a net positive charge when in water due to the presence of chemical groups such as amine whereas anionic dyes have a net negative charge due to sulfonate groups (Fernandes *et al.*, 2020). The continued use of synthetic dyes has resulted in a growing challenge to develop efficient, reliable, environmentally friendly, and low-cost technologies to reduce contamination of water resources.

Various technologies exist for the treatment of contaminated water including membrane separation (Liu *et al.*, 2015), electrocoagulation (Dermentzis *et al.*, 2011)(Kobya *et al.*, 2011), electrodeposition (Verduzco *et al.*, 2019), chemical oxidation(Mohan and Pittman, 2007), ozone treatment,, reverse osmosis (Mahdavi and Rahimi, 2018), co-precipitation (Mohan and Pittman, 2007), ion exchange (El Torky *et al.*, 2016), simple adsorption (Ballav, Maity and Mishra, 2012) and a combination of two or more processes (Ibrahim *et al.*, 2019).

Adsorption is a simple and reliable method as it has been extensively used on a variety of contaminants. It is a process that uses adsorbents for the removal of substances from liquid or gaseous solutions followed by adsorption of the substances onto the surface of the adsorbent. This technique has been used extensively owing to its great advantages ease of use and operation, financial feasibility, wide availability, little to no sludge generation and high removal efficiencies, therefore it is applicable in wastewater treatment on a large-scale. For adsorption to work effectively, the experiments conditions such as pH range, metal concentration, adsorbent type, ligand concentration, particle size, and competing for ions are to be optimised (Nicomel *et al.*, 2015)(Li *et al.*, 2019)(Ahmad *et al.*, 2015)(Awang *et al.*, 2018). The adsorption process strongly depends on the type of adsorbent used and commonly used adsorbents include chitosan (Neeraja *et al.*, 2016), bottom ash (Jarusiripot, 2014), natural zeolites (Sannino *et al.*, 2012), nanomaterials such as activated carbon, graphene, carbon nanotubes (Sadegh *et al.*, 2017)(Ilavský, Barloková and Marton, 2020)(Sujitha and Ravindhranath, 2016), activated alumina(Adegoke *et al.*, 2017), Hydrous zirconium oxide (Kumar *et al.*, 2018), rice husk ash(Vieira *et al.*, 2014), fly ash(Adegoke *et al.*, 2017), and agriculture by-products (Batmaz *et al.*, 2014).

Recently, the focus has increasingly been on the exploration of greener technological solutions, leading to increased interest in the use of cellulosic materials for applications in various fields. Cellulose is the most abundant natural polymer being a major component of higher plants, alongside lignin and hemicellulose (George and Sabapathi, 2015). The global production of cellulose has been estimated to be 1.5×10^{12} tons (Tavakolian, Jafari and Ven, 2020). To date, much of the cellulose in use has been

from wood sources (Pennells *et al.*, 2020) but other sources, particularly agricultural wastes e.g., sugarcane bagasse, corn husks, hemp fibres, banana rachis etc are attracting significant attention.

Cellulose is suitable for organic and inorganic pollutant remediation due to the presence of hydroxyl functional groups which can also be modified to improve adsorption (Jamshaid *et al.*, 2017)(Tavakolian, Jafari and Ven, 2020). Through various treatments, cellulose nanomaterials can be extracted various techniques. Acid hydrolysis using most often, mineral acids e.g., sulphuric acid, is used to synthesize nanocrystals (Sartika *et al.*, 2019). Work by Isogai and colleagues also showed that TEMPO-catalysed oxidation can be used to generate nanofibres with lengths up to 3 μm (Isogai, Saito and Fukuzumi, 2011). Importantly, both cellulose nanocrystals and nanofibres can be further modified with cationic or anionic surface groups in order to improve the adsorption capacity for organic and inorganic contaminants (Singh, Sinha and Srivastava, 2015)(Carpenter, de Lannoy and Wiesner, 2015)

1.2 Study aims and objectives

In South Africa, hemp production results of wastes rich in cellulose which is available at lower cost due to their wide local availability and renewability. For this reason, the use of these agricultural wastes in science research has become of great interest. Therefore, the current work aimed to use of hemp fibres as cellulose sources renewable and biodegradable material for applications in water remediation studies. The following objectives were pursued to achieve this goal:

i. To investigate green approaches for the extraction of cellulose from hemp waste using organic and mineral acids using response surface methodology for the selection of reaction conditions i.e., acid type, acid concentration, reaction temperature and duration.
ii. To characterise extracted cellulose for their physical and chemical properties using scanning electron microscope (SEM), X-ray diffraction (XRD). thermogravimetric analysis (TGA), and Fourier-transform infrared spectroscopy (FTIR).
iii. To modify the surface of extracted cellulose fibres by cationic moieties using glycidyl trimethylammonium chloride (GTMAC).
iv. To determine the removal efficiency of anionic dyes from water using cationised cellulose.

1.3 Research justification

Natural Cellulose is a renewable, low-cost, and biodegradable material that can be extracted from a variety of living and non-living organisms. Hemp bast fibres is a great source of cellulose (78%) and with legal hemp farming in South Africa increased production of hemp waste could result. Further resulting in a surge of under-utilised waste material that are burnt unused. Adsorption is a simple, low-cost, and reliable process that has been vastly used for remediation of organic and in organic

contaminants using cellulose materials as a natural adsorbent. To our best knowledge, there is no literature that has covered the use cationised cellulose extracted from hemp bast fibres for remediation of anionic dyes (methyl orange and sunset yellow) from aqueous solutions

1.4 Dissertation outline

Chapter 1: Introduction to study

This chapter gives a brief background introduction into the world of water scarcity on a global scale, pollution caused by synthetic dyes, extraction techniques and use of agricultural cellulose residue and cellulose material as adsorbents. It also highlights information of the main research aim and objectives for the work to be conducted, and the research justification.

Chapter 2: Literature review

This chapter is the core component of the dissertation in which phrases are defined and elaborated. Hemp bast fibre as a cellulose source is discussed with focus on preparation and extraction techniques. Response surface methodology (RSM) as an optimisation method and cellulose modification techniques are discussed. Furthermore, synthetic dye water remediation using cationised cellulose fibres is discussed in the following chapter.

Chapter 3: Research methodology

i. The major intention of this chapter is to clarify on experimental protocol of the research. It brings attention to all chemical reagents, equipment, Characterisation techniques, and adsorption experimental procedures. The experimental procedures were divided into a series of activities outlined below:
ii. Preparation and extraction of cellulose fibres from Industrial Hemp (*Cannabis sativa* L.) bast fibres waste through alkali and bleaching treatments. ii. Green chemistry synthesis of cellulose microfibres (CMFs) through mineral and organic acid hydrolysis coupled with ultrasonication method.

iii. Preparation of cationised cellulose fibres using GTMAC, as cationising agent.

iv. Characterisation techniques employed for all cellulose derived fibres were Scanning Electron Microscope (SEM), Fourier Transform Infrared (FTIR) spectroscopy, X-ray diffraction (XRD) analysis and Thermogravimetric analysis (TGA).

v. Adsorption parameters included solution pH, initial concentrations, adsorbent dosage, temperature effects, and contact time. Ultraviolet-visible (UV-vis) spectroscopy was used to measure the dye concentration after adsorption

Chapter 4: Chemically treated cellulose and its cellulose microfibres extracted from hemp fibres: Isolation and Characterisation

This chapter focuses on the acid hydrolysis extraction and characterisation of cellulose microfibres extracted from industrial hemp (*Cannabis Sativa* L.) plant fibres

Chapter 5: Optimisation of acid hydrolysis of hemp fibres using response surface methodology

In this chapter a response surface methodology with 3^3 full factorial experimental design was adapted to optimise organic and mineral hydrolysis in respect to acid concentration, temperature, and reaction time to obtain fibres high in crystallinity.

Chapter 6: Synthesis and application of cationised cellulose for adsorption of anionic dyes

This chapter presents the results of experiments conducted to examine the removal of azo dyes, methyl orange and sunset yellow by cationised cellulose. The chemical and physical characteristics of modified and unmodified cellulose are fully compared and discussed here. The adsorption efficiencies of raw plant fibre treated cellulose and cationised cellulose for remediation azo dyes are compared and discussed, primarily focusing on the influence of the following adsorption parameters: solution pH, mass of adsorbent, initial adsorbate concentration, contact time and reaction temperature. The applicability of the adsorbent on tap and seawater were also investigated. Adsorption isotherms and kinetic modelling were used to describe the adsorption behavior between adsorbate-adsorbent interactions.

Chapter 7: Conclusions and Recommendations

The general concluding remarks on the work covered in the study and future recommendations are made in this chapter.

1.5 References

Adegoke, K. A., Oyewole, R. O., Lasisi, B. M., and Bello, O. S. (2017) 'Abatement of organic pollutants using fly ash-based adsorbents', *Water Science and Technology*, 76(10), pp. 2580–2592. doi:

10.2166/wst.2017.437.

Ahmad, M., Ahmed, S., Swani, B. L., and Ikram, S. (2015) 'Adsorption of heavy metal ions: Role of chitosan and cellulose for water treatment', *International Journal of Pharmacognosy*, 2(6), pp. 280–289. doi: 10.13040/ijpsr.0975-8232.ijp.2(6).280-89.

Awang, N. A., Salleh, W. N. W., Ismail, A. F., Yusof, N., Aziz, F., and Jaafar, J. (2018) 'Adsorption Behavior of Chromium (VI) onto Regenerated Cellulose Membrane', *Industrial and Engineering Chemistry Research*, pp. 1–30. doi: 10.1021/acs.iecr.8b02366

Basheer, A. A. (2018) 'New generation nano-adsorbents for the removal of emerging contaminants in water', *Journal of Molecular Liquids*, 261, pp. 583–593. doi: 10.1016/j.molliq.2018.04.021.

Batmaz, R., Mohammed, N., Zaman, M., Minhas, G., Berry, R. M., and Tam, K. C. (2014) 'Cellulose nanocrystals as promising adsorbents for the removal of cationic dyes', *Cellulose*, 21(3), pp. 1655–1665. doi: 10.1007/s10570-014-0168-8.

Carpenter, A. W., de Lannoy, C. F. and Wiesner, M. R. (2015) 'Cellulose nanomaterials in water treatment technologies', *Environmental Science and Technology*,49(9), pp. 5277–5287. doi: 10.1021/es506351r.

Dermentzis, K., Christoforidis, A., Valsamidou, E., Lazaridou, A., and Kokkinos, N. (2011) 'Removal of Hexavalent Chromium From Electroplating Wastewater By Electrocoagulation With Iron Electrodes' , *Global NEST Journal,* 13(4), pp. 412–418.

El-Torky, A. M. M., Mostafa, H. Y., El-Masry, A. M. M., and Mahdi, M. E. (2016) 'Purification of Heavy Metals from Industrial Wastewater Using Grafted Corn Husks Pulp Ion Exchanger', *Sohag Journal of Sciences*, 1(1), pp. 53–64. doi: 10.18576/sjs/010107.

Fernandes, J. V., Rodrigues, A. M., Menezes, R. R., and de Araújo Neves, G. (2020) 'Adsorption of anionic dye on the acid-functionalized bentonite', *Materials*, 13(16), pp. 1–19. doi: 10.3390/MA13163600.

George, J. and Sabapathi, S. N. (2015) 'Cellulose nanocrystals: Synthesis, functional properties, and applications', *Nanotechnology, Science and Applications*, 8, pp. 45–54. doi: 10.2147/NSA.S64386.

Guppy, L. and Anderson, K. (2017) '*Global Water Crisis Report: the Facts'*, *United Nations University for Wter,Environment and Health*. Hamilton, Canada. Available at: http://inweh.unu.edu.

Hashem, A. and El-Shishtawy, R. M. (2001) 'Preparation and characterization of cationized cellulose for the removal of anionic dyes', *Adsorption Science and Technology*, 19(3), pp. 197–210. doi: 10.1260/0263617011494088.

Ibrahim, Y., Abdulkarem, E., Naddeo, V., Banat, F., and Hasan, S. W. (2019) 'Synthesis of super hydrophilic cellulose-alpha zirconium phosphate ion exchange membrane via surface coating for the removal of heavy metals from wastewater', *Science of the Total Environment*, 690, pp. 167–180. doi: 10.1016/j.scitotenv.2019.07.009.

Ilavský, J., Barloková, D. and Marton, M. (2020) 'Triazine herbicides removal from water with granular activated carbon', in *IOP Conference Series: Earth and Environmental Science*. IOP Publishing Ltd. doi: 10.1088/1755-1315/609/1/012088.

Isogai, A., Saito, T. and Fukuzumi, H. (2011) 'TEMPO-oxidized cellulose nanofibers', *Nanoscale*, 3(1), pp. 71–85. doi: 10.1039/c0nr00583e.

Jain, P., Varshney, S. and Srivastava, S. (2016) 'Functionalized nanobiomaterials : high-performance sorbents for chromium remediation from water streams', *International Journal of Environmental Science and Technology*, 13(12), pp. 2893–2904. doi: 10.1007/s13762-016-1115-z.

Jamshaid, A., Hamid, A., Muhammad, N., Naseer, A., Ghauri, M., Iqbal, J., Rafiq, S., Shah, N. S. (2017) 'Cellulose-based Materials for the Removal of Heavy Metals from Wastewater – An Overview', *ChemBioEng*, 4(4), pp. 1–18. doi: 10.1002/cben.201700002.

Jarusiripot, C. (2014) 'Removal of Reactive Dye by Adsorption over Chemical Pretreatment Coal based Bottom Ash', *Procedia Chemistry*, 9, pp. 121–130. doi: 10.1016/j.proche.2014.05.015.

Kaur, Y., Bhatia, Y., Chaudhary, S., and Chaudhary, G. R. (2017) 'Comparative performance of bare and functionalize ZnO nanoadsorbents for pesticide removal from aqueous solution', *Journal of Molecular Liquids*, 234, pp. 94–103. doi: 10.1016/j.molliq.2017.03.069.

Kobya, M., Gebologlu, U., Ulu, F., Oncel, S., and Demirbas, E. (2011) 'Removal of arsenic from drinking water by the electrocoagulation using Fe and Al electrodes', *Electrochimica Acta*, 56(14), pp. 5060–5070. doi: 10.1016/j.electacta.2011.03.086.

Konicki, W., Cendrowski, K., Bazarko, G., and Mijowska, E. (2015) 'Study on efficient removal of anionic, cationic and nonionic dyes from aqueous solutions by means of mesoporous carbon nanospheres with empty cavity', *Chemical Engineering Research and Design*, 94, pp. 242–253. doi:

10.1016/j.cherd.2014.08.006.

Kumar, R., Kim, S., Kim, K., Lee, S., Park, H., Jeon, B. (2018) 'Removal of hazardous hexavalent chromium from aqueous phase using zirconium oxide-immobilized alginate beads', *Applied Geochemistry*, 88, pp. 113–121. doi: 10.1016/j.apgeochem.2017.04.002.

Li, Z. J., Xue, H. D., Zhang, Y. Q., Hu, H., S., Zheng, X. D. (2019) 'Construction of a cationic organic network for highly efficient removal of anionic contaminants from water', *New Journal of Chemistry*, 43(29), pp. 11604–11609. doi: 10.1039/c9nj00886a.

Liu, Y., Ma, H., Liu, B., Hsiao, B. S., Chu, B. (2015) 'High-performance nanofibrous membrane for removal of Cr(VI) from contaminated water', *Journal of Plastic Film and Sheeting*, 31(4), pp. 379–400. doi: 10.1177/8756087915590645.

Mahdavi, H. and Rahimi, A. (2018) 'Zwitterion functionalized graphene oxide / polyamide thin film nanocomposite membrane: Towards improved anti-fouling performance for reverse osmosis', *Desalination*, 433, pp. 94–107. doi: 10.1016/j.desal.2018.01.031.

Mahida, V. P. and Patel, M. P. (2016) 'Removal of some most hazardous cationic dyes using novel poly (NIPAAm/AA/N-allylisatin) nanohydrogel', *Arabian Journal of Chemistry*, 9(3), pp. 430–442. doi: 10.1016/j.arabjc.2014.05.016.

Mohan, D. and Pittman, C. U. (2007) 'Arsenic removal from water/wastewater using adsorbents-A critical review', *Journal of Hazardous Materials*, 142(1–2), pp. 1–53. doi: 10.1016/j.jhazmat.2007.01.006.

Mukheibir, P. (2010) 'Water access, water scarcity, and climate change', *Environmental Management*, 45(5), pp. 1027–1039. doi: 10.1007/s00267-010-9474-6.

Neeraja, G., Raghunandana, S. K., Kumar, P. S., Cabana, H., Kumar, V. V. (2016) 'Adsorptive potential of dispersible chitosan coated iron-oxide nanocomposites toward the elimination of arsenic from aqueous solution', *Process Safety and Environmental Protection*, 104, pp. 185–195. doi: 10.1016/j.psep.2016.09.006.

Nicomel, N. R., Leus, K., Folens, K., Van Der Voort, P., and Laing, G. D. (2015) 'Technologies for Arsenic Removal from Water: Current Status and Future Perspectives', *Environmental Research and Public Health*, 13(62), pp. 1–24. doi: 10.3390/ijerph13010062.

Pennells, J., Godwin, I. D., Amiralian, N., Martin, D. J. (2020) 'Trends in the production of cellulose nanofibers from non-wood sources', *Cellulose*, 27(2), pp. 575–593. doi: 10.1007/s10570-019-02828-9.

Sadegh, H., Ali, G. A. M., Gupta, V. K., Makhlouf, A. S. H., Shahryari-ghoshekandi, R., Nadagouda, M. N., Sillanpää, M., and Megiel, E. (2017) 'The role of nanomaterials as effective adsorbents and their applications in wastewater treatment', *Journal of Nanostructure in Chemistry*, 7(1), pp. 1–14. doi: 10.1007/s40097-017-0219-4.

Sannino, F., Ruocco, S., Marocco, A., Esposito, S., and Pansini, M. (2012) 'Cyclic process of simazine removal from waters by adsorption on zeolite H-Y and its regeneration by thermal treatment', *Journal of Hazardous Materials*, 229–230, pp. 354–360. doi: 10.1016/j.jhazmat.2012.06.011.

Sartika, D., Syamsu, K., Warsiki, E., and Fahma, F. (2019) 'Optimization of Sulfuric Acid Concentration and Hydrolysis Time on Crystallinity of Nanocrystalline Cellulose: A Response Surface Methodology Study', in *IOP Conference Series: Earth and Environmental Science*, pp. 1–9. doi: 10.1088/1755-1315/355/1/012109.

Sharma, A., Tomer, A., Singh, J., Chhikara, B.S. (2019) 'Biosorption of metal toxicants and other water pollutants by Corn (Maize) plant: A comprehensive review', *Journal of Integrated Science and Technology*, 7(2), pp. 19–29. Available at: http://pubs.iscience.in/journal/index.php/jist/article/view/918.

Sharma, P. R., Sharma, S. K., Lindström, T., Hsiao, B. S. (2020) 'Nanocellulose-Enabled Membranes for Water Purification: Perspectives', *Advanced Sustainable Systems*, 4(5), pp. 1–28. doi: 10.1002/adsu.201900114.

Singh, K., Sinha, T. J. M. and Srivastava, S. (2015) 'Functionalized nanocrystalline cellulose: Smart biosorbent for decontamination of arsenic', *International Journal of Mineral Processing*, 139, pp. 51–63. doi: 10.1016/j.minpro.2015.04.014.

Sujitha, R. and Ravindhranath, K. (2016) 'Removal of Coomassie brilliant blue dye from waste waters using active carbon derived from barks of Ficus racemosa plant', *Der Pharmacia Lettre*, 8(10), pp. 72–83.

Szewczyk, R. and Ku, A. (2018) 'Chemosphere Ametryn removal by Metarhizium brunneum: Biodegradation pathway proposal and metabolic background revealed', 190, pp. 174–183. doi: 10.1016/j.chemosphere.2017.10.011.

Tavakolian, M., Jafari, S. M. and Ven, T. G. M. Van De (2020) 'A Review on Surface - Functionalized Cellulosic Nanostructures as Biocompatible Antibacterial Materials', *Nano-Micro Letters*, 12(73), pp. 1–23. doi: 10.1007/s40820-020-0408-4.

Verduzco, L E., Oliva, J., Oliva, A I., Macias, E., Garcia, C R., Herrera-trejo, M., Pariona, N., and Mtzenriquez, A I. (2019) 'Enhanced removal of arsenic and chromium contaminants from drinking water by electrodeposition technique using graphene composites', *Materials Chemistry and Physics*, 229, pp. 197–209. doi: 10.1016/j.matchemphys.2019.03.006.

Vieira, M. G. A., De Almeida Neto, A. F., Silva, M. G. C., Carneiro, C. N., and Melo Filho, A. A. (2014) 'Adsorption of Lead and Copper Ions from Aqueous Effluents on Rice Husk Ash In A Dynamic System', *Brazilian Journal of Chemical Engineering*, 31(02), pp. 519–529.

World Health Organization (2019) *Drinking-water*. Available at: https://www.who.int/news-room/factsheets/detail/drinking-water (Accessed: 22 May 2021).

World Population Prospects (2019).

.

CHAPTER 2: LITERATURE REVIEW

2.1 Hemp fibres (*Cannabis Sativa* L.)

Schultes wrote:

"Hemp is a green, very abundant and ubiquitous plant, economically valuable, a versatile and multipurpose product, possibly dangerous and certainly in many ways mysterious" (Schultes 1970)

Hemp (*Cannabis sativa* L.) is one of the most cultivated and used industrial crops worldwide. Hemp has an estimated world production of 214×10^3 tons per year (Rahman *et al.*, 2018). Hemp produces two types of natural fibres namely, bast fibres which are the fibrous form and woody core fibres (also known as Hurds) which is the granular form, and both are abundant in nature (Morin-Crini *et al.*, 2018). Hemp bast fibres are mainly composed of 76% cellulose, 14% hemicellulose, 5% lignin, 1% pectin's, and 6% of other substances, whereas Hurds are composed of 48% cellulose, 24% hemicellulose, 19% lignin, 2% ash and less than 5% of other substances (Väisänen *et al.*, 2018)(Salami *et al.*, 2020). Hemp fibres are low cost, biodegradable, environmentally friendly, durable, ease of processing, low density, and have good mechanical properties compared to synthetic fibres (Abraham, Wong and Puri, 2016)(Jarabo *et al.*, 2012). Furthermore hemp fibres have several industrial uses such as reinforcements for building materials, textile, paper processing, medicine, cosmetics, pharmaceuticals food manufacturing, detergent and bio-composites (Salami *et al.*, 2020)(Jarabo *et al.*, 2012)(Kassab *et al.*, 2020).

2.2 Cellulose and its hierarchical structure

Cellulose was first isolated in 1839 by the French chemist, Anselme Payen while studying various wood sources (Devabaktuni Lavanya, P.K.Kulkarni, Mudit Dixit, Prudhvi Kanth Raavi, 2011). Cellulose is a vital structural component of the cell walls of higher plants. It contributes up to 90 % of cotton, 80 % of hemp, 75 % of flax and 40-50% of wood (see Table 2.1) (Hokkanen, Bhatnagar and Sillanpää, 2016)(Huang *et al.*, 2020a). Cellulose can be found in a number of living organisms such as amoeba, algae, fungi and bacterium *acetobacter xylinum* and even in some aquatic animals e.g tunicates (Figure 2.1) (Dong, Roman and Long, 2014)(Mansoori *et al.*, 2020). Cellulose is the most abundant and renewable natural polymer on Earth. The global production of cellulose has been estimated to be 1.5×10^{12} tons each year (George and Sabapathi, 2015)(Tavakolian, Jafari and Ven, 2020). Cellulose has a wide range of physical and physiochemical properties such as high stiffness, high strength, biocompatibility, renewability, excellent thermal stability, high sorption capabilities and non-toxicity (Ratajczak and Stobiecka, 2020). Furthermore, due to previously mentioned properties and low cost, cellulose and other biopolymer materials attract more attention for applications in a variety of areas such as reinforcement

agents, water treatment, food packaging, textiles, bio-composite, medicine, and many more as shown in Figure 2.2(Abouzeid *et al.*, 2019) (Di Giorgio *et al.*, 2020)(Abiaziem *et al.*, 2019). Cellulose as a main component of biomass has been used for decades for a wide variety of applications and will continue to be investigated and applied in the future to contribute to environmental and economic improvement.

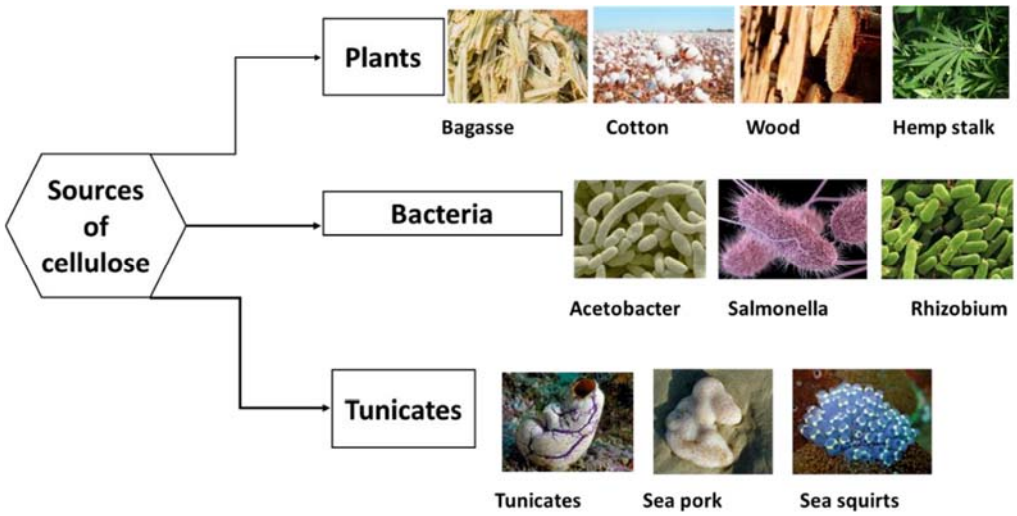

Figure 2.1: Sources of cellulose of various plant and animal species

Table 2.1: Cellulose, hemicellulose, and lignin as major components in the chemical composition of various plants materials.

Source	**Percentage composition (wt %)**			**Ref**
	Cellulose	**Hemicellulose**	**Lignin**	
Softwood	42	40	32	(Tarasov *et al*., 2018)
Hardwood	51	38	31	(Tarasov *et al*., 2018)
Hemp fiber	74	14	5	(Väisänen *et al*., 2018)
Corn husk	42	41	13	(De Carvalho Mendes *et al*., 2015)
Sugarcane bagasse	46	24	24	(Candido and Gonçalves, 2019)
Bamboo	35	27	11	(Wijaya *et al*., 2019)
Tea stalk	35	20	28	(Guo *et al*., 2020)

Rice husk	35	25	20	(Motaung and Linganiso, 2018)
Rice straw	37	29	23	(Ratnakumar *et al*., 2022)
Sorghum	46	15	17	(Motaung and Linganiso, 2018)
Maize stem	39	28	15	(Longaresi *et al*., 2019)
Banana trunks (*Musa acuminata*)	33	39	27	(Merais *et al*., 2022)
Banana rachis	34	8	16	(Gabriel *et al*., 2020)
***Calotropis procera* fiber**	64.1	19.5	9.7	(Song *et al*., 2019)
Corn stalk	38	46	16	(Chen *et al*., 2020)
Corn stover	40	28	10	(Hassan *et al*., 2016)
Garlic straw	41	18	6	(Kallel *et al*., 2016)
Yerba mate fiber	29	25	29	(Ju *et al*., 2020)
Peanut shell	30	19	29	(Chen *et al*., 2020)
Pineapple waste (roots)	42	32	19	(Maisyarah *et al*., 2019)
Kans grass (*Saccharum spontaneum*)	48	32	17	(Baruah *et al*., 2020)
Date seed (*Phoenix dactylifera* L.)	25	25	31	(Abu-thabit *et al*., 2020)
Eggplant plant (*Solanum melongena* L.)	63	7	23	(Bahloul, Kassab, El, *et al*., 2021)
Sugar palm fibers	37-54	4-8	17-25	(Ilyas *et al*., 2021)

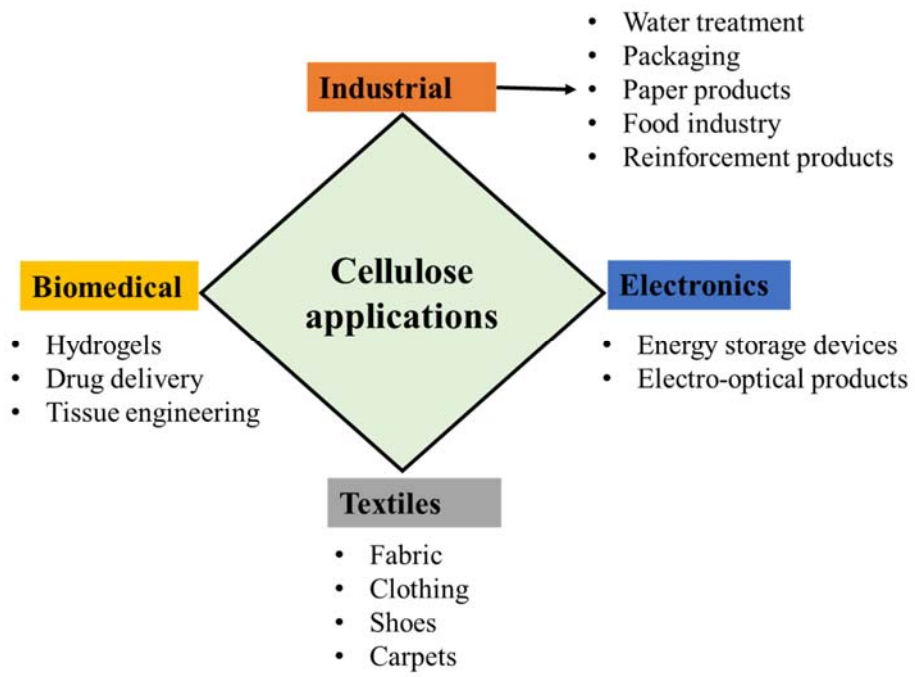

Figure 2.2: Applications of cellulose.

2.2.1 Cellulose structure and properties

Cellulose is a long linear polysaccharide chain consisting of repeating units of D-glucopyranose also commonly known as anhydroglucose units (AGU) in a chair conformation with molecular formula of $(C_6H_{11}O_5)_n$. The AGU are joined together by β-1,4-glycosidic linkages formed between C1 and C4 position to form a dimer of glucose known as cellobiose (Figure 2.3) (Mansoori *et al.*, 2020)(Hokkanen, Bhatnagar and Sillanpää, 2016)(Abouzeid *et al.*, 2019). Each repeating unit of AGU has three highly reactive hydroxyl (OH^-) groups which contribute to cellulose's properties (hydrophilicity, degradability, chirality), each one at position C2, C3, and C6 (Dong, Roman and Long, 2014). The hydroxyl groups at position C2 and C3 are secondary alcohols and the hydroxyl group at position C6 is a primary alcohol making them hydrophilic in nature. Moreover, cellulose does not dissolve in water and most common solvents (acetone, ethanol, methanol) due to strong hydrogen bonding interactions between cellulose chains (Jasmani and Thielemans, 2018). Within the cellulose chains, crystalline domains are formed due to van der Waals forces formed between the glucose units and hydrogen bonds formation between the cellulose chains (Hokkanen, Bhatnagar and Sillanpää, 2016). As shown in Figure 2.3, cellulose chains are made up of two chemically different ends: the non-reducing end is the one end with a closed ring structure and the reducing end is the opposite end which has a free anomeric carbon atom of hemiacetal nature in equilibrium with an aldehyde (Jasmani and Thielemans, 2018)(Eyley and Thielemans, 2014). The degree of polymerization (DP) as the number of glucose unit in a polysaccharide chain molecule given as **n,** strongly depends on the cellulose source and treatment

conditions applied for the isolation of cellulose (Jasmani and Thielemans, 2018)(Seddiqi *et al.*, 2021). The DP of cellulose materials can range from hundreds to a few thousands (Table 2.2).

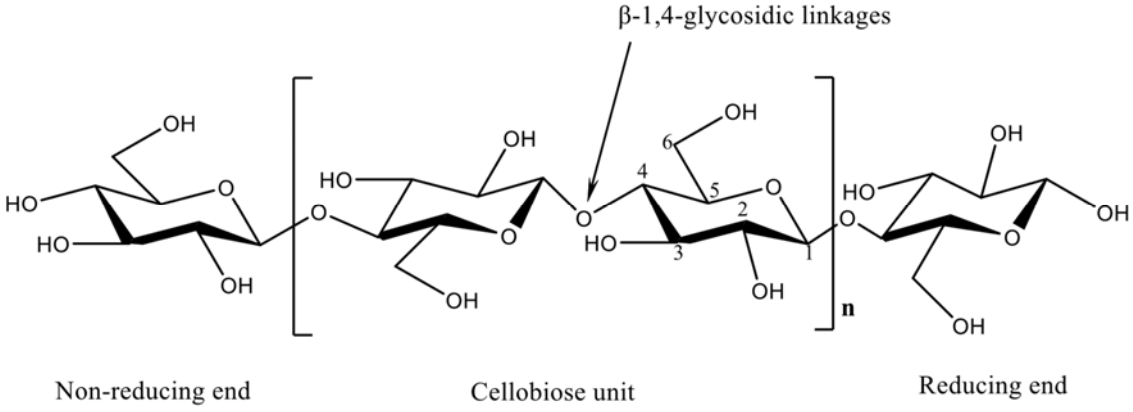

Figure 2.3: Molecular structure of cellulose showing the non-reducing ends, terminal reducing ends and cellobiose unit.

Table 2.2: Various sources of cellulose and their degree of polymerization (DP)

Source	Type	Degree of polymerization (DP)	Ref
Wood	Hardwood/softwood	1200-10,000	(Seddiqi *et al*., 2021)(Pei *et al*., 2013)
	Wood pulp	300-1700	(Dong *et al*., 2014)(Jasmani and Thielemans, 2018)
	Wood CNF	250-3500	(Seddiqi *et al*., 2021)
Plants	Cotton	800-10,000	(Jasmani and Thielemans, 2018)(Ioelovich, 2014)
	Sugarcane bagasse	974–1039	(Bian *et al*., 2014)
	Corn husk	50-300	(El-Torky *et al*., 2016)
	Hemp	200-1300	(Ji *et al*., 2021)
Bacteria		2000-16,000	(Yang *et al*., 2019)(Danafar, 2020)(Wang, Tavakoli and Tang *et al*., 2019)
Algae		Up to 10,000	(Santmarti and Lee, 2018)
Tunicate		700-3500	(Zhao and Li, 2014)

2.2.2 Cellulose microfibres (CMFs), cellulose nanofibres (CNFs), and cellulose nanocrystals (CNCs)

Over the years in order to improve cellulose application in various industries, cellulose fibres have been derived from several sources with the aim to improve cellulose's mechanical and physical properties such as low density, high tensile strength and stiffness, high aspect ratio, and high specific surface area for applications in water and wastewater treatment, paper making, biomedical engineering, and energy production (Abouzeid *et al.*, 2019)(Shak, Pang and Mah, 2018)(Xie *et al.*, 2018). Cellulose materials are thought of as emerging readily available biomass materials that is cost-effective, renewable, biocompatible, biodegradable, and causes little to no toxicity towards the environment.The Hierarchal nature cellulose is that it can be converted into different structures like microcrystalline cellulose (MCC), cellulose microfibres (CMFs), cellulose nanofibres (CNFs), cellulose nanocrystals (CNCs) using various treatments and approaches and Table 2.3 can be used to distinguish cellulose using their varying sizes (Figure 2.4).

Purified CMFs can isolated from raw biomass sources by chemical treatment methods such as alkaline treatment using NaOH to remove hemicellulose followed by bleaching treatment using sodium chlorite to remove lignin material to bleach the fibres (Puttaswamy, Srinikethan and Shetty, 2017)(Ait Benhamou *et al.*, 2022). Due to strong intra- and inter-molecular hydrogen bonds and van der Waals forces interactions within the cellulose molecular chain, the extraction and isolation of pure cellulose from the source is influenced by pretreatment methods that are used to aid the removal hemicellulose, lignin, pectin, ash, wax and other non-cellulosic materials from biomass materials (Wang, 2019)(Shamsabadi, Behzad and Bagheri, 2015). CMFs usually exhibit several micrometer-wide fiber diameters and are composed of both crystalline and amorphous regions (Risite *et al.*, 2022). Several other methods have also been used such as enzymatic hydrolysis, high-pressure homogenizer (SanchezSalvador *et al.*, 2019), organosolv pretreatment (Ferreira *et al.*, 2018), and steam explosion (Sonia and Dasan, 2013)(Tanpichai, Witayakran and Boonmahitthisud, 2019). CNFs are webbed-like cellulose particles composed of both crystalline and amorphous regions (Feng *et al.*, 2018). CNFs have diameters less than<100 nm and lengths of 500 nm or even longer (Du *et al.*, 2017). CNFs can be isolated from various cellulosic sources via mechanical treatments such as microfluidizer (Pacaphol and Aht-Ong, 2017), high-intensity ultrasonication (Kusumaningrum *et al.*, 2020), high-pressure homogenisation (Li *et al.*, 2014)(Wang *et al.*, 2015), cryocrushing (Alemdar and Sain, 2008), grinding process (Xie *et al.*, 2018), enzymatic hydrolysis (Tibolla, Pelissari and Menegalli, 2014), TEMPO oxidation method (Yang *et al.*, 2017), or a combination of two or more processes (Hu *et al.*, 2017)(Soni, Hassan and Mahmoud, 2015). CNCs are rod-like shaped cellulose particles of highly crystalline nature with diameter size of 5 - 30 nm and length size of 100 nm up to several μm (Wijaya *et al.*, 2019). CNCs can be isolated from cellulose using several methods for example, acid hydrolysis (Wijaya *et al.*, 2019), enzymatic hydrolysis (Cui *et al.*, 2016), high-pressure homogenisation (Lee *et al.*, 2018), high-sheer

homogenisation (Zhao *et al.*, 2013), microfluidisation (Khan *et al.*, 2014), and/or a combination of two or more methods (Tang *et al.*, 2014).

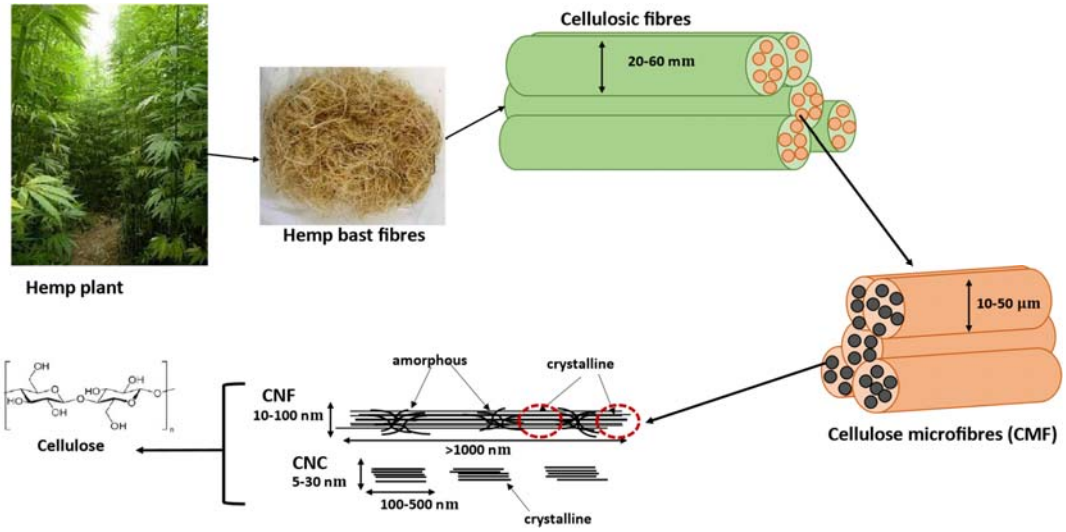

Figure 2.4: Schematic of showing cellulosic fibres, cellulose microfibres, cellulose nanofibres, and cellulose nanocrystals with their respective sizes.

Table 2.3: Type of nanocellulose with their respective average particle sizes

Type of nanocellulose	Sources of cellulose	Average particle size	Ref
Cellulose microfibers (CMFs)	Doum tree, pineapple leaves, hemp	Diameter of several micrometres	(Bahloul, Kassab, Aziz, *et al.*, 2021)(Tanpichai *et al.*, 2019)
Cellulose nanofibers (CNFs)	Wood, cotton, hemp, flax, straw, tunicin, algae, bacteria	Width: 5–60 nm. Length: few microns	(Wang, 2019)(Shak *et al.*, 2018)
Cellulose nanocrystals (CNCs)	Wood, cotton, hemp, flax, straw, tunicin	Width: 5–70 nm Length: 100 nm to several micrometres	(Hokkanen *et al.*, 2016)(Xie *et al.*, 2018)

2.3 Isolation techniques and their effects on crystallinity index and the surface morphology.

2.3.1 Chemical methods

Chemical methods such as acid hydrolysis and enzymatic hydrolysis have been of great interest for the isolation of nanocellulose from various sources.

2.3.1.1 Acid hydrolysis

Acid hydrolysis treatment breaks apart the β-glycosidic bonds of the amorphous regions and crystalline regions of cellulose. This removes amorphous regions resulting in a distinct single crystalline region called CNCs with rod-like configuration and high crystallinity (Figure 2.5) (Yang *et al.*, 2019)(Zimmermann *et al.*, 2016). During acid hydrolysis, the tightly packed cellulose chain undergoes an acid attack on the amorphous (disordered) regions during which the hydronium ions invade these regions encouraging the hydrolytic cleavage of glycosidic linkages in the process in order to isolate the acid attack resistant crystalline structures resulting in CNCs (Zimmermann *et al.*, 2016)(Pereira and Arantes, 2018). Acid hydrolysis is the most frequently used method to yield CNCs due to its high efficiency for CNC preparation, and this can be achieved by using sulfuric acid (Lu and Hsieh, 2010)(de Andrade *et al.*, 2019), hydrochloric acid (Huntley *et al.*, 2015), p-toluenesulfonic acid (p-TsOH) (Wang *et al.*, 2019), formic acid (Liu *et al.*, 2016), maleic acid (Seta *et al.*, 2020), phosphoric acid (Risite *et al.*, 2022), hydrobromic acid (Sadeghifar *et al.*, 2011), and other mixed acids (Wang *et al.*, 2019)(Frost and Johan Foster, 2020).

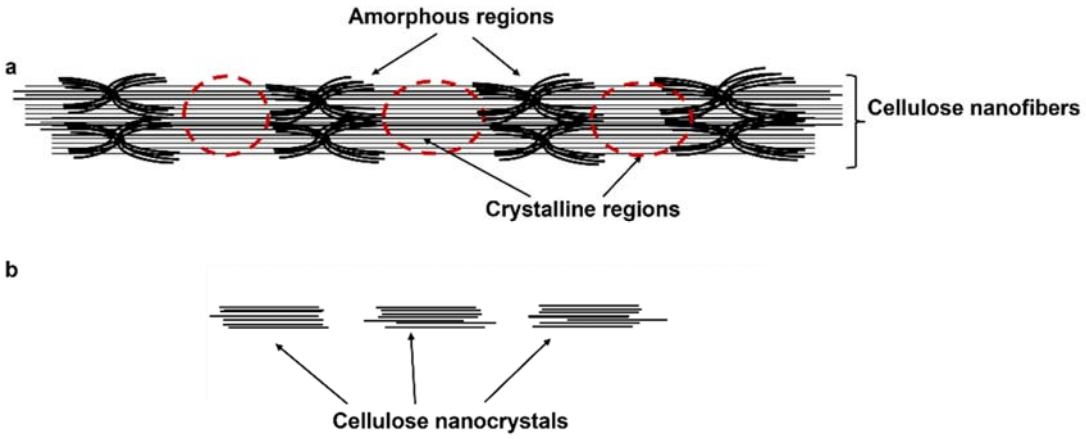

Figure 2.5: Cellulose acid hydrolysis mechanism.

2.3.1.2 Sulfuric acid hydrolysis

Sulfuric acid (SA) is a strong mineral acid (pK_a -3.0 and 2.0) and has the chemical formula H_2SO_4 (Almashhadani *et al.*, 2022). SA is most frequently used in lignocellulosic residues hydrolysis, as it produces negatively charged surface charges to produce more stable CNC suspensions with good dispersibility in water. Consequently, because of the sulfate groups on the crystalline surface, this reduces the thermal stability of the fibres (Xie *et al.*, 2018)(Jung, Choi and Yang, 2013). Shaheen *et al*, investigated the potential of commercially non-recyclable wood waste (sawdust) for the isolation of CNCs via acid hydrolysis together with ultrasonication technique. Alkaline treatment using 1.0 M NaOH was used to delignify sawdust material followed by sodium chlorite bleaching treatment for the removal of any non-cellulosic materials. Acid hydrolysis conditions of 65 wt% H_2SO_4 at 60℃ for 60

min were followed and CNCs were collected by centrifugation to remove traces of sulfate salts followed by dialysis to remove free acid then freeze-dried to produce CNC powder. From the results, the combination of sonication and chemical treatment had been effective for extraction of CNC with rodlike shape of the highly stiffened cellulose crystals like sticks and average diameter of 35.2 ± 7.4 nm were confirmed from SEM (Figure 2.6) and TEM, respectively. The CNC crystal structure is in accordance with cellulose type I with crystallinity index ~90%, according to the XRD data. (Shaheen and Emam, 2018).

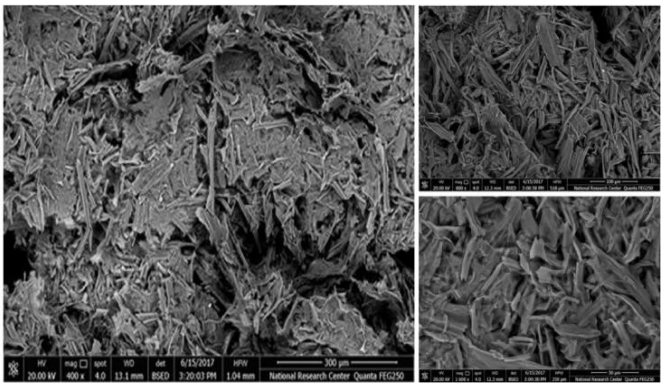

Figure 2.6: SEM images for the CNC at different magnification (300, 100 and 50 μm), (Image adapted from (Shaheen and Emam, 2018)).

Liu *et al,* also studied the extraction of CNCs from a waste material namely corncob residue (CCR). Prior to acid hydrolysis, alkaline and bleaching treatments were employed to treatment the CCR. Hydrolysis conditions of 64 wt% H_2SO_4 with 45°C for 60 min was used and produced rod-like nanocrystals with an average diameter of 5.5 ± 1.9 nm. The nanocrystals produced seemed to be well dispersed and individualized due to the presence of negatively charged sulfate groups on the surface of the CNCs and the crystallinity of the CNC was found to be 55.9% decreasing from raw CCR (61.5%). Furthermore, this could be explained by the fact that the strong acid distorted the amorphous portion of cellulose as well as the crystalline portion during hydrolysis (Liu *et al.*, 2016). In addition, Van Pham *et al*, studied the extraction of thermally stable CNCs from waste newspaper by sulfuric acid hydrolysis. The results showed that CNCs with rod-shaped structures were obtained with average diameters of about 12.3 ± 2.8 nm, high crystallinity index of 80.15%, and improved thermal stability with the crystalline regions of cellulose allowing for high temperature applications (Van Pham *et al.*, 2020) Although the use strong mineral acids such as sulfuric acid produces high crystallinity cellulose particles, there are a few drawbacks (non-environmentally friendly, high operational and maintenance costs, highly corrosive to equipment and not easily recovered). Organic acids as alternatives to improve cellulose acid hydrolysis has been studied. For this study, formic and maleic acid were compared with

sulfuric acid in terms of surface morphology, chemical analysis, crystallinity degree and thermal stability.

2.3.1.3 Formic acid hydrolysis

Formic acid (FA) is a weak organic acid with the chemical formula HCOOH. FA can be used to prepare CNC with longer rod-like structures under controlled conditions. As a result of its low boiling point (about 100.8 ℃), FA is readily recoverable and reusable in multiple reactions, less corrosion to equipment and is environmentally friendly (Li *et al.*, 2015) Liu *et al*, used 88 wt% formic acid to extract CNC from corncob residue and produced long rod-like nanocrystals with an average diameter of 6.5 ± 2.0 nm thereby forming agglomerated CNCs with high crystallinity of ~64% and good thermal stability (Liu *et al.*, 2016). In addition, Lv's *et al*, group demonstrated the tailored and integrated production of functional CNCs and CNFs through formic acid hydrolysis. CNCs and CNFs produced were tailored with sustainable characteristics appropriate for use in polymeric materials owing to the hydrophobic surfaces (see Figure 2.7). CNCs and CNFs exhibited high crystallinity index values of 79.1% and 61.0%, respectively. The surface morphology of the CNCs and CNFs was shown to be differentiable where CNCs had the average diameter of 11 nm, and average length of 141 nm, whereas CNFs microfibrils bundles of several length (Lv *et al.*, 2019). Formic acid hydrolysis was found to be able to isolate CNCs from oil palm empty fruit bunch (OPEFB). The resultant CNCs were found have high crystallinity index (69.82%) with needle-like structures (bin Jumhuri *et al.*, 2017).

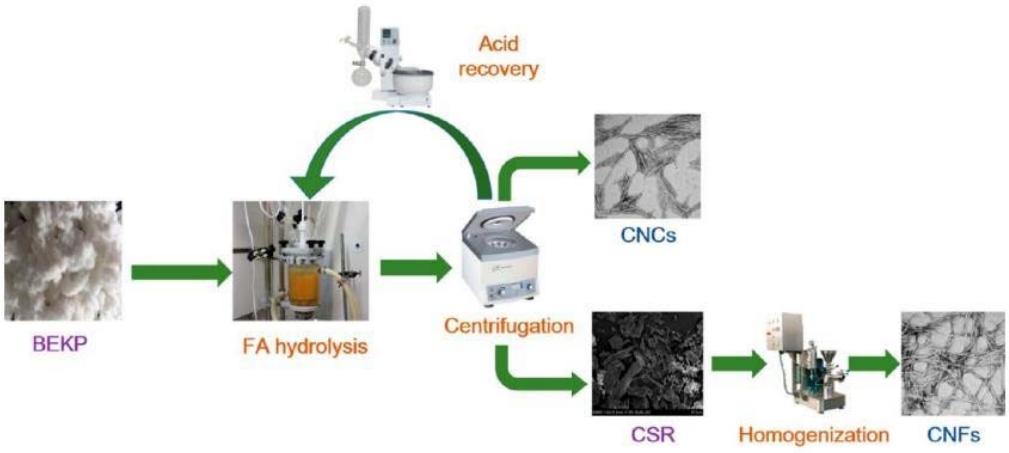

Figure 2.7: Schematic diagram of $FeCl_3$-catalyzed FA hydrolysis for the integrated production of CNCs and CNFs (Image adapted from (Lv *et al.*, 2019)).

2.3.1.4 Maleic acid hydrolysis

To overcome challenges faced with mineral acid hydrolysis, solid acids (maleic acid, oxalic acid, phosphotungstic acid) have been applied in hydrolysis as hydrolysis catalysts. Maleic acid (MA) is a solid organic acid and has chemical formula $HO_2CCH{=}CHCO_2H$. MA has considerable advantages

compared to mineral acids such as that it causes less corrosive to equipment, safe for storage, low transportation costs, cheap, environmentally friendly, easy to recover, uses milder reaction conditions, possible surface modification during hydrolysis, and higher boiling points (Wang *et al.*, 2019)(Seta, An and Liu, 2021)(Nurhadi *et al.*, 2022). Seta *et al*, used a green approach to isolate and extract CNCs through MA hydrolysis from bamboo fibres. To increase the accessibility of MA molecules and reveal more hydroxyl groups on the surface of bamboo fibers, ball-mill pre-treatment were done to the cellulose fibres. MA hydrolysis resulted in improved crystallinity (CrI = 85-91%) due to the removal of amorphous region in cellulose (Seta *et al.*, 2020). Wang *et al*, used MA to produce CNC and CNF extracted from bleached eucalyptus kraft pulp (BEP). Hydrolysis experiments were conducted using MA concentrations between 15–75 wt%, hydrolysis temperature ranges between 60–120℃, and hydrolysis reaction time between 5–300 min. The average length of CNCs produced was around 450−650 nm whereas CNFs produced were several micrometers longer and could not be deduced by AFM analysis (Wang *et al.*, 2017a). In addition, a research group by Bian *et al*, found that carboxylated CNFs extracted from bleached pulp fibres using recyclable MA have average height of about 6−20 nm with entangled fibril networks and average crystallinity index of about 80% (higher than the original BEP). It is worth noting that as the severity of hydrolysis conditions increased, CNF with a shorter length and smaller diameter resulted, and Cr*I* value was slightly reduced (Bian *et al.*, 2019).

Figure 2.8: Schematic diagram for the MA hydrolysis of bleached eucalyptus pulp to produce CNFs, along with acid crystallization, acid recovery, and acid reuse (Image adapted from (Bian *et al.*, 2019)).

2.3.1.5 Enzymatic hydrolysis

Cellulase is a multicomponent enzyme system that is widely utilised in enzymatic hydrolysis process, and it can be divided into three components namely endoglucanases (EG), cellobiohydrolases (CBH),

and β-glucosidase enzymes (Xie *et al.*, 2018)(Tibolla, Pelissari and Menegalli, 2014). These enzymes have targeted reactivity and selectivity, thus the hydrolysis occurs in three parts i) firstly, the EG enzyme decomposes the amorphous region of cellulose by randomly hydrolysing the β-1,4-glycosidic linkages in a cellulose chain generating smaller fibres with new terminal chains, ii) secondly, by removing the crystalline region of cellulose, the CBH enzyme primarily targets the terminal chains of cellulose to form cellobiose and iii) lastly, β-glucosidase enzymes are used to hydrolyse cellobiose into glucose (Yi *et al.*, 2020)(Tibolla *et al.*, 2017)(Kargarzadeh *et al.*, 2017). See mechanism for enzymatic hydrolysis in Figure 2.9.

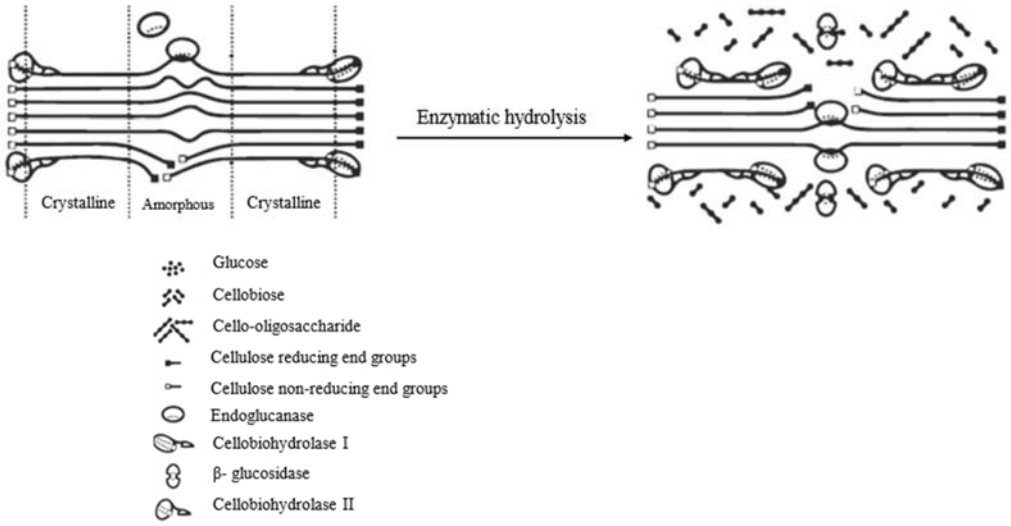

Figure 2.9: Diagrammatic representation of the effects of cellulase on cellulose (Image adapted from (Lynd *et al.*, 2002)).

Zhang *et al,* reported on production of CNFs using enzyme-assisted mechanical techniques and the results revealed that synthetized CNFs had diameters <100 nm, however the thermal stability of CNFs diminished as enzyme dosage was increased. This reduction in thermal stability of CNFs compared to original pulp reduces the applicability of CNFs in high temperature applications (Zhang *et al.*, 2018a). Additionally, Tao and colleagues conducted research on enzymatic pretreatment to separate cellulose nanofibrils from bagasse pulp. using cellulase, alkali pretreatment and combination of ultrafine grinding and high-pressure homogenisation techniques. It was discovered that the produced CNFs had a diameter of approximately 30 nm, reduced crystallinity, and the cellulose crystal structure transitioned from type I to type II. Furthermore, CNFs prepared had lower thermal stability and this was ascribed to the removal of amorphous regions of cellulose by pretreatment, grinding and high-pressure homogenisation methods leading smaller fibre dimensions with each treatment (Tao *et al.*, 2019). Long *et al*, stated that CNFs produced by xylanase-aided enzymatic pretreatment showed increased crystallinity. This increase

was attributed to the cleavage of the β-1,4-glucosidic linkages in the disordered region of cellulose fibre hence a decrease of polymerisation and an increase in crystallinity (Long *et al.*, 2017). Although enzymatic hydrolysis has been utilised for isolation of CNCs/CNFs, it has been combined with other processes (high-pressure homogenisation, ultrafine grinding, alkali pretreatment processes) to extract effectively. In addition, Li and associates, reported the considerable evidence in a review supporting the challenges such as expensive equipment needed for extraction, high investment costs, secondary contamination, and production of inhibitors limit large-scale application of enzyme hydrolysis in industries (Li *et al.*, 2022)

2.3.2 Mechanical methods

Mechanical methods including high intensity ultrasonication (HIUS), high-pressure homogenisation (HPH), cryocrushing, microfluidisation, and grinding have gained interest for CNFs extraction over the past decades

2.3.2.1 High Intensity Ultrasonication (HIUS)

Recently, the high-intensity ultrasonication (HIUS) technique has been vastly applied for the successful isolation and preparation of CNFs from various sources and it has attracted significant attention (Bracone, Luduena and Alvarez, 2022)(Dilamian and Noroozi, 2019)(Lee *et al.*, 2020)(Chen, Yu and Liu, 2011). During the HIUS process, the effect of ultrasonic energy is applied to the polysaccharide chains of cellulose via a cavitation process which involves the formation, growth and rapid collapse of cavities in water through intense shear forces, shockwaves, and microjets (Chen *et al.*, 2011)(Hu *et al.*, 2017)(Kargarzadeh *et al.*, 2017). Sonochemistry is the energy provided by the cavitation process which is between 10−100 $kJmol^{-1}$ of hydrogen bond energy scale, capable of gradually decomposing cellulose weak interfibrillar hydrogen linkages thus forming CNFs from micron-sized cellulose fibres as shown in Figure 2.10 (Chen *et al.*, 2011)(Ishak *et al.*, 2020)(Lu *et al.*, 2013)(Ji, Yu, Yagoub and Chen, 2021a). The characteristics of isolated CNFs by HIUS strongly depend on ultrasonic conditions such as process time, frequency, amplitude and solvent chemistry thus influencing the crystallinity degree, nanofibre size and thermal stability of nanofibres (Mazela *et al.*, 2020)(Ji *et al.*, 2020)(Ji, Yu, Yagoub, Chen, *et al.*, 2021b)(Lee *et al.*, 2020).

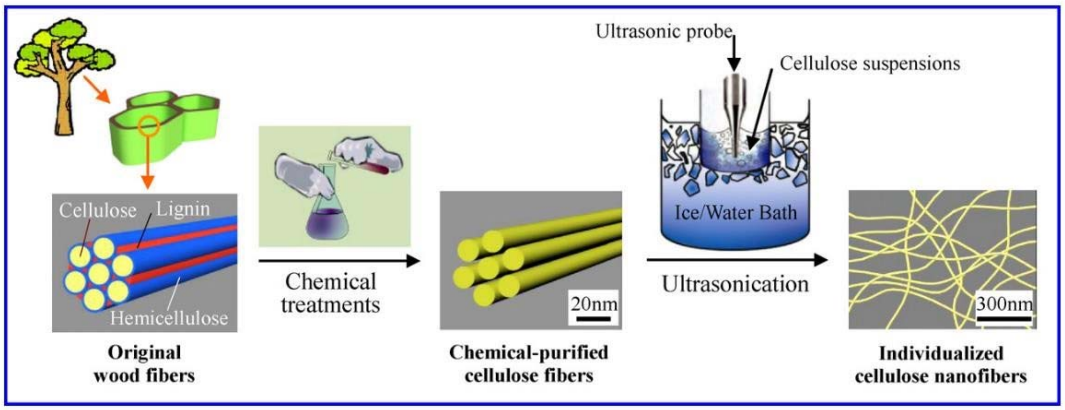

Figure 2.10: Schematic diagram showing the production of individualized CNFs using ultrasonic treatment (Imaged adapted from (Chen *et al.*, 2011)).

During the isolation of CNFs from culinary banana peel using HIUS with assisted chemical treatment, Khawas and Deka reported that increasing the ultrasonication output power reduced the size of CNFs forming thinner and needle-like structural fibrils compared to banana plant fibres. In addition, high crystallinity index values of about 63.64% and improved thermal stability was attained with higher power output during HIUS process, hence CNFs can be employed as a bio-nanocomposites due to its reinforcing properties. (Khawas and Deka, 2016). Abral *et al,* investigated the bacterial cellulose for the isolation of nano-sized bacterial cellulose (BC) particles via ultrasonication method and it was reported that nano-sized BC particles were successfully isolated with HIUS process. However, a decrease in crystallinity index values from 80% (no ultrasonication) to 68% (with ultrasonication) was reported which was attributed to reduced nano-sized BC particles isolated from the scission of the micro-length BC fibre by the high kinetic energy of a jet of liquid from acoustic cavitation produced by the ultrasonic equipment (Abral *et al.*, 2018). Quite recently, Szymańska-Chargot *et al*, reported on the production of CNFs extracted from Hop stems by HIUS treatments and how HIUS influences the properties of extracted CNFs. Extracted CNFs showed a decrease in crystallinity degree from 67% to 60% and a decrease in the fibre diameter up to 4 nm as longer HIUS treatments were applied. In addition, CNFs with higher thermal stability were produced, suitable for applications as natural reinforced or packaging biocomponents (Szymańska-Chargot *et al.*, 2022).

2.3.2.2 High-pressure homogenisation

High-pressure homogenisation (HPH) is one of the most widely used mechanical methods applied for preparation of CNFs as it is a simple, economically feasible, and high efficiency technique and it lacks organic solvents (Li *et al.*, 2012). The fundamental role of the HPH process is to cause high pressure (>150MPa), high shear, turbulence, and cavitation to cellulose pulp suspensions that is continuously

flowing through the homogenisation chamber (see Figure 2.11). Hence, this causes the disintegration of amorphous regions in cellulose, decreases size of cellulose fibres, results in dispersion of brokendown cellulose fractions thereby resulting in total cell disruption and consequently producing CNFs (Li *et al.*, 2014)(Pacaphol and Aht-Ong, 2017)(Yi *et al.*, 2020). In the past decade, most research shows that the cellulose fibre dimensions typically become smaller and more uniform as the number of homogenisation cycles increases. Therefore, high energy consumption can result due to increase in number of cycles, along with tedious equipment maintenance and low reliability (Yi *et al.*, 2020). Furthermore, as cellulose is insoluble in most organic solvents including water, homogenisation can result in valve clogging because of the numerous extensive cellulose networks of intra and/or intermolecular hydrogen bonds and therefore needs assistance by inorganic solvents or other pretreatment methods (Wang *et al.*, 2015)(Li *et al.*, 2012).

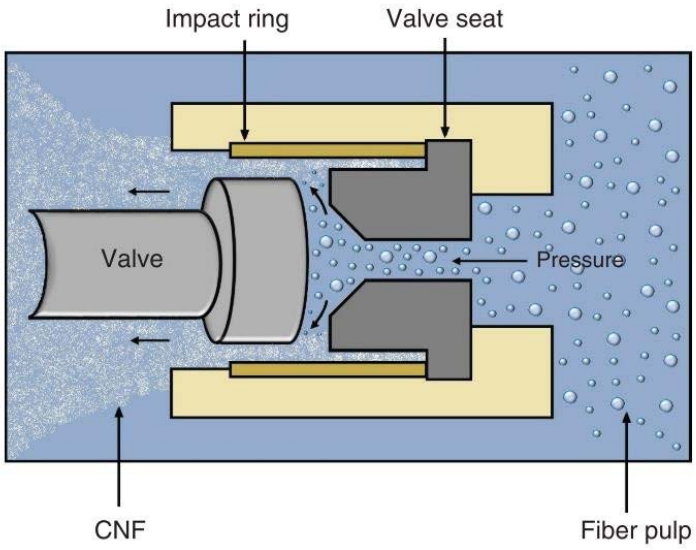

Figure 2.11: Schematic diagram of a high-pressure homogenizer used for the isolation of CNFs (Image adapted from (Kargarzadeh *et al.*, 2017))

Previous studies reported by Tibolla *et al*, have shown that CNFs obtained by acid hydrolysis and high-pressure homogenisation processes have potential to be applied as reinforcing agents of polymeric matrixes in food packaging industries. The study extracted CNFs from banana peel bran through chemical and mechanical treatments and it was reported that CNFs with mechanical treatments showed a higher crystallinity index (average Cr*I* ~66%) than those without mechanical treatments. In addition, as the number of cycles increases, the better the crystallinity index (Tibolla *et al.*, 2018). Bacterial nanofibrillated cellulose (BNFC) was isolated from bacterial (*Gluconacetobacter xylinus*) cellulose by varying levels of high-pressure homogenisation (Kawee, Lam and Sukyai, 2018). The crystal characteristics of the fibres showed that homogenisation had no effect of the crystal structure of

cellulose dispute different applied pressures. However, the crystal size and crystallinity index of BNFC decreased as the pressure increased due to the shear forces destroying inter and/or intramolecular hydrogen bonds of cellulose and leading to the breakdown of the crystal structure.

Table 2.4: Cellulose isolation techniques extracted from different sources.

Main process	Cellulose source	Pre-treatment	Main Treatment	Post-treatment	Crystallinity	Ref
Acid hydrolysis	Sugarcane bagasse waste	Bleaching and alkaline treatment	Acid hydrolysis using sulfuric acid.	Washing, centrifugation, dialysis, and sonication	~69%	(Wulandari *et al*., 2016)
	Waste office paper	Mechanical pre-treatment, alkaline, and bleaching treatment.	Maleic acid hydrolysis	Washing, centrifuging, dialysis, sonication, filtration and drying.	~81%	(Yeganeh *et al*., 2017)
	Sugarcane bagasse waste	Not applicable	Phosphoric acid hydrolysis with hydrogen peroxide treatment then homogenization.	Washing and dialysis	64%	(Wang *et al*., 2020)
	Brewery spent grain (BSG)	Acid and alkali treatment followed by bleaching step.	Acid hydrolysis using sulfuric acid	Washing, centrifugation, sonication, and freeze-drying.	76.3%	(Matebie *et al*., 2021)
	Ramie fibers	Chemical treatments (de-waxing, alkaline and bleaching treatments)	Acid hydrolysis using sulfuric acid	Washing, centrifugation, dialysis, and ultra-sonication.	80-91%	(Kusmono *et al*., 2020)

	Corn husk	Alkaline and bleaching treatment.	Acid hydrolysis using 64% sulfuric acid.	Washing, centrifugation, dialysis, and sonication	68.33%	(Kampeerapappun, 2015)
	Bleached softwood kraft pulp (BSKP)	$FeCl_3$ catalyst	Formic acid hydrolysis	CNFs−Centrifugation and high-pressure homogenization. CNCs with HPH	CNFs−52.91% CNCs−75.21%	(Du *et al*., 2017)
	Bleached softwood kraft pulp (BSKP)	Not applicable	Formic acid hydrolysis	Centrifugation and high-pressure homogenization.	49.0%−52.9%	(Du *et al*., 2016)
Enzymatic hydrolysis	Banana peel bran	Alkaline treatment, washing and centrifugation	Enzymatic hydrolysis using xylanase	Washing and centrifugation.	61.0%	(Tibolla *et al*., 2017)
	Cotton fibres	Fenton's pre-treatment	Enzymatic hydrolysis using cellulase.	Not applicable	~85%	(Jain and Vigneshwaran, 2012)
	Cotton fibres	DMSO and NaOH, ultrasonic treatments	Enzymatic hydrolysis with buffer solution of cellulose at 45℃	Centrifugation.	78.1%	(Chen *et al*., 2012)

	Flax and hemp fibres	Washing, drying, chemical /ultrasonic/microwave pre-treatment.	Enzymatic treatment in acetate buffer supplemented with endoglucanase and incubated in a shaker at 50°C.	Centrifugation, washing, ultrafiltration, freeze drying.	Not applicable	(Xu *et al*., 2013)
High-Intensity Ultrasonication (HIUS)	Apple pomace	Not applicable	Precipitate calcium carbonate was used to prepare 0.2 wt% cellulose suspension. Ultrasonication treatment (t = 30/60 min, P = 40, 60, or 80% of P_{max}).	Vacuum filtration, and drying	50-58%	(Szymańska-Chargot *et al*., 2018)
	Hop stems (*Humulus lupulus* L.)	Shredding, acid pre-treatment, alkaline, and bleaching treatment.	Ultrasonication treatment (power output 130W for 60 min) in an ice bath	Refrigeration a 5°C	~60%	(Szymańska-Chargot *et al*., 2022)

	Bamboo (*Phyllostachys pubescence*)	Soxhlet extractor for 6 hrs, $NaClO_2$ at 75℃ for 1 hr (repeat five times), 2wt% KOH at 90℃ for 2 hrs.	Dispersed in DI water (0.5 wt% solid content) Ultrasonication treatment (60 kHz, 30 min, output power of 1200 W)	Centrifugation, and drying.	58.73%	(Han *et al*., 2018)
	Waste coconut husk	Pre-washed, air-dried, and 24hrs of Soxhlet extraction. Ultrasonic-assisted solvent immersion with ultrasonic power (100 W), ultrasonic frequency (40 KHz), and solid- liquid ratio (1:30) Alkaline and bleaching treatment.	Ultrasonic treatment (output power 1000W) for 1 hr.	Centrifugation and stored at 4℃.	56.3%	(Wu *et al*., 2019)
High-pressure homogenization (HPH)	Cotton	1 % sodium hydroxide solution	High-pressure homogenization at pressure levels ranging from 40	Centrifugation and freeze drying	32.62%	(Wang *et al*., 2015)

	Microwave oven treatment of the 1 %(w/w) cellulose/[Bmim]Cl solution at ~130℃ while mixing	MPa to 140 MPa for up to 50 cycles.			
eucalyptus citriodora pulp	Microwave heating of 1% (w/w) [Bmim]Cl at 150℃ at 300W	High-pressure homogenization at pressure levels from 40 to 120 MPa and for up to 50 cycles.	Centrifugation and freeze drying	34.43%	(Wang *et al.*, 2017b)
Corn stover	Chemical treatments (alkali extraction and delignification)	High-pressure homogenization of 1% cellulose solutions at 500 bars of pressure.	Freeze drying	Not applicable	(Xu *et al*., 2018)
Okara cellulose	Degreasing, decolourizing, delignification, and bleaching processes.	High-pressure homogenization of 4wt% cellulose suspension at various conditions.	Freeze-drying	~69%	(Wu *et al.*, 2021a)

Combination of processes	Culinary bananas (*kachka*l)	Alkali pre-treatment and bleaching processes	Acid hydrolysis via 1% H_2SO_4 at 80℃ for 1 h. Ultrasonication treatment (25 kHz, 30℃, output power 400, 800 and 1000 W)	Washing and centrifugation. Stored at 4℃.	30-64%	(Xie *et al*., 2016)
	Pineapple leaf fibres	Alkali treatment and bleaching process	Acid hydrolysis (1^{st}-3.5M HCl at 50℃ for 12 hrs) and (2^{nd}-7.5 M HCl at 50℃ overnight). HPH HIUS	Washing	HPH - 69.4% HIUS - 61.7%	(Mahardika *et al*., 2018)
	Commercial MCC powder	Not applicable	Acid hydrolysis using sulfuric acid and ultrasonic treatment	Washing, centrifugation, dialysis and freeze-dried	73%	(Tang *et al*., 2014)

	Cassava roots	Alkali treatment, Q-chelating treatment, and bleaching step.	Acid hydrolysis and ultrasonic treatment	Washing, and centrifugation	~ 77%	(Leite *et al*., 2017)
	Commercial MCC (95%) powder derived from wheat straw	Not applicable	Enzymatic hydrolysis using acetate buffer and cellulase. Followed by ultrasonic treatment	Boiling, centrifugation, washing and freeze-dried	~ 77%	(Cui *et al*., 2016)

2.4 Response Surface Methodology

Response surface methodology (RSM) is a collection of statistical and mathematical modelling techniques employed to develop, improve, and optimise processes (Chang *et al.*, 2017)(Goudarzi, Kasra Kermanshahi and Jahed Khaniki, 2020). RSM model is useful to assess multiple regression analysis of quantitative data obtained from experiments to explain multivariate equations simultaneously (Amenaghawon *et al.*, 2013)(Ferreres *et al.*, 2017). Contrary to traditional univariate products, through which singleton variables are studied independently, RSM is principally designed to deal with several affecting factors useful even in the presence of complex interactions (Ferreres *et al.*, 2017)(Arslan and Araçoğlu, 2015). RSM has been extensively applied in research due to its resultant properties such that it allows successive models of increasing order to be built, gives an estimate of experimental error, robust presence of outliers in the data, cost-effective, allows for group experiments to be conducted, provides a good distribution and many more (Murray *et al.*, 1990).

Commonly used RSM designs are the 3^k factorial, the Box–Behnken design (BBD), and central composite design (CCD) are used to fit second-degree models (Dean *et al.*, 2015). BBD and CCD models are considered to be low-cost and time-saving due to the reduced number of experimental runs conducted in full factorial design when dealing with more than two variables (Goudarzi, Kasra Kermanshahi and Jahed Khaniki, 2020)(Sartika *et al.*, 2019). RSM has been extensively applied in modelling and optimisation of numerous acid hydrolysis experiments using cellulose extracted from plant materials.

2.4.1 Box-Behnken design (BBD)

BBD is a second-order multivariate technique based on a fractional three-level factorial design. BBD is an independent, rotatable or nearly rotatable quadratic design (Ferreres *et al.*, 2017)(Wan *et al.,* 2018). A 3^k factor BBD design is represented graphically in two forms: a cube defined by the midpoints of the edges of the process space and a centre point or three interlocking 2^2 factorial designs and a centre point as illustrated in Figure 2.12 (Dong, Roman and Long, 2014). For the BBD, the total number of runs, *N*, given by equation 2.1 below.

$$N = 2n \cdot (n - 1) + n_c \qquad 2.1$$

Where n is the number of factors and n_c is the number of centre points. BBD is advantageous over CCD as it avoids the design space corner points because runs at extreme conditions are difficult to perform. BBD has been widely applied to optimise the extraction of CNCs from plant natural sources.

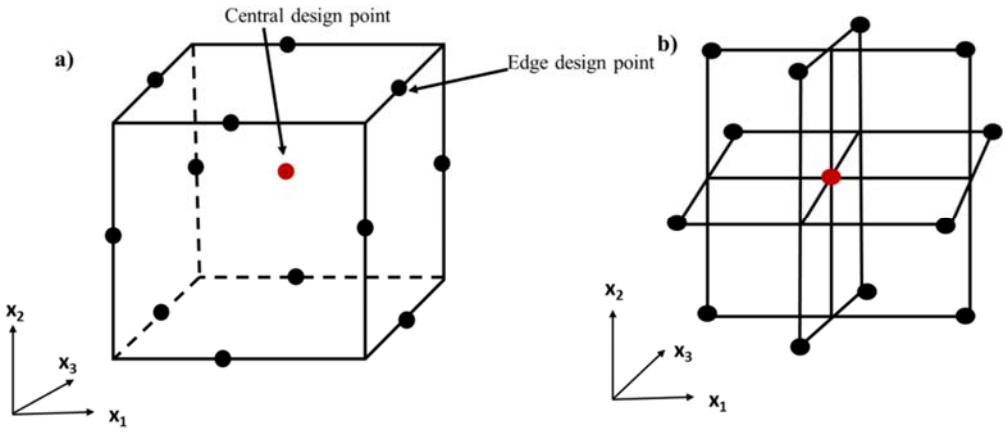

Figure 2.12: Geometry of 3^k factor Box-Behnken design a) cube defined by the midpoints of the edges and a centre point; (b) three interlocking 2^2 factorial designs and a centre point.

Song *et al*, investigated the effect of acid hydrolysis on nanocellulose crystals (NCCs) prepared with sulfuric acid using oil palm empty fruit bunch (Song *et al.*, 2016). A BBD RSM model was employed to optimise the following conditions: alkaline (NaOH) concentration, acid (H_2SO_4) concentration and hydrolysis time. From the particle size analysis results, isolated NCC had a particle size (z-average) below 300nm with typical elongated rod-like features. From RSM 3D contour plots, it was determined that at low NaOH and H_2SO_4 concentrations, the z-average diameter is increased due to the presence of hemicellulose/lignin material and insufficient exposure of cellulose crystalline regions for hydrolysis to occur. Hydrolysis time also played an important role as increasing hydrolysis time reduced the z-average diameter significantly (Song *et al.*, 2016). Chowdhury *et al*, studied the extraction of cellulose nanowhiskers (CNWs) from the leaves of an African baobab tree using the ultrasonication method (Chowdhury *et al.*, 2019). Two-level factorial BBD design was used to optimise the process parameters: ultrasonication power, hydrolysing time, and temperature. Ultrasonication power was determined as an significant factor influencing the extraction of CNWs from baobab leaves. Under optimum conditions (200 watts, 43.11 mins, 94 ℃), extracted CNWs were found to have high crystallinity index of 86.46 % and exhibited an average width of 15 – 20 nm (Chowdhury *et al.*, 2019).

2.4.2 Central composite design (CCD)

In RSM, a CCD model is one of the most used statistical experimental design models to optimise a vast amount of research problems. A CCD is a rapid well-suited technique used to fit second-order (quadratic) multivariate models based on a two-level full factorial design instead of the conventional three-level full factorial design (Bashiri and Farshbaf Geranmayeh, 2011)(Hang, Qu and Ukkusuri, 2011). A CCD includes three groups of design points: a) two-level factorial design points coded as +1 and −1, b) axial/star points located at a distance, α, from the centre, and c) centre points which represents

the number of replicate runs (see Figure 2.13) (Asghar, Raman and Daud, 2014). Depending on the alpha value, α, from equation 2.2, the design is either face centred, orthogonal, spherical, or rotatable and $|\alpha| > 1$. When α, the axial parameter is α = 1, the design is called the face centered cube design, when α = 1.287, the design is called orthogonal and when α = 1.682, the design called rotatable (Dong, Roman and Long, 2014)(Asghar, Raman and Daud, 2014).

$$\alpha = (2^k)^{0.25} \qquad 2.2$$

Given the design points, the total number of experimental runs, *N*, of a CCD is given by equation 2.3.

$$N = 2n + 2n + nc \qquad 2.3$$

Where *n* is the number of factors and n_c is the number of centre points. From the equation 2.3 above, the third term is used to determine experimental error and reproducibility of the data. A CCD model has been widely applied in scientific research fields, transportation, automotive engineering, and other fields.

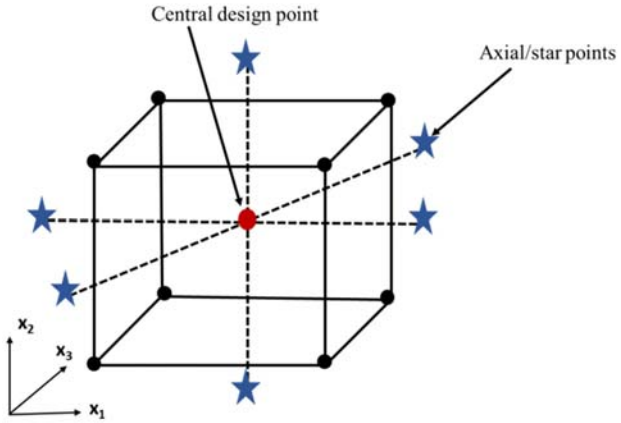

Figure 2.13: Geometry of central composite design in three factors.

Guo *et al,* investigated the optimisation of the hydrolysis of nanocellulose crystals (NCCs) prepared from abundant waste tea stalk (Guo *et al.*, 2020). They used CCD-RSM to evaluate and optimise the effect of the reaction conditions: H_2SO_4 acid concentration, hydrolysis temperature and hydrolysis time to achieve high yields of NCCs from tea stalk. According to the optimisation software, the maximum yield of 50.96 % was achieved at an acid concentration of 62.20 %, hydrolysis time of 123.35 min and hydrolysis temperature of 45℃. Furthermore, verification experiments obtained a yield of 49.8 % within the 97 % confidence interval of the software result. The tea stalk NCC also had good stability reports with dimensions of 4 – 8 nm wide and 6.36nm average width. Akhabue *et al*, investigated the optimum processing conditions for obtaining the maximum yield of MCC powder from orange peel waste (OPW)

by use of RSM (Akhabue and Osubor, 2017). CCD model was used to evaluate the optimum process conditions by investigating two factors: hydrolysis temperature and hydrolysis time. At optimum conditions 100.53℃ and 16.28 min, a maximum yield of 14.65% was obtained producing irregularly shaped fibrous MCC particles with particle size in the range 20–85 μm and average diameter of 56.57 μm. Kandhola *et al*, studied the production of CNCs and CNFs from pre-extracted loblolly pine kraft pulp using strong sulfuric acid hydrolysis method (Kandhola *et al.*, 2020). The effect of four parameters: acid concentration, temperature, hydrolysis time and pulp particle size were evaluated to optimise the yield and properties of CNCs using the CCD method of RSM. Maximum yield of 60% was obtained from optimum conditions of 60% acid concentration, 58℃, 60 min and 40 mesh particle size. From the results, it was observed that acid concentration and temperature had a significant effect on CNC yield. For CNC production, the use of strong acid concentrations is one of the most effective approaches, however, the process is not environmentally friendly due to harsh acid conditions. These conditions result in problems such as equipment corrosion, wastewater treatment and residual acid recycling (Wang *et al.*, 2019)(Kandhola *et al.*, 2020).

2.5 Cellulose surface modifications

As previously mentioned, cellulose materials can offer benefits of biodegradability, biocompatibility, high surface area, low cost, high thermal stability, and excellent mechanical qualities for various applications. However, the abundance of hydroxyl groups in cellulose chains reduces the processability of strong intra- and intermolecular hydrogen bonds, which commonly leads to fiber aggregation. To overcome the above-mentioned challenges, functionalisation of cellulose materials allows changes in the chemical structure by delivering unique properties to the material. By reacting hydroxyl groups with a modification reagent, additional functional groups can be added to the cellulose chain, enhancing its usefulness, and broadening its range of applications to various industries. 2,2,6,6tetramethylpiperidinyloxyl radical (TEMPO) oxidation (Patiño-Masó *et al.*, 2019), periodate oxidation (Sun *et al.*, 2015)(Strong *et al.*, 2018)(Yang, Chen and van de Ven, 2015), esterification (WillbergKeyriläinen and Ropponen, 2019; Her *et al.*, 2020; Beaumont *et al.*, 2021; Lease, Kawano and Andou, 2021; Liu *et al.*, 2021), acetylation (Beaumont *et al.*, 2020), amidation,(Gars *et al.*, 2020) carboxymethylation (Saber-Samandari *et al.*, 2016)(Veeramachineni *et al.*, 2016)(Eltaweil *et al.*, 2020), radical polymerization(Garcia-Valdez, Champagne and Cunningham, 2018), and cationisation(Gao *et al.*, 2016)(Gu *et al.*, 2020)(Rana *et al.*, 2021), are some of the chemical modifications previously studied (Vincent and Kandasubramanian, 2021).

2.5.1 TEMPO-mediated Oxidation

During TEMPO-mediated oxidation, negatively charged carboxyl groups are introduced onto cellulose surface by selective oxidization of the primary hydroxyl group at the C6 position of anhydroglucose

unit to form well dispersed individual nanofibrils or elementary fibrils in water (Figure 2.14) (Qu *et al.*, 2021)(Abou-Zeid *et al.*, 2020). Furthermore, it has been demonstrated that TEMPO-catalyzed oxidation does not oxidize the inside of crystalline microfibrils, which results in electrostatic repulsion between the fibrils, and primarily weakening the interfibrillar hydrogen bonds within cellulose structure (Kaffashsaie *et al.*, 2021)(Puangsin *et al.*, 2017)(Kondo, 2022). This method is one most promising, effective, and energy-saving pretreatments for converting plant cellulose fibres to nanofibres, however there are still several problems with the current method, including low processing efficiency, expensive catalyst, the use of toxic reagents, and difficulty in chemical recovery (Noremylia, Hassan and Ismail, 2022)(Du, Liu, Zhang, *et al.*, 2016). Nanocellulose isolation has been previously studied via TEMPOmediated oxidation reactions from different natural sources, bamboo (Tang *et al.*, 2017), softwood (Fraschini, Chauve and Bouchard, 2017), oil palm empty fruit branches (Hastuti, Kanomata and Kitaoka, 2019) (Indarti *et al.*, 2019), wheat straw (Qu *et al.*, 2021), raw wood (Kaffashsaie *et al.*, 2021), sugarcane bagasse (Rossi *et al.*, 2021) (Abou-Zeid *et al.*, 2020), cassava peel (Czaikoski, da Cunha and Menegalli, 2020),. Eucalyptus (Lv *et al.*, 2019), hemp bast (Puangsin *et al.*, 2017) and many more. In principle, the TEMPO oxidation reaction mechanism produces nitrosonium ions (+N=O) in situ when TEMPO radicals react with oxidants, and cellulose fibres are thereby oxidized in the process. As a result, the main alcohol groups are first changed to aldehydes and then to COOH groups through oxidation. At the same time, the cellulose depolymerization phenomenon appears. The depolymerization of cellulose can result in two different ways, first by β-elimination because of the presence of C6 aldehyde groups in an alkaline environment, and second by cleavage of a hydroglucose unit due to the presence of a hydroxyl radical (Noremylia, Hassan and Ismail, 2022).

According to Czaikoski *et al*, studied CNFs from cassava peel obtained by a combination of chemical and physical processes. During isolation, fibres were TEMPO oxidized with (CNFs-Tows) and without (CNFs-TOwos) ultrasonic treatment and it was found that CNFs-TOwos showed the widest distribution range. Larger dimensions were also observed for CNFs-TOwos, average length 3867±1597 nm and average diameter 16±14.0nm. Stable large negative zeta potential (above -40 mV) was observed with and without ultrasonic treatment which represented electrostatic stability as carboxylic groups were introduced on the surfaces of fibres during to catalytic oxidation (Czaikoski, da Cunha and Menegalli, 2020). Furthermore, Abou-Zeid *et al*. produced CNFs using TEMPO- periodate-chlorite in a series of oxidation stages. CNFs were produced by TEMPO oxidation, however, to improve adsorption efficiency for cationic species in water the carboxyl content was enhanced through periodate-chlorite oxidation. As the repulsive forces between the fibres grew, they recorded an increase in carboxylic content from 0.9 to 3.5 $mmolg^{-1}$ which further confirms the degradation of CNF fibres upon further oxidation (Abou-Zeid *et al.*, 2020). Puangsin and co-workers reported TEMPO mediated oxidation of hemp bast for preparation of cellulose nanofibres (TOHBC). It was reported that oxidizing conditions

of TEMPO/NaBr/NaClO system in water at pH 10, a considerable amount of carboxylate groups (up to 1.2 mmolg^{-1}) was introduced and at the same time sufficient delignification from the hemp bast fibres was achieved (Puangsin *et al.*, 2017).

On the other hand, Hassan *et al*, proved that coconut residues (shell and husk) successfully produced TEMPO-oxidized cellulose nanofibrils (CNFs) through alkali and bleaching pretreatment for removal of non-cellulosic content, followed by TEMPO/NaBr/NaClO oxidation approach for defibrillation of cellulose fibres. Functionalising the carboxyl groups on the surface of the fibres through TEMPO oxidation treatment enabled the defibrillation of cellulose microfibrils into cellulose nanofibrils (Hassan *et al.*, 2021). In addition, TEMPO oxidation of CNFs is known to reduce thermal stability of fibrils through the introduction of sodium carboxylate groups leading to decarbonation during heating process (Noremylia, Hassan and Ismail, 2022). In addition, TEMPO-oxidized CNFs prepared from aspen wood investigated by Jonasson *et al*, reported reduced thermal stability of nanocellulose (TOCNF) which can be attributed decarbonation of the oxidized anhydroglucose units (Jonasson *et al.*, 2020). Furthermore, isolation of CNCs prepared from lemon (*Citrus limon*) seeds by Zhang *et al*, was done through TEMPOmediated oxidation and acid hydrolysis. Lower thermal stability (256℃) and low crystallinity was observed for TEMPO oxidized CNCs caused by the development of sodium carboxylate groups on the surface of the cellulose, whereas nanocellulose from acid hydrolysis showed two decomposition stages (240℃ and 320℃), the first due to its highly sulfated regions, and the second due to decomposition unsulfated crystalline domains (Zhang *et al.*, 2020a).

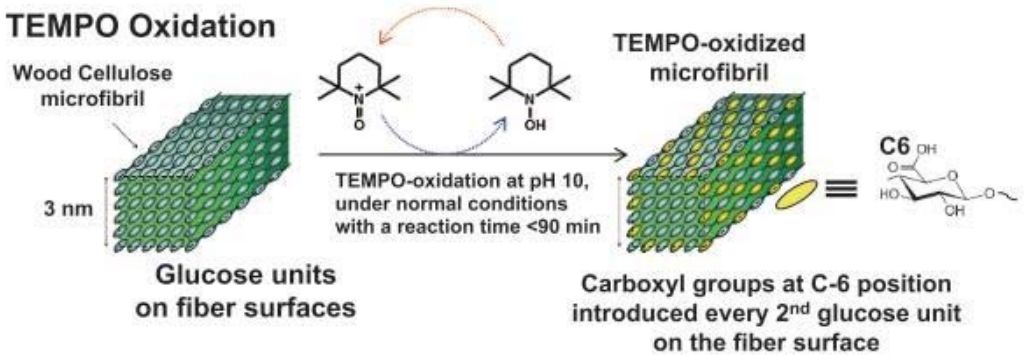

Figure 2.14: Schematic diagrams of a TEMPO-mediated oxidization process for nanocellulose isolation (Image adapted from (Kondo, 2022)).

2.5.2 Cationisation

Cationisation of cellulose fibres has been broadly utilized for preparation of modified cellulose. In the process, cellulose fibres are quaternised to introduce cationic functional groups on active hydroxyl group structures and nanofibrillation of cellulose fiber is facilitated by the electrostatic repulsion

between the quaternary ammonium cations (Xie *et al.*, 2018). Commonly used cationising agents include (2,3-epoxypropyl) trimethylammonium chloride (EPTMAC) (El Miri *et al.*, 2022)(Sehaqui *et al.*, 2015)(Sehaqui *et al.*, 2017)(Gao *et al.*, 2016), 3-chloro-2-hydroxypropyltrimethylammonium chloride (CHPTAC) (Morantes *et al.*, 2019)(Wang *et al.*, 2016)(Wang *et al.*, 2018)(Rana *et al.*, 2021)(Etale *et al.*, 2021), glycidyl trimethyl ammonium chloride (GTMAC) (Gao *et al.*, 2015) (Chaker and Boufi, 2015) (Pei *et al.*, 2013) (Willberg-Keyriläinen *et al.*, 2019) and (2-hydrazinyl- 2-oxoethyl)trimethylazanium chloride also known as Girard's reagent T (Huang *et al.*, 2020b) (Sirviö *et al.*, 2011)(Liimatainen *et al.*, 2014). Derivatives of cationic cellulose have several uses in the pulp and paper, textile, cosmetics, pharmaceutical, and dye industries (Jasmani *et al.*, 2016). Morantes *et al*, studied the use of highly charged CNCs as flocculants in water treatment processes. Acid-hydrolysed CNCs were modified CHPTAC resulting in CNC-EPTMAC. Results showed that grafting of cationic quaternary ammonium groups on the surface of the CNCs improved the zeta potential and thermal stability of the CNCs and gained flocculant properties (Morantes *et al.*, 2019). Zaman *et al*, investigated NCC modification with GTMAC and reported that altering the water content in the reaction system increased the cationic surface charge density of NCC. Due to an increased cationic surface charge, the modified NCC was stable and well dispersed in aqueous conditions, however, it has also been reported the main etherification reaction is subsequently accompanied by the alkaline hydrolysis reaction. Hence during cationisation reactions, two reactions can occur by; 1) a desirable cationisation of NCC and 2) the GTMAC hydrolysis reaction which is undesirable (Figure 2.15) (Rana *et al.*, 2021)(Zaman *et al.*, 2012). Although hydrolysis reactions cannot be avoided during cationisation as it results in high water content (Rana *et al.*, 2021), research has been explored on replacing a certain ratio of water with water-miscible organic solvents (dimethyl sulfoxide (DMSO), tetrahydrofuran (THF), or isopropanol). They found that when isopropanol and THF replaced 90% of water the reaction efficiency improved, and THF produced higher degrees of substitution (Odabas *et al.*, 2016) (Zaman *et al.*, 2012). Furthermore, studies conducted by Gao and co-workers report that surface cationisation of PC resulted in an improved zeta potential (67 mV) and charge density (+5.20 meq/g) over the unmodified cellulose and charge density increases with higher DMSO content up to a point. This is primarily caused by the presence of organic solvent, which prevents cationised PC from hydrolysing (Gao *et al.*, 2015). Additionally, it has been shown that cationised cellulose enhances the capacity for contaminant adsorption and significantly increases the antibacterial characteristics of the cellulose fibrils, therefore plays a significant role in wastewater treatment (Littunen *et al.*, 2016).

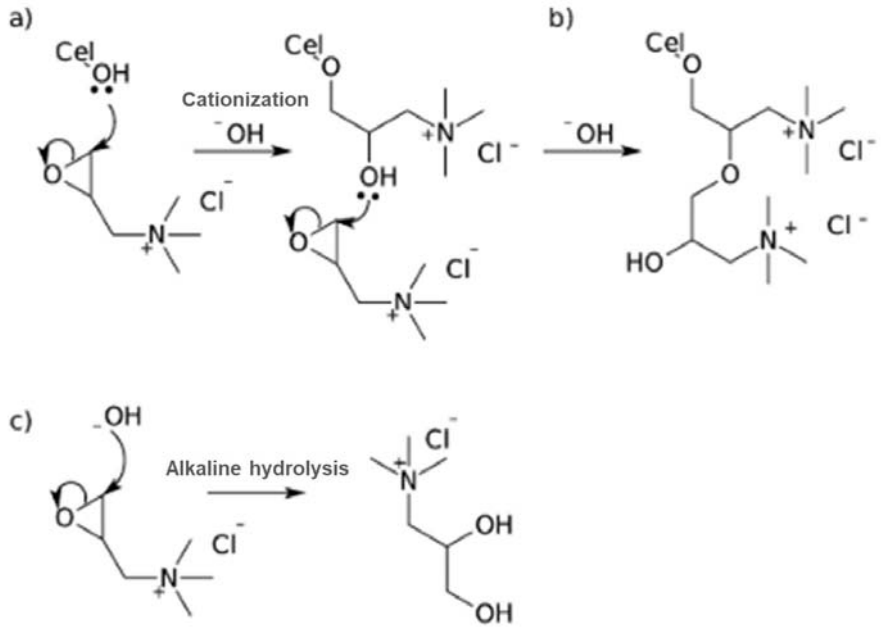

Figure 2.15: Mechanism of reaction between (a) epoxides and cellulose fibres, (desirable)(b) showing multiple substitution, and (c) alkaline hydrolysis of EPTMAC (undesirable) (Image adapted from (Eyley and Thielemans, 2014)).

Huang *et al,* used modified nanocellulose extracted from sugarcane bagasse for the effective removal of Cr (VI) using a Girard's reagent as a cationising agent. It was found that the cationic dialdehyde nanocellulose adsorbent (c-DAC) with the highest charge density showed an adsorption efficiency of 80.5 mg/g for Cr(VI) uptake and it was relieved that adsorption of anionic Cr(VI) was favored at a pH range 2-6 due to protonation of ^{-}OH and NH_2^{-} functional groups, leading to a highly cationic c-DAC surface (Huang *et al.*, 2020b). Sehaqui *et al*, evaluated the adsorption potential of anionic (F^-, NO_3^-, SO_4^{2-}, PO_4^{3-}) contaminants onto cationic CNFs synthesized from waste pulp residue. GTMAC was used as cationising agent and it was found that in comparison to unmodified CNFs, cationic CNFs displayed better adsorption capacity due to the presence of positive charges of the CNFs surface and wen all anions were present in solution, the adsorption of multivalent ions (SO_4^{2-}, PO_4^{3-}) was approximately twice as higher than monovalent ions (F^-, NO_3^-)(Sehaqui *et al.*, 2016). The removal of SO_4^{2-} ions from aqueous solutions using cationised CNFs was investigated by Muqeet *et al*, under a variety of experimental circumstances. Electrospinning was used to create nanofibre mats, which were then cationised with CHPTAC. A Langmuir isotherm model was used to determine the maximum adsorption capacity of 24.5 mgg^{-1}, and cationic CNF had an ammonium concentration of 0.134 $mmolg^{-1}$. From the adsorption data, pseudo-second order (PSO) kinetic model was best fitted for sulfate adsorption onto

cationic CNF. The average fibre diameter analysed by SEM micrographs was 280 10 nm, and a BET surface area and porosity analyser yielded a BET surface area of 5.04 m^2g^{-1} (Muqeet *et al.*, 2017).

Cationic modified has also been previously utilised for adsorptive removal of anionic dyes from waste. Jiang *et al*, investigated hydroxypropyloctadecyldimethylammonium as a modifying agent for preparation of cationised rice husk cellulose (CRHC) from rice husk cellulose (RHC). Adsorption of anionic dyes (Diamine Green B (DG-B), Acid Black 24 (AB-24) and Congo Red (CR)) was investigated in batch mode. FTIR, XRD, and SEM were used to characterize the structure and morphology of the materials. The findings revealed that the molecular structure and morphology of RHC had changed, and that the quaternary ammonium group were successfully grafted onto the RHC molecular structure. From the adsorption data, the adsorption performance and mechanism of DG-B, AB-24, and CR onto CRHC were best fit by pseudo-second order and Langmuir model. The maximal Langmuir adsorption capacity of DG-B, AB-24, and CR on the CRHC were determined to be 207.15, 268.88, and 580.09 mg g^{-1}, respectively, at 303.15 K. adsorption mechanism can be attributed to various factors including electrostatic attraction, hydrogen bonding, and the competition of OH^- ions (Jiang and Hu, 2019). Additionally, Pei *et al*, used mechanically pretreated wood pulp for quaternisation of cellulose nanofibrils with GTMAC. The generated quaternised cellulose nanofibrils (Q-NFC) reported trimethyl ammonium chloride content range of 0.59-2.31 mmol g^{-1}. With increased trimethylammonium chloride content on cellulose, the anionic dye adsorption ability of Q-NFC nanofibrils increased. (Pei *et al.*, 2013). To remove anionic dyes, the polyacrylamide grafted quaternised cellulose (PAM-g-QC) adsorbents were developed. The addition of CHPTAC, and acrylamide (AM) to cellulose could effectively improve its amino content, resulting in improved adsorption capability. SEM revealed a porous and three-dimensional framework structure in the adsorbents. The cellulose PAM-g-QC experimental results suited the pseudo-second-order kinetic model and the Langmuir isotherm well, and the highest theoretical adsorption capacity of the beads was 380.084 mg g^{-1} for Congo red (CR) and and 349.284 mg g^{-1} for Eriochrome blue SE (EBSE). The thermodynamic analyses gave support for the adsorption process being endothermic and spontaneous (Wang *et al.*, 2016).

Furthermore, anionic dye (Acid Orange 7, Direct Blue 75 and Direct Violet 31) adsorption was studied by Hashem and colleagues prepared from MCC with CHPTAC as a cationising agent. The results revealed that adsorption capacity was affected by adsorbent, temperature, type of dye, and van der Waals and hydrogen bonding. Cationised cellulose displayed significantly higher anionic dye adsorption capability than cellulose (Hashem and El-Shishtawy, 2001).

Table 2.5: Cellulose modifications from various sources

Modification	Source	Cellulose	Conditions	Findings	Ref
TEMPO oxidation	Bamboo dissolving pulp	Nanocellulose	TEMPO/NaBr/NaClO system at pH 10	TEMPO oxidized fibers showed fiber dimensions of 447 ± 5 µm, shorter than original sample. Crystallinity value = 69.5%	(Tang *et al*., 2017)
	Commercial bleached softwood kraft pulp	CNCs	TEMPO/NaBr/NaClO system at pH 10 with constant stirring	Introduction of carboxylate groups onto surface did not damage crystal structure, average length of the TEMPO-mediated oxidized crystals was 94 ±32 nm	(Fraschini *et al*., 2017)
	Oil Palm Empty Fruit Bunches	CNFs	TEMPO/NaBr/NaClO system at pH 10	TEMPO-oxidation increased carboxylate content without changing cellulose polymorph, fiber dimensions: The length:100–291 nm, width: 3–9 nm.	(Hastuti *et al*., 2019)
	Wheat straw	Cellulose fibers	TEMPO/NaBr/NaClO system at pH 10	Crystal structure change from cellulose I to II due to alkali treatment, however after TEMPO oxidation crystallinity did not change much meaning crystalline areas of cellulose could not be broken by the TEMPO-oxidized process.	(Qu *et al*., 2021)
	Raw wood particles of paulownia	CNFs	TEMPO/NaBr/NaClO system in water at pH 10	Average diameter of ± 3 nm showing elementary fibrils in individual or bundles form. Crystallinity value of 67%	(Kaffashsaie *et al*., 2021)

	Oil palm empty fruit bunch (OPEFB) strands	Nanocellulose	TEMPO/NaBr/NaClO system in water at pH 10	Crystallinity degree of 72%.	(Indarti *et al*., 2019)
	Walnut shell	Nanocellulose	TEMPO/NaBr/NaClO system in water at pH 10	Porous network with an irregular block structure was observed, low thermal stability	(Zheng *et al*., 2019)
	Sugarcane bagasse	CNFs	TEMPO/NaBr/NaClO system in water at pH 10.5	TEMPO-oxidized samples had an average length of 400 ± 200 nm, No significant changes in crystallite sizes	(Rossi *et al*., 2021)
	Cassava peel	CNFs	TEMPO/NaBr/NaClO system in water at pH 10	Diameter (5−16 nm) and high negative zeta potential values (around −30 mV).	(Czaikoski *et al*., 2020)
	Bagasse pulp	CNFs	TEMPO/NaBr/NaClO system in water at pH 10	high density of the carboxyl groups on CNFs thus improves adsorption, high crystallinity value of 83%, diameter of 20 nm, with different lengths up to a few micrometers.	(Abou-Zeid *et al*., 2020)
Cationization	bleached birch (Betula verrucose) commercial chemical pulp	Nanocellulose	Periodate oxidation Girard's reagent with aldehyde cellulose at pH 4.5 using HCl as catalyst.	Cationic group content increased from 2.85 to 4.7 $mmolg^{-1}$. An increase in temperature resulted in increased cationicity with low aldehyde content. improve solubility	(Sirviö *et al*., 2011)
	Hardwood bleached kraft pulp	Cellulose fibrils	EPTMAC as cationising agent	Cationization did not alter fiber length and width, however, it improved kink index and surface charge density +18.68 µeq/lg	(Gao *et al*., 2016)
	Sugarcane bagasse	Nanocellulose	Delignification of cellulose Periodate oxidation	Increase in DAC's degree of oxidation (from 6.32% to 18.91%) led to a significant increase in	(Huang *et al.*, 2020b)

		Girard's reagent at pH 4.5.	c-DAC's degree of oxidation, improving chromium adsorption	
Softwood	CNFs	GTMAC as cationising agent	Improved trimethylammonium chloride content up to 2.31 mmol/g. nucleophilic addition of alkali activated hydroxy groups of cellulose to epoxy moiety of GTMAC	(Pei *et al*., 2013)
Rice husk	Nanocellulose	Alkali and beaching treatments Epichlorohydrin as cationising agent	Reduced crystallinity due to production of quaternary ammonium groups through breakdown of original hydrogen bonds of rice. Cationization produced individual fibers with a smooth surface.	(Jiang and Hu, 2019)
Eucalyptus globulus	CNFs	Quaternization of cellulose fibers via GTMAC.	Nucleophilic addition of the hydroxyl groups to the epoxy moiety of GTMAC. DMAC was utilized as solvent to limit hydrolysis. NMR showed an $(CH_3)_3N^+$ at 55ppm	(Chaker and Boufi, 2015)
Bleached softwood kraft pulp	Nanocellulose	Cationised in systems with different water-miscible organic solvents. EPTMAC as cationising agent	replacing 90% of the water with isopropanol or tetrahydrofuran yielded higher degrees of substitution and increased reaction efficiencies	(Odabas *et al*., 2016)
Parenchyma cellulose (PC) from bagasse pith	Cellulose fibers	GTMAC was used as a cationization agent	Zeta potential and charge density on PC's surface increased in comparison to unmodified cellulose because of surface cationization.	(Gao *et al*., 2015)

2.6 Environmental pollutants

2.6.1 Synthetic Dyes

Dyes are organic compounds that consist of complex ionic aromatic structures featuring aryl groups that have delocalized electron systems, and by adsorption, dyes tend to give colour to substrates (TejadaTovar, Villabona-Ortíz and Gonzalez-Delgado, 2021). With over an estimate of 100,000 types of dyestuff commercially available are manufactured each year, and the annual global production of dyes lies at approximately 7×10^5 tons (Dawood and Sen, 2012)(Katheresan, Kansedo and Lau, 2018). Synthetic dyes with complex chemical structures are considered to be non-biodegradable and nonoxidisable in nature due to properties such as thermal, biological, physiochemical, and optical stability (Sun *et al.*, 2013)(Haddadian *et al.*, 2013)(Ata *et al.*, 2012). Unfortunately, up to 20% of dye solutions utilised in dyeing processes are discharged into industrial wastewater effluents and, become major environmental contaminants which can disrupt water ecosystems and affect human life (Veni and Brenda, 2021)(Haddadian *et al.*, 2013)(Abdel-Ghani *et al.*, 2017). A wide range of dyes can be classified as disperse, reactive, acid, basic, direct, azoic, sulfur, and direct dyes and these have been commonly used in textile industries (Hassan and Carr, 2018).

2.6.2 Azo dyes, environmental fate, and human health

Azo dyes are synthetic dyes which are distinguished by the presence of the azo moiety (–N=N–) in their chemical structure, linked with two identical symmetrical and/or asymmetrical or non-azo alkyl or aryl radicals (Weglarz-Tomczak and Górecki, 2012)(Benkhaya, M'rabet, and El Harf, 2020). Azo dyes are the largest and highly versatile class of dyes used and represent over 50% of total dyes manufactured worldwide (Benkhaya, M'rabet, and El Harf, 2020)(Chung, 2016). Due to their specific physiochemical properties and biological activities, azo dyes have been applied in various industries namely; pharmaceutical, plastics manufacturing, leather, cosmetic, food, dyeing/textile industry and analytical chemistry to impart color on final products (Hashem and El-Shishtawy, 2001)(Sun *et al.*, 2013)(Weglarz-Tomczak and Górecki, 2012)(Chukwuemeka-Okorie *et al.*, 2021). Due their distinct vivid bright colours (oranges, reds, and yellows), their presence in wastewater is significantly noticeable and dye effluents cannot be treated by the conventional wastewater treatment methods leading to lethal effects, genotoxicity, mutagenicity, and carcinogenicity to humans as well as animals (Chung, 2016). Azo dyes include Tartrazine, Methyl Yellow, Methyl Red, Congo Red, Orange II, Aniline Yellow, Sunset Yellow, Solvent Yellow 3, Direct Red 28, Methyl Orange and many more (Chung, 2016), however for this research study, the environmental fate and human health impact of methyl orange and sunset yellow will be discussed further below.

2.6.2.1 Synthetic dyes of interest

2.6.2.1.1 Methyl Orange

Methyl Orange (MO) is a common and typical azo anionic [Sulfonate (SO_3^-)] dye that is water-soluble (5 g L^{-1}, H_2O, 20°C) and is famous for its high colourability. The chemical characteristics of methyl orange are given in Table 2.6. MO has been applied in various industrial applications ranging from printing, dyeing, textile, pharmaceuticals, and research laboratories. Additionally, to industrial use, in laboratories MO can be used as a pH indicator (pH range 3.1–4.4) with a red to yellow colour change (Wu *et al.*, 2021b) (Alghamdi *et al.*, 2019) (Neethu and Choudhury, 2018) (Fernandes *et al.*, 2020). Industrial use can generate large volumes of wastewater effluent that is discharge into the environment containing dye residue leading to water pollution even at low dye concentration (less than 1 ppm). Dye effluent in the environment can cause a domino effect whereby light penetration into water can be limited by dye pollutants, subsequently reducing photosynthetic activity resulting in poor growth of aquatic species (fauna and flora). MO is a highly toxic azo dye that can cause mutagenic, teratogenic, and carcinogenic effects on human beings (Fernandes *et al.*, 2020) (Eljiedi and Kamari, 2017) (Liu *et al.*, 2022) (Zhang *et al.*, 2017).

Table 2.6: Chemical characteristics of Methyl Orange monoazo dye (Chiong *et al.*, 2016) (Iwuozor *et al.*, 2021)

Methyl Orange	
UIPAC name	Sodium;4-[[4-(dimethylamino) phenyl] diazenyl] benzenesulfonate
Chemical formula	$C_{14}H_{14}N_3NaO_3S$
Molecular weight ($gmol^{-1}$)	327.33
Colour index number (CI)	13,025
λ_{max} (nm)	522
Chemical structure	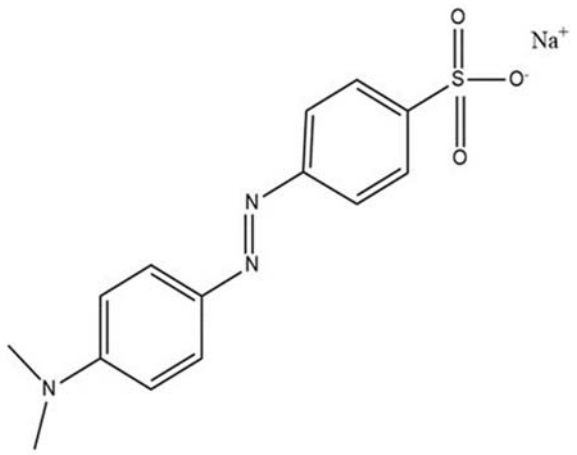

2.6.2.1.2 Sunset Yellow FCF

Sunset yellow FCF is a pyrazolone anionic dye that has been classified as a food additive used in food industry in products such as canned juices, sweets, sauces, jelly, pickles, soft drinks, orange squash, apricot jam, packet soups, and it has been applied in varying products including soaps, hair products, moisturizers, crayons, vitamins and medicinal capsule and many more (Dwivedi and Kumar, 2015)(do Nascimento *et al.*, 2020)(Ghaedi, 2012)(Ghaedi *et al.*, 2012). Sunset Yellow is known for its bright orange yellow colours and its chemical characteristics are given in Table 2.7 (Dwivedi and Kumar, 2015). Due to high frequent use of dyes in these industries, about 10-15% of dye-containing effluents are discharged into the environment without treatment (Chekir *et al.*, 2016)(Dawood and Sen, 2012). As a result, the Joint Food and Agricultural Organization (FAO)/World Health Organization (WHO) Expert Committee on Food Additives (JECFA) in 2011 determined and assessed safety data, such as acceptable daily intake (ADI) for Sunset Yellow FCF of 4 mg/kg /bw/day (EFSA, 2014).

However, there are food manufactures who continue to ignore regulations leading to excessive amounts of dye molecules in food items and in wastewater effluents produced by such industries. Prolonged use of Sunset Yellow dye in food items can have varying effects in children, adult humans, and the environment. Items marked by the presence of Sunset Yellow should be avoid in children suffering from attention deficit hyperactivity disorder (ADHD), and for individuals with aspirin intolerance as it can result in allergic reactions with symptoms varying from asthma, diarrhoea, cardiac arrest, hypersensitivity, immunosuppression, eczema, stomach pain, vomiting, swollen skin, and urticaria (Wawrzkiewicz, 2011)(Rovina, Perumal and Siddiquee, 2016)(Yayayürük *et al.*, 2020). Furthermore, dye molecules can have some of the following effects on the surrounding environment (a) dyed water bodies resulting in aesthetic issues, (b) reduces the ability of the receiving water to reoxygenate itself by blocking the sunlight, which disturbs photosynthetic processes within the aquatic system, and (c) can cause severe and chronic toxicity (do Nascimento *et al.*, 2020)(Mosallanejad and Arami, 2012)(Abdel-aziz and Abdel-gawad, 2020).

Table 2.7: Chemical characteristics of Sunset Yellow FCF monoazo dye (EFSA, 2009)

	Sunset Yellow FCF
UIPAC name	Disodium 6-hydroxy-5-[(4-sulfophenyl) azo]-2-naphthalenesulfonate
Chemical formula	$C_{16}H_{10}N_2Na_2O_7S_2$
Molecular weight ($gmol^{-1}$)	452.37
Colour index number (CI)	15,185
λmax (nm)	480

Chemical structure	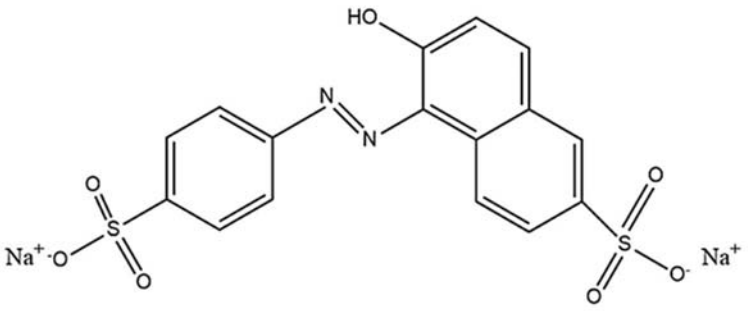

2.7 Conventional wastewater treatment methods

The presence of synthetic dyes in wastewater effluents continues to cause sustainable damage to human health and aquatic life. Therefore, over the past decade conventional wastewater treatment technologies aimed by reducing and/eradicating the issues have been developed and this has been crucial to achieving the Sustainable Development Goals (SDG). The methods for dye removal fall into three categories: chemical, biological, and physical methods. Table 2.8 identifies methods from each category which outlining their advantages and disadvantages.

2.7.1 Chemical method

Different chemical methods for dye removal can include advanced oxidation processes (AOPs), photochemical, Fenton reaction, and ozonation processes. The advanced oxidation processes (AOPs) are based on a treatment technique that uses hydroxyl radicals as oxidizing agents to remove dye molecules by attacking the chromogenic groups, which then generates organic peroxide radicals that eventually convert those groups into simple CO_2, H_2O, and inorganic salts. (Kamar *et al.*, 2022)(Sharma and Kaur, 2018). Fenton reaction is another common type of oxidation process which incorporates an oxidation process with or using Fenton reagent to completely degrade the contaminants and reducing them into compounds like CO_2, H_2O and inorganic salt (Zhang *et al.*, 2021). In addition, ozonation process uses ozone (short half-life) to act as a fast and effective oxidizing agent to oxidize chlorinated hydrocarbons, phenols, and other hydrocarbons, respectively (Vincenzo Naddeo, 2013)(Shah, 2018). Chemical methods are generally effective methods for remove of dye molecules, however the disadvantage of being expensive and producing large volumes sludge creates problems that can be possibly avoided by incorporating a different treatment method (Oller, Malato and Sánchez-Pérez, 2011)(Ledakowicz and Pázdzior, 2021).

2.7.2 Biological methods

Biological methods such as decolorization and degradation of dyes by fungi, algae and yeasts, adsorption by microbial biomass, enzyme degradation, and a range of aerobic-anaerobic methods are generally applied to wastewater treatment effluents to accumulate and degrade a diverse range

contaminant using a variety of microorganism (algae, bacteria, fungi, yeasts, algae) (Saratale *et al.*, 2011). The use of large amounts of chemical agents (as seen or chemical methods) can generate secondary pollution in the form of unwanted by-products and toxic sludge, however biological treatments can further mineralize dyes and their aromatic amine compounds, making effluents less harmful or even completely detoxifying them (Zhang *et al.*, 2021)(Chacko and Subramaniam, 2011). It is worth noting that due to its sensitivity to seasonal variation, use of some toxic chemicals, and lack of design and operating flexibility, biological treatment requires a considerably large space to operate and, therefore these drawbacks affect dye removal studies (Sivarajasekar, 2015)(Shah, 2018).

2.7.3 Physical methods

Common physical methods include membrane separation techniques (ultrafiltration, nanofiltration, reverse osmosis), ion-exchange, coagulation/flocculation, and adsorption processes. Membrane separation techniques act as physical barriers of species of ions, molecules or particles in a sample solution driven by either an electrical force, concentration differences or pressure in the system depending on particle size (Miculescu *et al.*, 2016)(Yin and Deng, 2015)(Li *et al.*, 2020). The ion exchange process has been investigated as dye removal technique since it is inexpensive, environmentally beneficial, and temperature resistant (Kaur and Jindal, 2018)(Wawrzkiewicz, 2011). The ion exchange process efficiently removes dyes from aqueous solutions by interacting strongly with charged dyes and functional groups on ion exchange resins. By exchanging ions, this procedure creates solid connections between the solutes and resins, thereby separating them. (Ahmad *et al.*, 2015)(Aragaw and Bogale, 2021). Anion exchangers or cation exchangers are two types of ion-exchange resins. (Bashir *et al.*, 2019). Another physical method is coagulation/flocculation (CF) process that has been vastly applied for its effectiveness for the removal of suspended from water effluents. Furthermore, CF processes also reduce water turbidity by removing toxic substances (organic and inorganic) and colloidal organic matter (Ugwu *et al.*, 2017)(Kamar *et al.*, 2022)(Barbosa *et al.*, 2018). Many suffer from disadvantages including high cost, difficultly to maintain and manage, generation of secondary pollution, toxic sludge generation, large amounts of chemicals used, severe membrane fouling, high energy consumption (Liu *et al.*, 2022)(Iwuozor *et al.*, 2021). Amongst the mentioned methods, adsorption process is considered to be the most used and effective methods for the removal of dye molecules from wastewater treatments as it is a simple and safe method that is characterised by minimal or no secondary pollution, low-cost, highly reliable and is capable of high removal efficiencies (Yue *et al.*, 2019)(Nethaji, Sivasamy and Mandal, 2013).

Table 2.8: Conventional water treatment techniques for dye removal.

Types of methods	Advantages	Disadvantages	Ref
Chemical methods			
Advanced oxidation processes (AOPs)	Simple method capable of dye removal from various effluents	Rigid and high-cost process. Undesirable by-products generated, pH dependent	(Sivarajasekar, 2015) (Katheresan, Kansedo and Lau, 2018) (Adegoke and Bello, 2015)
Photochemical	Effective for dye removal. Foul odors are generally reduced. No sludge generation	Produces unwanted by-products and has high-cost implications.	(Sivarajasekar, 2015) (Katheresan, Kansedo and Lau, 2018 (Adegoke and Bello, 2015)
Fenton reaction	Fenton reagent is a suitable chemical that is applicable for soluble and insoluble dye removal	High iron sludge generation. Time-consuming process.	(Katheresan, Kansedo and Lau, 2018)(Sivarajasekar, 2015) (Adegoke and Bello, 2015) (Sharma and Kaur, 2018)
Ozonation	No sludge production, effective for dye molecule removal. Ozone is applicable in its gaseous state	Non reusable method, toxic by-products generated, expensive, short half-life [20min]	(Sivarajasekar, 2015) (Katheresan, Kansedo and Lau, 2018) (Adegoke and Bello, 2015) (Sharma and Kaur, 2018)
Biological methods			

Aerobic−anaerobic methods	Economically feasible, no foam build-up, applicable to a wide variety of dye molecules	Low removal efficiency, time-consuming, sludge generation, rigid method, requires a lot of working space, By-products formed are methane and hydrogen sulphide	(Adegoke and Bello, 2015) (Katheresan, Kansedo and Lau, 2018)(Sivarajasekar, 2015)(Manavi *et al*., 2017)
Decolorization by white rot fungi	Dye degradation aided by enzymes	Unreliable enzyme production issues	(Sivarajasekar, 2015) (Adegoke and Bello, 2015) (Katheresan, Kansedo and Lau, 2018)(Saratale *et al*., 2011)(Srinivasan and Viraraghavan, 2010)
Enzyme degradation	Low-cost, high removal efficiency, environmentally friendly, reusable, and capable of using enzymes for dye uptake	Requires large amounts of enzyme for degradation	(Katheresan, Kansedo and Lau, 2018)(Bhatia *et al*., 2017)(Mojsov *et al*., 2016)(Chacko and Subramaniam, 2011)
Adsorption by microbial biomass	Microbial biomass has a strong affinity only towards a selection of dye molecules	Does not apply to all dye molecules	(Sivarajasekar, 2015)(Katheresan, Kansedo and Lau, 2018) (Adegoke and Bello, 2015)
Algae degradation	High removal efficiency for dyes, low-cost, environmentally friendly,	Unstable system	(Katheresan, Kansedo and Lau, 2018)(Bhatia *et al*., 2017)(Solís *et al*., 2012)

Physical methods			
Membrane separation	Effective removal method for a wide range of dye molecules, and water recovery and reuse.	Unsuitable for dye removal due to membrane fouling, concentrated sludge production, and expensive investment costs.	(Madhura *et al*., 2018)(Collivignarelli *et al*., 2018)(Adegoke and Bello, 2015) (Yadav *et al*., 2022)
Ion-exchange	Effective method for dye removal, results in high quality water, and can be easily regenerated.	Limited to certain dye molecules.	(Katheresan, Kansedo and Lau, 2018)(Sivarajasekar, 2015) (Adegoke and Bello, 2015)
Coagulation/flocculation	Simple operation and environmental impact. Suitable only for disperse, sulphur, and vat dye effluents, relatively cheap	pH dependent system, not suitable for a wide range of dyes (acid, azo, basic, and many more). High chemical usage and large volumes of concentrated sludge generated.	(Katheresan, Kansedo and Lau, 2018(Adegoke and Bello, 2015)(Aragaw and Bogale, 2021)(Han *et al*., 2016)
Adsorption	Effective and efficient dye removal method for a wide range of dyes. Simple and adsorbents can be regenerated	High-cost adsorbents	(Sivarajasekar, 2015) (Katheresan, Kansedo and Lau, 2018) (Adegoke and Bello, 2015) (Salleh *et al*., 2011)

2.8 Adsorption process

The removal of dye pollutants from aqueous environments by adsorption processes has been widely explored as it is a low cost, simple and reliable process with high removal efficiency outcomes, and has limited challenges related to the generation of toxic substances such as sludge or any by-products (Fernandes *et al.*, 2020) (Jarusiripot, 2014)(Taha, Samaka and Mohammed, 2013)(Nethaji, Sivasamy and Mandal, 2013)(Veni and Brenda, 2021). The adsorption process is a surface phenomenon which involves the removal of substances (called adsorbates) from a solution by mass transfer processes onto a solid surface (called adsorbents) with a highly porous surface structure via liquid-solid intermolecular forces of interactions (Khulbe and Matsuura, 2018) (Kandisa and Saibaba, 2016). Various adsorbents derived from activated carbon, bio-sorbents, biochar, clays, polymer and resins, nanoparticles and other low-cost materials have been previously studied for the removal of a variety of dye molecules (see Table 2.9) (Iwuozor *et al.*, 2021). The adsorption process strongly depends on different experimental conditions like solution pH, initial dye concentration, adsorbent used, adsorbent dosage, temperature, and reaction time (Ahmad, Ahmed and Ikram, 2015) (Dutta *et al.*, 2021). Physical adsorption (physisorption) and chemical adsorption (chemisorption) are the two primary mechanisms of adsorption, however there are also numerous other forces of interaction such as hydrogen (H-H) bonding, ion exchange, electrostatic interactions, hydrophobic interactions, π–π interactions etc., (Ibrahim, Creedon and Gharbia, 2022)(Ahmad *et al.*, 2015)(Dutta *et al.*, 2021). Physisorption usually occurs in typical solid/liquid or solid/gas interactions whereby adsorption onto the adsorbent surface is caused weak forces of interaction called van der Waal's forces, whereas chemisorption occurs via strong chemical bonds (covalent bonding) between adsorbate molecules and the adsorbent surface (Ibrahim, Creedon and Gharbia, 2022)(Khulbe and Matsuura, 2018)(Sadegh *et al.*, 2017). Additionally, it is simple to reverse physical adsorption, whereas chemical adsorption is generally irreversible in most cases (Shah, 2018). Mechanism of physisorption and chemisorption are shown below (Figure 2.16).

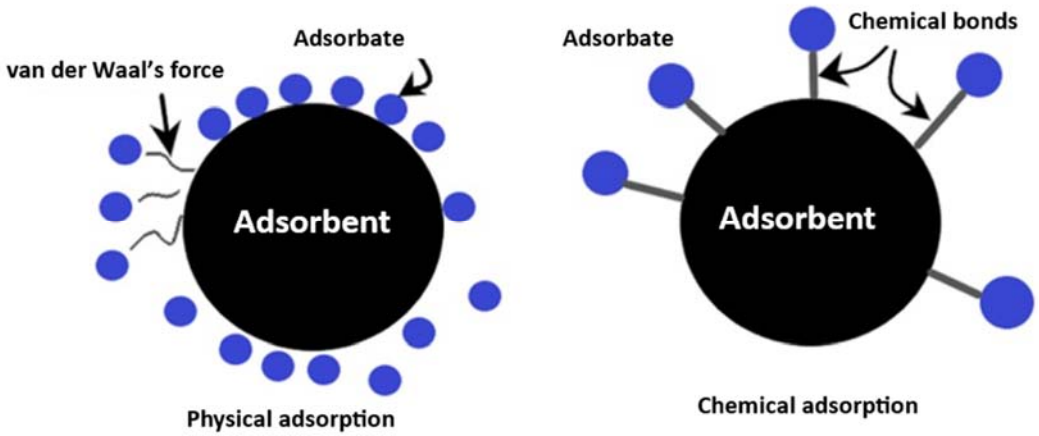

Figure 2.16: Schematic for physical and chemical adsorption mechanism (Image adapted from (Moosavi *et al.*, 2020)).

2.8.1 Adsorbents for dye removal

2.8.1.1 Activated carbon

Activated carbon (AC) is one of the most widely used adsorbents for the removal of dyes. AC adsorbents are carbon-based materials that undergo through physical or chemical processing in an effort to increase the material's potential for sorption (Iwuozor *et al.*, 2021)(Katheresan, Kansedo and Lau, 2018). Materials such as coal, charcoal, carbonised plant matter, peat and lignite are some ACs. AC is highly favored for adsorption processes because the adsorbents usually possess high surface area, high adsorption capacity, improved thermal stability, highly porous structures, surface reactivity, active free valences, and inertness (Iwuozor *et al.*, 2021)(Ahmad *et al.*, 2015)(Kumar and S, 2021). Research into low-cost natural plant materials and biomass as alternatives to commercial activated carbon has been done. Therefore activated carbon has been previously prepared from various materials such as coir pith(Namasivayam and Kavitha, 2002), rice husk(Saeed *et al.*, 2015), *lagerstroemia indica seed* (Kumar, Sivaprakash and Jayakumar, 2017), banana stems (Kumar and S, 2021), pomelo peels (Bello, Ahmad and Semire, 2015), corn husk (Khodaie *et al.*, 2013), Ficus *racemose* plant barks (Sujitha and Ravindhranath, 2016), *Juglans regia* shells (Nethaji, Sivasamy and Mandal, 2013), palm tree fibre (Alhogbi *et al.*, 2021) , *Nigella sativa* L. (Abdel-Ghani *et al.*, 2017), popcorn (Yu *et al.*, 2019), red pumpkin skin (Omari *et al.*, 2022), dragon fruit peels (Jawad *et al.*, 2021), pomegranate peels (Jawad *et al.*, 2018)(Nehaba, 2017)(Manimekalai *et al.*, 2015), papaya leaf (Ahmaruzzaman, 2012), custard apple (*Annona squamosa*) fruit shell (Khan, Shahjahan and Khan, 2018), cashew nut shells (Thang *et al.*, 2021), mangosteen peel (Suwattanamala, Prachuabmorn and Suwattanamala, 2021),cornelian cherry stones (*Cornus mas* L.) (Oguz Erdogan and Erdogan, 2018), and watermelon rinds (Ahmad, Ahmad and Bello, 2015) etc. for application as dye removal adsorbents.

El Maguana *et al*, investigated adsorption of MO from aqueous solutions onto activated carbon extracted from prickly pear seed cake via phosphoric acid activation. From previous studies, it was confirmed by FTIR analysis that oxygen and phosphorus functional groups were incorporated onto the activated carbon surface improving its adsorption capabilities. The adsorption process of MO was best described by the Freundlich isotherm and pseudo-second-order kinetic model, and furthermore, the mechanism for adsorption was determined to be physisorption with maximum adsorption capacity of 336.12 mgg^{-1}. Lastly, the authors concluded that activated carbon from prickly pear seed cake is suitable for dyes removal from aqueous solution (El Maguana *et al.*, 2020). Study for MO adsorption onto activated carbon from coffee grounds waste material has also been reported. Nitric acid was used for carbon activation and improving the surface porosity of the activated carbon adsorbent and

impregnating the surface with new functional groups essential for adsorption. At adsorption conditions, pH of 3, initial dye concentration of 300 mgL^{-1}, contact time of 90min and temperature of 30℃, the maximum adsorption capacity was 658 mgg^{-1}. MO dye was best fit by the Freundlich isotherm characterised with multi-layer adsorption. Adsorption of MO dye was furthermore described as a chemical adsorption mechanism and the nature of adsorption of MO onto activated carbon exothermic due to negative enthalpy value of -43.32 $kJ.mol^{-1}$ (Rattanapan, Srikram and Kongsune, 2017).

In addition, Sawasdee *et al*, reported using agricultural waste from sugarcane leaves to prepare activated carbon for the removal of MO dye in aqueous solutions. It was found that prepared activated carbon material was highly porous and most of the surface was rough due to activation processes. FTIR data further confirmed surface functionalisation with oxygen-containing functional groups that contribute adsorption properties for MO dye removal from aqueous solutions. The adsorption process was best described by the Freundlich isotherm, and pseudo-second-order kinetic models with a maximum adsorption capacity onto activated carbon of 12.50 mgg^{-1} at 30°C. It is worth noting that activated carbon prepared sugarcane leaves was effective for MO dye removal (%RE = 83.54%) at low costs than conventional activated carbon (Sawasdee *et al.*, 2020). A low-cost activated carbon adsorbent material was prepared from *Swietenia mahagoni* bark (industrial waste from wood processing) by Ghosh *et al*, for the adsorptive removal of MO dye from aqueous solution. Irregular, rough, and porous surface were found on the prepared activated carbon (SMBAC) adsorbent with new oxygen-containing functional groups reported. In addition, this also promotes MO dye adsorption onto SMBAC adsorbent. Maximum removal efficiency of MO dye by SMBAC was 92%, at adsorption conditions of pH 3.0, initial MO dye concentration 10.0 mg. L^{-1}, adsorbent dose 10.0 g. L^{-1} and contact time 120 min. The From the reported adsorption data, the Freundlich and Halsey isotherm models best fit the adsorption process showing that the multilayer adsorption on a heterogenous surface. The pseudo-second order kinetic model was favored for MO dye adsorption onto SMBAC and film diffusion as a adsorption mechanism was possible (Ghosh *et al.*, 2020).

Several research has been performed using activated carbon for SY dye removal by adsorption process. Becker *et al*, studied the potential of activated carbon prepared from straw for the adsorption of SY dye. Stalks and leaves of straw material was soaked in acid and alkali before carbonisation, and it was found that material soaked in alkali and carbonised at maximum temperature 700℃, straw material with a loose and porous structure was formed that was efficient for dye adsorption. The adsorption results showed that SY dye removal was significantly affected by changes in temperature and not much by pH (Becker *et al.*, 2022). The quinoa (*Chenopodium quinoa* Wild and *Quillaja Saponaria*) plant was used in a comparative study with commercial charcoal to remove SY dye, crystal violet and tartrazine. Porous surface structures with surface area of about 800 m^2g^{-1} for activated carbon was reported, however,

commercial charcoal showed the best adsorption efficiency during batch adsorption experiments for SY removal (Abril *et al.*, 2022). Oil palm trunk was utilised to prepare activated carbon to remove anionic dyes (SY and acid blue 25) from an aqueous solution. The equilibrium adsorption capacities of SY increased from 49.82 mgg^{-1} to 142.41 mgg^{-1} throughout an increase in initial dye concentration from 100 to 300 mgL^{-1}. For SY dye, the fitted isotherm followed non-linear Langmuir and kinetics was best fit by non-linear pseudo-second order model suggesting the adsorption mode of chemisorption in which adsorbate-adsorbent interaction is via electrostatic force of attraction (Lim *et al.*, 2022). In addition, Chukwuemeka-Okorie *et al*, studied anionic dyes (SY and tartrazine) adsorption onto activated carbon derived from cassava sievate biomass. Activated carbon characterisation showed that the adsorbent had a fine and highly porous structural surface with rough and irregular shapes. FTIR data also revealed new surface functional groups and with that said adsorbent material showed ideal properties for adsorbents with high adsorption capacity for removal of dyes. The experimental findings showed that low-cost and environmentally friendly cassava sievate biomass was suitable for the preparation of activated carbon and can be utilised for tartrazine and SY dyes removal from water (see Table 2.9 for adsorption results) (Chukwuemeka-Okorie *et al.*, 2021).

The drawbacks of using activated carbon material include high energy consumption during activation processes, loss of adsorbents during the deactivation, issues related to adsorbent regeneration, high costs and not environmentally friendly (Shah, 2018) (Sharma and Kaur, 2018)(Singla, Kaushal and Mahajan, 2016). However, from the reviewed studies, it is evident that low-cost agricultural biomass offers an advantage of widespread availability and biodegradability. This suggests that more work must be conducted resolve the issues involved in activated carbon production.

2.8.1.2 Low-cost adsorbents

Inclined growth in human population and the fast-growing industries, generation of industrial and agricultural waste residue is on the rise as these materials are usually burnt unused or pile up in landfills and this can result in both economic and environmental problems such as high transportation cost, lack of dumping site, and accumulation of high organic content material (Kadhom *et al.*, 2020)(Sulyman, Namiesnik and Gierak, 2017)(Bharathi and Ramesh, 2013). In recent decades, these biomass waste (industrial and agricultural waste) have been ultimately recognized as suitable material for dye removal in various waters. Advantageous of adsorbents prepared from biomass waste for dye removal include wide availability, low-cost, easy-handling, high efficiency, renewability, low energy consumption, simple maintenance, and high adsorption capacity hence resolving issues of waste disposal (Farhadi, Ameri and Tamjidi, 2021)(Bello *et al.*, 2015)(Adegoke and Bello, 2015)(Shelke, Jopale and Kategaonkar, 2022). Several agricultural wastes such a kenaf, flax, and ramie fibre (Kyzas, Christodoulou and Bikiaris, 2018), pineapple peel (Chaiyaraksa *et al.*, 2019), wheat bran (Ata *et al.*,

2012), raw oyster shell (Veni and Brenda, 2021), banana trunk fibres (Prasanna. *et al.*, 2014), yam leaf fibres (Vinoth *et al.*, 2010), camel thorn plant (MOGADDASI *et al.*, 2010), psyllium seed powder (Malakootian and Heidari, 2018), almond shell, olive stone and rye straw (Dardouri and Sghaier, 2017), sphagnum peat moss (Hemmati *et al.*, 2016), lady finger stem (Abbas *et al.*, 2012), sugarcane bagasse (Mohamed *et al.*, 2022)(Moharm *et al.*, 2022)(Mohamed *et al.*, 2017) dragon fruit (*Hylocereus polyrhizus*) peels (Jawad, Kadhum and Ngoh, 2018), , sunflower seeds (*Helianthus annuus* L.) (Jóźwiak *et al.*, 2020), jackfruit leaf powder (Chowdhury *et al.*, 2022), watermelon (*Citrullus Lanatus*) peels (Latif *et al.*, 2019) etc have been utilised for various dye molecule removal from different sources.

Subbaiah *et al*, investigated the use of pumpkin seed powder as an adsorbent for MO dye removal. The powder material was modified using ethanolamine and HCl to form aminated pumpkin seed powder (APSP). The batch experiments were used to study the effect of pH (3-11), initial dye concentration (100 to 1000 mgL^{-1}) contact time, and temperature (298, 308 and 313 K). The resultant material was characterised by SEM and FTIR techniques and it was reported that in SEM analysis, adsorbent material had irregular and porous surface which is suitable for adsorption of dye. The FTIR data also showed on the surface of the APSP adsorbent, amine and carboxyl functional groups were present. It was found that an increase in temperature influenced an increase on the removal rate of MO dye improving the adsorption efficiency of APSP. At equilibrium, the maximum adsorption capacity was determined to be 200.3 mgg^{-1} and the adsorption process followed the Langmuir isotherm model. Kinetic data showed the data was best fit with the pseudo-second-order kinetic model and desorption studies were successfully performed using 0.1 M NaOH with an efficiency of 93.5% (Subbaiah and Kim, 2016). Agriculture wastes such as date palm fibres (DPF), sawdust (SD), rice husk (RH) were studied without pretreatment for the removal of MO dye from industrial wastewater. The effect of various experiment conditions such as pH (2-10), initial dye concentration (100-500 mgL^{-1}), adsorbent dose [(0.1-1) g per 100 ml] and contact time (10-150 min) were evaluated and it was reported that as adsorbent dose (0.1-0.6 g) increased, the percentage of dye removal increased for all three adsorbents studied. The maximum adsorption capacities at equilibrium were found to be 61 mgg^{-1}, 53 mgg^{-1}, and 47 mgg^{-1} for DPF, SD, and RH, respectively. The adsorption data showed that all adsorbents adhered to the Langmuir isotherm model (Dakhil, 2020).

Mohamed and coworkers reported using polyethylenimine (PEI) modified sugarcane bagasse adsorbent for the adsorption of MO dye from aqueous solution. From the experimental parameters investigated and optimal adsorption results were achieved at contact time of 240 min, initial dye concentration of 0.01 gL^{-1}, adsorbent dosage of 0.15 g per 50 mL, temperature of 30°C and pH (7) with MO dye removal up to 82%. The study showed that PEI modified sugarcane has high potential as low-cost adsorbent for MO dye removal from wastewater (Mohamed *et al.*, 2017). Natural jackfruit leaves powder (JLP) has been investigated as an adsorbent for removal of MO dye by Dutta and colleagues. To evaluate the

effects of pH solution (2 - 8), adsorbent dose (0.03 - 0.5 g), initial MO concentration (10 - 30 mgL^{-1}), contact time (10 - 120 min), stirring speed (100 - 500 rpm), and temperature (300, 313, and 323 K), batch experiments were conducted. Prepared adsorbents were characterised using SEM, FTIR, XRD, and TGA techniques. SEM analysis showed adsorbent surfaces that were characterised by rough, irregular, and porous texture. FTIR, XRD, and TGA supported the suggested surface morphology of JLP adsorbent that has favorable properties suitable for MO dye removal. The adsorption data showed that the Langmuir model was well favored by exothermic monolayer adsorption and kinetics was best fit by the pseudo-second order kinetics and mixed diffusion process (bulk and intra-particle diffusion). The maximum sorption capacity of methyl orange on JLP adsorbent was found to be 32.89 mgg^{-1}. The analysis of thermodynamic variables showed that the adsorption was exothermic, physisorption, and spontaneous in nature (Dutta *et al.*, 2022).

Okodugha *et al*, investigated the behavior of low-cost agricultural biomass rice rusk treated with HCl and NH_4OH for the removal of MO dye from water. Batch studies were carried out to analyze and optimize the impact of different parameters on dye removal, including contact time, pH, initial dye concentrations, and adsorbent dosage. As initial concentration and contact time increased in HCl-treated husk, adsorption capacity increased; however, at higher pH and sorbent doses, adsorption capacity decreased. With an increase in the previously specified parameters, adsorption capacity decreased when NH_4OH-treated rice husk adsorbent was used. When compared to rice husk treated with NH_4OH, HCl treated rice husk adsorbent was found to show better removal efficiency for MO from aqueous solution and was best fit by the Freundlich isotherm model (Okodugha *et al.*, 2021). Shah and coworkers conducted batch experiments on the adsorption of MO onto populous tree adsorbents. Prepared adsorbents were characterised by SEM, BET, FTIR, and XRD techniques. Experimental parameters such as adsorbent dosage (0.2–0.6 g), pH solution 3–12, initial dye concentration (5–100 mgL^{-1}) and contact time (10–100 min) were evaluated for adsorption process. Langmuir and Freundlich isotherm models were used to fit the sorption data, and both were best fitted with the maximum Langmuir monolayer adsorptive capacity recorded as 90.44 mgg^{-1} at optimal adsorption conditions (pH 3, temperature 303.15 K). All prepared adsorbents were found to follow the pseudo-first order kinetic model. The adsorption process was exothermic according to the calculated thermodynamic parameters, and the spontaneous nature of the adsorption process was observed even at low temperatures (Shah *et al.*, 2021).

Song and coworkers performed comparative studies on the adsorption of SY dye onto modified methanol walnut shell (MMWS) adsorbent material. Batch experiments were performed using the following parameters pH, temperature, and initial concentration. The maximum capacity of SY onto MMWS at 298 K showed better adsorption than raw walnut shell, and the equilibrium data was best described by the Langmuir isotherm. Furthermore, it was shown that intra-particle diffusion was one of the rate-controlling phases in the adsorption process and that the adsorption kinetics suited the

pseudosecond-order model well. With that, the authors concluded that MMWS adsorbent is a promising adsorbent for wastewater dye removal (Yinghua *et al.*, 2021). Additionally, another study was carried out for the removal of SY dye from peanut husk waste as a low-cost adsorbent by Song *et al*. Batch mode experiments were carried out as a function of adsorption time, adsorbent dosage and initial SY concentration as well as temperature on SY adsorption. The maximum adsorption capacity was determined to be 25.89 mgg^{-1} under the optimal conditions of adsorbent dosage (2 gL^{-1}), initial concentration (95 mgL^{-1}), and solution pH 2 over a 24 h period at the temperature of 293K. The equilibrium data showed that the Langmuir isotherm and pseudo-second order kinetic models were favored for the adsorption process and the thermodynamic data suggested that a spontaneous exothermic physical adsorption process was favored (Song *et al.*, 2014).

Song *et al*, investigated removal SY dye from aqueous solution whereby peanut husk was crosslinked with epichlorohydrin and then modified with ethylenediamine for the adsorbent. The solution pH, contact time, temperature, and initial dye concentration were evaluated in batch experiments. It was determined that the ethylenediamine-modified peanut husk (EMPH) adsorbent had a maximum adsorption capacity for SY of 117.7 mgg^{-1} at 313 K and the Langmuir isotherm model best fitted the adsorption data more accurately. According to the calculated thermodynamic data, the process was a spontaneous endothermic adsorption process of SY dye onto peanut husk. The adsorption process was governed by intra-particle diffusion as the rate limiting step. Authors thereby concluded that ethylenediamine-modified peanut husk showed good performance for removing SY dye and may be employed as a very effective biomass adsorbent to treat dye containing wastewater (Song, Xu and Ren, 2015).

Table 2.9: Various materials used as adsorbents for removal of dyes via adsorption processes.

Adsorbent	**Dye**	**Adsorption capacity/ Removal efficiency**	**Adsorption isotherms, kinetics, and mechanism**	**Ref**
Modified walnut shell	Sunset yellow	18.35 mgg^{-1}	Langmuir, pseudo-second order, intraparticle diffusion	(Yinghua *et al*., 2021)
Dragon Fruit (*Hylocereusundatus*) Foliage	Methyl orange	21.05 mgg^{-1}	Freundlich, pseudo-second order, chemisorption and physisorption mechanism	(Haddadian *et al*., 2013)
Raw oyster shell	Coomassie brilliant blue	99.64%	Not applicable	(Veni and Brenda, 2021)
Chitosan	Sunset yellow Tartrazine Brilliant blue	1432.98 mgg^{-1} 1065.55 mgg^{-1} 814.27 mgg^{-1}	All dyes: physisorption mechanism	(Zhang *et al.*, 2020b)
Kaolinite Clay	Methyl orange	3.476 mgg^{-1}	Langmuir, pseudo second-order, chemisorption	(Aroke *et al*., 2020)
Pinecone powder	Congo red	Raw - 32.65 mgg^{-1} Acid-treated - 40.19 mgg^{-1}	Freundlich, pseudo-second order, intra particle diffusion	(Dawood and Sen, 2012)
Polyaniline and Fe_3O_4-hydrotalcite (Pan/MHT)	Methyl orange	156.25 mgg^{-1}	Freundlich, pseudo-second order, physical adsorption mechanism	(An Tran *et al.*, 2021)

Modified pineapple peel	Basic Red 9	82.03%	Temkin, pseudo-second order, Physical adsorption	(Chaiyaraksa *et al*., 2019)
	Direct Red	46.15%	Freundlich, pseudo-second order, Physical adsorption	(Chaiyaraksa *et al*., 2019)
Activated carbon derived from *Ficus racemose* barks	Coomassie brilliant blue	65.0 mgg^{-1}	Freundlich, pseudo-second order, heterogenous and multilayer adsorption process	(Sujitha and Ravindhranath, 2016)
Activated carbon from Camel thorn plant	Methyl Orange	Up to 80%	Langmuir, pseudo-second order, electrostatic interactions	(Mogaddasi *et al.*, 2010)
Cationized rice husk	Diamine Green	207.15 mgg^{-1}	Langmuir, pseudo-second-order, electrostatic attraction, hydrogen bonding, and van der Waals	(Jiang and Hu, 2019)
	Acid Black 24	268.88 mgg^{-1}	Langmuir, pseudo-second order, electrostatic attraction, hydrogen bonding, and van der Waals	(Jiang and Hu, 2019)
	Congo Red	580.09 mgg^{-1}	Langmuir, pseudo-second order, electrostatic attraction, hydrogen bonding, and van der Waals	(Jiang and Hu, 2019)
Banana peels	Methyl orange	17.2 mgg^{-1}	Freundlich, intraparticle diffusion	(Annadurai *et al*., 2002)
Orange peels	Methyl orange	15.8 mgg^{-1}	Langmuir, intraparticle diffusion	(Annadurai *et al*., 2002)
Activated carbon from coconut Shells	Sunset yellow (SY)	SY 18.12 mgg^{-1}	Both dyes: Freundlich, pseudo-first order	(Ademoriyo and Enyoh, 2020)

	Tartrazine	Tartrazine 20.67 mgg^{-1}		
Activated carbon from groundnut Shells	Sunset yellow (SY) Tartrazine	SY 19.02 mgg^{-1} Tartrazine 21.72 mgg^{-1}	Both dyes: Freundlich, pseudo-first order	(Ademoriyo and Enyoh, 2020)
Activated carbon from *Ficus racemosa* plant	Coomassie brilliant blue	65.0 mgg^{-1}	Freundlich, pseudo-second-order, chemisorption mechanism	(Sujitha and Ravindhranath, 2016)
Activated carbon from *Juglans regia* shell biomass	Malachite green (MG) Amido black 10B (AB)	MG – 2.53 mgg^{-1} AB – 2.55 mgg^{-1}	Freundlich, pseudo-second order, intraparticle diffusion and film diffusion played important roles for both dyes	(Nethaji *et al*., 2013)
Lala clam (*Orbicularia orbiculata*) shell	Methylene blue (MB) Methyl orange (MO)	MB – 9.615 mgg^{-1} MO – 0.212 mgg^{-1}	Freundlich isotherm, adsorption at multilayer heterogeneous surface	(Eljiedi and Kamari, 2017)
Modified coffee waste	Reactive Black 5 (RB5) Congo Red (CR)	RB5 - 77.52 mgg^{-1} CR - 34.36 mgg^{-1}	Langmuir, pseudo-second-order, chemisorption mechanism	(Wong *et al*., 2020)
Activated carbon from Corn cob	Methyl Orange	80.36%	Not applicable	(Abdullah *et al*., 2019)
Cellulose nanocrystals	Methylene blue	118 mgg^{-1}	Langmuir isotherm model, monolayer adsorption on a homogenous surface	(Batmaz *et al*., 2014)
Activated carbon from palm tree fiber waste	Congo red (CR) Rhodamine B (RhB)	CR - 10.4 mgg^{-1} RhB - 26.5 mgg^{-1}	Langmuir, pseudo-second-order, chemisorption mechanism	(Alhogbi *et al*., 2021)

Cellulose	Reactive red RB dye	8.94 mgg^{-1}	Langmuir, Elovich, Chemisorption mechanism	(Silva *et al*., 2015)
Cationic amphiphilic dextran hydrogel	Methyl Orange	705 mg g^{-1}	Langmuir, pseudo-second-order, chemical adsorption	(Stanciu and Nichifor, 2019)
Modified Coconut (*Cocos nucifera*) Mesocarp	Congo red (CR) Tartrazine	CR – 19.99 mgg^{-1} Tartrazine – 19.61 mgg^{-1}	CR - Dubinin–Radushkevic, fits all studied kinetic models Tartrazine - Freundlich, pseudo-second order, more than one mechanism responsible for adsorption processes	(Tejada-Tovar *et al*., 2021)
Mixed Fruit Peel Waste (MFPW)	Sunset yellow FCF	200 mgg^{-1}	Langmuir isotherm, pseudo-second order-kinetics, physisorption process	(Nafisa Begam *et al*., 2022)
Activated carbon derived from cassava sievate biomass	Sunset yellow (SY) FCF Tartrazine	SY FCF -0.091 mgg^{-1} Tartrazine - 20.83 mgg^{-1}	Freundlich, pseudo-second order for all dyes. Chemisorption mechanism	(Chukwuemeka-Okorie *et al*., 2021)
Wheat bran	Coomassie brilliant blue	6.41 mgg^{-1}	Freundlich, pseudo-second-order, monolayer sorption	(Ata *et al*., 2012)
Acid-Functionalized Bentonite	Methyl Orange Dye	RF1 – 67.4 mgg^{-1}, and RF2 47.8 mgg^{-1}	Sips equation, electrostatic attraction	(Fernandes *et al*., 2020)

Activated carbon entrapped in alginate	Sunset yellow	86%	Langmuir, monolayer adsorption on a homogenous surface	(Abdel-aziz and Abdel-gawad, 2020)

2.9 References

EFSA Panel on Food Additives and Nutrient Sources added to Food (ANS). Scientific Opinion on the re-evaluation of Sunset Yellow FCF (E 110) as a food additive on request from the European Commission., *European Food Safety Authority (EFSA) Journal*, 2009, 7(11), p. 1330. doi: 10.2903/j.efsa.2009.1330.

EFSA Panel on Food Additives and Nutrient Sources added to Food (ANS). Reconsideration of the temporary ADI and refined exposure assessment for Sunset Yellow FCF (E 110), *EFSA Journal*, 2014, 12(7), pp. 1–39. doi: 10.2903/j.efsa.2014.3765.

Abbas, A., Rehman, R., Murtaza, S., Shafique, U., Zahid, A., and Ayub, R. (2012) 'Adsorptive Removal of Congo Red and Sunset Yellow Dyes from Water Systems by Lady Finger Stem', *Journal of the Chemical Society of Pakistan*, 34(5), pp. 1241–1247.

Abdel-aziz, H. M,. and Abdel-gawad, S. A. (2020) 'Removal of sunset yellow azo dye using activated carbon entrapped in alginate from aqueous solutions', *Journal of science*, 4(1), pp. 1–6. doi: 10.15406/oajs.2020.04.00142.

Abdel-Ghani, N. T., El-Chaghaby, G. A., Rawash, E. A., and Lima, E. C. (2020). 'Adsorption of Coomassie Brilliant Blue R-250 dye onto novel activated carbon prepared from Nigella sativa L. waste: Equilibrium, kinetics and thermodynamics', *Journal of the Chilean Chemical Society*, 62(2), pp. 3505–3511. doi: 10.4067/S0717-97072017000200016.

Abdullah, N. H., Ghani, N. A. A., Razab, M. K. A. A.,Noor, A. M., Halim, A. Z. A., Rasat, M. S. M., Wong, K. N. S. W. S., and Amin, M. F. M. (2019) 'Methyl orange adsorption from aqueous solution by corn cob based activated carbon', in *AIP Conference Proceedings*. doi: 10.1063/1.5089335.

Abiaziem, C. V., Williams, A. B., Inegbenebor, A. I., Onwordi, C. T., EhiEromosele, C. O., and Petrik, L. F. (2019) 'Preparation and Characterisation of Cellulose Nanocrystal from Sugarcane Peels by XRD , SEM and CP/MAS 13 C NMR', in *Journal of Physics*, pp. 1–9. doi: 10.1088/17426596/1299/1/012123.

Abouzeid, R. E., Salama, A., Al-Ahmed, Z. A., Awwad, N. S., and Youssef, M A. (2020) 'Carboxylated cellulose nanofibers as a novel efficient adsorbent for water purification', *Cellulose Chemistry and Technology*, 54(3–4), pp. 237–245. doi: 10.35812/cellulosechemtechnol.2020.54.25.

Abouzeid, R. E., Khiari, R., El-Wakil, N., and Dufresne, A.L. (2019) 'Current State and New Trends in the Use of Cellulose Nanomaterials for Wastewater Treatment', *Biomacromolecules*, 20(2), pp. 573–597. doi: 10.1021/acs.biomac.8b00839.

Abraham, R. E., Wong, C. S. and Puri, M. (2016) 'Enrichment of cellulosic waste hemp (Cannabis sativa) hurd into non-toxic microfibres', *Materials*, 9(7), pp. 1–13. doi: 10.3390/MA9070562.

Abral, H., Lawrensius, V., Handayani, D., Sugiarti, E. (2018) 'Preparation of nano-sized particles from bacterial cellulose using ultrasonication and their characterization', *Carbohydrate Polymers*, 191, pp. 161–167. doi: 10.1016/j.carbpol.2018.03.026.

Abril, D., Ferrer, V., Mirabal-Gallardo, Y., Cabrera-Barjas, G., Segura, C., Marican, A., Pereira, A., Durán-Lara, E.F., and Valdés, O. (2022) 'Comparative Study of Three Dyes ' Adsorption onto Activated Carbon from Chenopodium quinoa Willd and Quillaja saponaria', *Materials*, 15, pp. 1–23.

Abu-thabit, N. Y., Abu, A., Hakeem, A. S., Ul-hamid, A., Umar, Y., and Ahmad, A. (2020) 'Isolation and characterization of microcrystalline cellulose from date seeds (Phoenix dactylifera L .)', *International Journal of Biological Macromolecules*, 155, pp. 730–739. doi: 10.1016/j.ijbiomac.2020.03.255.

Adegoke, K. A. and Bello, O. S. (2015) 'Dye sequestration using agricultural wastes as adsorbents', *Water Resources and Industry*, 12, pp. 8–24. doi: 10.1016/j.wri.2015.09.002.

Ademoriyo, C. and Enyoh, C. (2020) 'Batch Adsorption Studies of Sunset Yellow and Tartrazine Using Coconut and Groundnut Shells', *Journal of Biomedical Research and Environmental Sciences*, 1(5), pp.
163–172. doi: 10.37871/jbres1138.

Ahmad, A., Mohd-Setapar, S. H., Chuong, C. S., Khatoon, A., Wani, W. A., Kumar, R., and Rafatullah, M. (2015) 'Recent advances in new generation dye removal technologies: Novel search for approaches to reprocess wastewater', *RSC Advances*, 5(39), pp. 30801–30818. doi: 10.1039/c4ra16959j.

Ahmad, M., Ahmed, S., Swani, B. L., and Ikram, S. (2015) 'Adsorption of heavy metal ions: Role of chitosan and cellulose for water treatment', *International Journal of Pharmacognosy*, 2(6), pp. 280–289. doi: 10.13040/IJPSR.0975-8232.IJP.2(6).280-89.

Ahmad, M. A., Ahmad, N. and Bello, O. S. (2015) 'Removal of Remazol Brilliant Blue Reactive Dye from Aqueous Solutions Using Watermelon Rinds as Adsorbent', *Journal of Dispersion Science and Technology*, 36(6), pp. 845–858. doi: 10.1080/01932691.2014.925400.

Ahmaruzzaman, M. (2012) 'Removal of Methyl Orange from Aqueous Solution Using Activated Papaya Leaf', *Separation Science and Technology*, 47(16), pp. 2381–2390. doi: 10.1080/01496395.2012.671432.

Ait Benhamou, A., Kassab, Z., Boussetta, A., Salim, M. H., Ablouh, E., Nadifiyine, M., Qaiss, A. E., Moubarik, A., and El-Achaby, M. (2022) 'Beneficiation of cactus fruit waste seeds for the production of cellulose nanostructures: Extraction and properties', *International Journal of Biological Macromolecules*, 203, pp. 302–311. doi: 10.1016/j.ijbiomac.2022.01.163.

Akhabue, C. E. and Osubor, N. T. (2017) 'Optimization of extraction of microcrystalline cellulose from orange peel waste using response surface methodology', *Ife Journal of Science*, 19(2), pp. 227–235. doi: 10.4314/ijs.v19i2.3.

Alemdar, A. and Sain, M. (2008) 'Isolation and characterization of nanofibers from agricultural residues - Wheat straw and soy hulls', *Bioresource Technology*, 99(6), pp. 1664–1671. doi: 10.1016/j.biortech.2007.04.029.

Alghamdi, A. A., Al-Odayni, A. B., Saeed, W. S., Almutairi, M. S., Alharthi, F. A., Aouak, T., and Al-Kahtani, A. (2019) 'Adsorption of azo dye methyl orange from aqueous solutions using alkali-activated polypyrrole-based graphene oxide', *Molecules*, 24(20). doi: 10.3390/molecules24203685.

Alhogbi, B. G., Altayeb, S., Bahaidarah, E. A., and Zawrah, M. F. (2021) 'Removal of anionic and cationic dyes from wastewater using activated carbon from palm tree fiber waste', *Processes*, 9(3), pp. 1–21. doi: 10.3390/pr9030416.

Almashhadani, A. Q., Peng, C., Chan, S., Yew, C., and Goh, F. (2022) 'Nanocrystalline cellulose isolation via acid hydrolysis from non-woody biomass : Importance of hydrolysis parameters', *Carbohydrate Polymers*, 286, p. 119285. doi: 10.1016/j.carbpol.2022.119285.

Amenaghawon, A. N., Balogun, A., Agbonghae, E. E., Ogbeide, S. E., Okieimen, C. O., and Agbonghae, E. O. (2013) 'Modelling and Statistical Optimisation of Dilute Acid of Corn Stover using Response Surface Methodology', *Journal of Environment*, 02(02), pp. 34–40.

de Andrade, M. R., Nery, T. B. R., de Santana e Santana, T. I., Leal, I. L., Rodrigues, L. A. P., de Oliveira Reis, J. H., Druzian, J. I., and Machado, B. A. S.. (2019) 'Effect of Cellulose Nanocrystals from Different Lignocellulosic Residues to Chitosan / Glycerol Films', *Polymers*, 11(658), pp. 1–16.

Annadurai, G., Juang, R. S. and Lee, D. J. (2002) 'Use of cellulose-based wastes for adsorption of dyes from aqueous solutions', *Journal of Hazardous Materials*, 92(3), pp. 263–274. doi: 10.1016/S03043894(02)00017-1.

Aragaw, T. A. and Bogale, F. M. (2021) 'Biomass-Based Adsorbents for Removal of Dyes From Wastewater: A Review', *Frontiers in Environmental Science*, 9.pp 1-24. doi: 10.3389/fenvs.2021.764958.

Aroke, U. O., Momoh, R. O., Hamidu, L. A. J. and Buhari, U. (2020) 'Removal of Azo Dye Methyl Orange in Aqueous Solution by Kaolinite Clay : Equilibrium Kinetics and Error Analyses', *Saudi Journal of Engineering and Technology*, 5(11), pp. 422–433. doi: 10.36348/sjet.2020.v05i11.005.

Arslan, Y. and Araçoğlu, N. E. (2015) 'Response Surface Optimization Studies of the Acid- Catalysed Hydrolysis of Hazelnut Shells', *Gazi University Journal of Science*, 3(3), pp. 51–61.

Asghar, A., Raman, A. A. A. and Daud, W. M. A. W. (2014) 'A Comparison of Central Composite Design and Taguchi Method for Optimizing Fenton Process', *Scientific World Journal*, 2014. doi: 10.1155/2014/869120.

Ata, S., Imran Din, M., Rasool, A., Qasim, I., and Ul Mohsin, I. (2012) 'Equilibrium, thermodynamics, and kinetic sorption studies for the removal of coomassie brilliant blue on wheat bran as a low-cost adsorbent', *Journal of Analytical Methods in Chemistry*, 1(1), pp. 1–9. doi: 10.1155/2012/405980.

Ishak, N. A. M., Khalil, I., Abdullah, F. Z., Julkapli, N.M (2020) 'A correlation on ultrasonication with nanocrystalline cellulose characteristics', *Carbohydrate Polymers*, 246, p. 116553. doi: 10.1016/j.carbpol.2020.116553.

Bahloul, A., Kassab, Z., Aziz, F., Hannache, H., Bouhfid, R., Qaiss, A. E., Oumam, M., and El Achaby, M. (2021) 'Characteristics of cellulose microfibers and nanocrystals isolated from doum tree (Chamaerops humilis var. argentea)', *Cellulose*, 28(7), pp. 4089–4103. doi: 10.1007/s10570-02103793-y.

Bahloul, A., Kassab, Z., El Bouchti, M., Hannache, H., Qaiss, A.E., Oumam, M., and El Achaby, M. (2021) 'Micro- and nano-structures of cellulose from eggplant plant (Solanum melongena L) agricultural residue', *Carbohydrate Polymers*, 253, p. 117311. doi: 10.1016/j.carbpol.2020.117311.

Barbosa, A. D., da Silva, L. F., de Paula, H. M., Romualdo, L. L., Sadoyama, G., and Andrade, L. S.

(2018) ‘Combined use of coagulation (M. oleifera) and electrochemical techniques in the treatment of industrial paint wastewater for reuse and/or disposal’, *Water Research*, 145, pp. 153–161. doi: 10.1016/j.watres.2018.08.022.

Baruah, J., Chandra, R. and Kalita, E. (2020) ‘International Journal of Biological Macromolecules Greener production of microcrystalline cellulose (MCC) from Saccharum spontaneum (Kans grass): Statistical optimization’, *International Journal of Biological Macromolecules*, 154, pp. 672–682. doi: 10.1016/j.ijbiomac.2020.03.158.

Bashir, A., Malik, L. A., Ahad, S., Manzoor, T., Bhat, M. A., Dar, G. N., and Pandith, A. H. (2019) ‘Removal of heavy metal ions from aqueous system by ion-exchange and biosorption methods’, *Environmental Chemistry Letters*, 17(2), pp. 729–754. doi: 10.1007/s10311-018-00828-y.

Bashiri, M. and Farshbaf Geranmayeh, A. (2011) ‘Tuning the parameters of an artificial neural network using central composite design and genetic algorithm’, *Scientia Iranica*, 18(6), pp. 1600–1608. doi: 10.1016/j.scient.2011.08.031.

Batmaz, R., Mohammed, N., Zaman, M., Minhas, G., Berry, R. M., and Tam, K. C. (2014) ‘Cellulose nanocrystals as promising adsorbents for the removal of cationic dyes’, *Cellulose*, 21(3), pp. 1655–1665. doi: 10.1007/s10570-014-0168-8.

Beaumont, M., Winklehner, S., Veigel, S., Mundigler, N., Gindl-Altmutter, W., Potthast, A., and Rosenau, T. (2020) ‘Wet esterification of never-dried cellulose: a simple process to surface-acetylated cellulose nanofibers’, *Green Chemistry*, 22(17), pp. 5605–5609. doi: 10.1039/d0gc02116d.

Beaumont, M., Otoni, C. G., Mattos, B. D., Koso, T. V., Abidnejad, R., Zhao, B., Kondor, A., King, A. W. T., and Rojas, O. J. (2021) ‘Regioselective and water-assisted surface esterification of never-dried cellulose: nanofibers with adjustable surface energy’, *Green Chemistry*, 23(18), pp. 6966–6974. doi: 10.1039/d1gc02292j.

Bello, O. S., Adegoke, K. A., Olaniyan, A. A., and Abdulazeez, H. (2015) ‘Dye adsorption using biomass wastes and natural adsorbents: overview and future prospects’, *Desalination and Water Treatment*, 53(5), pp. 1292–1315. doi: 10.1080/19443994.2013.862028.

Bello, O. S., Ahmad, M. A. and Semire, B (2015) ‘Scavenging malachite green dye from aqueous solutions using pomelo (Citrus grandis) peels: kinetic, equilibrium and thermodynamic studies’, *Desalination and Water Treatment*, 56(2), pp. 521–535. doi: 10.1080/19443994.2014.940387.

Benkhaya, S., M'rabet, S., and El Harf. A. (2020) ‘Classifications , properties, recent synthesis and applications of azo dyes’, *Heliyon*, 6, pp. 1–26. doi: 10.1016/j.heliyon.2020.e03271.

Bharathi, K. S. and Ramesh, S. T. (2013) ‘Removal of dyes using agricultural waste as low-cost adsorbents: a review’, *Applied Water Science*, 3(4), pp. 773–790. doi: 10.1007/s13201-013-0117-y.

Bhatia, D., Sharma, N. R., Singh, J., and Kanwar, R. S. (2017) ‘Biological methods for textile dye removal from wastewater: A review’, *Critical Reviews in Environmental Science and Technology*, 47(19), pp. 1836–1876. doi: 10.1080/10643389.2017.1393263.

Bian, H., Luo, J., Wang, R., Zhou, X., Ni, S., Shi, R., Fang, G., and Dai, H. (2019) ‘Recyclable and Reusable Maleic Acid for Efficient Production of Cellulose Nanofibrils with Stable Performance’, *ACS Sustainable Chemistry and Engineering*, 7, pp. 20022–20031. doi: 10.1021/acssuschemeng.9b05766.

Bian, J., Peng, F., Peng, X. P., Xiao, X., Peng, P., Xu, F., and Sun, R. C. (2014) ‘Effect of [Emim]Ac pretreatment on the structure and enzymatic hydrolysis of sugarcane bagasse cellulose’, *Carbohydrate Polymers*, 100, pp. 211–217. doi: 10.1016/j.carbpol.2013.02.059.

bin Jumhuri, A. A., binti Fatanah, D. N. E., bin Mohamed, A. H., binti Che Hak, C. R., bin Mohamed Sapari, J., and binti Dzulkifli, N. N. (2017) ‘Characterization of cellulose nanocrystal isolated from oil palm empty fruit bunch using formic acid hydrolysis’, *International Journal of Agriculture*, 5, pp. 52–59. Available at: http://ijafp.com/wp-content/uploads/2017/10/AG-36.pdf.

Bracone, M. E., Luduena, L. N. and Alvarez, V. A. (2022) ‘Comparative study between mechanical and chemical treatments for the preparation of nanocellulose’, *Journal of Composite Materials*, 56(6), pp. 877–887. doi: 10.1177/00219983211044199.

Borsoi, C., Dahlem Junior, M. A., Beltrami, L. V. R., Hansen, B., Zattera, A.J., Catto, A.L. (2020) ‘Effects of alkaline treatment and kinetic analysis of agroindustrial residues from grape stalks and yerba mate fibers’, J*ournal of Thermal Analysis and Calorimetry,* 139. pp. 3275–3286. doi: 10.1007/s10973019-08666-y.

Candido, R. G. and Gonçalves, A. R. (2019) ‘Evaluation of two different applications for cellulose isolated from sugarcane bagasse in a biorefinery concept’, *Industrial Crops and Products*, 142. doi: 10.1016/j.indcrop.2019.111616.

Chacko, J. T. and Subramaniam, K. (2011) ‘Enzymatic Degradation of Azo Dyes – A Review’, *International Journal Of Environmetal Sciences*, 1(6), pp. 1250–1260. doi: 10.6088/ijes.00106020018.

Chaiyaraksa, C., Ruenroeng, C., Buaphuan, B., and Choksakul, S. (2019) 'Adsorption of cationic and anionic dye using modified pineapple peel', *Songklanakarin Journal of Science and Technology*, 41(1), pp. 199–206. doi: 10.14456/sjst-psu.2019.24.

Chaker, A. and Boufi, S. (2015) 'Cationic nanofibrillar cellulose with high antibacterial properties', *Carbohydrate Polymers*, 131, pp. 224–232. doi: 10.1016/j.carbpol.2015.06.003.

Chang, C. W., Yen, C. C., Wu, M. T., Hsu, M. C., and Wu, T. Y. (2017) 'Microwave-assisted extraction of cannabinoids in hemp nut using response surface methodology: Optimization and comparative study', *Molecules*, 22(11), pp. 1–15. doi: 10.3390/molecules22111894.

Chekir, N., Tassalit, D., Benhabiles, O., Merzouk, N.K., Ghenna, M., Abdessemed, A., and Issaadi, R. A. (2016) 'A comparative study of tartrazine degradation using UV and solar fixed bed reactors', *International Journal of Hydrogen Energy*, 42(13), pp. 8948–8954. doi: 10.1016/j.ijhydene.2016.11.057.

Chen, H., Liu, Z., Chen, X., Chen, Y., Dong, Z., Wang, X., and Yang, H. (2020) 'Comparative pyrolysis behaviors of stalk , wood and shell biomass : Correlation of cellulose crystallinity and reaction kinetics', *Bioresource Technology*, 310, p. 123498. doi: 10.1016/j.biortech.2020.123498.

Chen, W., Yu, H., Liu, Y., Chen, P., Zhang, M., and Hai, Y. (2011) 'Individualization of cellulose nanofibers from wood using high-intensity ultrasonication combined with chemical pretreatments', *Carbohydrate Polymers*, 83(4), pp. 1804–1811. doi: 10.1016/j.carbpol.2010.10.040.

Chen, W., Yu, H. and Liu, Y. (2011) 'Preparation of millimeter-long cellulose I nanofibers with diameters of 30 – 80 nm from bamboo fibers', *Carbohydrate Polymers*, 86(2), pp. 453–461. doi: 10.1016/j.carbpol.2011.04.061.

Chen, W., Yu, H., and Liu, Y. (2012) 'Controlled enzymolysis preparation of nanocrystalline cellulose from pretreated cotton fibers', *BioResources*, 7(3), pp. 4237–4248.

Chiong, T., Lau, S. Y., Lek, Z. H., Koh, B. Y., and Danquah, M. K. (2016) 'Enzymatic treatment of methyl orange dye in synthetic wastewater by plant-based peroxidase enzymes', *Journal of Environmental Chemical Engineering*, 4(2), pp. 2500–2509. doi: 10.1016/j.jece.2016.04.030.

Chowdhury, S. R., Roy, S. R., Ganguly, A., Ghosh, R., Majumder, S., Dasgupta, A., Das, R., Kumar,

A., Naskar, A., and Majumder, R. (2022) 'Biosorption of Acid dye by Jackfruit Leaf Powder: Isotherm, kinetics and Response surface methodology studies', *Journal of Experimental Biology and Agricultural Sciences*, 10(1), pp. 254–265. doi: 10.18006/2022.10(1).254.265.

Chowdhury, Z. Z., Chandran, R. R. R., Jahan, A., Khalid, K., Rahman, M. M., Al-Amin, M., Akbarzadeh, O., Badruddin, I. A., Khan, T. M.Y., Kamangar, S., Hamizi, N. A. B., Wahab, Y. A., Johan, R. B., and Adebisi, G. A. (2019) 'Extraction of cellulose nano-whiskers using ionic liquidassisted ultra-sonication: Optimization and mathematical modelling using Box-Behnken design', *Symmetry*. doi: 10.3390/sym11091148.

Chukwuemeka-Okorie, H.O., Ekuma, F.K., Akpomie, K.G., Nnaji, J.C., and Okereafor, A.G. (2021) 'Adsorption of tartrazine and sunset yellow anionic dyes onto activated carbon derived from cassava sievate biomass', *Applied Water Science*, 11(2), pp. 1–8. doi: 10.1007/s13201-021-01357-w.

Chung, K. T. (2016) 'Azo dyes and human health: A review', *Journal of Environmental Science and Health - Part C Environmental Carcinogenesis and Ecotoxicology Reviews*, 34(4), pp. 233–261. doi: 10.1080/10590501.2016.1236602.

Collivignarelli, M. C., Abbà, A., Benigna, I., Sorlini, S., and Torretta, V. (2018) 'Overview of the main disinfection processes for wastewater and drinking water treatment plants', *Sustainability (Switzerland)*, 10(1), pp. 1–21. doi: 10.3390/su10010086.

Cui, S., Zhang, S., Ge, S., Xiong, L., and Sun, Q. (2016) 'Green preparation and characterization of size-controlled nanocrystalline cellulose via ultrasonic-assisted enzymatic hydrolysis', *Industrial Crops and Products*, 83, pp. 346–352. doi: 10.1016/j.indcrop.2016.01.019.

Czaikoski, A., da Cunha, R. L. and Menegalli, F. C. (2020) 'Rheological behavior of cellulose nanofibers from cassava peel obtained by combination of chemical and physical processes', *Carbohydrate Polymers*, 248, p. 116744. doi: 10.1016/j.carbpol.2020.116744.

Dakhil, I. H. (2020) 'Recycling of Agriculture Wastes for Efficient Removal of Methyl Orange Dye Using Batch Adsorption Unit', in *3rd International Conference on Sustainable Engineering Techniques*, pp. 1–10. doi: 10.1088/1757-899X/881/1/012186.

Danafar, F. (2020) 'Recent development and challenges in synthesis of cellulosic nanostructures and their application in developing paper-based energy devices', *cellulose chemistry and technology*, 54(3–4), pp. 327–346. doi: 10.35812/cellulosechemtechnol.2020.54.34.

Dardouri, S. and Sghaier, J. (2017) ‘Adsorptive removal of methylene blue from aqueous solution using different agricultural wastes as adsorbents’, *Korean Journal of Chemical Engineering*, 34(4), pp. 1037–1043. doi: 10.1007/s11814-017-0008-2.

Dawood, S. and Sen, T. K. (2012) ‘Removal of anionic dye Congo red from aqueous solution by raw pine and acid-treated pine cone powder as adsorbent: Equilibrium, thermodynamic, kinetics, mechanism and process design’, *Water Research*, 46(6), pp. 1933–1946. doi: 10.1016/j.watres.2012.01.009.

Dean, A., Morris, M., Stufken, J., Bingham, D. (2015) 'Handbooks of Modern Statistical Methods'. *Handbook of Design and Analysis of Experiments*. *Chapman and Hall/CRC*, pp 1-946.

de Carvalho Mendes, C. A., de Oliveira Adnet, F. A., Leite, M. C. A. M., Furtado, C. R. G., and de Sousa, A. M. F (2015) ‘Chemical, physical, mechanical, thermal and morphological characterization of corn husk residue’, *Cellulose Chemistry and Technology*, 49(9–10), pp. 727–735.

Devabaktuni Lavanya, P.K.Kulkarni, Mudit Dixit, Prudhvi Kanth Raavi, L. N. V. K. (2011) ‘Sources of cellulose and their applications- A review’, *International Journal of Drug Formulation and Research*, 2(6), pp. 19–38.

Dilamian, M. and Noroozi, B. (2019) ‘A combined homogenization-high intensity ultrasonication process for individualizaion of cellulose micro-nano fibers from rice straw’, *Cellulose*, 26(10), pp. 5831–5849. doi: 10.1007/s10570-019-02469-y.

Dong, S., Roman, M. and Long, T. E. (2014) *Effects of acid hydrolysis conditions on cellulose nanocrystal yield and properties : A response surface methodology study*.

Du, H., Liu, C., Zhang, Y., Yu, G., Si, C., and Li, B. (2016) ‘Preparation and characterization of functional cellulose nanofibrils via formic acid hydrolysis pretreatment and the followed high-pressure homogenization’, *Industrial Crops and Products*, 94, pp. 736–745. doi: 10.1016/j.indcrop.2016.09.059.

Du, H., Liu, C., Wang, D., Zhang, Y., Yu, G., Si, C., Li, B., Mu, X., and Peng, H. (2017) ‘Sustainable preparation and characterization of thermally stable and functional cellulose nanocrystals and nanofibrils via formic acid hydrolysis’, *Journal of Bioresources and Bioproducts*, 2(1), pp. 10–15. doi: 10.21967/jbb.v2i1.68.

Dutta, S., Gupta, B., Srivastava, S. K., and Gupta, A. Kumar. (2021) 'Recent advances on the removal of dyes from wastewater using various adsorbents: A critical review', *Materials Advances*, 2(14), pp. 4497–4531. doi: 10.1039/d1ma00354b.

Dutta, S. K., Amin, M. K., Ahmed, J., Elias, Md., and Mahiuddin, Md. (2022) 'Removal of toxic methyl orange by a cost-free and eco-friendly adsorbent : Mechanism , phytotoxicity , thermodynamics , and kinetics', *South African Journal of Chemical Engineering*, 40, pp. 195–208. doi: 10.1016/j.sajce.2022.03.006.

Dwivedi, K. and Kumar, G. (2015) 'Genetic damage induced by a food coloring dye (sunset yellow) on meristematic cells of Brassica campestris L.', *Journal of Environmental and Public Health*, 2015. doi: 10.1155/2015/319727.

El Maguana, Y., Elhadiri, N., Benchanaa, M., and Chikri, R. (2020) 'Activated Carbon for Dyes Removal: Modeling and Understanding the Adsorption Process', *Journal of Chemistry*, 2020. doi: 10.1155/2020/2096834.

El Miri, N., Heggset, E.B., Wallsten, S., Svedberg, A., Syverud, K., and Norgren, M. (2022) 'A comprehensive investigation on modified cellulose nanocrystals and their films properties', *International Journal of Biological Macromolecules*, 219, pp. 998–1008. doi: 10.1016/j.ijbiomac.2022.08.057.

Eljiedi, A. A. A. and Kamari, A. (2017) 'Removal of methyl orange and methylene blue dyes from aqueous solution using lala clam (Orbicularia orbiculata) shell', *AIP Conference Proceedings*, 1847. doi: 10.1063/1.4983899.

Eltaweil, A. S., Elgarhy, G. S., El-Subruiti, G. M., and Omer, A. M. (2020) 'Carboxymethyl cellulose/carboxylated graphene oxide composite microbeads for efficient adsorption of cationic methylene blue dye', *International Journal of Biological Macromolecules*, 154, pp. 307–318. doi: 10.1016/j.ijbiomac.2020.03.122.

Etale, A., Nhlane, D. S., Mosai, A. K., Mhlongo, J., Khan, A., Rumbold, K., Nuapia, Y. B. (2021) 'Synthesis and application of cationised cellulose for removal of Cr(VI) from acid mine-drainage contaminated water', *AAS Open Research*, 4, p. 4. doi: 10.12688/aasopenres.13182.1.

El-Torky, A. M. M., Mostafa, H. Y., El-Masry, A. M. M., and Mahdi, M. E. (2016) 'Purification of Heavy Metals from Industrial Wastewater Using Grafted Corn Husks Pulp Ion Exchanger', *Sohag Journal of Sciences*, 1(1), pp. 53–64. doi: 10.18576/sjs/010107.

Eyley, S. and Thielemans, W. (2014) 'Surface modification of cellulose nanocrystals', *Nanoscale*, 6(14), pp. 7764–7779. doi: 10.1039/c4nr01756k.

Farhadi, A., Ameri, A. and Tamjidi, S. (2021) 'Application of Agricultural Wastes as a Low-cost Adsorbent for Removal of Heavy Metals and Dyes from Wastewater: A Review Study', *Physical Chemistry Research*, 9(2), pp. 211–226. doi: 10.22036/pcr.2021.256683.1852.

Feng, Y. H., Cheng, T. Y., Yang, W. G., Ma, P. T., He, H. Z., Yin, X. C., and Yu, X. X. (2018) 'Characteristics and environmentally friendly extraction of cellulose nanofibrils from sugarcane bagasse', *Industrial Crops and Products*, 111, pp. 285–291. doi: 10.1016/j.indcrop.2017.10.041.

Fernandes, J. V., Rodrigues, A. M., Menezes, R. R., and de Araújo Neves, G. (2020) 'Adsorption of anionic dye on the acid-functionalized bentonite', *Materials*, 13(16), pp. 1–19. doi: 10.3390/MA13163600.

Ferreira, F. V., Mariano, M., Rabelo, S. C., Gouveia, R. F., and Lona, L. M.F. F. (2018) 'Isolation and surface modification of cellulose nanocrystals from sugarcane bagasse waste: From a micro- to a nanoscale view', *Applied Surface Science*, 436, pp. 1113–1122. doi: 10.1016/j.apsusc.2017.12.137.

Ferreres, F., Grosso, C., Gil-Izquierdo, A., Valentão, P., Mota, A. T., and Andrade, P. B. (2017) 'Optimization of the recovery of high-value compounds from pitaya fruit by-products using microwaveassisted extraction', *Food Chemistry*, 230, pp. 463–474. doi: 10.1016/j.foodchem.2017.03.061.

Fraschini, C., Chauve, G. and Bouchard, J. (2017) 'TEMPO-mediated surface oxidation of cellulose nanocrystals (CNCs)', *Cellulose*, 24(7), pp. 2775–2790. doi: 10.1007/s10570-017-1319-5.

Frost, B. A. and Johan Foster, E. (2020) 'Isolation of thermally stable cellulose nanocrystals from spent coffee grounds via phosphoric acid hydrolysis', *Journal of Renewable Materials*, 8(2), pp. 187–203. doi: 10.32604/jrm.2020.07940.

García, G. E. J., Mora, K. R., and Bernal, C. (2020) 'Cellulose Nanofiber Production from Banana Rachis', *IJESC*, 10(2), pp. 24683–24689.

Gao, X., Chen, K., Zhang, H., and Yan, X. (2015) 'Characterization of cationic parenchyma cellulose derivative by rapid preparation of low microwave power', *Iranian Polymer Journal (English Edition)*, 24(9), pp. 747–758. doi: 10.1007/s13726-015-0363-y.

Gao, Y., Li, Q., Shi, Y., and Cha, R. (2016) 'Preparation and Application of Cationic Modified Cellulose Fibrils as a Papermaking Additive', *International Journal of Polymer Science*, 2016, pp. 1–8.

Garcia-Valdez, O., Champagne, P. and Cunningham, M. F. (2018) 'Graft modification of natural polysaccharides via reversible deactivation radical polymerization', *Progress in Polymer Science*, 76, pp. 151–173. doi: 10.1016/j.progpolymsci.2017.08.001.

George, J. and Sabapathi, S. N. (2015) 'Cellulose nanocrystals: Synthesis, functional properties, and applications', *Nanotechnology, Science and Applications*, 8, pp. 45–54. doi: 10.2147/NSA.S64386.

Ghaedi, M., Jah, A. H., Khodadoust, S., Sahraei, R., Daneshfar, A., Mihandoost, A., and Purkait, M. K. (2012) 'Cadmium telluride nanoparticles loaded on activated carbon as adsorbent for removal of sunset yellow', *Spectrochimica Acta Part A: Molecular and Biomolecular Spectroscopy*, 90, pp. 22–27. doi: 10.1016/j.saa.2011.12.064.

Ghaedi, M. (2012) 'Comparison of cadmium hydroxide nanowires and silver nanoparticles loaded on activated carbon as new adsorbents for efficient removal of Sunset yellow: Kinetics and equilibrium study', *Spectrochimica Acta - Part A: Molecular and Biomolecular Spectroscopy*, 94, pp. 346–351. doi: 10.1016/j.saa.2012.02.097.

Ghosh, G. C., Chakraborty, T. K., Zaman, S., Nahar, M. N., and Kabir, A. H. M. E. (2020) 'Removal of Methyl Orange Dye from Aqueous Solution by a Low- Cost Activated Carbon Prepared from Mahagoni (Swietenia mahagoni) Bark', *pollution*, 6(1), pp. 171–184. doi: 10.22059/poll.2019.289061.679.

Di Giorgio, L., Martín, L., Salgado, P. R., and Mauri, A. N. (2020) 'Synthesis and conservation of cellulose nanocrystals', *Carbohydrate Polymers*, 238, p. 116187. doi: 10.1016/j.carbpol.2020.116187.

Goudarzi, L., Kasra Kermanshahi, R. and Jahed Khaniki, G. (2020) 'Response Surface Design for Removal of Lead by Different Lactic Acid Bacteria', *Health Scope*, 9(3). doi: 10.5812/jhealthscope.101049.

Gu, H., Gao, X., Zhang, H., Chen, K., and Peng, L. (2020) 'Fabrication and characterization of cellulose nanoparticles from maize stalk pith via ultrasonic-mediated cationic etherification', *Ultrasonics Sonochemistry*, 66, p. 104932. doi: 10.1016/j.ultsonch.2019.104932.

Guo, Y., Zhang, Y., Zheng, D., Li, M., and Yue, J. (2020) 'Isolation and characterization of nanocellulose crystals via acid hydrolysis from agricultural waste-tea stalk', *International Journal of Biological Macromolecules*, 163, pp. 927–933. doi: 10.1016/j.ijbiomac.2020.07.009.

Haddadian, Z., Shavandi, M. A., Zainal, Z., Halim, M., and Ismail, S. (2013) 'Removal Methyl Orange from Aqueous Solutions Using Dragon Fruit (Hylocereusundatus) Foliage', *Chemical Science Transactions*, 2(3), pp. 900–910. doi: 10.7598/cst2013.439.

Han, G., Liang, C., Chung, T., Weber, M., Staudt, C., and Maletzko, C. (2016) 'Combination of forward osmosis (FO) process with coagulation / flocculation (CF) for potential treatment of textile wastewater', *Water Research*, 91, pp. 361–370. doi: 10.1016/j.watres.2016.01.031.

Han, S., Yao, Q., Jin, C., Fan, B., Zheng, H., and Sun, Q. (2018) 'Cellulose nanofibers from bamboo and their nanocomposites with polyvinyl alcohol: Preparation and characterization', *Polymer Composites*, 39(8), pp. 2611–2619. doi: 10.1002/pc.24249.

Hang, Y., Qu, M. and Ukkusuri, S. (2011) 'Optimizing the design of a solar cooling system using central composite design techniques', *Energy and Buildings*, 43(4), pp. 988–994. doi: 10.1016/j.enbuild.2010.12.024.

Hao, Y., Liu, M., Cheng, X., Liu, J., Geng, C., Li, Z., and Zhu, B. (2022) 'Preparation of activated carbon based on Straw and its adsorption on sunset yellow', *meteorological and environmental research*, 13(3), pp. 1–4..

Hashem, A. and El-Shishtawy, R. M. (2001) 'Preparation and characterization of cationized cellulose for the removal of anionic dyes', *Adsorption Science and Technology*, 19(3), pp. 197–210. doi: 10.1260/0263617011494088.

Hassan, M., Ding, W., Bi, J., Mehryar, E., Talha, Z. A. A., and Huang, H. (2016) 'Bioresource Technology Methane enhancement through oxidative cleavage and alkali solubilization pre-treatments for corn stover with anaerobic activated sludge', *Bioresource Technology*, 200, pp. 405–412. doi: 10.1016/j.biortech.2015.09.115.

Hassan, M. M. and Carr, C. M. (2018) 'A critical review on recent advancements of the removal of reactive dyes from dyehouse effluent by ion-exchange adsorbents', *Chemosphere*, 209, pp. 201–219. doi: 10.1016/j.chemosphere.2018.06.043.

Hassan, S. H., Velayutham, T. S., Chen, Y. W., and Lee, H. V. (2021) 'TEMPO-oxidized nanocellulose films derived from coconut residues: Physicochemical, mechanical and electrical properties', *International Journal of Biological Macromolecules*, 180, pp. 392–402. doi: 10.1016/j.ijbiomac.2021.03.066.

Hastuti, N., Kanomata, K. and Kitaoka, T. (2019) 'Characteristics of TEMPO-Oxidized Cellulose Nanofibers from Oil Palm Empty Fruit Bunches Produced by Different Amounts of Oxidant', *IOP Conference Series: Earth and Environmental Science*, 359(1). doi: 10.1088/1755-1315/359/1/012008.

Hemmati, F., Norouzbeigi, R., Sarbisheh, F., and Shayesteh, H. (2016) 'Malachite green removal using modified sphagnum peat moss as a low-cost biosorbent: Kinetic, equilibrium and thermodynamic studies', *Journal of the Taiwan Institute of Chemical Engineers*, 58, pp. 482–489. doi: 10.1016/j.jtice.2015.07.004.

Her, K., Jeon, S. H., Lee, S., Shim, B. S. (2020) 'Esterification of Cellulose Nanofibers with Valeric Acid and Hexanoic Acid', *Macromolecular Research*, 28(12), pp. 1055–1063. doi: 10.1007/s13233020-8146-5.

Hokkanen, S., Bhatnagar, A. and Sillanpää, M. (2016) 'A review on modification methods to cellulosebased adsorbents to improve adsorption capacity', *Water Research*, 91, pp. 156–173. doi: 10.1016/j.watres.2016.01.008.

Hu, Z., Zhai, R., Li, J., Zhang, Y., and Lin, J. (2017) 'Preparation and Characterization of Nanofibrillated Cellulose from Bamboo Fiber via Ultrasonication Assisted by Repulsive Effect', *International Journal of Polymer Science*, 2017. doi: 10.1155/2017/9850814.

Huang, L., Wu, Q., Wang, Q., and Wolcott, M. (2019) 'One-Step Activation and Surface Fatty Acylation of Cellulose Fibers in a Solvent-Free Condition', *ACS Sustainable Chemistry and Engineering*, 7(19), pp. 15920–15927. doi: 10.1021/acssuschemeng.9b01974.

Huang, S., Liu, X., Chang, C., and Wang, Y. (2020a) 'Recent developments and prospective food related applications of cellulose nanocrystals: a review', *Cellulose*, 27(6), pp. 2991–3011. doi: 10.1007/s10570-020-02984-3.

Huang, X., Dognani, G., Hadi, P., Yang, M., Job, A. E., and Hsiao, B.S. (2020b) 'Cationic Dialdehyde Nanocellulose from Sugarcane Bagasse for Efficient Chromium(VI) Removal', *ACS Sustainable Chemistry and Engineering*, pp. 1–57. doi: 10.1021/acssuschemeng.9b06683.

Huntley, C. J., Crews, K. D., Abdalla, M. A., Russell, A. E., and Curry, M. L. (2015) 'Influence of strong acid hydrolysis processing on the thermal stability and crystallinity of cellulose isolated from wheat straw', *International Journal of Chemical Engineering*, 2015. doi: 10.1155/2015/658163.

Ibrahim, Q., Creedon, L. and Gharbia, S. (2022) 'A Literature Review of Modelling and Experimental

Studies of Water Treatment by Adsorption Processes on Nanomaterials', *Membranes*, 12(4). doi: 10.3390/membranes12040360.

Ilyas, R.A., Sapuan, S.M., Hassan, S.A., Bangar, S.P., Sanjay, M.R., Atikah, M.S.N., Rushdan, I., Ainun, Z.M.A., Asrofi, M., and Harussani, M.M. (2021) 'Sugar Palm (Arenga Pinnata (*Wurmb* .) Merr) Lignocellulosic Fibre Hierarchy : From Macro To Nano Scale', in *International Conference on Sugar Palm and Allied Fibre Polymer Composites 2021*.

Indarti, E., Marwan, Rohaizu, R., and Wanrosli, W. D. (2019) 'Silylation of TEMPO oxidized nanocellulose from oil palm empty fruit bunch by 3-aminopropyltriethoxysilane', *International Journal of Biological Macromolecules*, 135, pp. 106–112. doi: 10.1016/j.ijbiomac.2019.05.161.

Ioelovich, M. (2014) 'Peculiarities of cellulose nanoparticles', *Tappi Journal*, 13(5), pp. 45–51. doi: 10.32964/tj13.5.45.

Iwuozor, K. O., . Ighalo, J. O., Emenike, E. C., Ogunfowora, L. A.,and Igwegbe, C.A. (2021) 'Current Research in Green and Sustainable Chemistry Adsorption of methyl orange : A review on adsorbent performance', *Current Research in Green and Sustainable Chemistry*, 4, p. 100179. doi: 10.1016/j.crgsc.2021.100179.

Jain, P. and Vigneshwaran, N. (2012) 'Effect of Fenton's pretreatment on cotton cellulosic substrates to enhance its enzymatic hydrolysis response', *Bioresource Technology*, 103(1), pp. 219–226. doi: 10.1016/j.biortech.2011.09.110.

Jarabo, R., Fuente, E., Monte, M. C., Savastano, H., Mutjé, P., and Negro, C. (2012) 'Use of cellulose fibers from hemp core in fiber-cement production. Effect on flocculation, retention, drainage and product properties', *Industrial Crops and Products*, 39(1), pp. 89–96. doi:

10.1016/j.indcrop.2012.02.017.

Jarusiripot, C. (2014) 'Removal of Reactive Dye by Adsorption over Chemical Pretreatment Coal based Bottom Ash', *Procedia Chemistry*, 9, pp. 121–130. doi: 10.1016/j.proche.2014.05.015.

Jasmani, L., Eyley, S., Schutz, C., Van Gorp, H., De Feyter, S., and Thielemans, W. (2016) 'One-pot functionalization of cellulose nanocrystals with various cationic groups', *Cellulose*, 23, pp. 3569–3576. doi: 10.1007/s10570-016-1052-5.

Jasmani, L. and Thielemans, W. (2018) 'Preparation of Nanocellulose and its Potential Application', *Journal of Forest Research*, 7(3), pp. 1–8. doi: 10.4172/2168-9776.1000222.

Jawad, A. H., Sauodi, M. H., Mastuli, M. S., Aouda, M. A., and Radzun, K. A. (2018) 'Pomegranate peels collected from fresh juice shop as a renewable precursor for high surface area activated carbon with potential application for methylene blue adsorption', *Desalination and Water Treatment*, 124, pp. 287–296. doi: 10.5004/dwt.2018.22725.

Jawad, A. H., Abdulhameed, A. S., Wilson, L. D., Syed-Hassan, S. S. A., ALOthman, Z. A., and Khan, M. R. (2021) 'High surface area and mesoporous activated carbon from KOH-activated dragon fruit peels for methylene blue dye adsorption: Optimization and mechanism study', *Chinese Journal of Chemical Engineering*, 32, pp. 281–290. doi: 10.1016/j.cjche.2020.09.070.

Jawad, A. H., Kadhum, A. M. and Ngoh, Y. S. (2018) 'Applicability of dragon fruit (Hylocereus polyrhizus) peels as low-cost biosorbent for adsorption of methylene blue from aqueous solution: Kinetics, equilibrium and thermodynamics studies', *Desalination and Water Treatment*, 109, pp. 231–240. doi: 10.5004/dwt.2018.21976.

Ji, A., Jia, L., Kumar, D., and Yoo, C. G. (2021) 'Recent advancements in biological conversion of industrial hemp for biofuel and value-added products', *Fermentation*, 7(1). doi: 10.3390/fermentation7010006.

Ji, Q., Yu, X., Yagoub, A. E. A., Li. M., Fakayode, O. A., Yan, D., Zhou, C., and Chen, L. (2020) 'Ultrasound - Ionic Liquid Pretreatment Enhanced Conversion of the Sugary Food Waste to 5 - Hydroxymethylfurfural in Ionic Liquid / Solid Acid Catalyst System', *Catalysis Letters* , 150, pp. 1373–1388. doi: 10.1007/s10562-019-03059-0.

Ji, Q., Yu, X., Yagoub, A. E. A. and Chen, L. (2021a) 'Efficient cleavage of strong hydrogen bonds in sugarcane bagasse by ternary acidic deep eutectic solvent and ultrasonication to facile fabrication of cellulose nanofibers', *Cellulose*, 28(10), pp. 6159–6182. doi: 10.1007/s10570-021-03876-w.

Ji, Q., Yu, Xi., Yagoub, A. E. A., Chen, L., Abiola, O., and Zhou, C. (2021b) 'Ultrasonics Sonochemistry Synergism of sweeping frequency ultrasound and deep eutectic solvents pretreatment for fractionation of sugarcane bagasse and enhancing enzymatic hydrolysis', *Ultrasonics Sonochemistry*, 73, p. 105470. doi: 10.1016/j.ultsonch.2021.105470.

Jiang, Z. and Hu, D. (2019) 'Molecular mechanism of anionic dyes adsorption on cationized rice husk cellulose from agricultural wastes', *Journal of Molecular Liquids*, 276, pp. 105–114. doi: 10.1016/j.molliq.2018.11.153.

Jonasson, S., Bünder, A., Niittylä, T., and Oksman, K. (2020) 'Isolation and characterization of cellulose nanofibers from aspen wood using derivatizing and non-derivatizing pretreatments', *Cellulose*, 27(1), pp. 185–203. doi: 10.1007/s10570-019-02754-w.

Jóźwiak, T., Filipkowska, U., Brym, S., and Kopeć, L. (2020) 'Use of aminated hulls of sunflower seeds for the removal of anionic dyes from aqueous solutions', *International Journal of Environmental Science and Technology*, 17(3), pp. 1211–1224. doi: 10.1007/s13762-019-02536-8.

Jung, J. Y., Choi, M. S. and Yang, J. K. (2013) 'Optimization of concentrated acid hydrolysis of waste paper using response surface methodology', *Journal of the Korean Wood Science and Technology*, 41(2), pp. 87–99. doi: 10.5658/WOOD.2013.41.2.87.

Kadhom, M., Albayati, N., Alalwan, H., and Al-Furaiji, M. (2020) 'Removal of dyes by agricultural waste', *Sustainable Chemistry and Pharmacy*, 16, p. 100259. doi: 10.1016/j.scp.2020.100259.

Kaffashsaie, E., Yousefi, H., Nishino, T., Matsumoto, T., Mashkour, M., Madhoushi, M., and Kawaguchi, H. (2021) 'Direct conversion of raw wood to TEMPO-oxidized cellulose nanofibers', *Carbohydrate Polymers*, 262, p. 117938. doi: 10.1016/j.carbpol.2021.117938.

Kallel, F., Bettaieb, F., Khiari, R., García, A., Bras, J., and Chaabouni, S. E. (2016) 'Isolation and structural characterization of cellulose nanocrystals extracted from garlic straw residues', *Industrial Crops and Products*, 87, pp. 287–296. doi: 10.1016/j.indcrop.2016.04.060.

Kamar, M. T., Elattar, H., Mahmoud, A. S., Peters, R.W., and Mostafa, M.K. (2022) 'A critical review of state-of-the-art technologies for electroplating wastewater treatment', *International Journal of Environmental Analytical Chemistry*, 00(00), pp. 1–34. doi: 10.1080/03067319.2022.2098486.

Kampeerapappun, P. (2015) 'Extraction and characterization of cellulose nanocrystals produced by acid hydrolysis from corn husk', *Jpurnal of Metals, Materials and Minerals*, 25(1), pp. 19–26.

Kandhola, G., Djioleu, A., Rajan, K., Labbé, N., Sakon, J., Carrier, D. J., Kim, J. W. (2020) 'Maximizing production of cellulose nanocrystals and nanofibers from pre-extracted loblolly pine kraft pulp: a response surface approach', *Bioresources and Bioprocessing*. doi: 10.1186/s40643-020-00302-0.

Kandisa, R. V. and Saibaba K.V, N. (2016) 'Dye Removal by Adsorption: A Review', *Journal of Bioremediation and Biodegradation*, 07(06). doi: 10.4172/2155-6199.1000371.

Kargarzadeh, H., Ioelovich, M., Ahmad, I., Thomas, S., and Dufresne, A. (2017) 'Methods for Extraction of Nanocellulose from Various Sources', *Handbook of Nanocellulose and Cellulose Nanocomposites*, pp. 1–49. doi: 10.1002/9783527689972.ch1.

Kassab, Z., Abdellaoui, Y., Salim, M. H., Bouhfid, R., Qaiss, A. E., and El Achaby, M. (2020) 'Micro- and nano-celluloses derived from hemp stalks and their effect as polymer reinforcing materials', *Carbohydrate Polymers*, 245, pp. 1–12. doi: 10.1016/j.carbpol.2020.116506.

Katheresan, V., Kansedo, J. and Lau, S. Y. (2018) 'Efficiency of various recent wastewater dye removal methods: A review', *Journal of Environmental Chemical Engineering*, 6(4), pp. 4676–4697. doi: 10.1016/j.jece.2018.06.060.

Kaur, K. and Jindal, R. (2018) 'Synergistic effect of organic-inorganic hybrid nanocomposite ion exchanger on photocatalytic degradation of Rhodamine-B dye and heavy metal ion removal from industrial effluents', *Journal of Environmental Chemical Engineering*, 6(6), pp. 7091–7101. doi: 10.1016/j.jece.2018.09.065.

Kawee, N., Lam, N. T. and Sukyai, P. (2018) 'Homogenous isolation of individualized bacterial nano fi brillated cellulose by high pressure homogenization', *Carbohydrate Polymers*, 179, pp. 394–401. doi: 10.1016/j.carbpol.2017.09.101.

Khan, A., Vu, K. D., Chauve, G., Bouchard, J., Riedl, B., and Lacroix, M. (2014) 'Optimization of microfluidization for the homogeneous distribution of cellulose nanocrystals (CNCs) in biopolymeric matrix', *Cellulose*, 21(5), pp. 3457–3468. doi: 10.1007/s10570-014-0361-9.

Khan, E. A., Shahjahan and Khan, T. A. (2018) 'Adsorption of methyl red on activated carbon derived from custard apple (Annona squamosa) fruit shell: Equilibrium isotherm and kinetic studies', *Journal of Molecular Liquids*, 249, pp. 1195–1211. doi: 10.1016/j.molliq.2017.11.125.

Khawas, P. and Deka, S. C. (2016) 'Isolation and characterization of cellulose nanofibers from culinary banana peel using high-intensity ultrasonication combined with chemical treatment', *Carbohydrate Polymers*, 137, pp. 608–616.

Khodaie, M., Ghasemi, N., Moradi, B., and Rahimi, M. (2013) 'Removal of methylene blue from wastewater by adsorption onto znclactivated corn husk carbon equilibrium studies', *Journal of Chemistry*, 2013. doi: 10.1155/2013/383985.

Khulbe, K. C. and Matsuura, T. (2018) 'Removal of heavy metals and pollutants by membrane adsorption techniques', *Applied Water Science*, 8(1), pp. 1–30. doi: 10.1007/s13201-018-0661-6.

Kondo, T. (2022) 'Cellulose Nanofibrils Pulverized from Biomass Resources :Past, Present, and Future Perspectives', *KONA Powder and Particle journal* , pp. 1–15.

Kumar, K. A. and S, S. (2021) 'Adsorption Kinetics of Malachite Green Dye Removal from Aqueous Solution by using Banana Stem', *International Journal of Engineering and Advanced Technology*, 10(5), pp. 215–220. doi: 10.35940/ijeat.e2756.0610521.

Kumar, P. S., Sivaprakash, S. and Jayakumar, N. (2017) 'Removal of Methylene Blue dye from aqueous solutions Using Lagerstroemia indica seed (LIS) activated carbon', *International Journal of Materials Science*, 12(1), pp. 107–116. Available at: http://www.ripublication.com.

Kusmono, Listyanda, R. F., Wildan, M. W., and Ilman, M. N. (2020) 'Preparation and characterization of cellulose nanocrystal extracted from ramie fibers by sulfuric acid hydrolysis', *Heliyon*. doi: 10.1016/j.heliyon.2020.e05486.

Kusumaningrum, W. B., Amanda, Putri., Suryanegara, L., and Masruchin, N. (2020) 'The effectivity of one-pot concentrated maleic anhydride hydrolysis for betung bamboo pulp (Dendrocalamus asper sp)', in *IOP Conference Series: Earth and Environmental Science*, pp. 1–11. doi: 10.1088/17551315/572/1/012044.

Kyzas, G. Z., Christodoulou, E. and Bikiaris, D. N. (2018) 'Basic dye removal with sorption onto lowcost natural textile fibers', *Processes*, 6(166), pp. 1–18. doi: 10.3390/pr6090166.

Latif, S., Rehman, R., Imran, M., Iqbal, S., Kanwal, A., and Mitu, L. (2019) 'Removal of Acidic Dyes from Aqueous Media Using Citrullus Lanatus Peels: An Agrowaste-Based Adsorbent for Environmental Safety', *Journal of Chemistry*, 2019. doi: 10.1155/2019/6704953.

Lease, J., Kawano, T. and Andou, Y. (2021) 'Esterification of cellulose with long fatty acid chain through mechanochemical method', *Polymers*, 13(24), pp. 1–12. doi: 10.3390/polym13244397.

Ledakowicz, S. and Pázdzior, K. (2021) 'Recent achievements in dyes removal focused on advanced oxidation processes integrated with biological methods', *Molecules*, 26(4). doi: 10.3390/molecules26040870.

Lee, D., Oh, Y., Yoo, J.K., Yi, J.W., Um, M.K., and Park, T. (2020) 'Rheological study of cellulose nanofiber disintegrated by a controlled high-intensity ultrasonication for a delicate', *Cellulose*, 27(16), pp. 9257–9269. doi: 10.1007/s10570-020-03410-4.

Lee, M., Heo, M. H., Lee, H., Lee, H. H., Jeong, H., Kim, Y. W., and Shin, J. (2018) 'Facile and ecofriendly extraction of cellulose nanocrystals: Via electron beam irradiation followed by high-pressure homogenization', *Green Chemistry*, 20(11), pp. 2596–2610. doi: 10.1039/c8gc00577j.

Leite, A. L. M. P., Zanon, C. D. and Menegalli, F. C. (2017) 'Isolation and characterization of cellulose nanofibers from cassava root bagasse and peelings', *Carbohydrate Polymers*, 157, pp. 962–970. doi: 10.1016/j.carbpol.2016.10.048.

Le Gars, M., Delvart, A., Roger, P., Belgacem, M. N., and Bras, J. (2020) 'Amidation of TEMPOoxidized cellulose nanocrystals using aromatic aminated molecules', *Colloid and Polymer Science*, 298, pp. 603–617.

Li, B., Xu, W., Kronlund, D., Määttänen, A., Liu, J., Smått, J. H., Peltonen, J., Willför, S., Mu, X., and Xu, C. (2015) 'Cellulose nanocrystals prepared via formic acid hydrolysis followed by TEMPOmediated oxidation', *Carbohydrate Polymers*, 133, pp. 605–612. doi: 10.1016/j.carbpol.2015.07.033.

Li, J., Wei, X., Wang, Q., Chen, J., Chang, G., Kong, L., Su, J., and Liu, Y. (2012) 'Homogeneous isolation of nanocellulose from sugarcane bagasse by high pressure homogenization', *Carbohydrate Polymers*, 90(4), pp. 1609–1613. doi: 10.1016/j.carbpol.2012.07.038.

Li, J., Wang, H., Yuan, X., Zhang, J., and Chew, J. W. (2020) 'Metal-organic framework membranes for wastewater treatment and water regeneration', *Coordination Chemistry Reviews*, 404, p. 213116. doi: 10.1016/j.ccr.2019.213116.

Li, M., Wang, L. J., Li, D., Cheng, Y. L., and Adhikari, B. (2014) 'Preparation and characterization of cellulose nanofibers from de-pectinated sugar beet pulp', *Carbohydrate Polymers*, 102(1), pp. 136–143. doi: 10.1016/j.carbpol.2013.11.021.

Li, X., Shi, Y., Kong, W., Wei, J., Song, W., and Wang, S. (2022) 'Improving enzymatic hydrolysis of lignocellulosic biomass by bio-coordinated physicochemical pretreatment—A review', *Energy Reports*, 8, pp. 696–709. doi: 10.1016/j.egyr.2021.12.015.

Liimatainen, H., Suopajärvi, T., Sirviö, J., Hormi, O., and Niinimäki, J. (2014) 'Fabrication of cationic cellulosic nanofibrils through aqueous quaternization pretreatment and their use in colloid aggregation', *Carbohydrate Polymers*, 103(1), pp. 187–192. doi: 10.1016/j.carbpol.2013.12.042.

Lim, A., Chew, J. J., Ismadji, S., Khaerudini, D. S., Darsono, N., and Sunarso, J. (2022) 'Kinetic and equilibrium adsorption study of anionic dyes using oil palm trunk-derived activated carbon', *Materials Today: Proceedings*, 64, pp. 1627–1638. doi: 10.1016/j.matpr.2022.04.918.

Littunen, K., De Castro, J. S., Samoylenko, A., Xu, Q., Quaggin, S., Vainio, S., and Seppälä, J. (2016) 'Synthesis of cationized nanofibrillated cellulose and its antimicrobial properties', *European Polymer Journal*, 75, pp. 116–124. doi: 10.1016/j.eurpolymj.2015.12.008.

Liu, C., Li, B., Du, H., Lv, D., Zhang, Y., Yu, G., Mu, X., and Peng, H. (2016) 'Properties of nanocellulose isolated from corncob residue using sulfuric acid, formic acid, oxidative and mechanical methods', *Carbohydrate Polymers*, 151, pp. 716–724. doi: 10.1016/j.carbpol.2016.06.025.

Liu, S., Zhang, Q., Gou, S., Zhang, L., Wang, Z. (2021) 'Esterification of cellulose using carboxylic acid-based deep eutectic solvents to produce high-yield cellulose nanofibers', *Carbohydrate Polymers*, 251, p. 117018. doi: 10.1016/j.carbpol.2020.117018.

Liu, Y., Xiang, Y., Xu, H., and Li, H. (2022) 'The reuse of nano-TiO_2 under different concentration of CO32 – using coagulation process and its photocatalytic ability in treatment of methyl orange', *Separation and Purification Technology*, 282, p. 120152. doi: 10.1016/j.seppur.2021.120152.

Long, L., Tian, D., Hu, J., Wang, F., and Saddler, J. (2017) 'A xylanase-aided enzymatic pretreatment facilitates cellulose nanofibrillation', *Bioresource Technology*, 243, pp. 898–904. doi: 10.1016/j.biortech.2017.07.037.

Longaresi, R. H., de Menezes, A. J., Pereira-da-Silva, M. A., Baron, D., and Mathias, S. L. (2019) 'The maize stem as a potential source of cellulose nanocrystal: Cellulose characterization from its phenological growth stage dependence', *Industrial Crops and Products*, 133, pp. 232–240. doi: 10.1016/j.indcrop.2019.02.046.

Lu, H., Gui, Y., Zheng, L., and Liu, X. (2013) 'Morphological, crystalline, thermal and physicochemical properties of cellulose nanocrystals obtained from sweet potato residue', *Food Research International*, 50(1), pp. 121–128. doi: 10.1016/j.foodres.2012.10.013.

Lu, P. and Hsieh, Y. (2010) 'Preparation and properties of cellulose nanocrystals: Rods, spheres, and network', *Carbohydrate Polymers*, 82(2), pp. 329–336. doi: 10.1016/j.carbpol.2010.04.073.

Lv, D., Du, H., Che, X., Wu, M., Zhang, Y., Liu, C., Nie, S., Zhang, X., and Li, B. (2019) 'Tailored and Integrated Production of Functional Cellulose Nanocrystals and Cellulose Nanofibrils via Sustainable Formic Acid Hydrolysis: Kinetic Study and Characterization', *ACS Sustainable Chemistry and Engineering*, 7(10), pp. 9449–9463. doi: 10.1021/acssuschemeng.9b00714.

Lynd, L. R., Weimer, P. J., Zyl, Willem H. V., Isak, S., van Zyl, W. H., and Prestorius, I. S. (2002) 'Microbial Cellulose Utilization : Fundamentals and Biotechnology', *Microbiology and Molecular Biology Reviews*, 66(3), pp. 506–577. doi: 10.1128/mmbr.66.3.506.

Madhura, L., Kanchi, S., Sabela, M. I., Singh, S., Bisetty, K., Inamuddin. (2018) 'Membrane technology for water purification', *Environmental Chemistry Letters*, 16(2), pp. 343–365. doi: 10.1007/s10311017-0699-y.

Mahardika, M., Abral, H., Kasim, A., Arief, S., and Asrofi, M. (2018) 'Production of nanocellulose from pineapple leaf fibers via high-shear homogenization and ultrasonication', *Fibers*, 6(2), pp. 1–12. doi: 10.3390/fib6020028.

Mansora, A. M., Lima, J.S., Anib, F.N., Hashima, H., and Ho, W.S. (2019) 'Characteristics of Cellulose , Hemicellulose and Lignin of MD2 Pineapple Biomass', *Chemical Engineering Transactions*, 72, pp. 79–84. doi: 10.3303/cet1972014.

Malakootian, M. and Heidari, M. R. (2018) 'Reactive orange 16 dye adsorption from aqueous solutions by psyllium seed powder as a low-cost biosorbent: kinetic and equilibrium studies', *Applied Water Science*, 8(7), pp. 1–9. doi: 10.1007/s13201-018-0851-2.

Manavi, N., Kazemi, A. S. and Bonakdarpour, B. (2017) 'The development of aerobic granules from conventional activated sludge under anaerobic-aerobic cycles and their adaptation for treatment of dyeing wastewater', *Chemical Engineering Journal*, 312, pp. 375–384. doi: 10.1016/j.cej.2016.11.155.

Manimekalai, T. K., Tamilarasan, G., Sivakumar, N., and Periyasamy, S. (2015) 'Kinetic, equilibrium and thermodynamic studies of synthetic dye removal using plastic waste activated carbon prepared by CO2 activation', *International Journal of ChemTech Research*, 8(6), pp. 225–240.

Mansoori, S., Davarnejad, R., Matsuura, T., and Ismail, A. F. (2020) 'Membranes based on nonsynthetic (natural) polymers for wastewater treatment', *Polymer Testing*, 84, pp. 1–34. doi: 10.1016/j.polymertesting.2020.106381.

Matebie, B. Y., Tizazu, B. Z., Kadhem, A. A., and Venkatesa Prabhu, S. (2021) 'Synthesis of Cellulose

Nanocrystals (CNCs) from Brewer's Spent Grain Using Acid Hydrolysis: Characterization and Optimization', *Journal of Nanomaterials*, 2021. doi: 10.1155/2021/7133154.

Mazela, B., Perdoch, W., Peplińska, B., and Mikołaj, Z. (2020) 'Influence of Chemical Pre-Treatments and Ultrasonication on the Dimensions and Appearance of Cellulose Fibers', *Materials*, 13, pp. 1–14.

Merais, M.S.; Khairuddin, N.; Salehudin, M.H.; Mobin Siddique, M.B.; Lepun, P.; Chuong, W.S. (2022) 'Preparation and Characterization of Cellulose Nanofibers from Banana Pseudostem by Acid Hydrolysis : Physico-Chemical and Thermal Properties'. *Membranes*, 12, 451. https://doi.org/10.3390/membranes12050451

Miculescu, M., Thakur, V. K., Miculescu, F., Voicu, S. I. (2016) 'Graphene-based polymer nanocomposite membranes: a review', *Polymers for Advanced Technologies*, 27(7), pp. 844–859. doi: 10.1002/pat.3751.

Mogaddasi, F., Heravi, M. M., Bozorgmehr, M.R., Ardalan, P., and Ardalan, T.(2010) 'Kinetic and Thermodynamic Study on the Removal of Methyl Orange From Aqueous Solution by Adsorption onto Camel Thorn Plant', *Asian Journal of Chemistry*, 22(7), pp. 5093–5100.

Mohamed, N.B., Ngadi, N., Lani, N. S., Ab Rahman, R. (2017) 'Polyethylenimine Modified Sugarcane Bagasse Adsorbent for Methyl Orange Dye Removal', *Chemical Engineering Transactions*, 56, pp. 103–108. doi: 10.3303/CET1756018.

Mohamed, N. B., Ngadi, N., Wong, S., Yahya, N. Y., Hassan, O., Inuwa, I. M., Opotu, L. A., and Ali, N. (2022) 'Facile synthesis of polyethylenimine-modified sugarcane bagasse adsorbent for removal of anionic dye in aqueous solution', *Scientific African*, 16, p. e01135. doi: 10.1016/j.sciaf.2022.e01135.

Moharm, A.E., El Naeem, G.A., Soliman, H. M. A., Abd-Elhamid, A. I., El-Bardan, A. .A., Kassem, T. S., Nayl, A.A., and Bräse.S. (2022) 'Fabrication and Characterization of Effective Biochar Biosorbent Derived from Agricultural Waste to Remove Cationic Dyes from Wastewater', *Polymers*, 14(13), p. 2587. doi: 10.3390/polym14132587.

Mojsov, K. D., Andronikov, D., Janevski, A., Kuzelov, A., and Gaber, S. (2016) 'The Application of Enzymes for the Removal of Dyes From Textile effluents', *Advanced technologies*, 5(1), pp. 81–86.

Moosavi, S., Lai, C. W., Gan, S., Zamiri, G., Pivehzhani, O. A., and Johan, M. R. (2020) 'Application of efficient magnetic particles and activated carbon for dye removal from wastewater', *ACS Omega*, 5(33), pp. 20684–20697. doi: 10.1021/acsomega.0c01905.

Morantes, D., Muñoz, E., Kam, D., and Shoseyov, O. (2019) 'Highly charged cellulose nanocrystals applied as a water treatment flocculant', *Nanomaterials*, 9(2), pp. 1–13. doi: 10.3390/nano9020272.

Morin-Crini, N., Loiacono, S., Placet, V., Torri, G., Bradu, C., Kostić, M., Cosentino, C., Chanet, G., Martel, B., Lichtfouse, E., and Crini, G. (2018) *Hemp-Based Materials for Metal Removal*, *Green Adsorbents for Pollutant Removal, Environmental Chemistry for a Sustainable World*. doi: 10.1007/978-3-319-92162-4_1.

Mosallanejad, N. and Arami, A. (2012) 'Kinetics and isotherm of sunset yellow dye adsorption on cadmium sulfide nanoparticle loaded on activated carbon', *Journal of Chemical Health Risks*, 2(2251–6719), pp. 31–40.

Motaung, T. E. and Linganiso, L. Z. (2018) *Critical review on agrowaste cellulose applications for biopolymers*, *International Journal of Plastics Technology*. Springer India. doi: 10.1007/s12588-0189219-6.

Muqeet, M., Malik, H., Mahar, R. B., Ahmed, F., Khatri, Z., and Carlson, K. (2017) 'Cationization of Cellulose Nanofibers for the Removal of Sulfate Ions from Aqueous Solutions', *Industrial and Engineering Chemistry Research*, 56(47), pp. 14078–14088. doi: 10.1021/acs.iecr.7b03739.

Mason, R. L., Gunst, R. F., Hess, J. L. (1990) Statistical Design and Analysis of Experiments: With Applications to Engineering and Science., *Journal of the American Statistical Association*. doi: 10.2307/2289624.

Nafisa Begam, M. N., Muthukumaran, K., Thamarai, P., and Joshua, J. P. (2022) 'Adsorption isotherm and kinetic studies for the decolorization of sunset yellow FCF dye using economically feasible lowcost adsorbent', *Global Nest Journal*, 24(2), pp. 276–285. doi: 10.30955/gnj.004266.

Namasivayam, C. and Kavitha, D. (2002) 'Removal of Congo Red from water by adsorption onto activated carbon prepared from coir pith, an agricultural solid waste', *Dyes and Pigments*, 54, pp. 47–

58.

do Nascimento, G. E., Cavalcanti, V. O.M., Santana, R. M.R., Sales, D. C.S., Rodríguez-Díaz, J. M., Napoleão, D. C., and Duarte, M. M.M.B. (2020) 'Degradation of a Sunset Yellow and Tartrazine Dye Mixture: Optimization Using Statistical Design and Empirical Mathematical Modeling', *Water, Air, and Soil Pollution*, 231(5), pp. 1–17. doi: 10.1007/s11270-020-04547-5.

Neethu, N. and Choudhury, T. (2018) 'Treatment of Methylene Blue and Methyl Orange Dyes in Wastewater by Grafted Titania Pillared Clay Membranes', *Recent Patents on Nanotechnology*, 12(3), pp. 200–207. doi: 10.2174/1872210512666181029155352.

Nehaba, S. S. (2017) 'Synthetic Textile Red Dye Removal From Aqueous Solution by Adsorption onto Pomegranate Peel', *Journal of Babylon University/Engineering Sciences*, 25(4), pp. 1439–1447.

Nethaji, S., Sivasamy, A. and Mandal, A. B. (2013) 'Adsorption isotherms, kinetics and mechanism for the adsorption of cationic and anionic dyes onto carbonaceous particles prepared from Juglans regia shell biomass', *International Journal of Environmental Science and Technology*, 10(2), pp. 231–242. doi: 10.1007/s13762-012-0112-0.

Noremylia, M. B., Hassan, M. Z. and Ismail, Z. (2022) 'Recent advancement in isolation, processing, characterization and applications of emerging nanocellulose: A review', *International Journal of Biological Macromolecules*, 206, pp. 954–976. doi: 10.1016/j.ijbiomac.2022.03.064.

Nurhadi, B., Angeline, A., Sukri, N., Masruchin, N., Arifin, R. H., and Saputra, R. A. (2022) 'Characteristics of microcrystalline cellulose from nata de coco: Hydrochloric acid versus maleic acid hydrolysis', *Journal of Applied Polymer Science*, 139(5), pp. 1–12. doi: https://doi.org/10.1002/app.51576.

Odabas, N., Amer, H., Bacher, M., Henniges, U., Potthast, A., and Rosenau, T. (2016) 'Properties of Cellulosic Material after Cationization in Different Solvents', *ACS Sustainable Chemistry and Engineering*, 4(4), pp. 2295–2301. doi: 10.1021/acssuschemeng.5b01752.

Oguz Erdogan, F. and Erdogan, T. (2018) 'Adsorption of Sunset Yellow FCF Onto MCM-41', *The Online Journal of Science and Technology*, 8(1), pp. 16–20. Available at: www.tojsat.net.

Okodugha, G. O., Okodugha, L. A., Chukwu, A., and Kingsley, A. O. (2021) 'Removal Of Methyl Orange Dye From Aqueous Solution By Adsorption On HCl And NH 4 OH Treated Rice Husk', *Nigeria Academic Forum*, 28(1), pp. 1–12.

Oller, I., Malato, S. and Sánchez-Pérez, J. A. (2011) 'Combination of Advanced Oxidation Processes and biological treatments for wastewater decontamination-A review', *Science of the Total Environment*, 409(20), pp. 4141–4166. doi: 10.1016/j.scitotenv.2010.08.061.

Omari, S., Nedjhioui, M., Hamidi, N., and Benkortbi, O. (2022) 'Synthesis and characterization of activated carbon from red pumpkin skin for the removal of ionic dyes', *Water Practice and Technology*, 17(5), pp. 1197–1217. doi: 10.2166/wpt.2022.038.

Pacaphol, K. and Aht-Ong, D. (2017) 'Preparation of hemp nanofibers from agricultural waste by mechanical defibrillation in water', *Journal of Cleaner Production*, 142, pp. 1283–1295. doi: 10.1016/j.jclepro.2016.09.008.

Patiño-Masó, J., Serra-Parareda, F., Tarrés, Q., Mutjé, P., Espinach, F. X., and Delgado-Aguilar, M. (2019) 'TEMPO-oxidized cellulose nanofibers: A potential bio-based superabsorbent for diaper production', *Nanomaterials*, 9(9). doi: 10.3390/nano9091271.

Pei, A., Butchosa, N., Berglund, L. A., and Zhou, Q. (2013) 'Surface quaternized cellulose nanofibrils with high water absorbency and adsorption capacity for anionic dyes', *Soft Matter*, 9(6), pp. 2047–2055. doi: 10.1039/c2sm27344f.

Pereira, B. and Arantes, V. (2018) 'Nanocelluloses From Sugarcane Biomass', *Advances in Sugarcane Biorefinery: Technologies, Commercialization, Policy Issues and Paradigm Shift for Bioethanol and By-Products*,, pp. 179–196. doi: 10.1016/B978-0-12-804534-3.00009-4.

Prasanna., N., Manivasagan, V., Pandidurai, S., Pradeep, D., and Leebatharushon, S.S. (2014) 'Studies on the Removal of Methyl Orange From Aqueous Solution Using Modified Banana Trunk Fibre', *International Journal of Advanced Research*, 2(4), pp. 341–349.

Puangsin, B., Soeta, H., Saito, T., and Isogai, A. (2017) 'Characterization of cellulose nanofibrils prepared by direct TEMPO-mediated oxidation of hemp bast', *Cellulose*, 24(9), pp. 3767–3775. doi: 10.1007/s10570-017-1390-y.

Puttaswamy, M., Srinikethan, G. and Shetty, V. K. (2017) 'Biocomposite composed of PVA reinforced with cellulose microfibers isolated from biofuel industrial dissipate: Jatropha Curcus L. seed shell', *Journal of Environmental Chemical Engineering*, 5(2), pp. 1990–1997. doi: 10.1016/j.jece.2017.04.004.

Qu, R., Tang, M., Wang, Y., Li, D., and Wang, L. (2021) 'TEMPO-oxidized cellulose fibers from wheat straw: Effect of ultrasonic pretreatment and concentration on structure and rheological properties of suspensions', *Carbohydrate Polymers*, 255, pp. 117386. doi: 10.1016/j.carbpol.2020.117386.

Rahman, N. S. A., Yhaya, M. F., Azahari, B., and Ismail, W. R. (2018) 'Utilisation of natural cellulose fibres in wastewater treatment', *Cellulose*, 25(9), pp. 4887–4903. doi: 10.1007/s10570-018-1935-8.

Rana, V., Malik, S., Joshi, G., Rajput, N. K., and Gupta, P. K. (2021) 'Preparation of alpha cellulose from sugarcane bagasse and its cationization: Synthesis, characterization, validation and application as wet-end additive', *International Journal of Biological Macromolecules*, 170, pp. 793–809. doi: 10.1016/j.ijbiomac.2020.12.165.

Ratajczak, K. and Stobiecka, M. (2020) 'High-performance modified cellulose paper-based biosensors for medical diagnostics and early cancer screening: A concise review', *Carbohydrate Polymers*, 229, p. 115463. doi: 10.1016/j.carbpol.2019.115463.

Ratnakumar, A., Samarasekara, B. A. M. P. and Amarasinghe, S. D. A. (2022) 'Effect of Sonication Time on Cellulose Nanofiber Disintegration from Locally Available Rice Straw', *Macromolecular symposia*, 402, pp. 1–5. doi: 10.1002/masy.202100425.

Rattanapan, S., Srikram, J. and Kongsune, P. (2017) 'Adsorption of Methyl Orange on Coffee grounds Activated Carbon', *Energy Procedia*, 138, pp. 949–954. doi: 10.1016/j.egypro.2017.10.064.

Risite, H., Salim, M. H., Oudinot, B. T., Ablouh, E., Joyeux, H. T., Sehaqui, H., Razafimahatratra, Jean H. A.,Qaiss, A. E., El Achaby, M., and Kassab, Z. (2022) 'Artemisia annua Stems a New Sustainable Source for Cellulosic Materials: Production and Characterization of Cellulose Microfibers and Nanocrystals', *Waste and Biomass Valorization*, 13(4), pp. 2411–2423. doi: 10.1007/s12649-02101658-w.

Rossi, B. R., Pellegrini, V. O.A., Cortez, A. A., Chiromito, E. M. S., Carvalho, A. J. F., Pinto, L. O., Rezende, C. A., Mastelaro, V. R., and Polikarpov, I. (2021) 'Cellulose nanofibers production using a set of recombinant enzymes', *Carbohydrate Polymers*, 256, pp. 117510. doi: 10.1016/j.carbpol.2020.117510.

Rovina, K., Perumal, P. and Siddiquee, S. (2016) 'Methods for the analysis of Sunset Yellow FCF (E110) in food and beverage products- a review', *Trends in Analytical Chemistry*, 85, pp. 47–56. doi: 10.1016/j.trac.2016.05.009.

Saber-Samandari, S., Saber-Samandari, S., Heydaripour, S., and Abdouss, M. (2016) 'Novel carboxymethyl cellulose based nanocomposite membrane: Synthesis, characterization and application in water treatment', *Journal of Environmental Management*, 166, pp. 457–465. doi:

10.1016/j.jenvman.2015.10.045.

Sadegh, H., Ali, G. A. M., Gupta, V. K., Makhlouf, A. S. H., Shahryari-ghoshekandi, R., Nadagouda, M. N., Sillanpää, M., and Megiel, E. (2017) 'The role of nanomaterials as effective adsorbents and their applications in wastewater treatment', *Journal of Nanostructure in Chemistry*, 7(1), pp. 1–14. doi: 10.1007/s40097-017-0219-4.

Sadeghifar, H., Filpponen, I., Clarke, S. P., Brougham, D. F., and Argyropoulos, D. S. (2011) 'Production of cellulose nanocrystals using hydrobromic acid and click reactions on their surface', *Journal of Materials Science*, 46(22), pp. 7344–7355. doi: 10.1007/s10853-011-5696-0.

Saeed, S., Khan, S., Saeed, S., Khan, R. (2015) 'Removal of dyes from textile waste water using adsorption by activated carbon of rice husk', *International Journal of Innovation and Scientific Research ISSN*, 17(1), pp. 2351–8014. Available at: http://www.ijisr.issr-journals.org/.

Salami, A., Raninen, K., Heikkinen, J., Tomppo, L., Vilppo, T., Selenius, M., Raatikainen, O., Lappalainen, R., and Vepsäläinen, J. (2020) 'Complementary chemical characterization of distillates obtained from industrial hemp hurds by thermal processing', *Industrial Crops and Products*, 155. doi: 10.1016/j.indcrop.2020.112760.

Salleh, M. A. M., Mahmoud, D. K., Karim, W. A. W. A., and Idris, A. (2011) 'Cationic and anionic dye adsorption by agricultural solid wastes: A comprehensive review', *Desalination*, 280(1–3), pp. 1–13. doi: 10.1016/j.desal.2011.07.019.

Sanchez-Salvador, J. L., Balea, A., Monte, M. C., Blanco, A., and Negro, C. (2019) 'Pickering emulsions containing cellulose microfibers produced by mechanical treatments as stabilizer in the food industry', *Applied Sciences*, 9(2). doi: 10.3390/app9020359.

Santmarti, A. and Lee, K. (2018) 'Crystallinity and Thermal Stability of Nanocellulose', in *Nanocellulose and Sustainability: Production, Properties, Applications, and Case Studies*, pp. 67–86. doi: 10.1201/9781351262927-5.

Saratale, R. G., Saratale, G. D., Chang, J. S., and Govindwar, S. P. (2011) 'Bacterial decolorization and degradation of azo dyes: A review', *Journal of the Taiwan Institute of Chemical Engineers*, 42(1), pp. 138–157. doi: 10.1016/j.jtice.2010.06.006.

Sartika, D., Syamsu, K., Warsiki, E., and Fahma, F. (2019) 'Optimization of Sulfuric Acid Concentration and Hydrolysis Time on Crystallinity of Nanocrystalline Cellulose: A Response Surface

Methodology Study', in *IOP Conference Series: Earth and Environmental Science*, pp. 1–9. doi: 10.1088/1755-1315/355/1/012109.

Sawasdee, S., Suwanputa, S., Seesaiya, C., Sritotesporn, S., Tosri, N., Sawangsup, N., Pumpikun, R., and Watcharabundit, P. (2020) 'Application of agricultural waste activated carbon prepared from sugarcane leaves for methyl orange removal in aqueous solution', *Food and Applied Bioscience Journal*, 8(3), pp. 1–18.

Seddiqi, H., Oliaei, E., Honarkar, H., Jin, J., Geonzon, L. C., Bacabac, R. G., and Klein-Nulend, J. (2021) 'Cellulose and its derivatives: towards biomedical applications', *Cellulose*, 28, pp 1893-1931. doi: 10.1007/s10570-020-03674-w.

Sehaqui, H., De Larraya, U. P., Tingaut, P., and Zimmermann, T. (2015) 'Humic acid adsorption onto cationic cellulose nanofibers for bioinspired removal of copper(ii) and a positively charged dye', *Soft Matter*, 11(26), pp. 5294–5300. doi: 10.1039/c5sm00566c.

Sehaqui, H., Mautner, A., De Larraya, U. P., Pfenninger, N., Tingaut, P., and Zimmermann, T. (2016) 'Cationic cellulose nanofibers from waste pulp residues and their nitrate, fluoride, sulphate and phosphate adsorption properties', *Carbohydrate Polymers*, 135, pp. 334–340. doi: 10.1016/j.carbpol.2015.08.091.

Sehaqui, H., Schaufelberger, L., Michen, B., and Zimmermann, T. (2017) 'Humic acid desorption from a positively charged nanocellulose surface', *Journal of Colloid and Interface Science*, 504, pp. 500–506. doi: 10.1016/j.jcis.2017.06.006.

Seta, F. T., An, X., Liu, L., Zhang, H., Yang, J., Zhang, W., Nie, S., Yao, S., Cao, H., Xu, Q., Bu, Y., and Liu, H. (2020) 'Preparation and characterization of high yield cellulose nanocrystals (CNC) derived from ball mill pretreatment and maleic acid hydrolysis', *Carbohydrate Polymers*, 234, pp. 1–9. doi: 10.1016/j.carbpol.2020.115942.

Seta, F. T., An, X. and Liu, H. (2021) 'Solid Acid Hydrolysis for Isolation of Cellulose Nanocrystals and Chitin Nanocrystals – A mini review', *Jurnal Selulosa*, 11(2), pp. 69–88.

Shah, M. P. (2018) 'Azo Dye Removal Technologies', *Austin Journal of Biotechnology and Bioengineering*, 5(1), pp. 1–6.

Shah, S. S., Sharma, T., Dar, B. A., and Bamezai, R. K. (2021) 'Adsorptive removal of methyl orange dye from aqueous solution using populous leaves: Insights from kinetics, thermodynamics and computational studies', *Environmental Chemistry and Ecotoxicology*, 3, pp. 172–181. doi: 10.1016/j.enceco.2021.05.002.

Shaheen, T. I. and Emam, H. E. (2018) 'Sono-chemical synthesis of cellulose nanocrystals from wood sawdust using Acid hydrolysis', *International Journal of Biological Macromolecules*, 107, pp. 1599–1606. doi: 10.1016/j.ijbiomac.2017.10.028.

Shak, K. P. Y., Pang, Y. L. and Mah, S. K. (2018) 'Nanocellulose: Recent advances and its prospects in environmental remediation', *Beilstein Journal of Nanotechnology*, 9(1), pp. 2479–2498. doi: 10.3762/bjnano.9.232.

Shamsabadi, M. A., Behzad, T. and Bagheri, R. (2015) 'Optimization of acid hydrolysis conditions to improve cellulose nanofibers extraction from wheat straw', *Fibers and Polymers*, 16(3), pp. 579–584. doi: 10.1007/s12221-015-0579-7.

Sharma, S. and Kaur, A. (2018) 'Various methods for removal of dyes from industrial effluents - a review', *Indian Journal of Science and Technology*, 11(12), pp. 1–21. doi: 10.17485/ijst/2018/v11i12/120847.

Shelke, B. N., Jopale, M. K. and Kategaonkar, A. H. (2022) 'Exploration of biomass waste as low cost adsorbents for removal of methylene blue dye: A review', *Journal of the Indian Chemical Society*, 99(7), p. 100530. doi: 10.1016/j.jics.2022.100530.

Silva, L. S., Lima, L. C. B., Ferreira, F. J. L., Silva, M. S., Osajima, J. A., Bezerra, R. D.S., and Silva Filho, E. C. (2015) 'Sorption of the anionic reactive red RB dye in cellulose: Assessment of kinetic, thermodynamic, and equilibrium data', *Open Chemistry*, 13(1), pp. 801–812. doi: 10.1515/chem-20150079.

Singla, S., Kaushal, J. and Mahajan, P. (2016) 'Removal of Dyes From Wastewater By Plant Waste', *International journal of Advance Research in Science and Engineering*, 5(3), pp. 228–239.

Sirviö, J., Honka, A., Liimatainen, H., Niinimäki, J., and Osmo, H. (2011) 'Synthesis of highly cationic water-soluble cellulose derivative and its potential as novel biopolymeric flocculation agent', *Carbohydrate Polymers*, 86, pp. 266–270. doi: 10.1016/j.carbpol.2011.04.046.

Sivarajasekar, N. (2015) 'Agriculture waste biomass valorisation for cationic dyes sequestration: A concise review Biosorption of cationic dyes View project Reverse micelles View project', *Journal of Chemical and Pharmaceutical Research*, 7(9), pp. 737–748. Available at: www.jocpr.com.

Solís, M., Solís, A., Pérez, H. I., Manjarrez, N., and Flores, M. (2012) 'Microbial decolouration of azo dyes: A review', *Process Biochemistry*, 47(12), pp. 1723–1748. doi: 10.1016/j.procbio.2012.08.014.

Song, K., Zhu, X., Zhu, W., and Li, X. (2019) 'Preparation and characterization of cellulose nanocrystal extracted from Calotropis procera biomass', *Bioresources and Bioprocessing*, 6(1). doi: 10.1186/s40643-019-0279-z.

Song, Y., Liu, Y., Chen, S., Xu, H., Liao, Y. (2014) 'Sunset Yellow adsorption by peanut husk in batch mode', *Fresenius Environmental Bulletin*, 23(4), pp. 1074–1079.

Song, Y. K., Chew, I. M. L., Choong, T. S. Y., Tan, J., and Tan, K. W. (2016) 'Isolation of Nanocrystalline Cellulose from oil palm empty fruit bunch - A response surface methodology study', *MATEC Web of Conferences*, 60, pp. 1–5. doi: 10.1051/matecconf/20166004009.

Song, Y., Xu, H. and Ren, J. (2015) 'Adsorption study for removal of sunset yellow by ethylenediamine-modified peanut husk', *Desalination and Water Treatment*, pp. 1–8. doi: 10.1080/19443994.2015.1086897.

Soni, B., Hassan, E. B. and Mahmoud, B. (2015) 'Chemical isolation and characterization of different cellulose nanofibers from cotton stalks', *Carbohydrate Polymers*, 134, pp. 581–589. doi: 10.1016/j.carbpol.2015.08.031.

Sonia, A. and Dasan, K. P. (2013) 'Chemical, morphology and thermal evaluation of cellulose microfibers obtained from Hibiscus sabdariffa', *Carbohydrate Polymers*, 92(1), pp. 668–674. doi: 10.1016/j.carbpol.2012.09.015.

Srinivasan, A. and Viraraghavan, T. (2010) 'Decolorization of dye wastewaters by biosorbents: A review', *Journal of Environmental Management*, 91(10), pp. 1915–1929. doi: 10.1016/j.jenvman.2010.05.003.

Stanciu, M. C. and Nichifor, M. (2019) 'Adsorption of anionic dyes on a cationic amphiphilic dextran hydrogel: equilibrium, kinetic, and thermodynamic studies', *Colloid and Polymer Science*, 297(1), pp. 45–57. doi: 10.1007/s00396-018-4439-z.

Strong, E. B., Kirschbaum, C. W., Martinez, A. W., and Martinez, N. W. (2018) 'Paper miniaturization via periodate oxidation of cellulose', *Cellulose*, 25(6), pp. 3211–3217. doi: 10.1007/s10570-018-1805-4.

Subbaiah, M. V. and Kim, D. S. (2016) 'Adsorption of methyl orange from aqueous solution by aminated pumpkin seed powder: Kinetics, isotherms, and thermodynamic studies', *Ecotoxicology and Environmental Safety*, 128, pp. 109–117. doi: 10.1016/j.ecoenv.2016.02.016.

Sujitha, R. and Ravindhranath, K. (2016) 'Removal of Coomassie brilliant blue dye from waste waters using active carbon derived from barks of Ficus racemosa plant', *Der Pharmacia Lettre*, 8(10), pp. 72–83.

Sulyman, M., Namiesnik, J. and Gierak, A. (2017) 'Low-cost adsorbents derived from agricultural byproducts/wastes for enhancing contaminant uptakes from wastewater: A review', *Polish Journal of Environmental Studies*, 26(2), pp. 479–510. doi: 10.15244/pjoes/66769.

Sun, B., Hou, Q., Liu, Z., and Ni, Y. (2015) 'Sodium periodate oxidation of cellulose nanocrystal and its application as a paper wet strength additive', *Cellulose*, 22(2), pp. 1135–1146. doi: 10.1007/s10570015-0575-5.

Sun, D., Zhang, X., Wu, Y., and Liu, T. (2013) 'Kinetic mechanism of competitive adsorption of disperse dye and anionic dye on fly ash', *International Journal of Environmental Science and Technology*, 10(4), pp. 799–808. doi: 10.1007/s13762-012-0130-y.

Suwattanamala, R., Prachuabmorn, A. and Suwattanamala, A. (2021) 'Application of Carbonized Mangosteen Peel As Low - Cost Biosorbent in Removing Hair Dye From Aqueous Solution', *Suranaree J. Sci. Technol.* 29(3). pp. 1–9.

Szymańska-Chargot, M., Cieśla, J., Chylińska, M., Gdula, K., Pieczywek, P. M., Kozioł, A., Cieślak, K. J., and Zdunek, A. (2018) 'Effect of ultrasonication on physicochemical properties of apple based nanocellulose-calcium carbonate composites', *Cellulose*, 25(8), pp. 4603–4621. doi: 10.1007/s10570018-1900-6.

Szymańska-Chargot, M., Cieśla, J., Pękala, P., Pieczywek, P. M., Żyła, M., Oleszek, W., Szkopek, Z., and Zdunek, A. (2022) 'The Influence of High-Intensity Ultrasonication on Properties of Cellulose Produced from the Hop Stems , the Byproduct of the Hop Cones Production', *Molecules*, 27, pp. 1–14.

Taha, N. D., Samaka, S. I. and Mohammed, L. A. (2013) 'Adsorptive removal of dye from industrial effluents using natural Iraqi palygors-kite clay as low-cost adsorbent', *Journal of Asian Scientific Research*, 3(9), pp. 945–955.

Tang, Y., Yang, S., Zhang, N., and Zhang, J. (2014) 'Preparation and characterization of nanocrystalline cellulose via low-intensity ultrasonic-assisted sulfuric acid hydrolysis', *Cellulose*, 21(1), pp. 335–346. doi: 10.1007/s10570-013-0158-2.

Tang, Z., Li, W., Lin, X., Xiao, H., Miao, Q., Huang, L., Chen, L., and Wu, H. (2017) 'TEMPOOxidized cellulose with high degree of oxidation', *Polymers*, 9(9), pp. 3–4. doi:

10.3390/polym9090421.

Tanpichai, S., Witayakran, S. and Boonmahitthisud, A. (2019) 'Study on structural and thermal properties of cellulose microfibers isolated from pineapple leaves using steam explosion', *Journal of Environmental Chemical Engineering*, 7(1), p. 102836. doi: 10.1016/j.jece.2018.102836.

Tao, P., Zhang, Y., Wu, Z., Liao, X., and Nie, S. (2019) 'Enzymatic pretreatment for cellulose nanofibrils isolation from bagasse pulp: Transition of cellulose crystal structure', *Carbohydrate Polymers*, 214, pp. 1–7. doi: 10.1016/j.carbpol.2019.03.012.

Tarasov, D., Leitch, M. and Fatehi, P. (2018) 'Lignin-carbohydrate complexes: Properties, applications, analyses, and methods of extraction: A review', *Biotechnology for Biofuels*, 11(1), pp. 1–28. doi: 10.1186/s13068-018-1262-1.

Tavakolian, M., Jafari, S.M., and van de Ven, T. G. M. (2020) 'A Review on Surface - Functionalized Cellulosic Nanostructures as Biocompatible Antibacterial Materials', *Nano-Micro Letters*, 12(73), pp. 1–23. doi: 10.1007/s40820-020-0408-4.

Tejada-Tovar, C., Villabona-Ortíz, Á. and Gonzalez-Delgado, Á. D. (2021) 'Adsorption of azo-anionic dyes in a solution using modified coconut (Cocos nucifera) mesocarp: Kinetic and equilibrium study', *Water* , 13(10). doi: 10.3390/w13101382.

Thang, N.H., Khang, D.S., Hai, T.D., Nga, D.T., and Tuanb, P.D. (2021) 'Methylene blue adsorption mechanism of activated carbon synthesised from cashew nut shells', *RSC Advances*, 11(43), pp. 26563–26570. doi: 10.1039/d1ra04672a.

Tibolla, H., Pelissari, F. M., Rodrigues, M. I., and Menegalli, F. C. (2017) 'Cellulose nanofibers produced from banana peel by enzymatic treatment: Study of process conditions', *Industrial Crops and Products*, 95, pp. 664–674. doi: 10.1016/j.indcrop.2016.11.035.

Tibolla, H., Pelissari, F. M., Martins, J. T., Vicente, A. A., and Menegalli, F. C. (2018) 'Cellulose nanofibers produced from banana peel by chemical and mechanical treatments: Characterization and cytotoxicity assessment', *Food Hydrocolloids*, 75, pp. 192–201. doi: 10.1016/j.foodhyd.2017.08.027.

Tibolla, H., Pelissari, F. M. and Menegalli, F. C. (2014) 'Cellulose nanofibers produced from banana peel by chemical and enzymatic treatment', *LWT - Food Science and Technology*, 59, pp. 1311–1318. doi: 10.1016/j.lwt.2014.04.011.

An Tran, T.T., Duong, H. T. L., Pham, T. T. P., Nguyen, T., Nguyen, T.D., and An Tran B. (2021) 'Preparation of Magnetic Composite Polyaniline / Fe_3O_4 − Hydrotalcite and Performance in Removal of Methyl Orange', *Adsorption Science and Technology*, 2021, pp. 1–18.

Ugwu, S. N., Umuokoro, A. F., Echiegu, E. A., Ugwuishiwu, B. O., and Enweremadu, C. C. (2017) 'Comparative study of the use of natural and artificial coagulants for the treatment of sullage (domestic wastewater)', *Cogent Engineering*, 4(1). doi: 10.1080/23311916.2017.1365676.

Van-Pham, D.T., Pham, T. Y. N., Tran, M.C., Nguyen, C. N., and Miyata, Q. T. C. (2020) 'Extraction of thermally stable cellulose nanocrystals in short processing time from waste newspaper by conventional acid hydrolysis', *Materials Research Express*, 7, pp 1-12. https://doi.org/10.1088/20531591/ab9668.

Väisänen, T., Batello, P., Lappalainen, R., and Tomppo, L. (2018) 'Modification of hemp fibers (Cannabis Sativa L.) for composite applications', *Industrial Crops and Products*, 111, pp. 422–429. doi: 10.1016/j.indcrop.2017.10.049.

Veeramachineni, A. K., Sathasivam, T., Muniyandy, S., Janarthanan, P., Langford, S. J., and Yan, L.Y. (2016) 'Optimizing extraction of cellulose and synthesizing pharmaceutical grade carboxymethyl sago cellulose from Malaysian sago pulp', *Applied Sciences (Switzerland)*, 6(6). doi: 10.3390/app6060170.

Veni, V. K. and Brenda, T. H. (2021) 'Preparation of raw oyster shell for removal of coomassie brilliant blue R-250 dye from aqueous solution', in *IOP Conference Series: Earth and Environmental Science*, pp. 1–8. doi: 10.1088/1755-1315/765/1/012039.

Vincent, S. and Kandasubramanian, B. (2021) 'Cellulose nanocrystals from agricultural resources : Extraction and functionalisation', *European Polymer Journal*, 160, p. 110789. doi: 10.1016/j.eurpolymj.2021.110789.

Vincenzo Naddeo, A. C. (2013) 'Wastewater Treatment by Combination of Advanced Oxidation Processes and Conventional Biological Systems', *Journal of Bioremediation and Biodegradation*, 04(08). doi: 10.4172/2155-6199.1000208.

Vinoth, M., Lim, H.Y., Xavier, R., Marimuthu, K., Sreeramanan, S., Mas Rosemal, H.M.H., and Kathiresan, S. (2010) 'Removal of Methyl Orange from Solutions using Yam Leaf Fibers', *International Journal of ChemTech Research*, 2(4), pp. 1892–1900.

Wan, Y., Liu, X., Liu, P., Zhao, L., and Zou, W. (2018) 'Optimization adsorption of norfloxacin onto polydopamine microspheres from aqueous solution: Kinetic, equilibrium and adsorption mechanism studies', *Science of the Total Environment*, 639, pp. 428–437. doi: 10.1016/j.scitotenv.2018.05.171.

Wang, D. (2019) 'A critical review of cellulose-based nanomaterials for water purification in industrial processes', *Cellulose*, 26(2), pp. 687–701. doi: 10.1007/s10570-018-2143-2.

Wang, J., Wang, Q., Wu, Y., Bai, F., Wang, H., Si, S., Lu, Y., Li, X., and Wang, S. (2020) 'Preparation of cellulose nanofibers from bagasse by phosphoric acid and hydrogen peroxide enables fibrillation via a swelling, hydrolysis, and oxidation cooperative mechanism', *Nanomaterials*, 10(11), pp. 1–15. doi: 10.3390/nano10112227.

Wang, J., Tavakoli, J. and Tang, Y. (2019) 'Bacterial cellulose production, properties and applications with different culture methods – A review', *Carbohydrate Polymers*, 219, pp. 63–76. doi: 10.1016/j.carbpol.2019.05.008.

Wang, R., Chen, L., Zhu, J. Y., and Yang, R. (2017a) 'Tailored and integrated production of carboxylated cellulose nanocrystals (CNC) with nanofibrils (CNF) through maleic acid hydrolysis', *ChemNanoMat*, 3(5), pp. 328–335. doi: 10.1002/cnma.201700015.

Wang, S., Wang, F., Song, Z., Song, X., Yang, X., and Wang, Q. (2019) 'Preparation of cellulose nanocrystals using highly recyclable organic acid treated softwood pulp', *BioResources*, 14(4), pp. 9331–9351. doi: 10.15376/biores.14.4.9331-9351.

Wang, Y., Wei, X., Li, J., Wang, F., Wang, Q., Chen, J., and Kong, Lingxue. (2015) 'Study on nanocellulose by high pressure homogenization in homogeneous isolation', *Fibers and Polymers*, 16(3), pp. 572–578. doi: 10.1007/s12221-015-0572-1.

Wang, Y., Zhao, L., Peng, H., Wu, J., Liu, Z., and Guo, X. (2016) 'Removal of Anionic Dyes from Aqueous Solutions by Cellulose-Based Adsorbents: Equilibrium, Kinetics, and Thermodynamics', *Journal of Chemical and Engineering Data*, 61(9), pp. 3266–3276. doi: 10.1021/acs.jced.6b00340.

Wang, Y., Wei, X., Li, J., Wang, F., Wang, Q., Zhang, Y., and Kong, L. (2017b) 'Homogeneous isolation of nanocellulose from eucalyptus pulp by high pressure homogenization', *Industrial Crops and Products*, 104, pp. 237–241. doi: 10.1016/j.indcrop.2017.04.032.

Wang, Y., Zhao, L., Hou, J., Peng, H., Wu, J., Liu, Z., and Guo, X. (2018) 'Kinetic, isotherm, and thermodynamic studies of the adsorption of dyes from aqueous solution by cellulose-based adsorbents', *Water Science and Technology*, 77(11), pp. 2699–2708. doi: 10.2166/wst.2018.229.

Wawrzkiewicz, M. (2011) 'Sorption of Sunset Yellow dye by weak base anion exchanger-kinetic and equilibrium studies', *Environmental Technology*, 32(4), pp. 455–465. doi: 10.1080/09593330.2010.502188.

Weglarz-Tomczak, E. and Górecki, Ł. (2012) 'Azo dyes - Biological activity and synthetic strategy', *Chemik*, 66(12), pp. 1298–1307.

Wijaya, C. J., Ismadji, S., Aparamarta, H. W., and Gunawan, S. (2019) 'Optimization of cellulose nanocrystals from bamboo shoots using Response Surface Methodology', *Heliyon*, 5(11), pp. 1–7. doi: 10.1016/j.heliyon.2019.e02807.

Willberg-Keyriläinen, P., Pitkänen, P., Hulkko, J., Asikainen, M., and Setälä, H. (2019) 'The effect of mixing and consistency on cellulose cationization', *Heliyon*, 5(3), pp. 1–15. doi: 10.1016/j.heliyon.2019.e01349.

Willberg-Keyriläinen, P. and Ropponen, J. (2019) 'Evaluation of esterification routes for long chain cellulose esters', *Heliyon*, 5(11). doi: 10.1016/j.heliyon.2019.e02898.

Wong, S., Ghafar, N. A., Ngadi, N., Razmi, F. A., Inuwa, I. M., Mat, R., and Amin, N. A. S. (2020) 'Effective removal of anionic textile dyes using adsorbent synthesized from coffee waste', *Scientific Reports*, 10(1), pp. 1–13. doi: 10.1038/s41598-020-60021-6.

Wu, C., Julian, D., He, M., Zheng, L., Tian, T., Teng, F., and Li, Y. (2021a) 'Preparation and characterization of okara nanocellulose fabricated using sonication or high-pressure homogenization treatments', *Carbohydrate Polymers*, 255, p. 117364. doi: 10.1016/j.carbpol.2020.117364.

Wu, J., Du, X., Yin, Z., Xu, S., Xu, S., and Zhang, Y. (2019) 'Preparation and characterization of cellulose nanofibrils from coconut coir fibers and their reinforcements in biodegradable composite films', *Carbohydrate Polymers*, 211, pp. 49–56. doi: 10.1016/j.carbpol.2019.01.093.

Wu, L., Liu, X., Lv, G., Zhu, R., Tian, L., Liu, M., Li, Y., Rao, W., Liu, T., and Liao, L. (2021b) 'Study on the adsorption properties of methyl orange by natural one-dimensional nano-mineral materials with different structures', *Scientific Reports*, 11(1), pp. 1–11. doi: 10.1038/s41598-021-90235-1.

Wulandari, W. T., Rochliadi, A. and Arcana, I. M. (2016) 'Nanocellulose prepared by acid hydrolysis of isolated cellulose from sugarcane bagasse', *IOP Conference Series: Materials Science and Engineering*, 107(1). doi: 10.1088/1757-899X/107/1/012045.

Xie, H., Du, H., Yang, X., and Si, C. (2018) 'Recent Strategies in Preparation of Cellulose Nanocrystals and Cellulose Nanofibrils Derived from Raw Cellulose Materials', *International Journal of Polymer Science*, pp. 1–25. doi: 10.1155/2018/7923068.

Xie, J., Hse, C., De Hoop, C. F., Hu, T., Qi, J., and Shupe, T. F. (2016) 'Isolation and characterization of cellulose nanofibers from bamboo using microwave liquefaction combined with chemical treatment and ultrasonication', *Carbohydrate Polymers*, 151, pp. 725–734. doi: 10.1016/j.carbpol.2016.06.011.

Xu, J., Krietemeyer, E. F., Boddu, V. M., Liu, S. X., and Liu, W. C. (2018) 'Production and characterization of cellulose nanofibril (CNF) from agricultural waste corn stover', *Carbohydrate Polymers*, 192, pp. 202–207. doi: 10.1016/j.carbpol.2018.03.017.

Xu, Y., Salmi, J., Kloser, E., Perrin, F., Grosse, S., Denault, J., and Lau, P. C. K. (2013) 'Feasibility of nanocrystalline cellulose production by endoglucanase treatment of natural bast fibers', *Industrial Crops and Products*, 51, pp. 381–384. doi: 10.1016/j.indcrop.2013.09.029.

Yadav, A., Vardhan, R., Prakash, C., Kumar, P., and Kumar, V. (2022) 'Physicochemical and Engineering Aspects Experimental study and numerical optimization for removal of methyl orange using polytetrafluoroethylene membranes in vacuum membrane distillation process', *Colloids and Surfaces A: Physicochemical and Engineering Aspects*, 635, p. 128070. doi: 10.1016/j.colsurfa.2021.128070.

Yang, H., Chen, D. and van de Ven, T. G. M. (2015) ‘Preparation and characterization of sterically stabilized nanocrystalline cellulose obtained by periodate oxidation of cellulose fibers’, *Cellulose*, 22(3), pp. 1743–1752. doi: 10.1007/s10570-015-0584-4.

Yang, X., Han, F., Xu, C., Jiang, S., Huang, L., Liu, L., and Xia, Z. (2017) ‘Effects of preparation methods on the morphology and properties of nanocellulose (NC) extracted from corn husk’, *Industrial Crops and Products*, 109, pp. 241–247. doi: 10.1016/j.indcrop.2017.08.032.

Yang, Y., Chen, Z., Zhang, J., Wang, G., Zhang, R., and Suo, D. (2019) ‘Preparation and Applications of the Cellulose Nanocrystal’, *International Journal of Polymer Science*, 2019. doi: 10.1155/2019/1767028.

Yayayürük, O., Erdem, A., Özmen, P., and Karagöz, B. (2020) ‘PDMAEMA grafted microspheres as an efficient adsorbent for the removal of Sunset yellow from pharmaceutical preparations , beverages and waste water’, *European Polymer Journal*, 141, p. 110089. doi: 10.1016/j.eurpolymj.2020.110089.

Yeganeh, F., Behrooz, R. and Rahimi, M. (2017) ‘The effect of Sulfuric acid and Maleic acid on characteristics of nano-cellulose produced from waste office paper’, *International Journal of Nano Dimension* , 8(3), pp. 206–215.

Yi, T., Zhao, H., Mo, Q., Pan, D., Liu, Y., Huang, L., Xu, H., Hu, B., and Song, H. (2020) ' From Cellulose to Cellulose Nanofibrils—A Comprehensive Review of the Preparation and Modification of Cellulose Nanofibril', *Materials*. 13(22), pp 1-32. doi: 10.3390/ma13225062.

Yin, J. and Deng, B. (2015) ‘Polymer-matrix nanocomposite membranes for water treatment’, *Journal of Membrane Science*, 479, pp. 256–275. doi: 10.1016/j.memsci.2014.11.019.

Yinghua, S., Rong, P., Lili, G., and Mei, Y. (2021) ‘Removal of sunset yellow by methanol modified walnut shell’, *Iranian Journal of Chemistry and Chemical Engineering*, 40(4), pp. 1095–1104. doi: 10.30492/ijcce.2020.101424.3429.

Yu, Y., Qiao, N., Wang, D., Zhu, Q., Fu, F., Cao, R., Wang, R., Liu, W., and Xu, B. (2019) ‘Fluffy honeycomb-like activated carbon from popcorn with high surface area and well-developed porosity for ultra-high efficiency adsorption of organic dyes’, *Bioresource Technology*, 285, p. 121340. doi: 10.1016/j.biortech.2019.121340.

Yue, X., Huang, J., Jiang, F., Lin, H., and Chen, Y. (2019) ‘Synthesis and characterization of cellulosebased adsorbent for removal of anionic and cationic dyes’, *Journal of Engineered Fibers and Fabrics*, 14. doi: 10.1177/1558925019828194.

Zaman, M., Xiao, H., Chibante, F., and Ni, Y. (2012) 'Synthesis and characterization of cationically modified nanocrystalline cellulose', *Carbohydrate Polymers*, 89(1), pp. 163–170. doi: 10.1016/j.carbpol.2012.02.066.

Zhang, C., Chen, H., Xue, G., Liu, Y., Chen, S., and Jia, C. (2021) 'A critical review of the aniline transformation fate in azo dye wastewater treatment', *Journal of Cleaner Production*, 321, p. 128971. doi: 10.1016/j.jclepro.2021.128971.

Zhang, H., Luan, Q., Tang, H., Huang, F., Zheng, M., Deng, Q., Xiang, X., Yang, C., Shi, J., Zheng, C., and Zhou, Q. (2017) 'Removal of methyl orange from aqueous solutions by adsorption on cellulose hydrogel assisted with Fe_2O_3 nanoparticles', *Cellulose*, 24(2), pp. 903–914. doi: 10.1007/s10570-0161129-1.

Zhang, H.; Chen, Y.; Wang, S.; Ma, L.; Yu, Y.; Dai, H.; Zhang, Y. (2020a) 'Extraction and comparison of cellulose nanocrystals from lemon (Citrus limon) seeds using sulfuric acid hydrolysis and oxidation methods', *Carbohydrate Polymers*, 238(2), p. 116180. doi: 10.1016/j.carbpol.2020.116180.

Zhang, K., Zhang, Y., Yan, D., Zhang, C., and Nie, S. (2018a) 'Enzyme-assisted mechanical production of cellulose nanofibrils: thermal stability', *Cellulose*, 25(9), pp. 5049–5061. doi: 10.1007/s10570-0181928-7.

Zhang, L., Sellaoui, L., Franco, D., Dotto, G. L., Bajahzar, A., Belmabrouk, H., Bonilla-Petriciolet, A., Oliveira, Marcos L. S., and Li, Z. (2020b) 'Adsorption of dyes brilliant blue, sunset yellow and tartrazine from aqueous solution on chitosan: Analytical interpretation via multilayer statistical physics model', *Chemical Engineering Journal*, 382. doi: 10.1016/j.cej.2019.122952.

Zhao, J., Zhang, W., Zhang, X., Zhang, X., Lu, C., and Deng, Y. (2013) 'Extraction of cellulose nanofibrils from dry softwood pulp using high shear homogenization', *Carbohydrate Polymers*, 97(2), pp. 695–702. doi: 10.1016/j.carbpol.2013.05.050.

Zhao, Y. and Li, J. (2014) 'Excellent chemical and material cellulose from tunicates: Diversity in cellulose production yield and chemical and morphological structures from different tunicate species', *Cellulose*, 21(5), pp. 3427–3441. doi: 10.1007/s10570-014-0348-6.

Zheng, D., Zhang, Y., Guo, Y., and Yue, J. (2019) 'Isolation and Characterization of Nanocellulose with a Novel Shape from Walnut (Juglans Regia L.) Shell Agricultural Waste', *Polymers*, 11, p. 1130.

Zimmermann, M. V. G., Borsoi, C., Lavoratti, A., Zanini, M., Zattera, A. J., and Santana, R. M.C.

(2016) ‘Drying techniques applied to cellulose nanofibers’, *Journal of Reinforced Plastics and Composites*, 35(8), pp. 682–697. doi: 10.1177/0731684415626286.

CHAPTER 3: RESEARCH METHODOLOGY

3.1 Chemicals

Corn husk fibres supplied from Johannesburg Street vendors, hemp stem and branch fibres were obtained locally. All chemicals used were of analytical grade. Sulfuric acid (H_2SO_4), formic acid (CH_2O_2), maleic acid ($C_4H_4O_4$), sunset yellow FCF ($C_{16}H_9AlN_2O_7S_2$; Mw = 452.37 g/mol) and Methyl orange ($C_{14}H_{14}N_3NaO_3S$, Mw = 327.34), Glycidyl trimethylammonium chloride (GTMAC; $C_6H_{14}ClNO$, > 90 wt % in H_2O, Mw = 151.63 g/mol) and Tetrahydrofuran (THF, 99.5 % purity) were acquired from Merck, Sigma-Aldrich, Germany. Hydrochloric acid (HCl, 32 %), sodium hydroxide (NaOH), sodium chlorite ($NaClO_2$), glacial acetic acid (CH_3COOH) was acquired from Ace Chemicals, South Africa. Solutions of required lower concentrations were prepared by diluting the stock solutions. The pH of the solutions was adjusted using 0.1 mol L^{-1} HCl and/or 0.1 mol L^{-1} NaOH solutions. All solutions were prepared with double deionised water. Glassware and polypropylene vials were washed, soaked in a 1 M HNO_3 acid bath for at least 24 hr., and rinsed with deionised water before use.

3.2 Equipment

For all mass measurements, an analytical balance with up to 4 decimal places and 220 g capacity supplied by OHAUS (Johannesburg, South Africa) was used. Deionised water was obtained from a Millipore water system (Massachusetts, USA). pH measurements were performed on a Five easy FE20 pH meter (Mettler Toledo, Johannesburg, South Africa). Batch adsorption experiments were performed in triplicate on a room temperature Labcon electrical shaker (Johannesburg, South Africa) and temperature sensitive BIOASE electrical shaker (Johannesburg, South Africa). Cellulose microfibre samples were freeze-dried in an LABCONCO freeze dryer for several days. Cellulose samples were dried in an Wisecube air-circulating oven (Johannesburg, South Africa). Acid washing experiments and adsorbent-adsorbate separations were achieved using the Eppendorf centrifuge (Johannesburg, South Africa). To homogenize the sample the Scilogex D500 homogenizer (Johannesburg, South Africa) was used. Scanning electron microscopy (SEM, Jeol JSM IT300, Tokyo, Japan) at an acceleration voltage of 10 kV was used to examine the morphology of the cellulose derived samples. Before analysis, the samples were coated with 5 µm gold in an SCD 005 Cool Sputter Coater (BalTec, Germany) at a current of 25 µA applied for 50 s. Fourier Transform Infrared (FTIR) spectroscopy was used to study the surface chemical functional groups in cellulose derived samples. FTIR spectroscopy was performed on a Tensor 27 Infrared Spectrometer (Massachusetts, USA). The spectra were collected in the range 500 – 4500 cm^{-1} in the absorption mode.

Thermal stability of the fibres was determined on a thermal analyser (STA 6000; Perkin Elmer, United states). Approximately 10 mg of the fibre samples were weighed and placed in an alumina crucible to

be evaluated at heating temperatures between 35℃ to 900℃. All measurements were carried out at a heating rate of 10 ℃ min^{-1} in nitrogen gas, at a flow rate of 20 mL min^{-1}. The loss of weight was obtained from the TGA curve of a plot of weight loss (%) versus temperature (℃). X-ray diffraction (XRD) patterns were obtained to determine the crystallinity of the cellulose derived samples. XRD patterns of CMFs were collected on a Bruker D2 phase diffractometer (Massachusetts, USA) with a Cu-Kα (λ= 0.154 nm) radiation source fitted with a LynxEye detector, using a 30 kV X-ray tube at a current of 30 mA. The scan range was $5\ ^\circ \leq 2\theta \leq 90\ ^\circ$ in a 0.02 ° measurement step. The crystallinity of the fibres was determined by applying Segal's equation (3.1) (Segal *et al.*, 1959).

$$\text{CrI}\ (\%) = \frac{I_{200} - I_{am}}{I_{200}} \times 100\% \qquad (3.1)$$

where I_{200} represents the crystalline peak corresponding to the intensity at about 22.5°, and I_{am} represents the amorphous peak corresponding to the intensity at approximately between 14-18°.

Quantitative determination of methyl orange and sunset yellow concentrations in the aqueous medium was carried out using a Cary Series UV-vis Spectrophotometer (Agilent Technologies, United States). UV-vis analysis of methyl orange and sunset yellow were determined at the wavelength of 465 nm and 485 nm, respectively.

3.3 References

Segal, L., Creely, J. J., Martin, A. E., and Conrad, C. M. (1959) 'An Empirical Method for Estimating the Degree of Crystallinity of Native Cellulose Using the X-Ray Diffractometer', *Textile Research Journal*, 29(10), pp. 786–794. doi: 10.1177/004051755902901003.

CHAPTER 4: CHEMICALLY TREATED CELLULOSE AND ITS CELLULOSE MICROFIBRES FROM HEMP FIBRES: ISOLATION AND CHARACTERISATION

4.1 Introduction

Agricultural biomass is increasingly recognized as a valuable source of cellulose due to the low lignin content and the wide range of plant sources. With an estimated global annual production of 214×10^3 tonnes, hemp (*Cannabis sativa L.*) is one of the most cultivated industrial crops from which fibrous (bast) fibres and granular fibres can be extracted (Morin-Crini *et al.*, 2018). Hemp bast fibres comprise approximately 76% cellulose, 14% hemicellulose, 5% lignin, 1% pectin, and 6% of other non-cellulosic substances (Väisänen *et al.*, 2018)(Salami *et al.*, 2020). The use of hemp fibres as an alternative to synthetic fibres for reinforcement of polymer composites is of interest because hemp fibres are lower in cost, renewable, biodegradable, and environmentally friendly (Abraham, Wong and Puri, 2016)(Jarabo *et al.*, 2012)(Pejić *et al.*, 2020). Hemp fibres also have applications in paper processing, medicine, cosmetics, pharmaceuticals, food manufacturing, detergent and bio-composites (Salami *et al.*, 2020)(Jarabo *et al.*, 2012)(Kassab *et al.*, 2020).

Micro- and nano-cellulose materials can be extracted by chemical and mechanical methods. Cellulose microfibres with diameters of 10 μm and several micrometres in length have been obtained using chemical, mechanical or a combination of both processes (Tanpichai, Witayakran and Boonmahitthisud, 2019)(Reddy *et al.*, 2016)(Elanthikkal *et al.*, 2010). Acid hydrolysis breaks the glycosidic bonds of the crystalline regions and amorphous regions of cellulose (Wang *et al.*, 2019)(Frost and Johan Foster, 2020). This can be achieved by using a variety of organic and mineral acids including sulfuric acid (Elanthikkal *et al.*, 2010), hydrochloric acid, phosphoric acid (Sherif, Gadalla and Kamel, 2021), hydrobromic acid, or mixtures of different acids (Rehman *et al.*, 2018). CNFs, on the other hand, have been extracted using mechanical treatment; ultrasonic treatment, cryo-crushing, and high-pressure homogenisation to produce fibres of diameter ranging from 10 – 100 nm and lengths up to several microns (Du *et al.*, 2017). However, for some applications including water treatment, there is evidence suggesting that it may not be necessary to process cellulose all the way to the nanoscale. Chen *et al,* (Chen *et al.*, 2019), calculated a maximum adsorption of As(III) as 344.82 and 357.14 mg g^{-1}, for nanofibrillated and microfibrillated cellulose, respectively. Periodate oxidation resulted in functionalisation of a large surface area within the fibres, providing high surface areas for adsorption. Finding more sustainable green approaches for the extraction and purification of cellulose is also a matter of increasing concern for upholding the sustainability credentials of cellulose-derived materials. These studies suggest that the properties of cellulose microfibres are influenced by hydrolysis conditions where various parameters can be optimised to obtain fibres with desired properties. The aim of this study was to investigate the extraction and synthesis of cellulose microfibres with high crystallinity index from hemp bast fibres. To our knowledge, no studies have compared the performance

of the selected acids (sulfuric, maleic, and formic acids) in the extraction of CMFs. Thus, this study presents an opportunity for comparing the chemical and physical properties of CMFs produced from organic and mineral acids.

4.2 Methods

4.2.1 Extraction and purification of cellulose

Cellulose fibres were extracted from dried stems and branches of Cannabis sativa plants (Figure 4.1). The stems and branches were soaked in water overnight and the fibres peeled off the woody cores. Dried hemp fibres were treated with 4 wt% NaOH at 80℃ for 2 hr, 3 times. Treated cellulose were bleached using equal parts of $NaClO_2$ (1.7 wt%) and acetate buffer (pH 4.8) for 1 hr at 100℃, and this was done until fibres were white in colour. The bleaching solution was disposed, fibres were washed with ultrapure distilled water and dried before further use in experiments.

4.2.2 Synthesis of cellulose microfibres

CMFs were extracted from bleached cellulose fibres via acid hydrolysis using different types of acids (sulfuric acid, formic acid, maleic acid) and different hydrolysis conditions determined through RSM design summarised in

Experiment 1 involved the use of 45% H_2SO_4 with 20 mL g^{-1} of cellulose fibre. The hydrolysis process was conducted by heating the suspension to 45℃ for 30 min under constant mechanical stirring. Cold distilled water was added to the reaction vessel by 10-fold dilution to stop the hydrolysis reaction. After the hydrolysis reaction, the suspension was washed by centrifuging for 20 min at 7800 rpm to remove excess acid. This cycle was repeated several times by washing with distilled water until pH 7. Using a Scilogex D500 homogenizer, the samples were homogenised for 10 min at a medium speed then it was stored in a freezer, freeze-dried for several days, and later characterised as demonstrated in Figure 4.1. The rest of the experimental conditions conducted were followed according to Table 5.1.

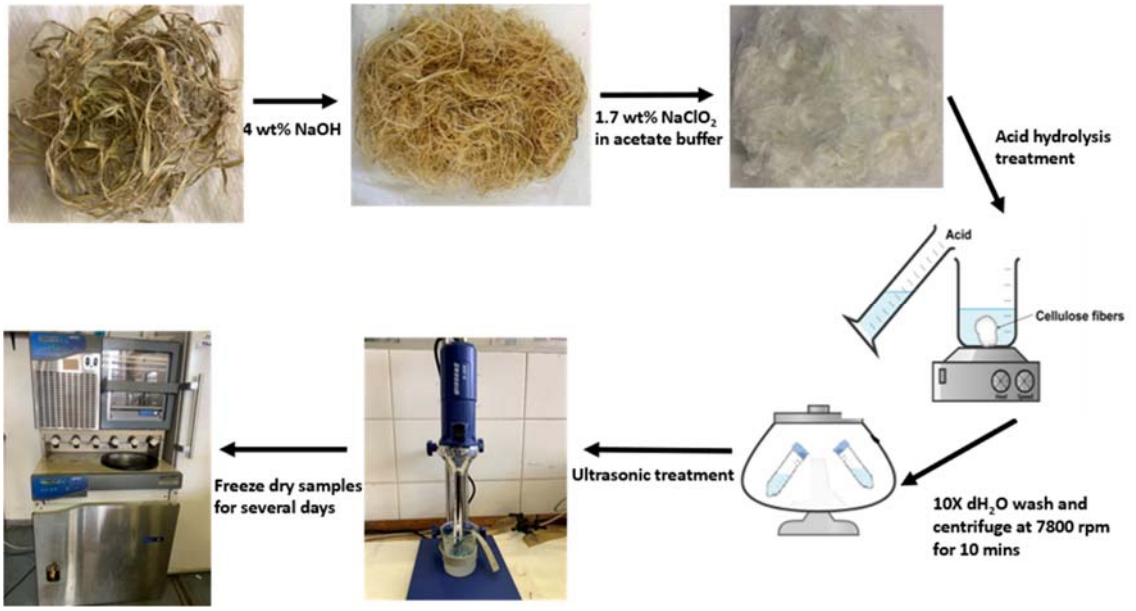

Figure 4.1: Schematic showing extraction and preparation of cellulose microfibres from hemp bast fibres through acid hydrolysis process coupled with ultrasonic treatment.

4.3 Results and discussion

In this work, various acids (sulfuric acid, maleic acid, and formic acid) were used for the synthesis of cellulose microfibres at different acid concentrations, hydrolysis time and temperatures.

4.3.1. Pretreatment of cellulose

According to Figure 4.2, cellulose fibres were extracted from hemp bast fibres using a series of pretreatment procedures, including an alkali treatment step and a bleaching treatment step. Hemp bast fibres were subjected to alkaline treatment (4 wt% NaOH) to aid the removal of hemicellulose and other noncellulosic content from the fibres, resulting in brown hemp fibres (Abiaziem *et al.*, 2020)(Malucelli *et al.*, 2019). This process was achieved by three subsequent alkaline treatment rounds to help reduce any non-cellulosic content. Jiang *et al*, studied the effects of various concentrations of alkali treatments and found that 3 wt% NaOH was effective in the removal of non-cellulosic material (Jiang and Hsieh, 2015) Furthermore, lignin removal was achieved after several rounds of bleaching using a bleaching agent, 1.7% sodium chlorite ($NaClO_2$) in acetate buffer with 1 hr duration rounds to remove any hemicellulose and lignin content resulting a white cellulose fibres (Abiaziem *et al.*, 2020)(Ilyas, Sapuan and Ishak, 2018). Similar reported were recorded from previous studies from cellulose extracted from *Helicteres isora* plant (Chirayil *et al.*, 2014), bamboo plant (Xie *et al.*, 2016), and banana peels (Pelissari, Sobral and Menegalli, 2014). The alkaline and bleaching treatment improved the surface area of hemp bast fibres to make polysaccharides more accessible to acid hydrolysis reactions.

4.3.2 Acid hydrolysis followed by ultrasonic treatment

Acid hydrolysis process was performed using sulfuric acid, formic acid, and maleic acid to produce CMFs with various physical and chemical characteristics. Sulfuric acid (pKa -3.0) is a strong mineral acid commonly used to isolate CNCs and CNFs from natural plant sources. As shown in Figure 4.2a, during sulfuric acid hydrolysis, the typical mechanism of hydrolysis is that the hydrogen ions (-OH) of cellulose are converted to negatively charged sulfate ions ($-OSO_3H$) thereby weakening amorphous regions. This process breaks down the β-1,4-glycosidic linkages between the anhydroglucose units (AGU) and preserves the crystalline regions of cellulose (Jiang and Hsieh, 2015)(Wulandari, Rochliadi and Arcana, 2016). This type of hydrolysis strongly depends on the acid concentration, hydrolysis time, temperature, and acid: cellulose ratio. It was observed that for 1SA- CMFs and 2SA- CMFs reactions, a white suspension was formed during the hydrolysis process. For 3SA- CMFs, after addition of acid, the fibres and acid suspension turned light brown due to high temperature. This later changed color to a white suspension during distilled water washing with successive centrifugation. For 4SA- CMFs ,5SA- CMFs and 6SA- CMFs resulted in a black-dark brown suspension. These changed can be attributed to partial-complete digestion of cellulose fibres due to increased acid concentration, longer hydrolysis time and higher reaction temperature. Similar observations were reported by Leite *et al*, investigating isolation and characterisation of CNFs from cassava root bagasse and peelings via acid hydrolysis treatment (Leite, Zanon and Menegalli, 2017). Sulfuric acid concentration range was 30-50%, the hydrolysis time range 30-90 min and the reaction temperatures were maintained at 60℃. It was observed that higher acid concentrations and longer hydrolysis resulted in dark brown suspension due to carbonisation of cellulose fibres during hydrolysis process.

Weak organic acids such as formic acid (pKa 3.77) and maleic acid have also been used for acid hydrolysis process and Figure 4.2b and c, represent formic acid and maleic acid hydrolysis, respectively. Isolation of formic acid hydrolysed CMFs from bleached cellulose formed white colloidal suspension before freezing into white fibres. From the observed reactions, through variations of acid concentration, hydrolysis time and temperature, no significant changes were observed with the naked eye. During formic acid hydrolysis, the amorphous regions of cellulose can be digested to form nanosized fibres with a large surface area, however, a secondary process can result in the formation of cellulose formate (bin Jumhuri *et al.*, 2017)(Du, Liu, Zhang, *et al.*, 2016). As shown in Figure 4.2c, maleic acid hydrolysis can be expected to react with exposed hydrogen ions (-OH) of the cellulose chain to form carboxyl groups on the CMFs surface. No visible changes were observed through the naked eye during hydrolysis at various acid concentrations, hydrolysis time and temperature. During the acid hydrolysis process (Figure 4.2c), maleic acid has three functions:1) maleic acid molecules react with β-1,4-glycosidic linkages between AGU in cellulose chains and release cellulose with small and uniform particle size; 2) maleic acid can hydrolyse the amorphous regions to release the crystalline regions of cellulose; and

3) maleic acid can catalyze cellulose molecules through the esterification process of hydroxyl groups (OH) with rich maleic anhydride anionic groups (Seta *et al.*, 2020). Further characterisation to determine the size, morphology, chemical functional moiety, thermal stability, and crystallinity of the CMFs is to follow.

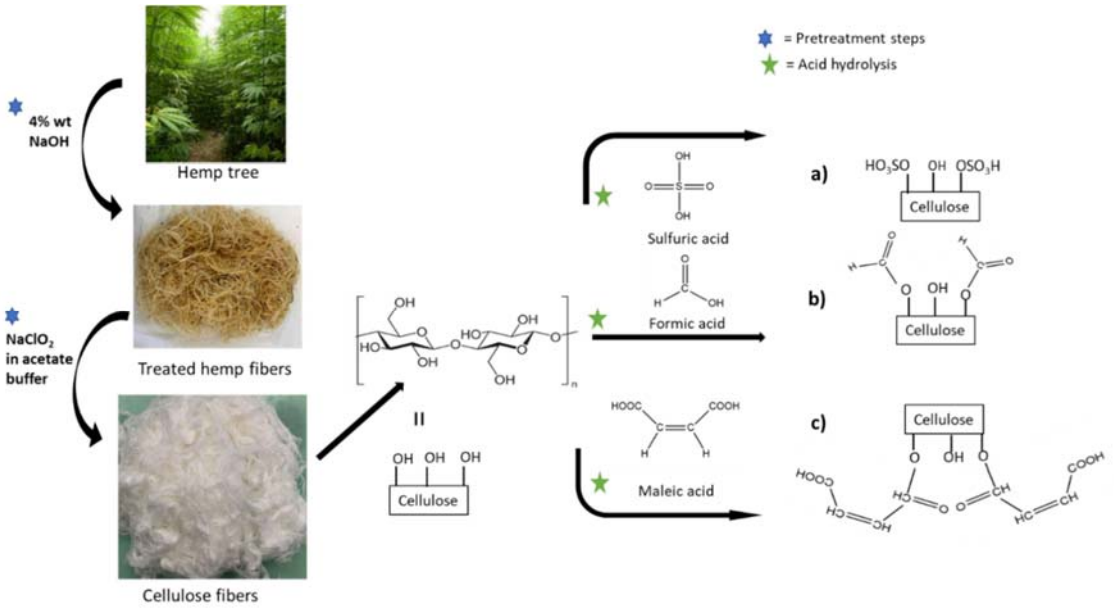

Figure 4.2: Schematic showing the production of a) sulfuric acid, b) formic acid and c) maleic acid hydrolysis process from cellulose derived from hemp bast fibres.

4.3.3 Scanning Electron Microscope analysis

Detailed morphology in the structure of bleached cellulose fibres was investigated by using SEM analysis as shown in Figure 4.3. Hemp bast fibres were subjected to alkaline treatment (4 wt% NaOH) to aid the removal of hemicellulose and other non-cellulosic content, resulting in brown hemp fibres. Furthermore, lignin removal was achieved after several rounds of bleaching to remove any hemicellulose and lignin content resulting in white cellulose fibres. Jiang *et al*, studied the effects of various concentrations of alkali treatments and found that 3 wt% NaOH was effective in the removal of non-cellulosic material (Jiang and Hsieh, 2015). Various publications also observed similar trends (Malucelli *et al.*, 2019)(Abiaziem *et al.*, 2020)(Ilyas, Sapuan and Ishak, 2018). Micrographs of the dried cellulose fibres (1000x magnification) show that the fibres have smooth flat surfaces with average diameters of 9.18 ± 3.17 µm (Figure 4.3a, b). Further, the fibres were micrometre thick as seen in the SEM micrographs. The results correspond to native cellulose SEM images reported in many studies using cellulose extracted from palm tree trunk (Abd Hamid, Chowdhury and Karim, 2014), and recycled Tetra Pak Food Packaging Waste (Akgün, 2022)

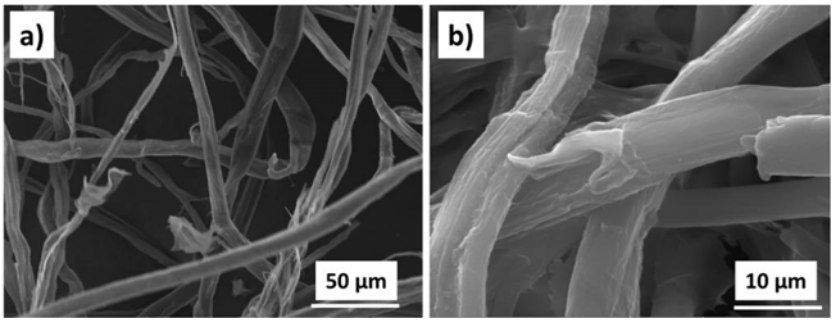

Figure 4.3: SEM images of bleached cellulose a) 50 µm magnification and b) 10 µm magnification.

The CMFs extracted from hemp cellulose fibre were examined by SEM analysis at 50 µm magnification as shown in Figure 4.4(a-r) with varying morphologies and sizes. Prior to freezing and freeze-drying to remove any water molecules and to produce white fluffy mass of fibrillated structures, CMFs suspension samples were subjected to ultrasonic treatment to help reduce the structural deformation of the fibres. After hydrolysis using various sulfuric acid concentrations at varying conditions the following morphology was observed (Figure 4.4a - b). Fibres (1SA- CMFs, 2SA- CMFs) extracted using 45% H_2SO_4 at temperatures below 55°C were a few hundreds of micrometres in length and had rod-like morphologies, whereas when the temperature was increased to 65°C (3SA- CMFs), shorter fibres were obtained as the material was much more degraded. Due to high hydrolysis conditions, there was not enough sample for SEM images for 4SA- CMFs samples. Fibres from the 5SA- CMFs conditions showed rod-like features and smaller fibre diameters due to higher acid concentrations and longer reaction time. The structural deformation observed in 6SA- CMFs can be linked to cellulose swelling and dissolvability caused by high concentrations, longer reactions times conditions, and high temperatures, which was also observed in other studies (Jung, Choi and Yang, 2013). At high hydrolysis conditions (7SA- CMFs), the fibres appear to have sheet-like and rod-like features in morphology. It results could be due to insufficient hydrolysis and damage caused by ultrasonic treatment.

CMFs preparation strongly depends on the acid concentration, temperature conditions and reaction times. Considering that formic acid is a weak organic acid, assisted hydrolysis using ultrasonic treatment is essential. Resultant CMFs had similar morphology throughout varying treatment conditions (Figure 4.4g–l). From the various conditions, it was observed that 1FA- CMFs, 2FA- CMFs, and 5FA- CMFs showed signs of incomplete hydrolysis and inhomogeneity resulting in a mixture of fibres of different sizes such as the partially hydrolysed microfibres and long CMFs. This can be attributed to low acid concentrations (pKa value 3.745), low reaction temperatures or even low reaction time. Similar results were recorded when Du and colleagues studied the preparation and characterisation of thermally stable CNFs via a sustainable approach of $FeCl_3$-catalyzed formic acid hydrolysis. The results obtained showed hydrolysis carried out using formic acid with low catalyst concentration, hydrolysis was incomplete and inhomogeneous (Du, Liu, Mu, *et al.*, 2016). Previous studies observed that formic

hydrolysis can result in incomplete hydrolysis resulting in CNFs/CNCs that are large and aggregation of fibres. However to improve fibre diameter various changing can be implemented namely introducing a catalyst, high pressure ultrasonic treatment, higher acid conditions, high temperatures and longer reaction times (Du, Liu, Zhang, *et al.*, 2016)(Lv *et al.*, 2019)(Du *et al.*, 2017).

Maleic acid is another relatively weak organic acid that can be used for hydrolysis produce CMFs as shown in Figure 4.4(m-r). Figure 4.4m representing 1MA- CMFs hydrolysis at low acid concentration and temperature was characterised by interwoven web-like structural features. As the hydrolysis conditions were increased (e.g higher acid concentrations, higher temperature, and longer reaction time), improvement in structural morphology was observed where fibres with rod-like structures were formed. Formic acid and maleic acid hydrolysed fibres showed similarities in morphologies, although fibres formed from hydrolysis with maleic acid showed more advanced degradation, and this was likely because maleic acid is a stronger acid (pKa = 1.9) than formic acid. The average diameter for fibres extracted using maleic acid was found to be between 8.32±1.85 µm and 11.27±2.01 µm.

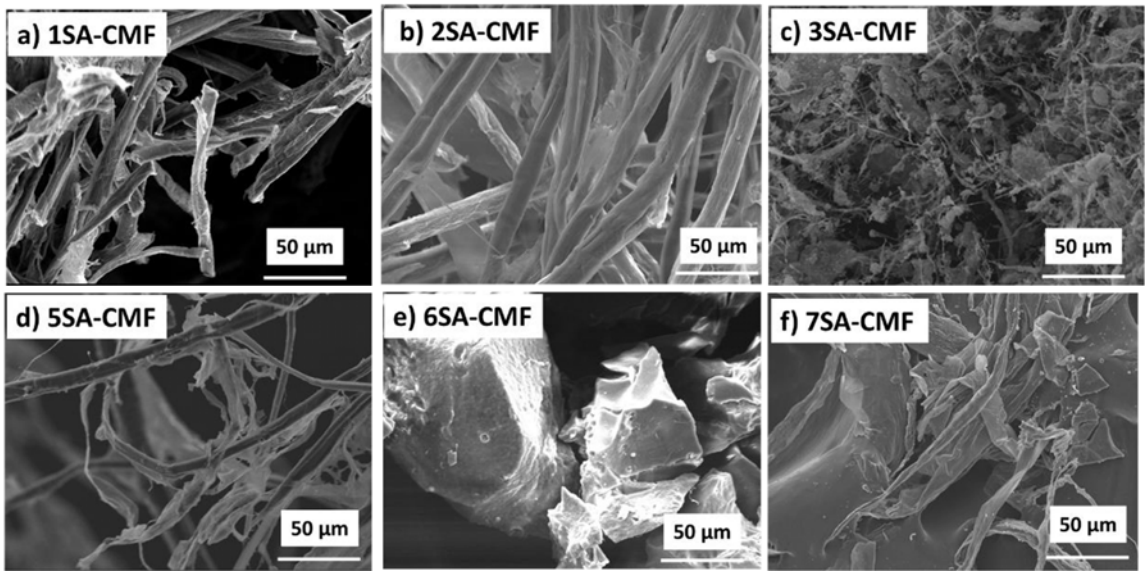

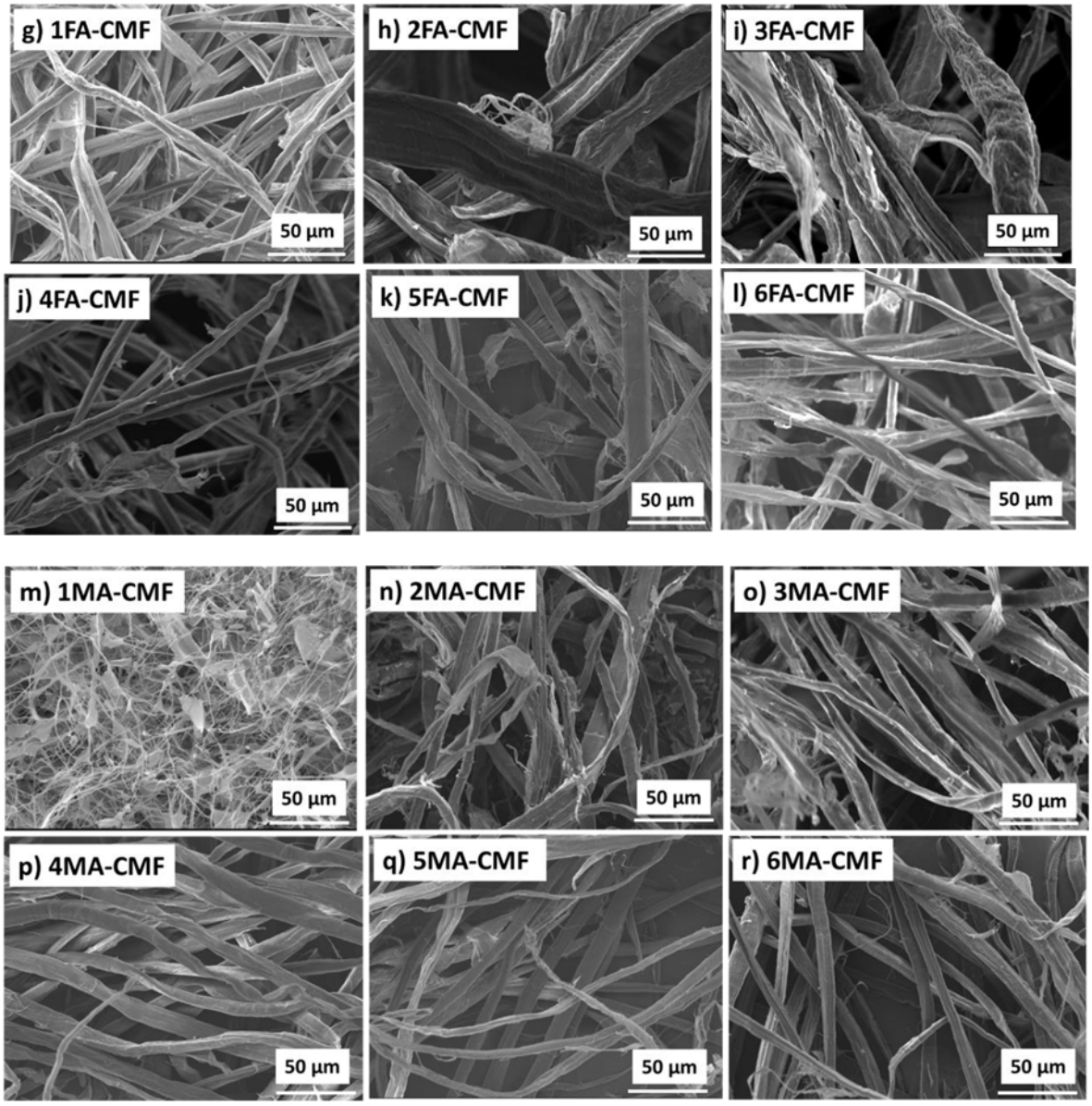

Figure 4.4: SEM images of hemp cellulose microfibres after acid hydrolysis

4.3.4 Fourier Transform Infrared spectroscopy

FTIR spectroscopy is a suitable technique used to assign the vibrations/ stretch of samples caused by physical or chemical treatments on the chemical structure. The FTIR spectrum of raw hemp fibres and bleached cellulose are represented below in Figure 4.5 and recorded in Table 4.1. The absorption peaks that appear on the range between 1158 cm^{-1}, and 1019 cm^{-1} including 1056 cm^{-1} are associated with C-O stretching, C-O-C asymmetric stretching, and C-H deformation vibrations of the pyranose ring skeletal of cellulose. The increase in intensity of the absorption bands between 1158-1019 cm^{-1} from raw hemp fibre to bleached cellulose fibres shows the increase in the cellulose content (Reddy *et al.*, 2016). Some peaks observed on raw hemp fibre spectrum did not appear on the spectrum of bleached

fibres in 1736 cm^{-1}, 1509 cm^{-1}, and 1236 cm^{-1}. The peak at 1736 cm^{-1} is most likely from vibrations of acetyl and uronic ester groups of hemicellulose or from the ester linkages between carboxylic group of the ferulic and *p*-coumaric acids of lignin (Matebie *et al.*, 2021)(Ventura-Cruz and Tecante, 2019)(Zhang *et al.*, 2019). The absence of the aforementioned peaks in the bleached cellulose spectrum can be attributed to the elimination of hemicellulose and lignin content. Banana peels (Pelissari, Sobral and Menegalli, 2014), sugarcane bagasse (Wulandari, Rochliadi and Arcana, 2016), and bamboo (Xie *et al.*, 2016) all showed similar results. The peaks at 1509 cm^{-1} and 1236 cm^{-1} on the raw hemp fibres spectrum could be attributed to C=C aromatic ring skeletal vibrations and C-O stretching vibrations of the guaiacyl ring of lignin, respectively. These groups were greatly weakened in the bleached cellulose spectrum because of partial or complete removal of lignin components after bleaching treatment of raw hemp fibres (Pelissari, Sobral and Menegalli, 2014)(Tibolla, Pelissari and Menegalli, 2014)(Dominic *et al.*, 2020).

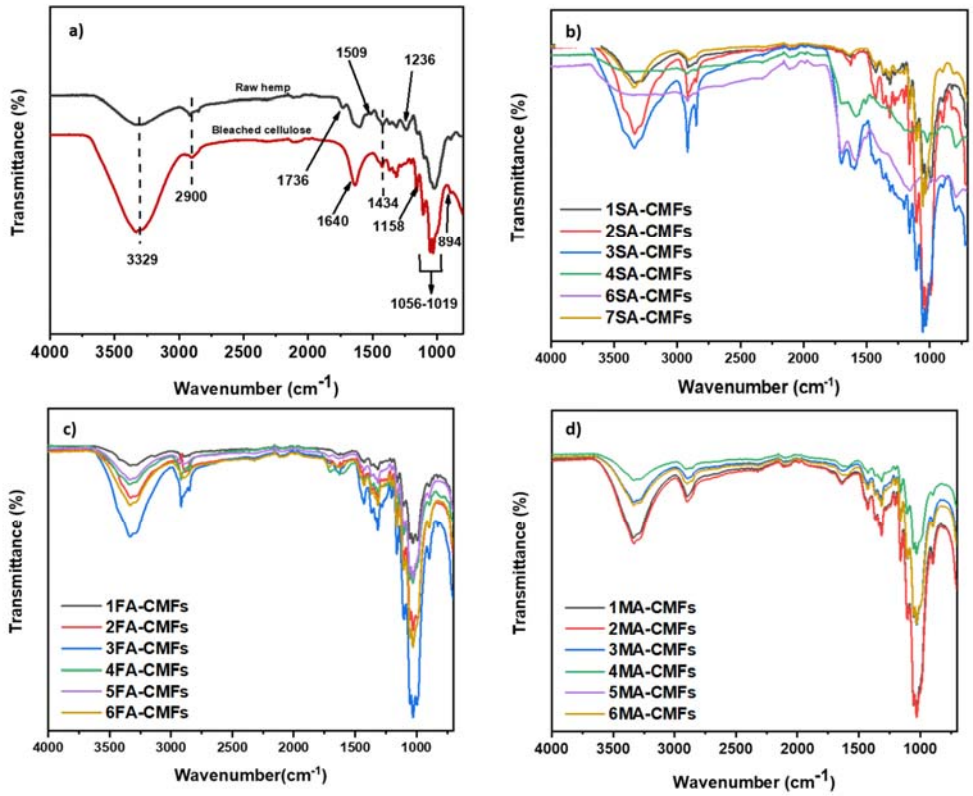

Figure 4.5: FTIR spectra of a) raw hemp fibre and bleached cellulose, b) sulfuric acid hydrolysed CMFs, c) formic acid hydrolysed CMFs, and d) maleic acid hydrolysed CMFs.

FTIR spectrum of bleached cellulose was later compared to that of CMFs as shown by Figure 4.5(b-d). From the FTIR spectra shown in Figure 4.5(b-d), the absorption bands at 3329 cm^{-1} and 2900 cm^{-1} were assigned to the hydroxyl group (-OH) stretching vibration and carbonyl (C-H) stretching vibration in

the CH_2 and CH_3 groups of cellulose, respectively (Syafri *et al.*, 2018)(Tang *et al.*, 2014)(Mahardika *et al.*, 2018). The characteristic absorption band at 1640 cm^{-1} is due to the bending vibration mode of absorbed moisture (Li *et al.*, 2014)(Rana *et al.*, 2021).Characteristic absorption peaks at 1434 cm^{-1}, 1368 cm^{-1}, and 894 cm^{-1} could be attributed to intermolecular hydrog.en attraction at C_6, C-H deformations and C-O bonds in the polysaccharide aromatic ring and β-glycosidic linkages between the anhydroglucose units within cellulose, respectively (Ilyas, Sapuan and Ishak, 2018)(Pelissari, Sobral and Menegalli, 2014)(Rana *et al.*, 2021). Figure 4.5(b), which represents sulfuric acid hydrolysed CMFs shows that with less harsh hydrolysis conditions, CMFs showed weak chemical changes whereas higher acid conditions revealed advanced chemical changes. Figure 4.5(c, and d) represent formic acid and maleic acid hydrolysed CMFs and the absorption peak at 1714 cm^{-1} corresponds to C=O stretching vibrations in the carbonyl group from cellulose (Liu *et al.*, 2016). However, the hydrolysis effects on the fibres can be observed with the peak strength varying between low to moderate esterification taking place. These results show that the main molecular structure of cellulose was not altered during extraction except in 5SA/6SA- CMFs spectrum which could be attributed to high sulfuric acid concentration leading to the breakdown of cellulose chain to glucose (Yang *et al.*, 2017). Similar CMFs s FTIR spectra were also reported by other researchers working with other types of natural cellulose sources; rose stems (Ventura-Cruz and Tecante, 2019), banana peels (Tibolla *et al.*, 2018), bamboo (Han *et al.*, 2018), lettuce peel (Zhang *et al.*, 2019) and many more.

Table 4.1: Chemical functional groups of cellulose and hydrolysed cellulose derivatives.

Wavenumber range (cm^{-1})	**Chemical peak assignments**	**Ref**
3329	-OH stretching	(Chirayil *et al*., 2014)(Syafri *et al*., 2018)
2900	-CH symmetrical stretching	(Tang *et al*., 2014)(Mahardika *et al*., 2018)
1714	C=O stretching vibration	(Zhang *et al*., 2019)(Nurhadi *et al*., 2022)
1640	-OH bending of absorbed moisture	(Li *et al*., 2014)(Rana *et al*., 2021)
1510	C-O-C out of plane stretching vibrations of aryl groups	(Nurhadi *et al*., 2022)(Tian *et al*., 2017)
1434	-CH_2 and OCH in the plan bending vibrations	(Matebie *et al*., 2021)(Tian *et al*., 2017)
1368	-CH bending deformations vibrations	(Pelissari *et al*., 2014)(Rana *et al*., 2021)

1240	C=C aromatic rings	(Ventura-Cruz and Tecante, 2019)(Dominic *et al*., 2020)
1150	C-O-C asymmetrical stretching vibrations	(Saurabh *et al*., 2016)(Widiarto *et al*., 2019)
1109, 1056, 1019	C-C, C-O-H and C-H pyranose ring and side group stretching vibrations of cellulose	(Saurabh *et al*., 2016)(Widiarto *et al*., 2019)(Elanthikkal *et al*., 2010)
894	C-O deformation and stretching/ glycosidic β linkages of cellulosic chain	(Ilyas *et al*., 2018)(Matebie *et al*., 2021)

4.3.5 X-ray diffraction analysis

XRD analysis is widely used to determine the crystallinity in individualized microfibres which plays an important role to determine the mechanical and thermal properties of microfibres. The X-ray diffractograms in Figure 4.6a-d for the cellulose fibres present intense peaks at 2θ angles of 14 – 18°, 22 – 24° and 34.6° which reflect on the crystallographic planes of (101), (002) and (004) respectively. This represents a preserved native cellulose type Iβ crystal structure even after acid hydrolysis, indicating that ultrasonic treatment can not alter characteristic XRD peaks of cellulose (Radakisnin *et al.*, 2020)(Wang *et al.*, 2019)(Kouadri and Satha, 2018). The crystallinity index (Cr*I*) of fibres as determined using the Segal method are shown in Table 4.2. Raw hemp fibre and bleached cellulose (Figure 4.6a) showed an increase in Cr*I* from 60% to 73% with improved peak intensity. This could be attributed to the removal of non-cellulosic content such as hemicellulose, lignin, and ash residue after alkali pretreatment and bleaching treatment cycles (Nagarajan, Balaji and Ramanujam, 2019). X-ray diffractogram of bleached cellulose has been studied to have a well-defined crystalline structure due to hydrogen bonding and van der Waals inter-actions existing between adjacent cellulose molecules compared to raw hemp fibres which have hemicellulose and lignin content and are amorphous in nature (Chirayil *et al.*, 2014). Similar results were reported by Wu and colleagues after isolation and characterisation purified coir cellulose fibres (PCC) from coconut coir fibres (CC). It is noteworthy to mention that the crystallinity increased from 35.8% in coconut coir fibres to 57.2% in purified coir cellulose, also due to chemical pretreatments aiding the removal of lignin and hemicellulose contents (Wu *et al.*, 2019).

CMFs isolation is strongly dependent on acid concentration, hydrolysis time and temperature of the hydrolysis reaction. After alkali and bleaching steps, cellulose fibres were acid hydrolysed using different hydrolysis conditions and Figure 4.6(b-d) represent the X-ray diffractograms of acid hydrolysed CMFs. Sulfuric acid hydrolysed CMFs resulted in Cr*I* values ranging between 52% to 75% as the conditions of hydrolysis changed (Figure 4.6b). The hydrolysis conditions play a major role in crystallinity of CMFs. As shown in Figure 4.6b, at low hydrolysis conditions,1SA-CMFs, showed high

Cr*I* value of about 75% whereas at high hydrolysis conditions (increased concentration, increased temperature, increased reaction time), 6SA-CMFs showed a low Cr*I* value of 59%. At lower conditions of hydrolysis, acid treated CMFs with high crystallinity could be due to the removal of amorphous regions of cellulose, whereas at higher acid conditions can result in removal of amorphous and crystalline regions of cellulose, producing low crystallinity CMFs which can be attributed to the harsh hydrolysis conditions and ultrasonic treatment step which altered not only the amorphous regions of the hemp cellulose but also severely damage the crystalline regions leading to more disordered domains in the cellulose, hence reduced crystallinity. These changes are consistent with literature findings that have been reported by various researchers such as Wang *et al*, who was working on the preparation of CNFs using highly recyclable organic acid treated softwood pulp which resulted in similar results (Wang *et al.*, 2019). The XRD pattern of 4SA- CMFs (Figure 4.6b) had an intense peak at 2θ = 22 – 24° with crystallinity index of 71%. Thus, the higher the acid concentration, contributes to the higher the crystallinity peak of CMFs. Due to improved crystallinity, acid hydrolysis and ultrasonic treatments play an significant role in removing the hemicellulose and lignin as also observed from others such as Revati *et al*, investigating the extraction of cellulose nanofibres from Napier grass fibres (*Pennisetum purpureum)* using acid hydrolysis process (Revati *et al.*, 2019).

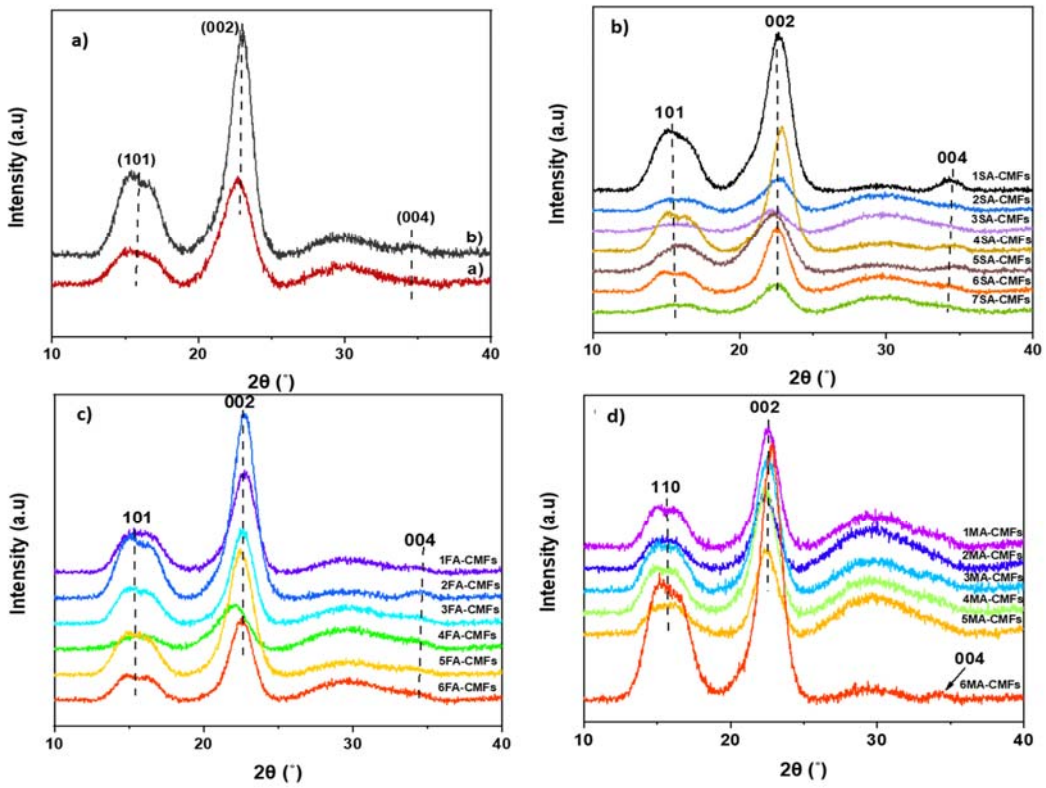

Figure 4.6: X-ray diffractogram patterns of a) fibres (raw hemp fibre-red and bleached cellulose fibreblack), b) sulfuric acid hydrolysed CMFs, c) formic acid hydrolysed CMFs, and d) maleic acid hydrolysed CMFs produced from hemp fibres.

From the formic acid hydrolysed CMFs presented in the X-ray diffractograms (Figure 4.6c), the Cr*I* values of CMFs range from 50 - 70% at different hydrolysis conditions. The Cr*I* values for 1FA- CMFs and 6FA- CMFs were determined to be 55% and 61%, respectively. Since formic acid is a relatively weak acid, changes in hydrolysis conditions did not significantly affect the thermal and mechanical stability of CMFs extracted. Formic acid hydrolysis coupled with high-pressure homogenisation process has been previously studied to produce CNFs with 52.91% crystallinity (Du *et al.*, 2017). Du *et al,* investigated cellulose nanofibre preparation using formic acid hydrolysis coupled with high-pressure homogenisation and it was found that the crystallinity increased from 49.0% to 52.9% with increased hydrolysis time (2 to 6 hr) (Du, Liu, Zhang, *et al.*, 2016). For maleic acid hydrolysed CMFs X-ray diffractograms (Figure 4.6d), Cr*I* values were calculated to range between 40 - 67% with varying hydrolysis conditions. The Cr*I* values for 1MA- CMFs and 6MA- CMFs were reported to be 40% and 67%, respectively. With improved maleic acid hydrolysis conditions, the crystallinity of CMFs also increases as shown in studies using waste office paper (Yeganeh, Behrooz and Rahimi, 2017) and mixed hardwood kraft pulp (Bian *et al.*, 2017). Changes in crystallinity can be attributed to chemical treatment, and acid hydrolysis treatment effects onto cellulose fibres to produce CMFs. Ultrasonic treatment also has been proven to significantly affect the crystallinity of CNFs/ CNCs by removing amorphous and crystalline regions in cellulose (Tang *et al.*, 2014)(Cui *et al.*, 2016).

Table 4.2: The crystallinity index (Cr*I* %), thermal degradation onset temperature (T_{onset}), and max degradation temperature (T_{max}) of cellulose microfibres obtained from XRD, TG, and DTG curves respectively.

Sample ID	**Cr*I* (%)**	**Main thermal degradation**			**Char residue amount at 900 ℃ (%)**
		T*onset* (℃)	T*max* (℃)	Weight loss (%)	
Raw hemp fibres	60	244	386	72	14
Bleached cellulose fibres	73	262	384	82	10
1SA- CMF	75	289	378	78	11
2SA- CMF	52	198	410	70	18
3SA- CMF	53	152	441	71	19
4SA- CMF	71	256	377	85	5

5SA- CMF	76	244	373	85	4
6SA- CMF	59	190	522	48	48
7SA- CMF	66	244	323	53	22
1FA- CMF	55	208	364	72	18
2FA- CMF	50	247	378	81	9
3FA- CMF	66	252	380	83	8
4FA- CMF	59	238	387	86	7
5FA- CMF	70	235	389	81	9
6FA- CMF	61	262	370	85	5
1MA- CMF	40	203	368	67	18
2MA- CMF	55	244	386	84	8
3MA- CMF	61	253	385	84	8
4MA- CMF	65	245	389	84	7
5MA- CMF	54	261	385	87	3
6MA- CMF	67	265	384	86	4

4.3.6 Thermogravimetric (TG) and Derivative Thermogravimetric (DTG) analysis

The thermal stability of cellulose microfibres was determined to evaluate their potential use in high-temperature applications such as thermal processing, reinforcing agents, thermoplastics, bio-composite processing and many more. Figure 4.7-4.10 show the thermogravimetric (TG) and derivative thermogravimetric (DTG) curves of raw hemp fibres, bleached cellulose fibres and cellulose microfibres (CMF) samples. The thermal degradation onset temperatures (T_{onset}), maximum thermal degradation temperatures (T_{max}), weight loss (%) and residual ash amount at maximum temperature (900℃) for all samples are listed in **Error! Reference source not found.** above. It is worth noting that all samples showed an initial weak weight loss of less than 5% at a temperature range between 45℃ to 100 ℃, mostly caused by vaporization and removal of absorbed water molecules in the sample surfaces (Chirayil *et al*., 2014)(Du *et al*., 2016). The thermal decomposition of raw hemp fibres, bleached cellulose and acid hydrolysed fibres occurs in two stages, also known as cellulose pyrolysis curve and the mechanism of pyrolysis is affected by two main factors, chemical factors such as presence of impurities (cellulose and non-cellulose content), crystallinity of cellulose samples, type of cellulose used, and physical factors such as temperature, heating time and type of atmospheric conditions adapted during the decomposition measurements (Radakisnin *et al*., 2020)(Santmarti and Lee, 2018).

From the TG curves of all samples, the first stage of decomposition takes place in the temperature range 220 ℃ to 300℃, where β-glycosidic bonds of cellulose breakdown and this can attributed to thermal depolymerization of hemicellulose contents (Longaresi *et al*., 2019). The second stage of decomposition occurs in the temperature range 220℃ to 450℃, which can be attributed to cellulose decomposition

and lastly lignin decomposes in the wider region of 450℃ to 900 ℃ a result of released gases (CO_2, CO, H_2O) contributing to the formation of solid char residue at maximum temperature (Tanpichai et al., 2019)(Wu *et al*., 2019)(Santmarti and Lee, 2018)(Shaikh *et al*., 2021). As shown from the TG and DTG curves (Figure 4.7), the thermal degradation of raw hemp fibres and bleached cellulose fibres starts at T_{onset} of 244℃ and 262℃, with a maximum rate at T_{max} of 386℃ and 384℃, respectively. After chemical treatment, the weight loss (%) increased from 72% (raw hemp fibres) to 82% (bleached cellulose fibres) and ash residue amount at 900℃ is 14% and 10% for raw hemp fibres and bleached cellulose fibres, respectively. Thermal stability of bleached cellulose fibres is better than raw hemp fibres. Thermal decomposition temperatures similar to that of the current study were reported from the production of nanocellulose from pineapple leaf fibres and raw pineapple fibres T_{onset} at 215℃ and bleached fibres T_{onset} at 230 ℃ (Mahardika *et al*., 2018). This trend can be attributed to absence of non-cellulosic components (ash and lignin) in the fibres due to the removal of hemicellulose and lignin content during chemical treatment steps (Chirayil *et al*., 2014). High crystallinity of bleached cellulose fibres samples along with the low solid ash residue provide better thermal stability. Similar results were reported by Dominic *et al*, where at maximum temperature of 700℃, raw *Cuscuta reflexa* fibres and alkali-treated *Cuscuta reflexa* fibres had char residue amount of 17% and 8%, signifying improved thermal stability (Dominic *et al*., 2020).

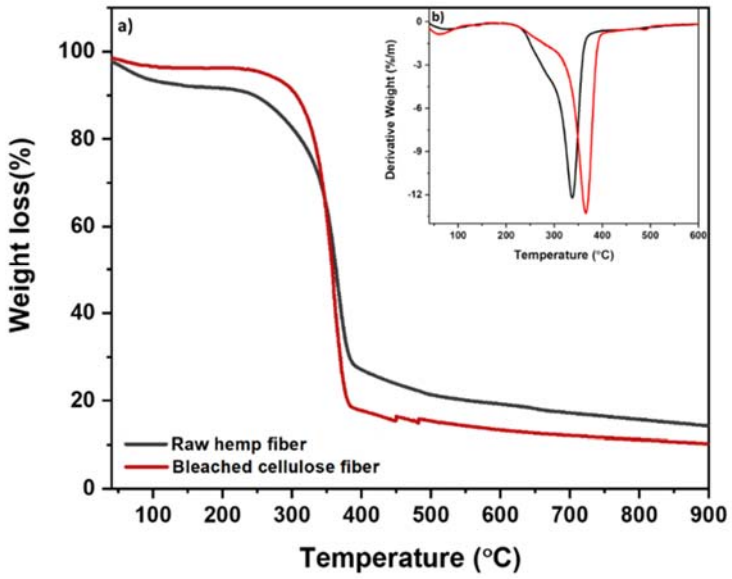

Figure 4.7: TG a) and DTG b) curves of raw hemp fibres and bleached cellulose fibres extracted from hemp fibre waste.

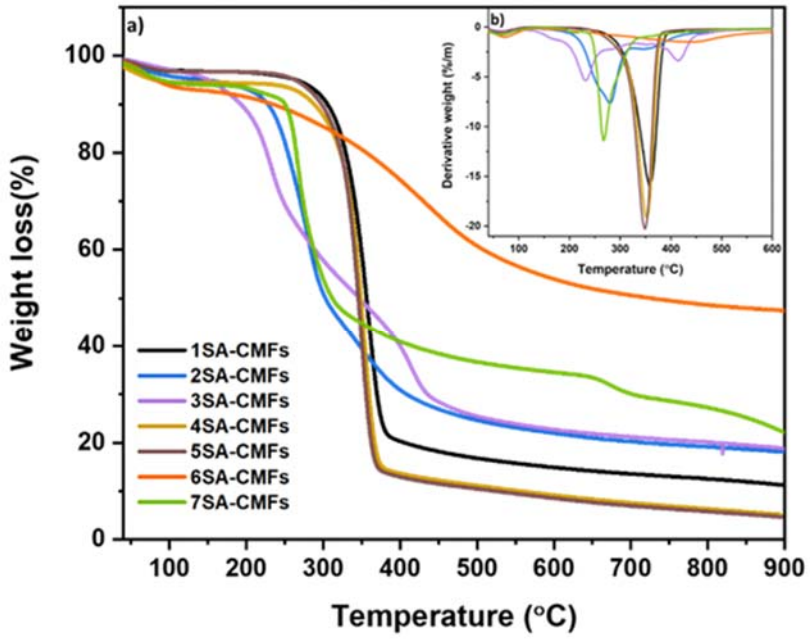

Figure 4.8: TG a) and DTG b) curves of sulfuric acid hydrolysed microfibres extracted from hemp fibres waste.

As shown in Figure4.8a and b, improved thermal stability of sulfuric acid hydrolysed CMF followed the order: 1SA-CMF <4SA-CMF <5SA-CMF <7SA-CMF <6SA-CMF <2SA-CMF <3SA-CMF. 1SA-CMF had the highest thermal stability with an onset decomposition temperature of 289℃ and maximum decomposition temperature of 378℃. High thermal stability of CMF can be attributed to the removal of amorphous regions of cellulose e.g., hemicellulose, lignin and other non-cellulose content after hydrolysis and homogenising treatment of cellulose samples (Du *et al*., 2017)(Lv *et al*., 2019). Sulfuric acid extracted CMF, however, e.g., 3SA-CMF had reduced thermal stability and a lower T_{onset} at 152℃. Two mechanisms can be considered to contribute to this phenomenon, The first is that sulfuric acid already leads to greater depolymerisation of the cellulose chains and the shorter cellulose chains are more easily degraded (Liu *et al*., 2016)(Sofla *et al*., 2016). Secondly, the presence of sulphate half ester groups leads to the generation sulfuric acid in the initial dehydration step. This stronger acid catalyses greater cellulose dehydration than the weaker carboxylic acid (generated from the dehydration of maleic and formic acid treated cellulose). The weight loss (%) of 1SA-CMF and 3SA-CMF were determined to be 78% and 74%, respectively. Moreover, the ash residue amount at 900℃ of the previously mentioned CMF were also determined to be 11% and 19%, respectively. The high weight loss (%) and low ash residue recorded in 1SA-CMF signifies the lack of any non-cellulose contents (hemicellulose, lignin, wax). Chirayil *et al,* (Chirayil *et al*., 2014), investigated and found similar results on acid treated cellulose extracted from *Helicteres isora* plant which had low carbon residue at maximum temperature 800℃.

Figure4.9a and b, represent the TG and DTG curves of formic acid hydrolysed CMF. The thermal stability of CMF extracted using formic acid follow the order: 6FA- CMF >3FA-CMF >2FA-CMF >4FA-CMF >5FA-CMF >1FA- CMF as it decreases. Both the T_{onset} and T_{max} of 6FA-CMF were determined to be higher than the T_{onset} and T_{max} of 1FA-CMF (see **Error! Reference source not found.**). High thermal stability can be attributed to the removal of disordered regions of cellulose and hemicellulose during hydrolysis, whereas low thermal stability can be attributed to insufficient hydrolysis by weak formic acid (Liu *et al*., 2016)(Seta *et al*., 2020). This is also in line with the relatively low crystallinity index of 1FA-CMF showed on the X-ray diffractograms and the high ash residue of 28% at maximum temperature 900℃.

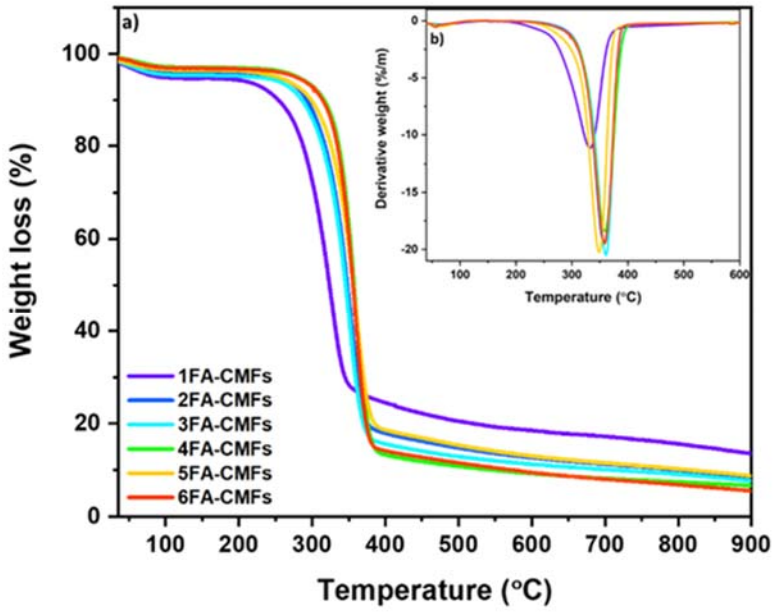

Figure 4.9: TG a) and DTG b) curves of formic acid hydrolysed microfibres extracted from hemp fibres waste.

Figure4.10a and b, show the TG and DTG curves of maleic acid hydrolysed microfibres. The thermal stability of maleic acid hydrolysed microfibres can be arranged in ascending order: Figure4.10a show that 1MA-CMF have low degradation temperature T_{onset} 203℃ to T_{max} 368℃ and 6MA-CMF have a high degradation temperature of T_{onset} 265℃ to T_{max} 384℃. Furthermore, 1MA-CMF has a lower crystallinity and high ash residue than 6MA-CMF. The lower acid concentration and lower temperature in 1MA- CMF likely resulted in less hemicellulose removal, leading to lower thermal stability and crystallinity (Peretz *et al*., 2019)(H. Bian *et al*., 2019). From all results, it is noteworthy to mention that TGA data analysis can be collaborated with the FTIR and XRD analysis results to support the notion that acid hydrolysis using various acid conditions and ultrasonic treatment of microfibres could not

modify the chemical composition, crystal structure, and thermal stability of microfibres, however only structural changes were observed via SEM analysis. Similar results were reported in previous studies (Nurhadi *et al*., 2022).

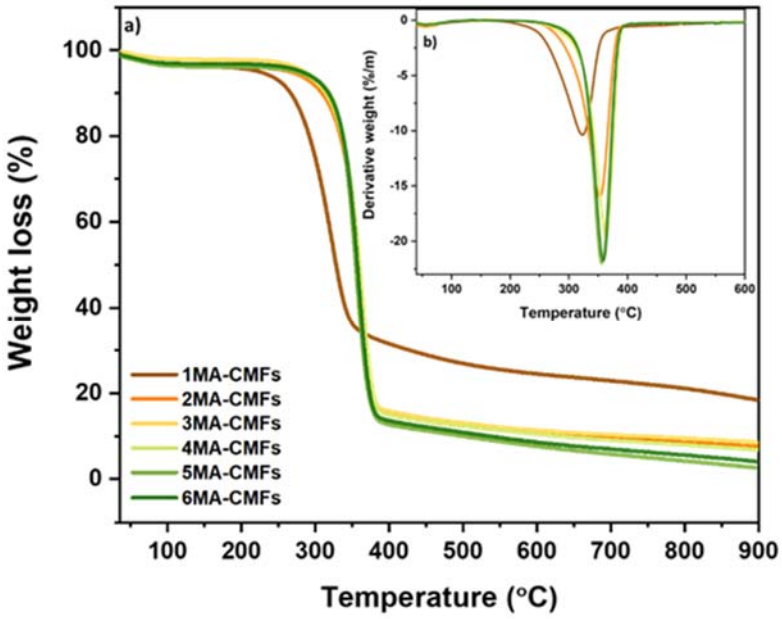

Figure 4.10: TG a) and DTG b) curves of maleic acid hydrolysed microfibres extracted from industrial hemp fibres waste.

4.4 Conclusion

CMFs were successfully extracted from Hemp (*Cannabis Sativa* L.) bast fibres by alkali pre-treatment followed by subsequent bleaching processes. Additionally, acid hydrolysis combined with ultrasonic treatment was utilised for further isolation. The surface morphology, chemical analysis, crystalline, and thermal properties of the untreated, treated and acid hydrolysed fibres was determined using SEM, FTIR, XRD and TGA. SEM analysis confirmed that hydrolysis produced CMFs of varying size and morphology. Bleached cellulose fibres showed have smooth flat surfaces with average diameters of 9.18 ± 3.17 µm whereas acid hydrolysed fibres showed more deformity on the surface due to acid hydrolysis and ultrasonic treatment. FTIR spectra of acid-hydrolysed fibres showed that the main chemical structure of cellulose was not altered during the hydrolysis process. The values of crystallinity calculated from XRD for raw fibre and bleached cellulose fibres were 60% and 73%, respectively. Xray diffraction results confirmed that non-cellulosic content (hemicellulose, lignin, and ash residue) was partially or completely removed by alkali pretreatment and bleaching treatments. On the other hand, CMFs after hydrolysis and ultrasonic treatment showed reduced crystallinity. Thermal stability of some of the CMFs was significantly improved than the bleached cellulose and raw fibres. Thermal

decomposition of raw hemp fibre, bleached cellulose and acid hydrolysed fibres occurred in three stages which involved release of adsorbed moisture, at around 100℃, a 2nd rapid stage at about 360℃ involving dehydration and decarboxylation reactions and lastly a slow decomposition step of the remaining char residue. Fibres with reduced thermal stability were affected by weak hydrolysis conditions leading incomplete hydrolysis of fibres. TGA also showed that CMFs with high crystallinity resulted in good thermal stability which is a favorable property for high temperature applications such as use as a flame-retardant agent, thermal processing, etc. Furthermore, this study revealed that bleached cellulose and CMFs can be extracted from hemp bast fibres and therefore, this contributes as future knowledge to use cellulose and/or CMFs extracted from hemp as low-cost, green material for application in various industrial applications.

4.5 References

Abd Hamid, S. B., Chowdhury, Z. Z. and Karim, M. Z. (2014) 'Catalytic extraction of microcrystalline cellulose (MCC) from Elaeis guineensis using central composite design (CCD)', *BioResources*, 9(4), pp. 7403–7426. doi: 10.15376/biores.9.4.7403-7426.

Abiaziem, C. V., Williams, A. B., Inegbenebor, A. I., Onwordi, C. T., Ehi-Eromosele, C. O., and Petrik, L. F (2020) 'Isolation and Characterisation of Cellulose Nanocrystal Obtained From Sugarcane Peel', *Rasayan Journal of Chemistry*, 13(1), pp. 177–187.

Abraham, R. E., Wong, C. S. and Puri, M. (2016) 'Enrichment of cellulosic waste hemp (Cannabis sativa) hurd into non-toxic microfibres', *Materials*, 9(7), pp. 1–13. doi: 10.3390/MA9070562.

Akgün, D., Özcan, D. O. and Övez, B. (2022) 'Optimization and Characterization of Cellulose Nanocrystal Production from Aseptic Tetra Pak Food Packaging Waste', *Journal of the Turkish Chemical Society Section A: Chemistry*, 9(1), pp. 131–148.

Bian, H., Chen, L., Dai, H., and Zhu, J. Y. (2017) 'Effect of fiber drying on properties of lignin containing cellulose nanocrystals and nanofibrils produced through maleic acid hydrolysis', *Cellulose*, 24(10), pp. 4205–4216. doi: 10.1007/s10570-017-1430-7.

Bian, H., Luo, J., Wang, R., Zhou, X., Ni, S., Shi, R., Fang, G., and Dai, H. (2019) 'Recyclable and Reusable Maleic Acid for Efficient Production of Cellulose Nanofibrils with Stable Performance', *ACS Sustainable Chemistry and Engineering*, 7, pp. 20022–20031. doi: 10.1021/acssuschemeng.9b05766.

Chen, H., Sharma, S. K., Sharma, P. R., Yeh, H., Johnson, K., and Hsiao, B. S. (2019) 'Arsenic(III)

Removal by Nanostructured Dialdehyde Cellulose-Cysteine Microscale and Nanoscale Fibers', *ACS Omega*, 4(26), pp. 22008–22020. doi: 10.1021/acsomega.9b03078.

Chirayil, C. J., Joy, J., Mathew, L., Mozetic, M., Koetz, J., and Thomas, S. (2014) 'Isolation and characterization of cellulose nanofibrils from Helicteres isora plant', *Industrial Crops and Products*, 59, pp. 27–34. doi: 10.1016/j.indcrop.2014.04.020.

Cui, S., Zhang, S., Ge, S., Xiong, L., and Sun, Q. (2016) 'Green preparation and characterization of size-controlled nanocrystalline cellulose via ultrasonic-assisted enzymatic hydrolysis', *Industrial Crops and Products*, 83, pp. 346–352. doi: 10.1016/j.indcrop.2016.01.019.

Dominic, M. C. D., Joseph, R., Begum, P. M.S., Joseph, M., Padmanabhan, D., Morris, L.A., Kumar, A. S., and Formela, K. (2020) 'Cellulose nanofibers isolated from the Cuscuta Reflexa plant as a green reinforcement of natural rubber', *Polymers*, 12(4). doi: 10.3390/POLYM12040814.

Du, H., Liu, C., Zhang, Y., Yu, G., Si, C., and Li, B (2016) 'Preparation and characterization of functional cellulose nanofibrils via formic acid hydrolysis pretreatment and the followed high-pressure homogenization', *Industrial Crops and Products*, 94, pp. 736–745. doi: 10.1016/j.indcrop.2016.09.059.

Du, H., Liu, C., Mu, X., Gong, W., Lv, D., Hong, Y., Si, C., and Li, B. (2016) 'Preparation and characterization of thermally stable cellulose nanocrystals via a sustainable approach of FeCl3catalyzed formic acid hydrolysis', *Cellulose*, 23(4), pp. 2389–2407. doi: 10.1007/s10570-016-0963-5.

Du, H., Liu, C., Wang, D., Zhang, Y., Yu, G., Si, C., Li, B., Mu, X., and Peng, H. (2017) 'Sustainable preparation and characterization of thermally stable and functional cellulose nanocrystals and nanofibrils via formic acid hydrolysis', *Journal of Bioresources and Bioproducts*, 2(1), pp. 10–15. doi: 10.21967/jbb.v2i1.68.

Elanthikkal, S., Gopalakrishnapanicker, U., Varghese, S., and Guthrie, J. T. (2010) 'Cellulose microfibres produced from banana plant wastes: Isolation and characterization', *Carbohydrate Polymers*, 80(3), pp. 852–859. doi: 10.1016/j.carbpol.2009.12.043.

Frost, B. A. and Foster, E. J. (2020) 'Isolation of thermally stable cellulose nanocrystals from spent coffee grounds via phosphoric acid hydrolysis', *Journal of Renewable Materials*, 8(2), pp. 187–203. doi: 10.32604/jrm.2020.07940.

Han, S., Yao, Q., Jin, C., Fan, B., Zheng, H., and Sun, Q. (2018) 'Cellulose nanofibers from bamboo and their nanocomposites with polyvinyl alcohol: Preparation and characterization', *Polymer Composites*, 39(8), pp. 2611–2619. doi: 10.1002/pc.24249.

Ilyas, R. A., Sapuan, S. M. and Ishak, M. R. (2018) 'Isolation and characterization of nanocrystalline cellulose from sugar palm fibres (Arenga Pinnata)', *Carbohydrate Polymers*, 181, pp. 1038–1051. doi:

10.1016/j.carbpol.2017.11.045.

Jarabo, R., Fuente, E., Monte, M. C., Savastano, H., Mutjé, P., and Negro, C. (2012) 'Use of cellulose fibers from hemp core in fiber-cement production. Effect on flocculation, retention, drainage and product properties', *Industrial Crops and Products*, 39(1), pp. 89–96. doi: 10.1016/j.indcrop.2012.02.017.

Jiang, F. and Hsieh, Y. Lo (2015) 'Cellulose nanocrystal isolation from tomato peels and assembled nanofibers', *Carbohydrate Polymers*, 122, pp. 60–68. doi: 10.1016/j.carbpol.2014.12.064.

bin Jumhuri, A. A., binti Fatanah, D. N. E., bin Mohamed, A. H., binti Che Hak, C. R., bin Mohamed Sapari, J., and binti Dzulkifli, N. N. (2017) 'Characterization of cellulose nanocrystal isolated from oil palm empty fruit bunch using formic acid hydrolysis', *International Journal of Agriculture*, 5, pp. 52–59. Available at: http://ijafp.com/wp-content/uploads/2017/10/AG-36.pdf.

Jung, J. Y., Choi, M. S. and Yang, J. K. (2013) 'Optimization of concentrated acid hydrolysis of waste paper using response surface methodology', *Journal of the Korean Wood Science and Technology*, 41(2), pp. 87–99. doi: 10.5658/WOOD.2013.41.2.87.

Kassab, Z., Abdellaoui, Y., Salim, M. H., Bouhfid, R., Qaiss, A. E., and El Achaby, M. (2020) 'Micro- and nano-celluloses derived from hemp stalks and their effect as polymer reinforcing materials', *Carbohydrate Polymers*, 245, pp. 1–12. doi: 10.1016/j.carbpol.2020.116506.

Kouadri, I. and Satha, H. (2018) 'Extraction and characterization of cellulose and cellulose nanofibers from Citrullus colocynthis seeds', *Industrial Crops and Products*, 124, pp. 787–796. doi: 10.1016/j.indcrop.2018.08.051.

Leite, A. L. M. P., Zanon, C. D. and Menegalli, F. C. (2017) 'Isolation and characterization of cellulose nanofibers from cassava root bagasse and peelings', *Carbohydrate Polymers*, 157, pp. 962–970. doi: 10.1016/j.carbpol.2016.10.048.

Li, M., Wang, L. J., Li, D., Cheng, Y. L., and Adhikari, B. (2014) 'Preparation and characterization of cellulose nanofibers from de-pectinated sugar beet pulp', *Carbohydrate Polymers*, 102(1), pp. 136–143. doi: 10.1016/j.carbpol.2013.11.021.

Liu, C., Li, B., Du, H., Lv, D., Zhang, Y., Yu, G., Mu, X., and Peng, H. (2016) 'Properties of nanocellulose isolated from corncob residue using sulfuric acid, formic acid, oxidative and mechanical methods', *Carbohydrate Polymers*, 151, pp. 716–724. doi: 10.1016/j.carbpol.2016.06.025.

Longaresi, R. H., de Menezes, A. J., Pereira-da-Silva, M. A., Baron, D., and Mathias, S. L. (2019) 'The maize stem as a potential source of cellulose nanocrystal: Cellulose characterization from its phenological growth stage dependence', *Industrial Crops and Products*, 133, pp. 232–240. doi: 10.1016/j.indcrop.2019.02.046.

Lv, D., Du, H., Che, X., Wu, M., Zhang, Y., Liu, C., Nie, S., Zhang, X., and Li, B. (2019) 'Tailored and Integrated Production of Functional Cellulose Nanocrystals and Cellulose Nanofibrils via Sustainable Formic Acid Hydrolysis: Kinetic Study and Characterization', *ACS Sustainable Chemistry and Engineering*, 7(10), pp. 9449–9463. doi: 10.1021/acssuschemeng.9b00714.

Mahardika, M., Abral, H., Kasim, A., Arief, S., and Asrofi, M. (2018) 'Production of nanocellulose from pineapple leaf fibers via high-shear homogenization and ultrasonication', *Fibers*, 6(2), pp. 1–12. doi: 10.3390/fib6020028.

Malucelli, L. C., Matos, M., Jordão, C., Lomonaco, D., Lacerda, L. G., Carvalho Filho, M. A.S., and Magalhães, W. L.E. (2019) 'Influence of cellulose chemical pretreatment on energy consumption and viscosity of produced cellulose nanofibers (CNF) and mechanical properties of nanopaper', *Cellulose*, 26(3), pp. 1667–1681. doi: 10.1007/s10570-018-2161-0.

Matebie, B. Y., Tizazu, B. Z., Kadhem, A. A., and Venkatesa Prabhu, S. (2021) 'Synthesis of Cellulose Nanocrystals (CNCs) from Brewer's Spent Grain Using Acid Hydrolysis: Characterization and Optimization', *Journal of Nanomaterials*, 2021. doi: 10.1155/2021/7133154.

Morin-Crini, N., Loiacono, S., Placet, V., Torri, G., Bradu, C., Kostić, M., Cosentino, C., Chanet, G., Martel, B., Lichtfouse, E., and Crini, G. (2018) Hemp-Based Materials for Metal Removal, *Green Adsorbents for Pollutant Removal, Environmental Chemistry for a Sustainable World*. doi: 10.1007/978-3-319-92162-4_1.

Nagarajan, K. J., Balaji, A. N. and Ramanujam, N. R. (2019) 'Extraction of cellulose nanofibers from cocos nucifera var aurantiaca peduncle by ball milling combined with chemical treatment', *Carbohydrate Polymers*, 212, pp. 312–322. doi: 10.1016/j.carbpol.2019.02.063.

Nurhadi, B., Angeline, A., Sukri, N., Masruchin, N., Arifin, R. H., and Saputra, R. A. (2022) 'Characteristics of microcrystalline cellulose from nata de coco: Hydrochloric acid versus maleic acid hydrolysis', *Journal of Applied Polymer Science*, 139(5), pp. 1–12. doi: https://doi.org/10.1002/app.51576.

Pejić, B. M., Kramar, A. D., Obradović, B. M., Kuraica, M. M., Žekić, A. A., and Kostić, M. M. (2020) 'Effect of plasma treatment on chemical composition, structure and sorption properties of lignocellulosic hemp fibers (Cannabis sativa L.)', *Carbohydrate Polymers*, 236. pp 1-9 doi: 10.1016/j.carbpol.2020.116000.

Pelissari, F. M., Sobral, P. J. D. A. and Menegalli, F. C. (2014) 'Isolation and characterization of cellulose nanofibers from banana peels', *Cellulose*, 21(1), pp. 417–432. doi: 10.1007/s10570-013-0138-6.

Peretz, R., Sterenzon, E., Gerchman, Y., Kumar, V., Luxbacher, T., and Mamane, H. (2019) 'Nanocellulose production from recycled paper mill sludge using ozonation pretreatment followed by recyclable maleic acid hydrolysis', *Carbohydrate Polymers*, 216, pp. 343–351. doi: 10.1016/j.carbpol.2019.04.003.

Radakisnin, R., Majid, M. S. A., Jamir, M. R. M., Jawaid, M., Sultan, M. T. H., and Tahir, M. F. M. (2020) 'Structural, morphological and thermal properties of cellulose nanofibers from napier fiber (Pennisetum purpureum)', *Materials*, 13(18). doi: 10.3390/ma13184125.

Rana, V., Malik, S., Joshi, G., Rajput, N. K., and Gupta, P. K. (2021) 'Preparation of alpha cellulose from sugarcane bagasse and its cationization: Synthesis, characterization, validation and application as wet-end additive', *International Journal of Biological Macromolecules*, 170, pp. 793–809. doi: 10.1016/j.ijbiomac.2020.12.165.

Reddy, K. O., Maheswari, C. U., Dhlamini, M. S., and Kommula, V. P. (2016) 'Exploration on the characteristics of cellulose microfibers from Palmyra palm fruits', *International Journal of Polymer Analysis and Characterization*, 21(4), pp. 286–295. doi: 10.1080/1023666X.2016.1147799.

Rehman, N., Alam, S., Amin, N. U. Mian, I., and Ullah, H. (2018) 'Ecofriendly isolation of cellulose from eucalyptus lenceolata: A novel approach', *International Journal of Polymer Science*, 2018. doi: 10.1155/2018/8381501.

Revati, R., Majid, M. S.A., Ridzuan, M. J.M., and Nasir, N. F.M. (2019) 'Characterisation of structural and physical properties of cellulose nanofibers from Pennisetum purpureum', *IOP Conference Series: Materials Science and Engineering*, 670(1). doi: 10.1088/1757-899X/670/1/012043.

Salami, A., Raninen, K., Heikkinen, J., Tomppo, L., Vilppo, T., Selenius, M., Raatikainen, O., Lappalainen, R., and Vepsäläinen, J. (2020) 'Complementary chemical characterization of distillates obtained from industrial hemp hurds by thermal processing', *Industrial Crops and Products*, 155. doi: 10.1016/j.indcrop.2020.112760.

Santmarti, A. and Lee, K. (2018) 'Crystallinity and Thermal Stability of Nanocellulose', in *Nanocellulose and Sustainability: Production, Properties, Applications, and Case Studies*, pp. 67–86. doi: 10.1201/9781351262927-5.

Saurabh, C. K., Mustapha, A., Masri, M. M., Owolabi, A. F., Syakir, M. I., Dungani, R., Paridah, M. T., Jawaid, M., and Abdul Khalil, H. P.S. (2016) 'Isolation and characterization of cellulose nanofibers from gigantochloa scortechinii as a reinforcement material', *Journal of Nanomaterials*, 2016. doi: 10.1155/2016/4024527.

Seta, F. T., An, X., Liu, L., Zhang, H., Yang, J., Zhang, W., Nie, S., Yao, S., Cao, H., Xu, Q., Bu, Y., and Liu, H. (2020) 'Preparation and characterization of high yield cellulose nanocrystals (CNC) derived from ball mill pretreatment and maleic acid hydrolysis', *Carbohydrate Polymers*, 234, pp. 1–9. doi: 10.1016/j.carbpol.2020.115942.

Shaikh, H. M., Anis, A., Poulose, A. M., Saeed, M. A., Madhar, N. A., Alhamidi, A., and Alam, M. A. (2021) 'Isolation and characterization of alpha and nanocrystalline cellulose from date palm (Phoenix dactylifera l.) trunk mesh', *Polymers*, 13(11). doi: 10.3390/polym13111893.

Sherif, N., Gadalla, M. and Kamel, D. (2021) 'Acid–hydrolysed furfural production from rice straw bio-waste: Process synthesis, simulation, and optimisation', *South African Journal of Chemical Engineering*, 38, pp. 34–40. doi: 10.1016/j.sajce.2021.08.002.

Sofla, M. R. K., Brown, R. J., Tsuzuki, T., and Rainey, T. J. (2016) 'A comparison of cellulose nanocrystals and cellulose nano fibres extracted from bagasse using acid and ball milling methods', *Advances in Natural Sciences: Nanoscience and Nanotechnology*, 7, pp. 1–10.

Syafri, E., Kasim, A., Abral, H., Sudirman, Sulungbudi, G. T., Sanjay, M. R., and Sari, N. H. (2018) 'Synthesis and characterization of cellulose nanofibers (CNF) ramie reinforced cassava starch hybrid

composites', *International Journal of Biological Macromolecules*, 120, pp. 578–586. doi: 10.1016/j.ijbiomac.2018.08.134.

Tang, Y., Yang, S., Zhang, N., and Zhang, J. (2014) 'Preparation and characterization of nanocrystalline cellulose via low-intensity ultrasonic-assisted sulfuric acid hydrolysis', *Cellulose*, 21(1), pp. 335–346. doi: 10.1007/s10570-013-0158-2.

Tanpichai, S., Witayakran, S. and Boonmahitthisud, A. (2019) 'Study on structural and thermal properties of cellulose microfibers isolated from pineapple leaves using steam explosion', *Journal of Environmental Chemical Engineering*, 7(1), p. 102836. doi: 10.1016/j.jece.2018.102836.

Tian, Z., Chen, J., Ji, X., Wang, Q., Yang, G., and Fatehi, P. (2017) 'Dilute sulfuric acid hydrolysis of Pennisetum (sp.) Hemicellulose', *BioResources*, 12(2), pp. 2609–2617. doi: 10.15376/biores.12.2.2609-2617.

Tibolla, H., Pelissari, F. M., Martins, J. T., Vicente, A. A., and Menegalli, F. C. (2018) 'Cellulose nanofibers produced from banana peel by chemical and mechanical treatments: Characterization and cytotoxicity assessment', *Food Hydrocolloids*, 75, pp. 192–201. doi: 10.1016/j.foodhyd.2017.08.027.

Tibolla, H., Pelissari, F. M. and Menegalli, F. C. (2014) 'Cellulose nanofibers produced from banana peel by chemical and enzymatic treatment', *LWT - Food Science and Technology*, 59, pp. 1311–1318. doi: 10.1016/j.lwt.2014.04.011.

Väisänen, T., Batello, P., Lappalainen, R., Tomppo, L. (2018) 'Modification of hemp fibers (Cannabis Sativa L.) for composite applications', *Industrial Crops and Products*, 111, pp. 422–429. doi: 10.1016/j.indcrop.2017.10.049.

Ventura-Cruz, S. and Tecante, A. (2019) 'Extraction and characterization of cellulose nanofibers from Rose stems (Rosa spp.)', *Carbohydrate Polymers*, 220, pp. 53–59. doi: 10.1016/j.carbpol.2019.05.053.

Wang, S., Wang, F., Song, Z., Song, X., Yang, X., and Wang, Q. (2019) 'Preparation of cellulose nanocrystals using highly recyclable organic acid treated softwood pulp', *BioResources*, 14(4), pp. 9331–9351. doi: 10.15376/biores.14.4.9331-9351.

Widiarto, S., Pramono, E., Suharso, Rochliadi, A., and Arcana, I. M. (2019) 'Cellulose nanofibers preparation from cassava peels via mechanical disruption', *Fibers*, 7(5), pp. 2–11. doi: 10.3390/FIB7050044.

Wu, J., Du, X., Yin, Z., Xu, S., Xu, S., and Zhang, Y. (2019) 'Preparation and characterization of cellulose nanofibrils from coconut coir fibers and their reinforcements in biodegradable composite films', *Carbohydrate Polymers*, 211, pp. 49–56. doi: 10.1016/j.carbpol.2019.01.093.

Wulandari, W. T., Rochliadi, A. and Arcana, I. M. (2016) 'Nanocellulose prepared by acid hydrolysis of isolated cellulose from sugarcane bagasse', *IOP Conference Series: Materials Science and Engineering*, 107(1). doi: 10.1088/1757-899X/107/1/012045.

Xie, J., Hse, C., De Hoop, C. F., Hu, T., Qi, J., and Shupe, T. F. (2016) 'Isolation and characterization of cellulose nanofibers from bamboo using microwave liquefaction combined with chemical treatment and ultrasonication', *Carbohydrate Polymers*, 151, pp. 725–734. doi: 10.1016/j.carbpol.2016.06.011.

Yang, X., Han, F., Xu, C., Jiang, S., Huang, L., Liu, L., and Xia, Z. (2017) 'Effects of preparation methods on the morphology and properties of nanocellulose (NC) extracted from corn husk', *Industrial Crops and Products*, 109, pp. 241–247. doi: 10.1016/j.indcrop.2017.08.032.

Yeganeh, F., Behrooz, R. and Rahimi, M. (2017) 'The effect of Sulfuric acid and Maleic acid on characteristics of nano-cellulose produced from waste office paper', *International Journal of Nano Dimension (Ijnd)*, 8(3), pp. 206–215.

Zhang, G., Wu, F., Ma, T., Zhang, B., Manyande, A., and Du, H. (2019) 'Preparation and characterization of cellulose nanofibers isolated from lettuce peel', *Cellulose Chemistry and Technology*, 53(7–8), pp. 677–684. doi: 10.35812/CelluloseChemTechnol.2019.53.66.

CHAPTER 5: OPTIMISATION OF ACID HYDROLYSIS OF HEMP FIBRES USING RESPONSE SURFACE METHODOLOGY

5.1 Introduction

RSM has been extensively applied in modelling and optimisation of numerous acid hydrolysis experiments using cellulose extracted from plant material. Commonly used RSM designs include the Box–Behnken design (BBD), and central composite design (CCD) (Dean *et al.*, 2015). Guo *et al,* used a CCD to determine optimal conditions for the extraction of CNCs from tea stalk using sulfuric acid (Guo *et al.*, 2020). The maximum yield of 50.96% was achieved at an acid concentration of 62.20%, hydrolysis time of 123.35 minutes and hydrolysis temperature of 45 ℃. The predicted yield was closer to the experimental yield of 49.8%. Akhabue and colleagues used RSM to determine optimal conditions for maximum yield of MCC powder from orange peel waste (OPW) (Akhabue and Osubor, 2017). They found that a maximum experimental yield of 14.12% was predicted when the hydrolysis temperature of 100.53 ℃ and 16.28 minutes hydrolysis time was applied. Chowdhury *et al*, studied the extraction of CNCs from African baobab tree leaves (Chowdhury *et al.*, 2019). Optimum conditions were determined as: 200 watts sonication, 43.11 minutes, 94 ℃. The extracted CNCs (15 – 20 nm diameter) were found to have high crystallinity index of 86.46%. Similarly, the production of CNCs and CNFs from pine kraft pulp using sulfuric acid hydrolysis was found to require 60 % acid concentration, 58℃ hydrolysis temperature, 60 minutes hydrolysis time for a 60% yield (Kandhola *et al.*, 2020). In this endeavour, RSM can be a useful tool for comparing quantitative data from experiments in order to determine conditions that may be applied to achieve desired results; in this case conditions that may be used with organic acids, to achieve fibre properties similar to those obtained using mineral acids (Amenaghawon *et al.*, 2013)(Ferreres *et al.*, 2017). Further, RSM allows for achieving this goal with minimal number of experiments, thus reducing cost and time (Chang *et al.*, 2017)(Goudarzi, Kasra Kermanshahi and Jahed Khaniki, 2020)(Murray *et al.*, 1990).

The objective of this work was to study the hydrolysis of hemp bast fibres with sulfuric acid, formic acid and maleic acid at different temperatures, reaction time, and acid concentrations. Response surface methodology with 3^3 full factorial experimental design was adapted to optimize the hydrolysis of cellulose microfibres to obtain fibres with high crystallinity and improved thermal stability suitable for application at high temperature.

5.2. Methods

Cellulose fibress and microfibres were extracted according to the method described in section 4.2.1. and 4.2.2.

5.2.1 Response Surface Methodology experimental design

The experimental procedure variables such as acid concentration, hydrolysis time, temperature and type of acid used which influenced the physical and chemical characteristics CMFs were optimised by using RSM.

Table 5.1 presents the level of process variables chosen. A full factorial design comprising of 21 experiment runs was created in MODDE 13.1 (Sartorius Stedim Biotech, Malmö, Sweden), to assess CMFs hydrolysis. The partial least square regression will be applied to evaluate the fitting of the model and response surface. The adequacy of the models will be evaluated by the R^2 (model fit) and Q^2 (estimate of the future prediction precision) values. The *F*-test will be used to assess the significance of the coefficients of regression and the modelling will be done with a quadratic model (Murray *et al.*, 1990)(Dean *et al.*, 2015).

Table 5.1: Experimental conditions and the types of acids to achieve optimum cellulose microfibres hydrolysis.

Exp No	**Temperature (℃)**	Hydrolysis time (**min)**	Acid concentration **(%)**	Type of **Acid**	**Sample ID**
1	45	30	45	Sulfuric acid	1SA-CMFs
2	45	60	45	Formic acid	1FA- CMFs
3	45	90	45	Maleic acid	1MA- CMFs
4	55	30	45	Sulfuric acid	2SA- CMFs
5	55	60	45	Formic acid	2FA- CMFs
6	55	90	45	Maleic acid	2MA- CMFs
7	65	30	45	Formic acid	3FA- CMFs
8	65	60	45	Maleic acid	3MA- CMFs
9	65	90	45	Sulfuric acid	3SA- CMFs
10	45	30	64	Maleic acid	4MA- CMFs
11	45	60	64	Sulfuric acid	4SA- CMFs
12	45	90	64	Formic acid	4FA- CMFs
13	55	30	64	Formic acid	5FA- CMFs
14	55	60	64	Maleic acid	5MA- CMFs
15	55	90	64	Sulfuric acid	5SA- CMFs
16	65	30	64	Maleic acid	6MA- CMFs

17	65	60	64	Sulfuric acid	6SA-CMFs
18	65	90	64	Formic acid	6FA-CMFs
19	55	60	55	Sulfuric acid	7SA-CMFs
20	55	60	55	Sulfuric acid	7SA-CMFs
21	55	60	55	Sulfuric acid	7SA-CMFs

5.3 Results and discussion

5.3.1 Interpretation of residual and coefficient plots

The MODDE 13 statistical software was used to optimise the acid hydrolysis process for CMFs production of which were extracted from hemp bast fibres. The design matrix was provided with reaction conditions; type of acid, acid concentration, hydrolysis time, and hydrolysis temperature for all 21 experimental runs with the output response of crystallinity index (%) for CMFs. Figure 5.1 shows the linear regression plot for the predicted versus the observed crystallinity index (%) and summarised in table form below (Table 5.2). As seen on the linear plots, the crystallinity index of the predicted model was close to the crystallinity index (%) of observed experiments, exhibiting R^2 value of 0.985 close to unity. Therefore, the model was accurate for optimizing the experimental conditions. Chowdhury *et al,* found similar results with a slight difference (R^2 = 0.986) in crystallinity index of predicted and experimental samples producing cellulose nanowhiskers from extracted African baobab leaves (Chowdhury *et al.*, 2019). R^2 value of 0.95 for the percentage crystallinity was found by Abd Hamid and colleagues while they investigated the extraction of MCC from palm trunk (Abd Hamid, Chowdhury and Karim, 2014).

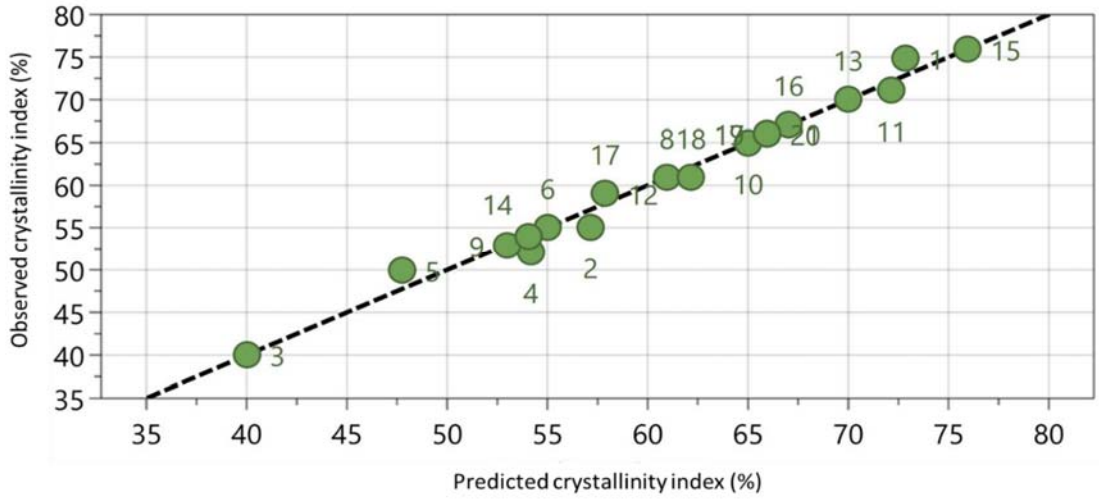

Figure 5.1: Residual plot of predicted versus observed crystallinity indexes (%) of CMFs extracted from hemp fibres.

Table 5.2: Results from the RSM-CCD experimental design and response data for sulfuric, formic, and maleic acid hydrolysis of cellulose extracted from *Cannabis sativa* L. bast fibres.

Sample ID	**Crystallinity degree (%)**	
	Predicted	Observed
1SA-CMFs	72.8	75
1FA- CMFs	57.2	55
1MA- CMFs	40	40
2SA- CMFs	54.2	52
2FA- CMFs	47.8	50
2MA- CMFs	55	55
3FA- CMFs	66	66
3MA- CMFs	61	61
3SA- CMFs	53	53
4MA- CMFs	65	65
4SA- CMFs	72.1	71
4FA- CMFs	57.9	59
5FA- CMFs	70	70
5MA- CMFs	54	54
5SA- CMFs	76	76
6MA- CMFs	67	67
6SA-CMFs	57.9	59
6FA-CMFs	62.1	61
7SA-CMFs	66	66
7SA-CMFs	66	66
7SA-CMFs	66	66
	62.1	61

A positive regression coefficient indicates a direct proportionality effect to crystallinity, whereas the negative coefficient value indicates the effect of an inverse relationship with crystallinity (Sartika *et al.*, 2019). From Figure 5.2, it is illustrated that the linear factors (various types of acids and temperature) show that there is both a positive and negative correlation with the crystallinity, whereas other linear factors, acid concentration and reaction time show positive and negative effects, respectively. An increase in acid concentration resulted in an increase in crystallinity degree of CMFs extracted from

hemp bast fibres and vice versa. However, the regression coefficients interactions between acid concentration and acid type varied i.e., a positive interaction was observed with sulfuric acid, but the opposite effect was possible when maleic or formic acid were used. The regression coefficients of the quadratic form of the acid concentration (aci*aci) had a strong significant negative effect on CMFs, whereas the reaction time (rea*rea) had a positive effect Therefore, from the observed trends an increase in the interaction of factors and squares between each factor can result in a decrease in crystallinity degree or vice versa.

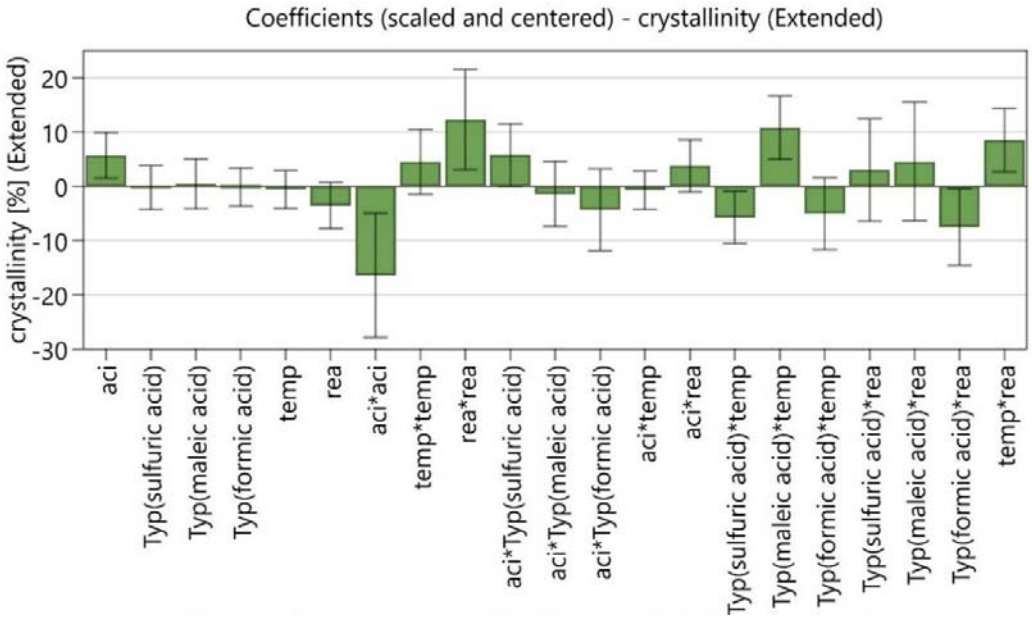

Figure 5.2: Coefficients plot for acid hydrolysed CMFs crystallinity index (%).

5.3.2 ANOVA analysis and lack of fit

The ANOVA of the regression model and statistical information corresponding to the second-order polynomial quadratic model has been summarised in Table 5.3. Several factors have been determined for a good regression model, namely the significance of the regression model, coefficient of determination (R^2), coefficient of variation (CV), standard deviation (SD), and adequate precision of the model (Sartika *et al.*, 2019). The significance level (p-value<0.05) of each independent factor involved in hydrolysis, namely type of acid, acid concentration, hydrolysis time, and temperature have a statistically significant effect on the crystallinity index (%) from the model. The significance of the regression model from the p-value was determined to be 0.034 which is smaller than the 0.05 significance threshold. The values of p less than 0.05 indicate that the regression model terms are significant, whereas values greater than 0.10 indicate that regression model terms are insignificant (Amenaghawon *et al.*, 2013). The variables of the acid concentration, hydrolysis temperature and reaction time, had a significant effect on the crystallinity degree (%) of CMFs. The regression model *F*

value was given as 11.41. This was determined to be greater than $F_{0.05}$ 3.20 at a level of 5%, (Table 5.3). The coefficient of determination (R^2) of the model is a measure of the linear relationship between the observed and predicted values (Sharmada *et al.*, 2016)(Shet *et al.*, 2018). The R^2 value and adjusted R^2 value are 0.985 and 0.898, respectively and moreover, with R^2 close to unity it signifies a strong correlation between the observed and predicted Cr*I* (%) of CMFs and validates the fitted model well. Coefficient of variation (CV) of the model in this study was determined to be 4.07%. A lower CV value signifies high accuracy and reliability of the experimental model (Ahmadi *et al.*, 2005), and the standard deviation value of 2.84 indicates that the experimental model has satisfying precision, reliability, and reproducibility. Finally, the adequate precision values which is a measure of the "signal and noise ratio" was also examined. Values above 4 signify a desirable model (Amenaghawon *et al.*, 2013)(Fatriasari *et al.*, 2021). From the data (Table 5.3), adequate precision value was given as 9.59, which indicates adequate signal. Similar results were reported in various scientific experimental results. Matebie *et al.*, 2021, Kandhola *et al.*, 2020, and Akhabue and Osubor, 2017 studied cellulose nanomaterials extracted from Brewer's Spent Grain, loblolly pine kraft pulp, and orange peel waste that also obtained the adequate signal, respectively.

Table 5.3: Analysis variance estimated by ANOVA and statistical information for the crystallinity index (%) as a response from the optimisation of sulfuric, formic, and maleic acid hydrolysis treatment

Source	**DF**	**Sum of squares**	**Mean square**	***F***	***p***
Regression	17	1564.09	92.0051	11.41	0.034*
Residual	3	24.2	8.8.67		
Lack of fit	1	24.2	24.2	--	--
Pure error	2	0.00	0		
Total corrected	21	1588.21			
R^2	0.985		**Coefficient of variance (CV) (%)**	4.07	
Adjusted R^2	0.898		**Adequate precision**	9.59	
Std.Dev	2.84		**Q^2**	-0.524	

*p<0.05 is significant

5.3.3 Interpretation of Response Contour and Surface Contour plots

Response contour plots as well as surface plot analysis (Figure 5.3 and Figure 5.5) were used to describe the relationship between varying factors within the experimental range, while one factor was kept constant at the centre point. The shapes of the contour plots indicate the nature and scope of the

interactions. Circular plots describe insignificant interaction between two variables whereas noncircular (elliptical) plots represent a significant interaction (Chen *et al.*, 2018). The response contour plot for sulfuric acid (Figure 5.3) suggests that for microfibres produced using sulfuric acid, the degree of crystallinity was high when hemp cellulose was exposed to an acid concentration range of 51 – 65%, and temperature of about ~50 ℃ for 60 min (Figure 5.3a). In general, crystallinity seemed to be maximised when acid concentration was higher than 52% regardless of the reaction time (Figure 5.3b), and by manipulation of reaction time and hydrolysis temperature (Figure 5.3c), at low reaction time and low temperature, the crystallinity degree increased. Figure 5.3d shows the surface plots of sulfuric acid hydrolysis and confirmed the same trend shown in the contour plots that an increase in crystallinity is influenced by an increase in acid concentration even at low temperatures. Furthermore, from the results obtained, the crystallinity degree decreases when high sulfuric acid concentrations are adopted, and this can be attributed to complete hydrolysis of cellulose to soluble sugars and other by-products (Akhabue and Osubor, 2017). Song *et al*, reported that excessive treatment using H_2SO_4 either in higher concentration or longer treatment conditions NCC yield percentage did not improve but rather NCC would be degraded into other products (Song *et al.*, 2016). The contour plots show non-circular lines, and this can be attributed to a significant interaction between variables.

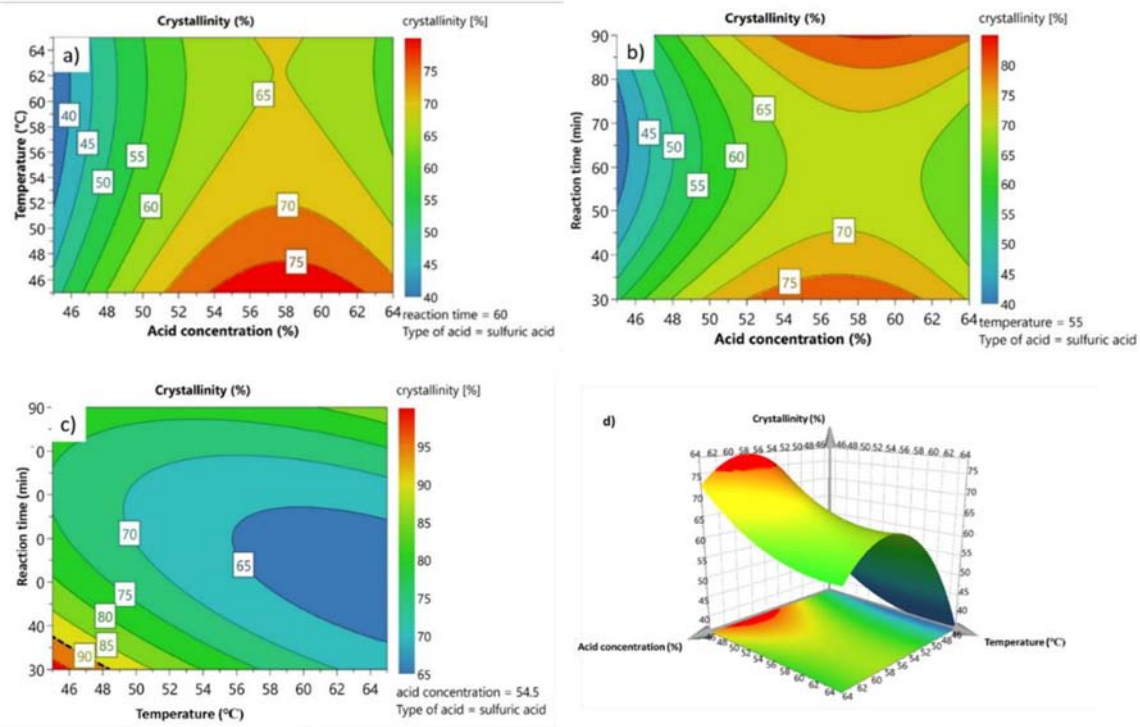

Figure 5.3: Response contour plots for the response between a) hydrolysis temp vs acid conc., b) reaction time vs acid conc., c) reaction time vs hydrolysis temp and d) response surface plot from sulfuric acid hydrolysis.

In accordance with the contour plots results, Figure 5.4a-c shows non-circular contour lines representing a significant interaction between the formic acid concentration and hydrolysis temperature, acid concentration and reaction time, and reaction time and hydrolysis temperature. From the surface plot (Figure 5.4d), higher crystallinity was observed with an increase in formic acid concentration in the range of 50 – 62% and at lower temperatures as also shown by the contour plot (Figure 5.4a).

In the contour plots (Figure 5.5a-c), the relationships between maleic acid concentration and hydrolysis temperature, maleic acid concentration and reaction time, and reaction time and hydrolysis temperature are presented. The results show a non-circular nature of the plots, and this can be attributed to significant interaction between two variables. From Figure 5.5a, the crystallinity is highly influenced by an increase in temperature and an increase in acid concentration. The reaction time and hydrolysis temperature contour plot show that the crystallinity degree is highly influenced by extreme hydrolysis conditions (temperature and time). Figure 5.5d, shows the surface plot relationship to crystallinity and an increase in crystallinity degree was observed at low temperatures and maleic acid concentration range 50 –61%.

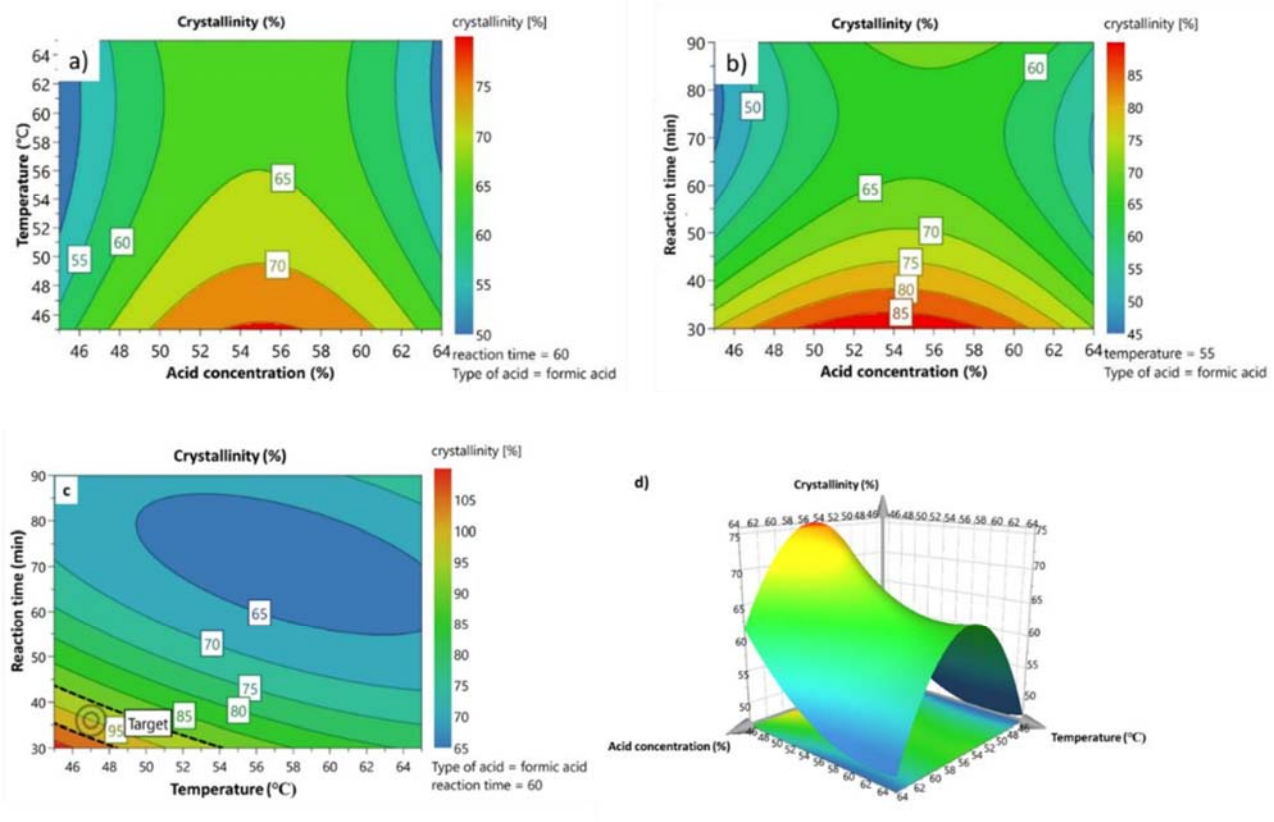

Figure 5.4: Response contour plots for the response between a) hydrolysis temp vs acid conc., b) reaction time vs acid conc., c) reaction time vs hydrolysis temp and d) response surface plot from formic acid hydrolysis.

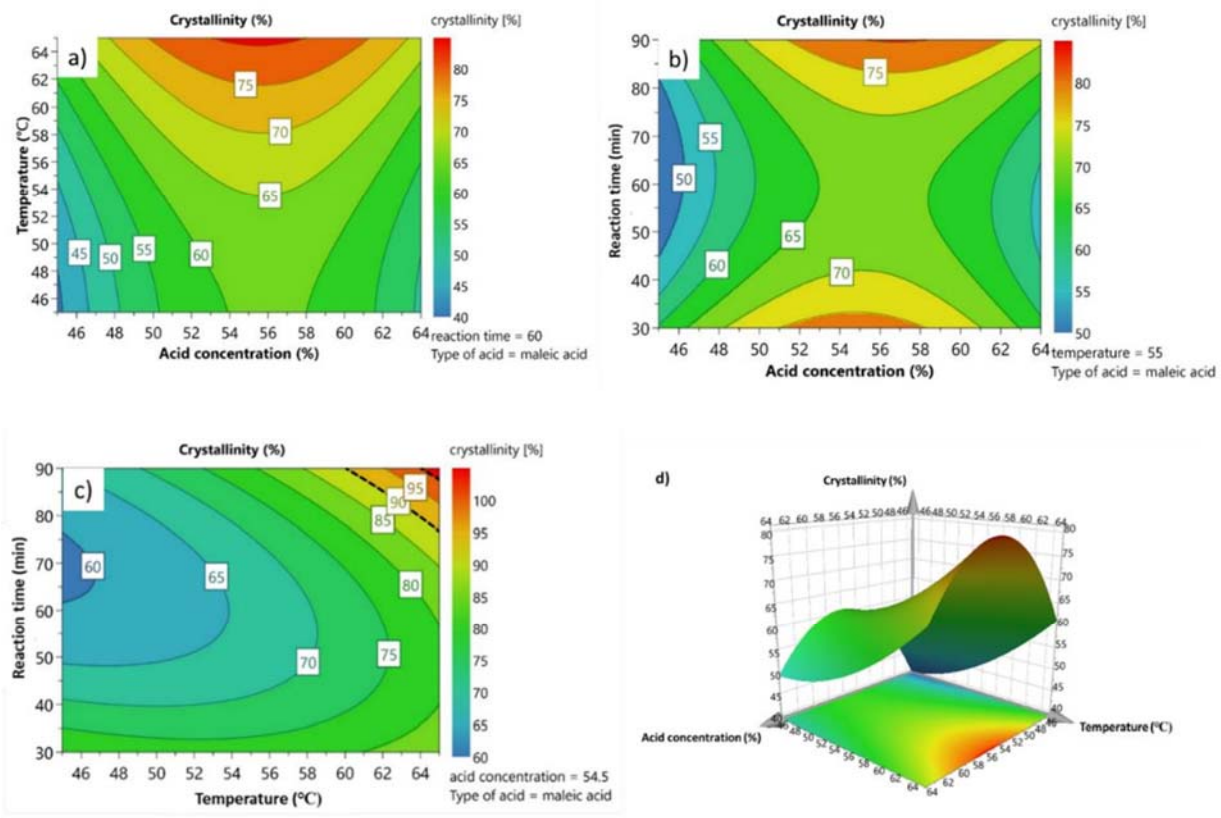

Figure 5.5: Response contour plots for the response between a) hydrolysis temp vs acid conc., b) reaction time vs acid conc., c) reaction time vs hydrolysis temp and d) response surface plot from maleic acid hydrolysis.

5.3.4 Optimisation and model verification

To select the optimum conditions and their respective levels, the RSM-CCD model was analysed. The maximum crystallinity degree of CMFs predicted from the model was determined to be 83.69% with optimum hydrolysis conditions as detailed in Table 5.4. To confirm the validity of the model for predicting the maximum crystallinity degree for CMFs, experiments were repeated three times using the optimum conditions. From the three replicate experiments, the results obtained showed an average crystallinity degree of 82%, which is significantly closer to the predicted optimum value. Therefore, the results verified the validity of the model to produce CMFs extracted from cellulose.

Table 5.4: Observed vs predicted results of the optimum crystallinity index (%)

	Observed results	**Predicted results**
Acid type	Formic acid	Formic acid
Acid concentrations (%)	62	62.1
Hydrolysis temperature (°C)	47	47

Reaction time (min)	36	36
Maximum crystallinity index (%)	82	83.69

5.4 Conclusion

In the present work, a 3^3 full factorial design response surface study using a central composite design model was employed to investigate the effect of various hydrolysis conditions on the extracted CMFs. From the contour plots, it was observed that harsh hydrolysis conditions (acid concentration and temperature) can have an effect on the crystallinity index of cellulose fibres (high conditions, higher crystallinity index value). Optimum hydrolysis conditions were obtained while using formic acid as the acid choice at 62 % acid concentration, 47 ℃ hydrolysis temperature and 36 minutes of reaction time with maximum obtained crystallinity degree of 82 %. This study established that the wide available bast fibre can be regarded as a greener and sustainable waste for the preparation of CMFs and RSM-CCD can be used to optimise extraction conditions.

5.5 References

Abd Hamid, S. B., Chowdhury, Z. Z. and Karim, M. Z. (2014) 'Catalytic extraction of microcrystalline cellulose (MCC) from Elaeis guineensis using central composite design (CCD)', *BioResources*, 9(4), pp. 7403–7426. doi: 10.15376/biores.9.4.7403-7426.

Ahmadi, M., Vahabzadeh, F., Bonakdarpour, B., Mofarrah, E., and Mehranian, M. (2005) 'Application of the central composite design and response surface methodology to the advanced treatment of olive oil processing wastewater using Fenton's peroxidation', *Journal of Hazardous Materials*, 123(1–3), pp. 187–195. doi: 10.1016/j.jhazmat.2005.03.042.

Akhabue, C. E. and Osubor, N. T. (2017) 'Optimization of extraction of microcrystalline cellulose from orange peel waste using response surface methodology', *Ife Journal of Science*, 19(2), pp. 227–235. doi: 10.4314/ijs.v19i2.3.

Amenaghawon, A. N., Balogun, A., Agbonghae, E. E., Ogbeide, S. E., Okieimen, C. O., and Agbonghae, E. O. (2013) 'Modelling and Statistical Optimisation of Dilute Acid of Corn Stover using Response Surface Methodology', *Journal of Environment*, 02(02), pp. 34–40.

Chang, C. W., Yen, C. C., Wu, M. T., Hsu, M. C., and Wu, T. Y. (2017) 'Microwave-assisted extraction of cannabinoids in hemp nut using response surface methodology: Optimization and comparative study', *Molecules*, 22(11), pp. 1–15. doi: 10.3390/molecules22111894.

Chen, X., Wei, Z., Zhu, L., Yuan, X., Wei, D., Peng, W., and Wu, C. (2018) 'Efficient approach for the extraction and identification of red pigment from zanthoxylum bungeanum maxim and its antioxidant activity', *Molecules*, 23(5). doi: 10.3390/molecules23051109.

Chowdhury, Z. Z., Chandran, R. R. R., Jahan, A., Khalid, K., Rahman, M. M., Al-Amin, M., Akbarzadeh, O., Badruddin, I. A., Khan, T. M.Y., Kamangar, S., Hamizi, N. A. B., Wahab, Y. A., Johan, R. B., and Adebisi, G. A. (2019) 'Extraction of cellulose nano-whiskers using ionic liquidassisted ultra-sonication: Optimization and mathematical modelling using Box-Behnken design', *Symmetry*. doi: 10.3390/sym11091148.

Dean, A., Morris, M., Stufken, J., Bingham, D. (2015) 'Handbooks of Modern Statistical Methods'. *Handbook of Design and Analysis of Experiments*. *Chapman and Hall/CRC*, pp 1-946.

Fatriasari, W., Ulwan, W., Aminingsih, T., Sari, F. P., Fitria, Suryanegara, L., Iswanto, A.H., Ghozali, M., Kholida, L. N., Hussin, M. H., Fudholi, A., and Hermiati, E. (2021) 'Optimization of maleic acid pretreatment of oil palm empty fruit bunches (OPEFB) using response surface methodology to produce reducing sugars', *Industrial Crops and Products*, 171, pp. 1–15.

Ferreres, F., Grosso, C., Gil-Izquierdo, A., Valentão, P., Mota, A. T., and Andrade, P. B. (2017) 'Optimization of the recovery of high-value compounds from pitaya fruit by-products using microwaveassisted extraction', *Food Chemistry*, 230, pp. 463–474. doi: 10.1016/j.foodchem.2017.03.061.

Goudarzi, L., Kermanshahi, R. K. and Khaniki, G. J. (2020) 'Response Surface Design for Removal of Lead by Different Lactic Acid Bacteria', *Health Scope*, 9(3). doi: 10.5812/jhealthscope.101049.

Guo, Y., Zhang, Y., Zheng, D., Li, M., and Yue, J. (2020) 'Isolation and characterization of nanocellulose crystals via acid hydrolysis from agricultural waste-tea stalk', *International Journal of Biological Macromolecules*, 163, pp. 927–933. doi: 10.1016/j.ijbiomac.2020.07.009.

Kandhola, G., Djioleu, A., Rajan, K., Labbé, N., Sakon, J., Carrier, D. J., Kim, J. W. (2020) 'Maximizing production of cellulose nanocrystals and nanofibress from pre-extracted loblolly pine kraft pulp: a response surface approach', *Bioresources and Bioprocessing*. doi: 10.1186/s40643-020-00302-0.

Matebie, B. Y., Tizazu, B. Z., Kadhem, A. A., and Prabhu, S. V. (2021) 'Synthesis of Cellulose Nanocrystals (CNCs) from Brewer's Spent Grain Using Acid Hydrolysis: Characterization and Optimization', *Journal of Nanomaterials*, 2021. doi: 10.1155/2021/7133154.

Mason, R. L., Gunst, R. F., Hess, J. L. (1990) Statistical Design and Analysis of Experiments: With Applications to Engineering and Science., *Journal of the American Statistical Association*. doi: 10.2307/2289624.

Sartika, D., Syamsu, K., Warsiki, E., and Fahma, F. (2019) 'Optimization of Sulfuric Acid Concentration and Hydrolysis Time on Crystallinity of Nanocrystalline Cellulose: A Response Surface Methodology Study', in *IOP Conference Series: Earth and Environmental Science*, pp. 1–9. doi: 10.1088/1755-1315/355/1/012109.

Sharmada, N., Punja, A., Shetty, S. S., Shet, V. B., Goveas, L. C., and Rao, C. V. (2016). 'Optimization of pre-treatment of de-oiled oil seed cake for release of reducing sugars by response surface methodology', *Bioethanol*, 2(1), pp. 94–102. doi: 10.1515/bioeth-2016-0006.

Shet, V. B., Sanil, N., Bhat, M., Naik, M., Mascarenhas, L. N., Goveas, L. C., Rao, C. V., Ujwal, P., Sandesh, K., and Aparna, A. (2018) 'Acid hydrolysis optimization of cocoa pod shell using response surface methodology approach toward ethanol production', *Agriculture and Natural Resources*, 52(6), pp. 581–587. doi: 10.1016/j.anres.2018.11.022.

CHAPTER 6: SYNTHESIS AND APPLICATION OF CATIONISED CELLULOSE FOR ADSORPTION OF ANIONIC DYES

6.1 Introduction

With over 10,000 types of dyes commercially manufactured, approximately 7×10^5 tonnes of dyes are produced annually worldwide and 50% of these are azo dyes (Hashem and El-Shishtawy, 2001; Chukwuemeka-Okorie *et al.*, 2021). Synthetic dyes represent a major class of organic pollutants found in wastewater and are commonly used in industries such as textile, plastics, paper printing, food, and pharmaceuticals to give colour to final products (Santos *et al.*, 2017; Katheresan, Kansedo and Lau, 2018). These dyes have complex aromatic structures that offer thermal, biological, physiochemical, and optical stability, hence not biodegradable and non-oxidizable in nature (Haddadian *et al.*, 2013; Sun *et al.*, 2013; Veni and Brenda, 2021). Therefore, when used in industrial processes, up to 20% of dye solutions end up in industrial wastewater effluents making their way into the environment (Stanciu and Nichifor, 2019; Veni and Brenda, 2021). Azo dyes such as methyl orange and sunset are highly toxic, carcinogenic, and mutagenic to humankind and aquatic life. The presence of such dyes in wastewater can adversely affect aquatic life by preventing light penetration into the water body, thereby inhibiting photosynthetic activity (Haddadian *et al.*, 2013; Abdel-Ghani *et al.*, 2017). Harmful human effects induced by dyes include allergies related to the skin, and eyes, as well as the respiratory and gastrointestinal tracts when dye contaminated water is ingested (Stanciu and Nichifor, 2019; Veni and Brenda, 2021) Due to the aforementioned negative impacts, various decontamination techniques such as chemical coagulation/flocculation, chemical oxidation, membrane filtration (Khumalo *et al.*, 2019), electrocoagulation , adsorption (Chen and Zhao, 2009), and many more have been explored and employed in treating wastewater containing dyes (Dawood and Sen, 2012; Katheresan, Kansedo and Lau, 2018; Stanciu and Nichifor, 2019) Membrane fouling, toxic sludge generation, high operation and investment costs are some of the disadvantages associated with some of the techniques (Katheresan, Kansedo and Lau, 2018). Adsorption process is a widely used technique for dye removal as it is a low cost, simple and reliable process with high removal efficiency outcomes, and has limited hurdles associated with the generation of toxic substances (Dawood and Sen, 2012; Stanciu and Nichifor, 2019). Adsorption is principally the separation of solute molecules (dye molecules) by transfer onto the surface of an adsorbent. Adsorbents (zeolites, activated carbon, biomaterials, etc) act as filter materials for the removal of dyes from aqueous solutions (Veni and Brenda, 2021). Activated carbons are some of the most used adsorbents for the removal of toxic organic pollutants with high removal efficiencies but high operational and investment costs and difficulty in regeneration for reuse remains a cause for (Zhu *et al.*, 2007; Ma *et al.*, 2011). The use of agricultural waste material as adsorbents is common in today's scientific research due to its low cost, wide availability, renewability and biodegradability impacts (Gao *et al.*, 2016). Cellulose is one of the most abundant natural polymers found on earth, and it makes up

the structural component of plants' cell wall (Gao *et al.*, 2016; Kassab *et al.*, 2020). Industrial raw hemp (*Cannabis sativa L.*) stalks are composed mainly of ~72% cellulose (Kassab *et al.*, 2020), but are currently an under-utilised agricultural cellulose source. Cationisation of cellulose fibres can introduce amine or quaternary ammonium groups allowing for their use in adsorption. Cationisation has also been shown to imbue cellulose with antibacterial properties (Hashem and El-Shishtawy, 2001), allowing for dual approach to water treatment. To our best knowledge, no studies have been conducted using hemp fibre cellulose cationised using GTMAC as a cationising agent, for the removal of methyl orange and sunset yellow from aqueous solutions

6.2. Methods

6.2.1 Cationisation of cellulose fibres

To functionalise cationic cellulose fibres, a two necked round bottom flask equipped with a condenser was utilised (Figure 6.1), 5 g of cellulose fibres was added to 225 mL THF solution and stirred for 1 hr at ambient temperature (21 ± 2℃). After 1 hr, 2.5 mL of 10 M NaOH was added into the mixture and stirred for an additional 30 min. After NaOH addition, 17.8 mL of GTMAC was added into the reaction vessel and further allowed to stir for 15 hr at 40℃. After 15 hr, 12.5 mL of 4 M HCl was then added to the reaction vessel to stop the reaction. The cationisation solution was decanted then the fibres were dried and then washed several times with ultrapure water until stable neutral pH. The fibres were then dried and further stored for characterisation and use in experiments. For referral cationised cellulose fibres were labelled GT-cellulose fibres.

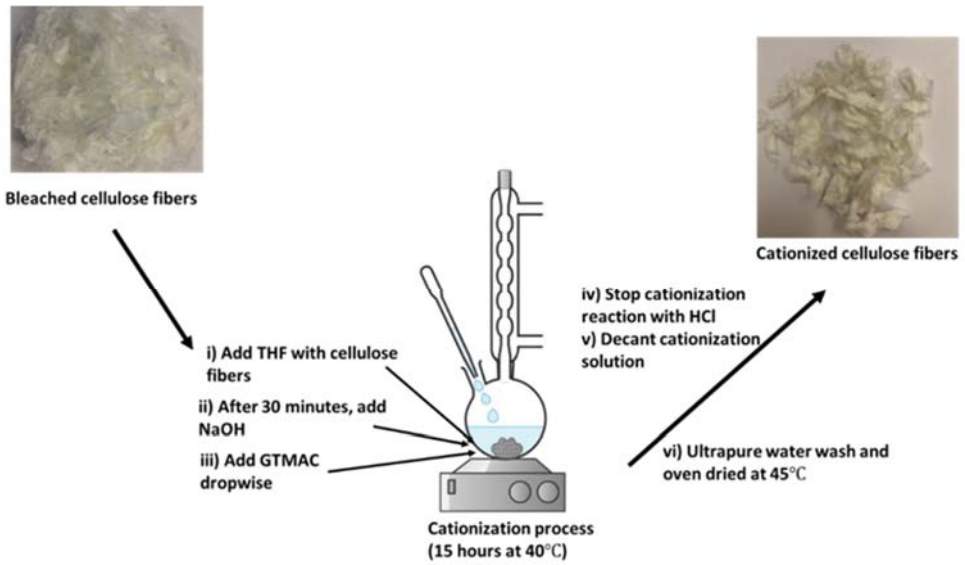

Figure 6.1: Schematic showing the preparation of cationised cellulose fibres extracted from hemp (*Cannabis sativa* L.) bast fibres.

6.2.2 Methyl orange and sunset yellow dye adsorption studies

6.2.2.1 Batch adsorption experiments

Adsorption measurements were determined by batch experiments of 50 mg of the adsorbent sample with 20 ml (20 mgL^{-1}) of aqueous dye solutions. The pH of dye solution was adjusted with 0.1 M HCl or NaOH solution. The mixture was shaken in a thermostatic shaker bath at 120 rpm and room temperature for 24 hrs. After a shaking time was completed, the suspension was centrifuged at 4000 rpm for 10 min. The equilibrium concentration of dye solution was measured using a UV-Vis spectrophotometer at the dye's maximum wavelengths, 465 and 485 nm for methyl orange and sunset yellow, respectively. All assays were carried out in triplicate and the presented data represented the mean values of the experimental results. The amount of dye adsorbed by GT-cellulose (mgg^{-1}) (q_e) and the percentage of dye removal (% R) were calculated by using following equations, respectively. The adsorption capacity (q_e) and percentage removal (% R) were calculated using Equation 6.1 and 6.2, respectively.

$$q_e = \frac{(C_0 - C_e) \times V}{M} \quad (6.1)$$

$$\%R = \frac{(C_0 - C_e)}{C_0} \times 100 \quad (6.2)$$

Where qe is the amount of dye adsorbed by the GT-cellulose (mgg^{-1}), C_0 (mgL^{-1}) and C_e (mgL^{-1}) are the initial and equilibrium concentrations of the dye in solution, respectively, V (L) is the solution volume and M (g) is the sorbent mass. The experiments were carried out by varying the pH of the dye solutions (2-10), adsorbent mass (10-60 mg), initial dye concentration (5-200 mgL^{-1}), contact time (5630 min).

6.2.2.2 Application to real environmental waters.

Application studies were performed using tap and drain water from the environmental chemistry laboratory (Wits university), and seawater from Mdhloti (Durban, South Africa). The sorption experiments were performed with 20 mL each of the effluent's samples spiked with 20 mgL^{-1} dye concentrations. Adsorbent was added to the mixture and stirred for 24 hr at room temperature. After 24 hrs, samples were centrifuged at 4000 rpm for 10 min and analysed as before.

6.2.3 Adsorption isotherms, kinetics, and thermodynamic parameters

6.2.3.1 Adsorption isotherm model

Three isotherm models were fitted to the adsorption data: Langmuir, Freundlich and Temkin isotherm. The Langmuir isotherm model assumes monolayer adsorption on a structurally homogenous surface where there is no interaction between molecules adsorbed on adjacent sites (Ibrahim, Ang and Wang,

2009). The non-linear Langmuir is given by the equation below and the calculated values are given in Table 6.3:

$$q_e = \frac{q_m K_L C_e}{1+K_L C_e} \quad (6.3)$$

Where C_e (mgL^{-1}) is the dye concentration at equilibrium, q_e (mgg^{-1}) is the amount of dye adsorbed per GT-cellulose adsorbent used, K_L (Lmg^{-1}) is the Langmuir constant related to binding sites affinity and adsorption energy, and q_{max} (mgg^{-1}) is the maximum monolayer capacity of adsorption.

The Freundlich isotherm model assumes multilayer adsorption on a heterogeneous adsorbent surface with uneven distribution of adsorption heat and affinity (Ilgin, Ozay and Ozay, 2020). The non- linear Freundlich is given by the equation below and the calculated values are given in Table 6.3:

$$q_e = K_f C_e^{1/n} \quad (6.4)$$

Where K_F ((mgg^{-1}) (mgL^{-1}) $^{(-1/n))}$ and n (dimensionless) are Freundlich constant related to the adsorption intensity and adsorption capacity, respectively. The n values indicate the favourability of the adsorption process.

The Temkin isotherm is used to describes a heterogenous adsorption between the adsorbed and adsorbent interaction. Adsorption heat decreases linearly with increasing interactions between adsorbents and adsorbates, and the adsorption binding energies are distributed uniformly (Wang *et al.*, 2016). The non-linear Temkin isotherm is given by the equation below and the calculated values are given in Table 6.3:

$$q_e = \frac{RT}{B_T} \ln(K_T C_e) \quad (6.5)$$

where C_e and q_e are the same meaning as previously described, and K_T (L mg^{-1}) and B_T (J mol^{-1}) are the Temkin constants. R (8.314 J mol^{-1} K^{-1}) is the universal gas constant, and T (K) is the absolute temperature.

Dubinin-Radushkevich (D-R) isotherm is useful in determining on the nature of adsorption process as a physical or a chemical adsorption (Ayawei, Ebelegi and Wankasi, 2017). D-R isotherm is given as follows and calculated parameters are presented in Table 6.3:

$$\ln q_e = \ln q_{max} - \beta\varepsilon^2 \quad (6.6)$$

$$\varepsilon = RT \ln(1 + {}^{1}/_{C_e}) \quad (6.7)$$

$$E = \frac{1}{\sqrt{2\beta}} \quad (6.8)$$

Where q_e, q_{max}, and C_e are the same meaning as previously described. β is the Dubinin-Radushkevich constant ($mol^2\ kJ^{-2}$), and ε is the Polanyi potential (kJ mol^{-1}), R (8.314 J mol^{-1} K^{-1}) is the universal gas constant, and T (K) is the absolute temperature. E is the average adsorption energy (kJ mol^{-1}), which is used to determine the type of adsorption mechanism (Günay, Arslankaya and Tosun, 2007). when E is less than 8 kJ mol^{-1}, physical adsorption is favoured and when E greater than 8 kJ mol^{-1}, chemisorption is favoured (An Tran *et al.*, 2021).

6.2.3.2 Adsorption kinetics model

To further investigate the adsorption mechanism and its potential rate-controlling steps such as mass transfer, diffusion control, and chemical reaction, the adsorption kinetics models: Pseudo first order (PFO) kinetic, Pseudo second order (PSO) kinetic, and intraparticle diffusion (IPD) were investigated.

The Pseudo first-order equations is expressed in the non-linearized form is given as follows (Ho and McKay, 1998) (Fungaro, Borrely and Carvalho, 2013)

$$q_t = q_e(1 - \exp^{(K_1 t)}) \quad (6.10)$$

Where q_e is the amount of dye adsorbed per mass of GT-cellulose adsorbent at equilibrium, (mg g^{-1}), q_t is the amount of dye adsorbed per unit mass of GT-cellulose adsorbent at a certain time, (mg g^{-1}), t is the removal of time t, K_1 is the rate constant of pseudo first-order adsorption (g (mg min)$^{-1}$). The plots of q_t vs. t are used to determine K_1 and q_e from the slope and intercept of the plot, respectively.

Pseudo second-order model is more suitable to understand adsorption on heterogeneous surfaces adsorption and multiple adsorption layers. The non-linear form of pseudo second-order model is given as follows (Fungaro, Borrely and Carvalho, 2013)(Ho and McKay, 1998):

$$q_t = \frac{q_e^2.K_2.t}{1+q_e.K_2.t} \quad (6.11)$$

Where q_t, q_e, and t have the same meaning as in the pseudo-first order model and K_2 is the rate constant of pseudo second-order model (g (mg min)$^{-1}$). The plots of q_t vs. t are employed to determine K_2 and q_e from the slope and intercept of the plot, respectively.

Intraparticle diffusion model is also used to study the adsorption kinetic of a chemical process. The intraparticle diffusion model equation is given as follows (Gandhi, Sirisha and Chandra Sekhar, 2016)(Nethaji, Sivasamy and Mandal, 2013):

$$q_t = k_{id}\sqrt{t} + C_i \quad (6.12)$$

K_{id} is the slope which refer to the intraparticle diffusion rate constant (g (mg min)$^{-1}$).and C (mg g^{-1}) is the intercept which is a constant related to the thickness of the boundary layer. t is the same as previously described. The plots of qt vs. $t^{0.5}$ are used to determine K_{id} and C_i from the slope and intercept of the plot, respectively.

6.2.3.3 Thermodynamic analysis

Adsorption thermodynamic studies were conducted at various temperatures (298 - 318 K). Interaction between adsorbent and adsorbate during adsorption process was evaluated using thermodynamic parameters such as Gibbs free energy (ΔG, kJ mol^{-1}), enthalpy (ΔH, kJ mol^{-1}), and entropy (ΔS, J molK^{1}). By plotting a lnK_c versus 1/T curve, the parameters were calculated and given in Table 6.7 as follows:

$$\Delta G^\circ = \Delta H^\circ - T\Delta S^\circ \quad (6.13)$$

$$\Delta G^\circ = -RT\ln K_c \quad (6.14)$$

$$K_c = \frac{q_e}{C_e} \quad (6.15)$$

$$\ln K_c = \frac{\Delta S^\circ}{R} - \frac{\Delta H^\circ}{RT} \quad (6.16)$$

where C_e is equilibrium concentration in dye solution (mg L^{-1}), q_e is the amount of dye adsorbed per mass of GT-cellulose adsorbent at equilibrium, (mg g^{-1}), T is the temperature (K) and R is the gas constant (8.314 J mol^{-1} K^{-1}) (Ebelegi, Ayawei and Wankasi, 2020)(Konicki *et al.*, 2015).

6.3 Results and discussion

6.3.1 Characterisation of bleached treated and cationised cellulose

In this work, bleached cellulose fibres extracted from hemp bast fibres were cationised using GTMAC, a highly effective and commercially available cationisation and NaOH as a base catalyst (Mohammed, Grishkewich and Tam, 2018). Changes in intramolecular and intermolecular bonds of cellulose during cationisation are improved using NaOH as a catalyst base (Willberg-Keyriläinen *et al.*, 2019). To synthesize cationic cellulose, the introduction of the trimethylammonium chloride groups of GTMAC

was carried out through nucleophilic addition reaction between the alkali activated hydroxyl groups of cellulose and reactive epoxy moiety of GTMAC shown in Figure 6.2. Similar studies were reported by Hasani *et al*., working on cationic functionalisation of CNCs produced from cotton using a cationic surfactant EPTMAC (Hasani *et al.*, 2015) (Zaman *et al.*, 2012)(Chaker and Boufi, 2015). It has been reported in literature that the main etherification reaction is accompanied by an alkaline hydrolysis reaction during the cationisation process in the presence of a water content. Therefore, to eliminate undesirable side reactions involved in alkaline hydrolysis of GTMAC, THF has been employed as an organic solvent of choice as also studied in various literature (Rajesh and Hemraz, 2018) (Odabas *et al.*, 2016).

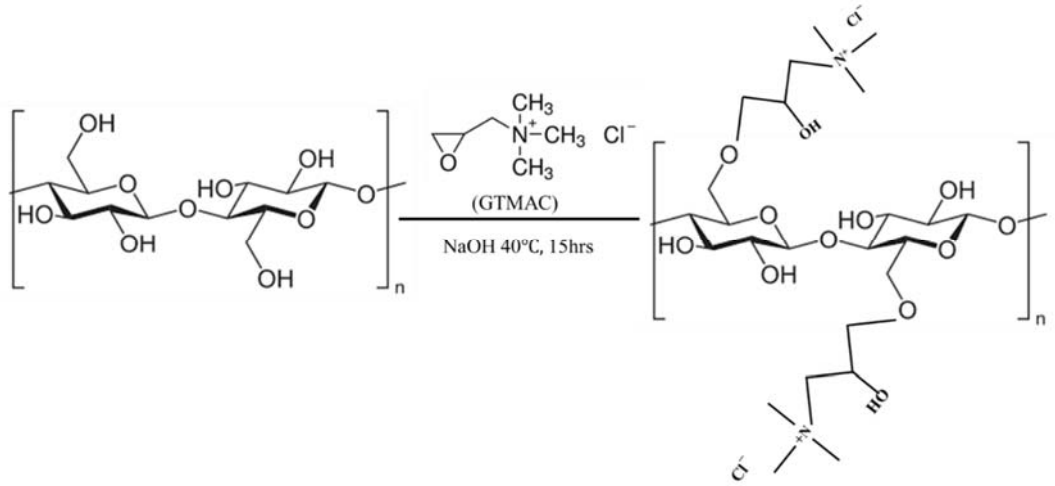

Figure 6.2: Desirable reaction scheme for the cationisation of cellulose using GTMAC.

6.3.2 Scanning Electron Microscope analysis

SEM was conducted to determine the surface morphology of bleached cellulose and cationised cellulose samples in Figure 6.3. Figure 6.3 (a) represents bleached cellulose from the hemp plant and shows a typical cellulose structure forming long fibrous structures of cylindrical cross-section referred to as the fibre bundles. Figure 6.3 (c) representing GTMAC modified cellulose shows fibres with similar surface morphology to the bleached cellulose fibres. Due to the entanglement of long cellulose fibres and twisted morphologies, the length bundles could not be easily deduced with the SEM image, however, only the average diameter could be deduced. The average diameter of bleached cellulose and cationised cellulose fibres were determined to be 10.1 ± 0.21 µm and 9.2 ± 0.87 µm, respectively using ImageJ software. From the results, cationisation process did not substantially affect the shape and/or the size of fibres. The small changes in diameter noted in GT-cellulose can be attributed to structural breakdown during cationisation, improving the active surface area, hence preferrable for effective adsorption studies (Hasani *et al.*, 2015) (Fungaro, Borrely and Carvalho, 2013). Muqeet and coworkers also

reported that while working on cationisation of CNFs for the removal of sulfate ions from aqueous solutions, cationisation did not enact any major modifications to the size and/shape of fibres (Muqeet *et al.*, 2017).

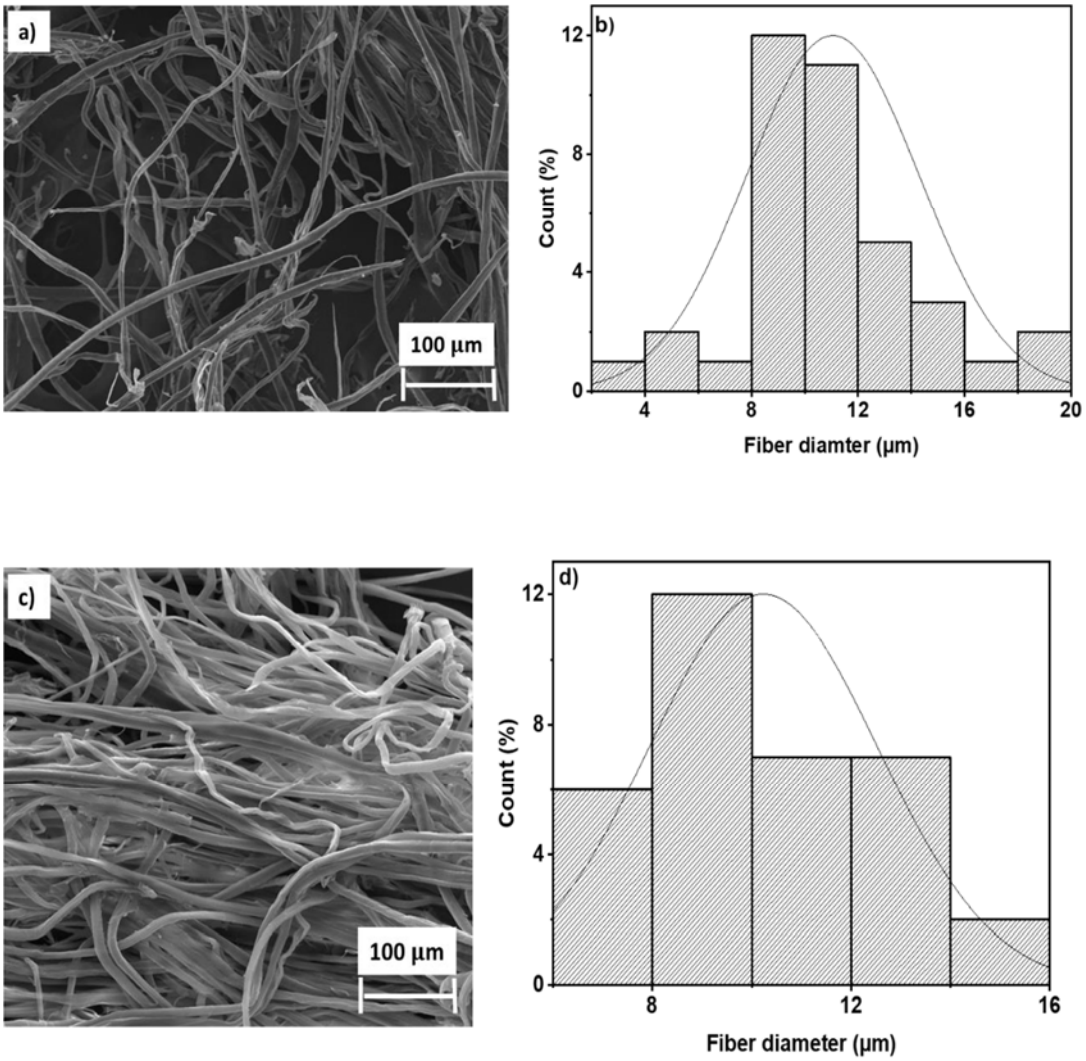

Figure 6.3: SEM images of a) bleached and c) cationised cellulose, and histograms of b) bleached and d) cationised cellulose.

6.3.3 Fourier Transform Infrared spectroscopy

FTIR analysis of raw plant fibres, bleached cellulose, GTMAC and cationised cellulose (GT-cellulose) samples are shown in Figure 6.4 and Table 6.1. FTIR analysis is conducted to present detailed information about the chemical groups on the surface of the samples. In all spectrum, strong characteristic absorption bands at 3340 cm^{-1} and 2905 cm^{-1} are assigned to the O-H stretching vibration in hydroxyl groups involved in hydrogen bonding and the carbon hydrogen (C-H) asymmetric

stretching vibration, respectively (Zaman *et al.*, 2012). The band observed at 1640 cm^{-1} was ascribed to the hydroxyl bending vibrations of absorbed water in the cellulose samples (Gu *et al.*, 2020). At 1368 cm^{-1} can be ascribed to the stretching and deformation vibration of carbon-hydrogen (C-H) group in the glucose unit of cellulose. The characteristic bands at 1426, 1158, 1113 and 894 cm^{-1} are thought to be typical bonds of cellulose 1β (Du, Liu, Mu, *et al.*, 2016). The weakening band at 1426 cm^{-1} can be attributed to the disruption in intermolecular and/or intramolecular hydrogen bonding between the hydroxyl groups of cellulose from bleached fibres to cationised cellulose fibres (Yue *et al.*, 2019)(Gu *et al.*, 2020). The peaks in the range 1113-1028 cm^{-1} are ascribed to the C-O-C pyranose ring skeletal vibration and the 894 cm^{-1} is due to the carbon-hydrogen (C-H) bond deformation mode of the βglycosidic linkages between the glucose units of cellulose (Gu *et al.*, 2020). The GTMAC spectrum, Figure 6.4b, a strong band appears at 1480 cm^{-1} due to $-CH_2$ symmetric bending modes which correspond to the trimethyl groups of the cationic substituent which is also apparent on the GT-cellulose spectrum on Figure 6.4a (Etale *et al.*, 2021). Kaboorani and Riedl successfully modified CNCs by a cationic surfactant, hexadecyltrimethylammonium (HDTMA) bromide, leading to the presence of quaternary ammonium groups. They observed that a weak intensity peak at 1480 cm^{-1} on the FTIR spectrum associated with $-CH_2$ rocking for CNC modified with high concentrations of HDTMA (Kaboorani and Riedl, 2015). Lastly, the increase in intensity at 1113 cm^{-1} and 1028 cm^{-1} provides evidence of grafting of GTMAC onto the surface of cellulose as shown in Figure 6.4a. Similar results were reported by Rana and co-workers while working on preparing cationised alpha cellulose extracted from sugarcane bagasse, whereby on the FTIR spectrum of synthesized cationic alpha cellulose, characteristic band at 1477 cm^{-1} and was assigned to C-N stretching vibrations formed due to the introduction of quaternary ammonium group in cellulosic structure (Rana *et al.*, 2021).

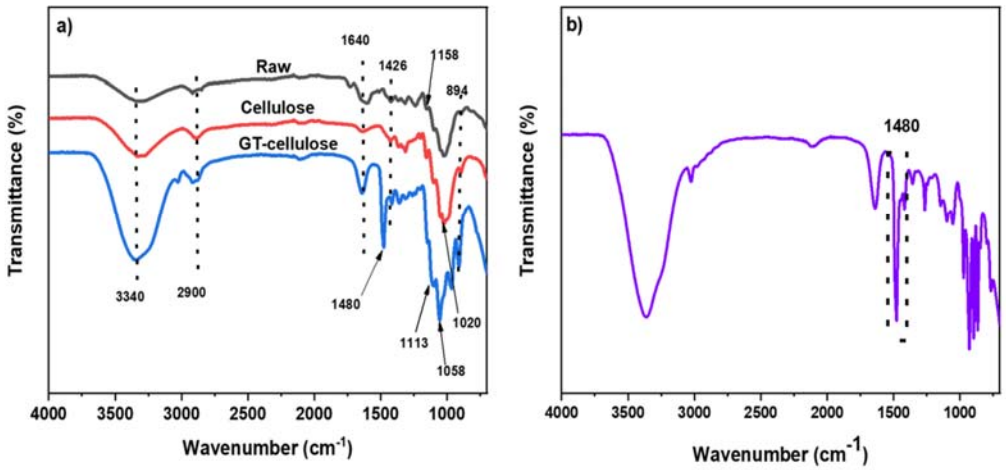

Figure 6.4: a) FTIR spectrum of raw plant fibre, bleached cellulose, and GT-cellulose and b) FTIR spectrum of GTMAC solution.

Table 6.1: The main functional groups observed on raw plant fibre, bleached cellulose, and GT-cellulose by FTIR spectroscopy and their corresponding wavenumbers.

Wavelength (cm^{-1})	**Functional groups**	**Ref**
3340	OH stretching vibration	(Syafri *et al*., 2018)(Alhogbi *et al*., 2021)
2900	C-H symmetrical stretching vibration	(Alhogbi *et al*., 2021)(Mahardika *et al*., 2018)
1640	OH bending vibration	(Li *et al*., 2014)(Gao *et al*., 2016)
1480	-CH_2 bending vibrations	(Gao *et al*., 2015)(Gao *et al*., 2016)
1426	-COOH stretching vibrations	(Yue *et al*., 2019)(Eltaweil *et al*., 2020)
1368	C-H bending vibrations	(Konicki *et al*., 2015)(Huang *et al.*, 2020b)
1158	C-O stretching vibrations	(Zaman *et al*., 2012)(Gao *et al*., 2016)
1100-1028	C-O-C pyranose ring skeletal vibration	(Tejada-Tovar *et al*., 2021)(Yin *et al*., 2017)
894	C-H deformation vibrations	(Zaman *et al*., 2012)

6.3.4 X-ray diffraction analysis

The XRD patterns of raw plant fibres, bleached cellulose, and GT-cellulose are presented in Figure 6.5. The crystallinity of fibres can be affected by any chemical or mechanical treatment subjected to the material thereby affecting the size and shape of the fibres. From the X-ray diffractograms, all the diffraction patterns are characterised by two peaks at around 2θ=16.3° and 22.5° corresponding to the (110) and (002) crystallographic planes respectively and all of them are related to cellulose type I, and an amorphous broad hump (2θ=18-19°) (Hemmati *et al.*, 2018). The crystallinity of raw plant fibres, bleached cellulose and GT-cellulose were calculated as 60%, 73% and 54% respectively (shown in Table 6.2), corresponding to similar results recorded by Rosli and colleagues working on Agave angustifolia fibres (Rosli, Ahmad and Abdullah, 2013). During the alkali (4 wt% NaOH) and bleaching (aqueous chlorite in acetate buffer) treatment, the crystallinity increased from 60% to 73% due to the reduction and removal of amorphous regions such as hemicellulose and lignin content (Rosli, Ahmad

and Abdullah, 2013)(García-García *et al.*, 2018). Upon cationisation with GTMAC, the crystallinity decreased to 44% due to the breaking down of intermolecular hydrogen bonds in the structure of cellulose hindering the formation of crystalline regions (Etale *et al.*, 2021)(Sajjan, Premakshi and Kariduraganavar, 2015).

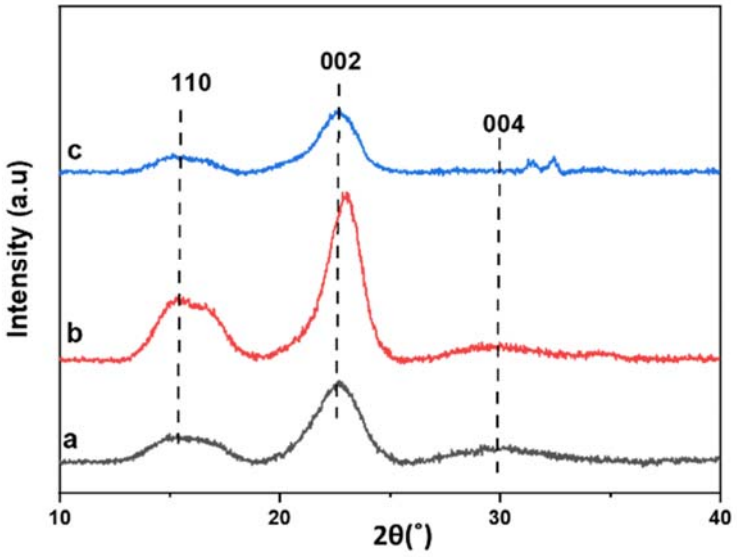

Figure 6.5: XRD spectrums of a) raw plant fibre, b) bleached cellulose and c) GT-cellulose.

Table 6.2: Crystallinity Index (CrI), Onset Temperature (T_{onset}), Maximum Degradation Temperature (T_{max}), and Char Residuals at 900 °C Obtained from XRD, TGA and DTG plots.

Samples	**CrI (%)**	**Cellulose thermal degradation**		
		T_{onset} (℃)	**T_{max} (℃)**	**Ash amount at 900℃ (%)**
Raw plant fibres	60	279.25	386.14	14.2
Bleached cellulose	73	259.66	383.71	10.3
GT-cellulose	44	228.26	365.90	9.5

6.2.5 Thermogravimetric and Derivative Thermogravimetric analysis

The TGA was performed to evaluate the thermal stability of raw plant fibre, bleached cellulose, and GT-cellulose fibres in a temperature range of 30-900℃ with the heating rate 10 ℃. min^{-1}. The TGA and DTG curves of raw plant fibre, bleached cellulose and GT-cellulose are shown in Figure 6.6a) and

b), respectively. The thermal degradation onset temperatures, maximum thermal degradation temperatures and residual ash amount at 900 ℃ are also listed in Table 6.2. In the temperature range 30-150 ℃, an initial weight loss of approximately 10 % is observed for all samples, which can attributed to moisture loss from absorbed water (Ilgin, Ozay and Ozay, 2020)(Tejada-Tovar, Villabona-Ortíz and Gonzalez-Delgado, 2021). Raw plant fibre and bleached cellulose samples resulted in a two-step mechanism process for degradation and cationised cellulose involved a three-step mechanism process of degradation. As seen on the raw plant fibre curve, a second weight loss of about 64.4% from 260−400 ℃ and it was associated with the presence of non-cellulosic material such as hemicellulose and lignin, whereas bleached cellulose resulted in weight loss 80.2% from 320−380 ℃ which can be attributed hemicellulose and lignin degradation from alkali and bleaching treatment (Tejada-Tovar, Villabona-Ortíz and Gonzalez-Delgado, 2021)(Liu *et al.*, 2016)(Silva *et al.*, 2015). The cationised cellulose sample was observed to have reduced onset thermal degradation at approximately 228℃ and due to further removal of non-cellulosic material and addition of quaternary ammonium groups onto cellulose fibres after cationisation, resulting in lowered thermal stability and reduced crystallinity (Gao *et al.*, 2016)(Rana *et al.*, 2021).

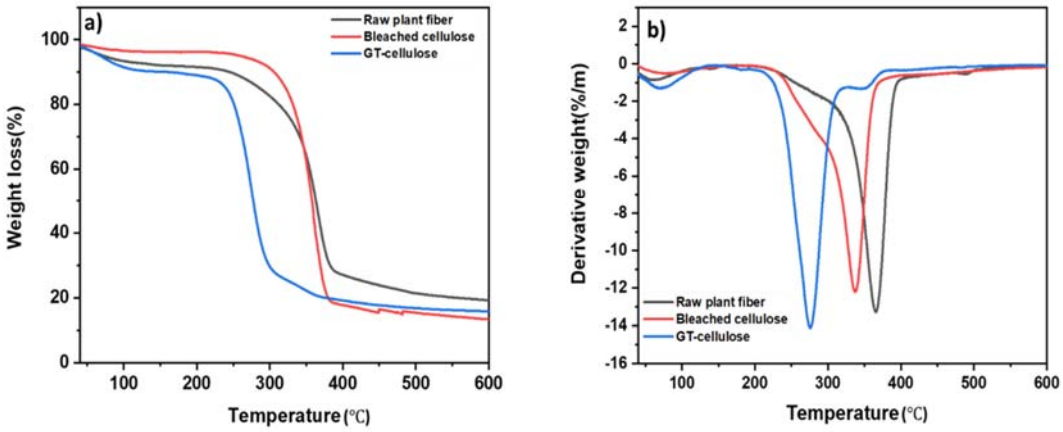

Figure 6.6: a) TGA and b) DTA curves of raw plant fibre, bleached cellulose, and GT-cellulose.

6.4 Adsorption experiments

6.4.1 Effect of pH

The point of zero charge(pH_{pzc}) of an adsorbent plays a significant role in mode of adsorption at different pH and it helps determine the pH at which the surface of the adsorbent has net electrical neutrality. From the point of zero charge graph on Figure 6.7(a), the pH_{pzc} of the cationised adsorbent is 4.01, hence the surface charge is positive at pH values lower than pH_{PZC}, neutral at pH_{pzc} =4.01, and negative at pH values higher than the pH_{pzc} (Abidi *et al.*, 2019). The effect of pH on the uptake of methyl orange

(MO) and sunset yellow (SY) onto GT-cellulose is shown in Figure 6.7(b). The pH of a solution is known to significantly affect the adsorption of pollutants onto adsorbents surface, however, from the results obtained we observed that the solution pH did have affect the dyes uptake onto GT-cellulose. For MO, it was observed that the dye removal efficiency increased from pH 2 (4.2 %) to pH 4 (98 %), with a slight decrease in removal uptake after pH 5(b). At lower adsorbate pH, the adsorbent surface has a higher protonation degree leading to an increase in hydrogen (H^+) ions concentration therefore resulting in increased electrostatic attraction between the positively charged adsorbent and negatively-charged MO dye molecules and at higher adsorbate pH, the positively charged sites on the adsorbent are reduced (less H^+, more OH^-) resulting in less attraction (electrostatic repulsion) of the dyes on the surface of GT-cellulose (Wong *et al.*, 2020). A similar result was recorded for the removal of methyl orange from aqueous solutions using dragon fruit foliage as an adsorbent (Haddadian *et al.*, 2013). As for SY, results show that the solution pH did not have a significant effect of the uptake onto GT-cellulose. As shown in Figure 6.7(b), the dye uptake slightly increased from pH 2 (97 %) to pH 8 (99 %) and this interaction between the adsorbent's surface and dye molecules may not be solely described by simple electrostatic interactions, nonetheless, Van der Waals forces, hydrogen bonding or ion-ion interactions may contribute largely to the adsorption mechanism between the cationised adsorbent and anionic dyes (Sujitha and Ravindhranath, 2016). For further experiments, all dye solutions were prepared at pH 4.

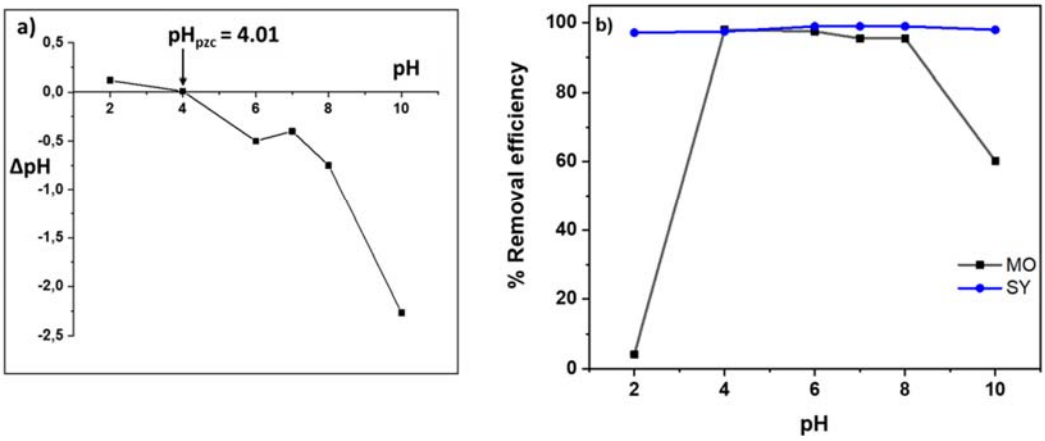

Figure 6.7: a) Point of zero charge graph and b) Effect of solution pH of dyes (MO and SY) adsorbed onto GT-cellulose adsorbent.

6.4.2 Effect of adsorbent dosage

The adsorbent dose governs the capacity of adsorbent for a given initial concentration of dye (20 mg g^{-1}), and it is an important parameter in adsorption studies. The effect of adsorbent dosage on the adsorption of MO and SY onto GT-cellulose is shown in Figure 6.8. From the results, Figure 6.8,

represents the removal efficiency and adsorption capacity of dyes, and it shows that an increase in adsorbent dose results in an increase removal efficiency and a decrease in adsorption capacity. This trend can be explained that there is an increase in available sorption active sites on the surface of the adsorbent as the adsorbent dosage increases, however, further increment of the adsorbent amount could lead to possible surface agglomeration of the GT-cellulose fibres, hindering access to the adsorbent's sorption sites during the adsorption process (Chukwuemeka-Okorie *et al.*, 2021). The abovementioned relationship is observed for both dyes. For MO dye in Figure 6.8 (a), at adsorbent dosage of 10 mg and 60 mg resulted in removal efficiencies of 88 % and 98 %, respectively whereas the adsorption capacity was reduced significantly to 34.8 mg g^{-1} and 6.46 mg g^{-1}, respectively. Figure 6.8 (b) represents the removal efficiency of SY from the sample solution onto the adsorbent surface and it was observed that SY uptake was significant from 10 mg (89 %) and 60 mg (100 %) with an adsorption capacity of 36.6 mg g^{-1} and 6.76 mg g^{-1}, respectively (Jarusiripot, 2014). A similar trend was reported by Taha and colleagues while using natural Iraqi palygors-kite clay as low-cost adsorbent for adsorptive removal of Basic Red 2 from industrial effluents (Taha, Samaka and Mohammed, 2013). Since 10 mg adsorbent amount resulted in the highest adsorption capacity for both dyes, it was selected as the optimal mass for further experiments.

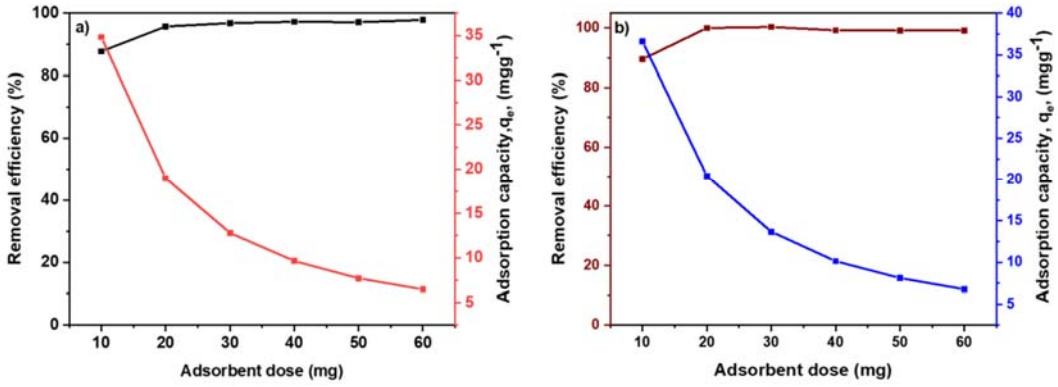

Figure 6.8: Effect of adsorbent dosage on the uptake of MO onto GT-cellulose adsorbent and b) Effect of adsorbent dosage on the uptake of SY onto GT-cellulose adsorbent

6.4.3 Effect of initial concentration

The influence of the initial dye's concentration onto GT-cellulose was carried out at a fixed adsorbent dosage (10 mg), solution volume (0.02 L), a solution pH of 4, and various dye concentrations (5-200 mg L^{-1}) at 298.15 K. As shown in Figure 6.9, increasing the concentration of the dyes from 5 to 200 mg L^{-1}, greatly increases the adsorption capacity of dyes onto GT-cellulose from 10.53-154.54 mg g^{-1} (93 % - 36 %) in MO dye and from 8.19-52.73 mg g^{-1} (85 % - 16 %) in SY dye, thereby decreasing the removal efficiency. A similar trend was observed by Vena and colleagues, working on the preparation

of raw oyster shell for removal of Coomassie brilliant blue R-250 dye from aqueous solution (Veni and Brenda, 2021). This could postulate that more adsorbates have the ability bind to the active sites on the adsorbent at higher dye concentration, resulting in higher adsorption capacities (Haddadian *et al.*, 2013). At 200 mg L^{-1} dye concentration, the removal efficiency was given as 8.34 % for MO and 4.79 % for SY, meaning that there are fewer active sites available for sufficient complete removal of dyes. This can also be observed on similar studies for the removal of Sunset Yellow Azo dye using activated carbon entrapped in alginate from aqueous solutions (Abdel-aziz and Abdel-gawad, 2020).

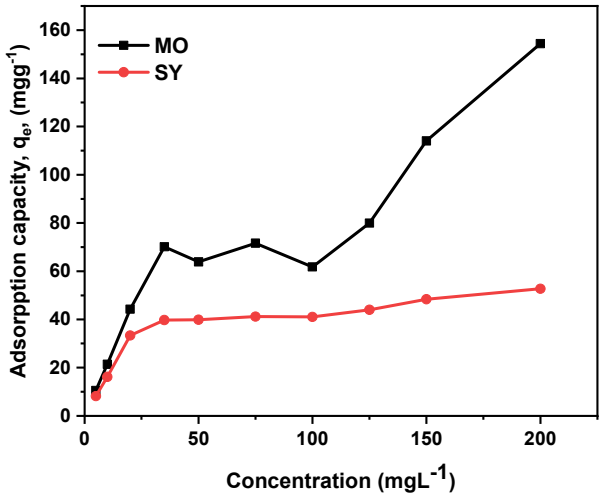

Figure 6.9: Effect of initial dye concentration on the uptake of MO and SY onto GT-cellulose adsorbent at 298.15 K.

6.4.4 Effect of temperature

The effect of temperature experiments for MO and SY uptake was carried out at different temperatures (298.15, 308.15, 318.15 K) at various dye concentration (10, 20, 35, 50 mg g^{-1}). For MO dye at 20 mg L^{-1} in Figure 6.10a, it was observed that as the temperature increases from 298.15 K to 318.15 K, the adsorption capacity decreases from 44.27 mg g^{-1} to 33.30 mg g^{-1}, a similar trend was observed for SY dye at 20 mg L^{-1} (Figure 6.10b), the adsorption capacity decreases from 33.34 mg g^{-1} to 25.89 mg g^{-1}. Figure 6.10 (a and b) demonstrates that an increase in temperature, decreases the adsorption capacity of adsorbent for the anionic dyes. This could be attributed to the bond dissociation occurring on the adsorbent surface sites as the temperature increases increasing the kinetic energy within the system (Chukwuemeka-Okorie *et al.*, 2021).

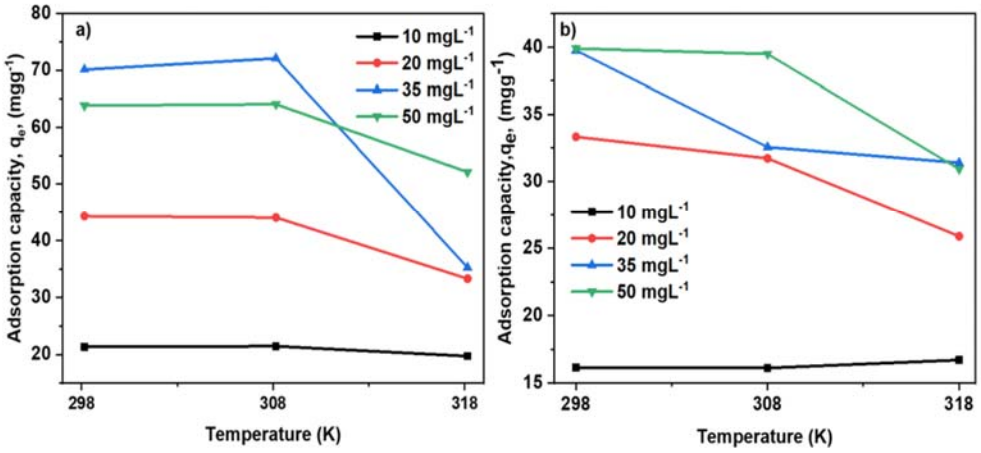

Figure 6.10: a) Effect on temperature on the uptake of MO onto GT-cellulose adsorbent and b) Effect on temperature on the uptake of SY onto GT-cellulose adsorbent.

6.10.5 Effect of contact time

The effect of contact time on the uptake of MO and SY onto GT-cellulose was studied over a period of 630 min (Figure 6.11a and b). At 20 ppm, the equilibrium adsorption capacity MO was determined to be 32.18 mg g^{-1}at 120 min (SY dye q_e= 40.04 mg g^{-1} at 270 min) with a removal efficiency of 91 % (SY dye 97 %). After 120 min for MO uptake and 270 min for SY uptake, slight changes were recorded in the adsorption capacity. Therefore, this can be attributed to the abundant surface binding sites on the adsorbent which become saturated as contact time increases that suggest equilibrium adsorption is attained (Chukwuemeka-Okorie *et al.*, 2021)(Abdel-Ghani *et al.*, 2017). A similar trend was reported by Abdel-Ghani and colleagues while studying Coomassie Brilliant Blue R-250 dye adsorption by activated carbon from *Nigella sativa L*. (Abdel-Ghani *et al.*, 2017).

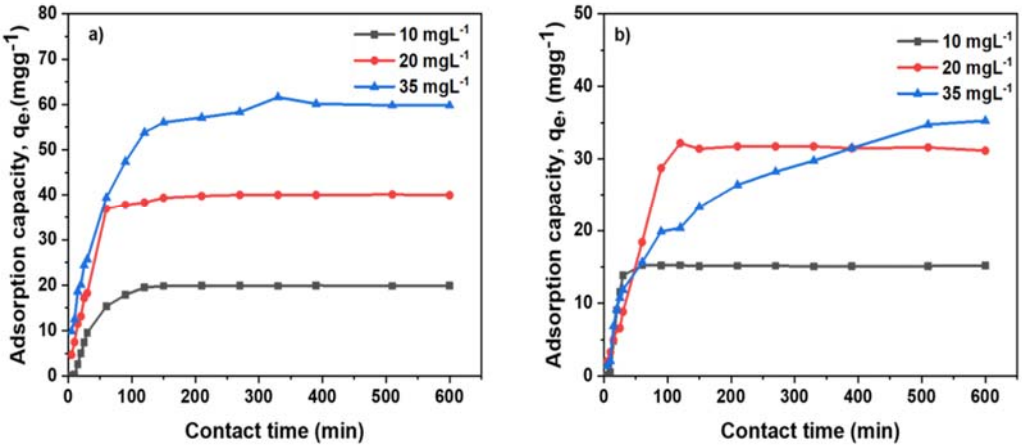

Figure 6.11: a) Effect of contact time of MO dye onto GT-cellulose adsorbent over a period of 630 min and b) Effect of contact time of SY dye onto GT-cellulose adsorbent over a period of 630 min.

6.5 Adsorption isotherms, kinetics, and thermodynamic parameters

6.5.1 Adsorption isotherm models

Adsorption isotherm studies for MO onto GT-cellulose by comparing Langmuir, Freundlich, Temkin and D-R adsorption isotherm model were studied and the calculated correlation coefficients (R^2) at 298 K were given as 0.996, 0.708, 0.857 and 0.732, respectively (see Table 6.3 below). According to the given R^2 values, the adsorption of MO onto GT-cellulose was best fit by the Langmuir isotherm model and such results indicate monolayer adsorption and homogeneous onto the surface of GT-cellulose. Similar results were reported in adsorption of anionic dyes on a cationic amphiphilic dextran hydrogel (Stanciu and Nichifor, 2019). Furthermore, the values of 1/n could mean, easy adsorption when $0.5 < 1/n \leq 1$; difficult adsorption when 1/n is greater than 1; and excellent favourable adsorption when $0.1 < 1/n \leq 0.5$. From the 1/n data given in Table 6.3, MO adsorption onto GT-cellulose adsorbent undergoes favourable excellent adsorption under the optimised adsorption conditions and a maximum adsorption capacity of 69.71 mg g^{-1} from Langmuir adsorption isotherm model is observed. For SY adsorption isotherm studies onto GT-cellulose, the Langmuir isotherm was the best fit model as the R^2 value was greater ($R^2 = 0.992$) than that of Freundlich ($R^2 = 0.619$), Temkin ($R^2 = 0.634$), D-R ($R^2 = 0.626$) isotherm models. This confirms the applicability of Langmuir adsorption isotherm indicating the monolayer adsorption and homogenous surface of the adsorbent. Relatable data was also reported in the removal of sunset yellow azo dye using activated carbon entrapped in alginate from aqueous solution (Abdel-aziz and Abdel-gawad, 2020). The 1/n values of SY onto GT-cellulose adsorption are in support of a favourable excellent adsorption process and maximum adsorption capacity from Langmuir adsorption isotherm model was 42.85 mg g^{-1}. From the D-R isotherm, the evaluated average adsorption energies for MO and SY adsorption onto GT-cellulose under optimised conditions are all above E= 8 kJ mol^{-1}, supporting chemisorption processes as the adsorption mechanism. Similar studies are tabulated in Table 6.4.

Table 6.3: Adsorption isotherm parameters for the adsorption of MO and SY onto GT-cellulose.

	Isotherm parameters					
	Methyl orange			**Sunset yellow**		
T (K)	**Langmuir**					
	q_{max} (mgg^{-1})	**K_L (Lmg^{-1})**	**R^2**	**q_{max} (mgg^{-1})**	**K_L (Lmg^{-1})**	**R^2**

298	69.71	1.12	0.996	42.85	1.06	0.992
308	71.63	1.05	0.998	40.44	0.89	0.939
318	55.06	0.37	0.945	34.00	1.77	0.977
	Freundlich					
	1/n	**K_F (Lmg^{-1})**	**R^2**	**1/n**	**K_F (Lmg^{-1})**	**R^2**
298	0.297	32.32	0.708	0.291	21.64	0.604
308	0.299	33.06	0.706	0.248	18.64	0.619
318	0.371	20.19	0.897	0.234	17.39	0.843
	Temkin					
	B_T ($Jmol^{-1}$)	**K_T (Lmg^{-1})**	**R^2**	**B_T ($Jmol^{-1}$)**	**K_T (Lmg^{-1})**	**R^2**
298	252.19	26.65	0.857	387.49	26.58	0.634
308	250.93	24.28	0.858	404.41	17.46	0.779
318	284.30	6.52	0.967	542.03	44.92	0.894
	Dubinin-Radushkevich (D-R)					
	β	**E ($kJ.mol^{-1}$)**	**R^2**	**β**	**E ($kJ.mol^{-1}$)**	**R^2**
298	2.2×10^{-3}	15.18	0.732	2.1×10^{-3}	15.46	0.626
308	2.1×10^{-3}	15.61	0.735	1.7×10^{-3}	17.27	0.639
318	2.4×10^{-3}	14.42	0.902	1.4×10^{-3}	18.87	0.851

Table 6.4: Comparison of other adsorbents adsorption isotherm parameters.

Dye contaminant	**Adsorbent**	**q_{max} (mgg^{-1})**	**Ref**

Methyl orange	Hydroxyethyl starch/p(sodium acrylate) (HES/p(NaAAc)) hydrogel	2.84	(Ilgin *et al*., 2020)
	Dragon Fruit (Hylocereusundatus) Foliage	17.67	(Haddadian *et al*., 2013)
	Cationic dextran hydrogel	705	(Stanciu and Nichifor, 2019)
	3-chloro-2-hydroxypropyl trimethyl ammonium (CTA) modified chitosan magnetic composite adsorbent (CS-CTA- MCM)	2.55	(Li *et al*., 2016)
	Natural bentonite	2.26	(Fernandes *et al*., 2020)
	Magnetic Composite Polyaniline/Fe_3O_4 −Hydrotalcite and	156.3	(An Tran *et al.*, 2021)
	Magnetic cellulose/Fe_2O_3 hydrogels	7.51	(Zhang *et al*., 2017)
	Cationized cellulose (GT-cellulose)	69.71	This work
Sunset yellow	Cassava sievate biomass	0.091	(Chukwuemeka-Okorie *et al*., 2021)
	Activated carbon entrapped in alginate beads (AG-AC)	5.40	(Abdel-aziz and Abdel-gawad, 2020)
	Silver nanoparticles loaded on activated carbon	37.04	(Ghaedi, 2012)
	Amberlite FPA51	130.6	(Wawrzkiewicz, 2011)
	Layered double hydroxide (LDH)	142.86	(Abd Malek and Yasin, 2012)

	Cadmium sulfide nanoparticles loaded onto activated carbon (CdSN-AC)	83.33	(Mosallanejad and Arami, 2012)
	Cationized cellulose (GT-cellulose)	42.85	This work

6.5.2 Adsorption kinetic models

The kinetic models for MO and SY adsorption onto GT-cellulose was evaluated using three models: Pseudo first-order, pseudo second order and intraparticle diffusion. Calculated kinetic constants (K_1, K_2, K_{id}), adsorption capacity at equilibrium (q_e) and correlation coefficients (R^2) are presented in Table 6.6 above. From the data in Table 6.6, pseudo first-order model is the best fit model for the adsorption process of MO and SY onto GT-cellulose surface due to high R^2 values of 0.967 and 0.883, respectively. While comparing the experimental value for adsorption capacity for MO and SY strongly agree with the calculated adsorption capacity at equilibrium (Given in Table 6.5).

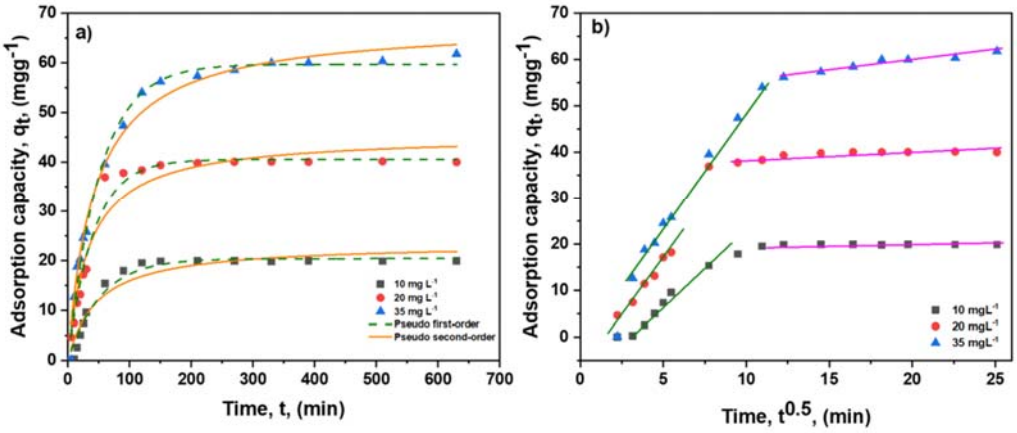

Figure 6.12: Effect of contact time on MO adsorption and kinetic data fit to (a) pseudo first order and pseudo second order non-linear models. (b) Intra-particle diffusion for adsorption of MO onto GT-cellulose at 298.15 K.

Table 6.5: Maximum experimental adsorption capacity of MO and SY onto GT-cellulose (adsorbent dosage = 10 mg, initial dye concentration= 75 mg L^{-1}, contact time = 24 hr).

T(K)	**298**	**308**	**318**
Methyl orange, $q_{max}^{experimental}$(mg g^{-1})	71.65	72.11	64.51

Sunset yellow, $q_{max}^{experimental}$(mg g^{-1})	41.19	41.42	39.98

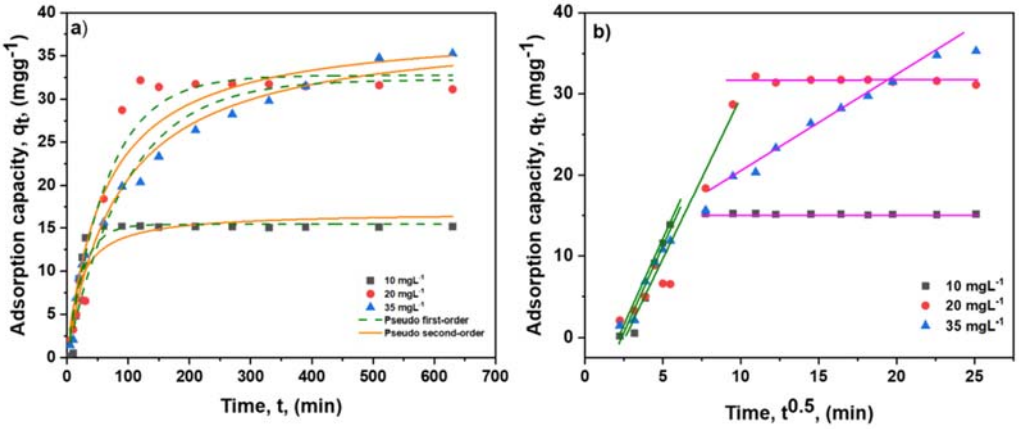

Figure 6.13: Effect of contact time on SY adsorption and kinetic data fit to (a) pseudo first order and pseudo second order non-linear models. (b) Intra-particle diffusion for adsorption of SY onto GT-cellulose at 298.15 K.

To evaluate and determine the mechanism and rate-limiting steps for the adsorption of MO and SY onto GT-cellulose, the intraparticle diffusion parameters were studied. Plots of $t^{0.5}$ vs q_t in Figure 6.12(b) and Figure 6.13(b) showed multi-linearly indicating that adsorption is given by two or more rate controlling steps of adsorption, namely: Step 1: The transport of dye to the surface of the adsorbent (film diffusion), (b) the transport of dye within the pores of the adsorbent (particle diffusion), and (c) adsorption of dye on the interior surface of the pores of the adsorbent (Wawrzkiewicz, 2011)(Wu, Tseng and Juang, 2009). Intraparticle diffusion is only the rate-limiting step if the plots in Figure 6.12 (b) and Figure 6.13 (b) yield a straight line that passes through the origin (where C = 0) (Ghaedi, 2012) (Ghaedi *et al.*, 2011)(Zhang *et al.*, 2018b). From the data presented in Table 6.6, it suggests that the 1st linear plots occurred due to film diffusion and 2nd linear plots support intraparticle diffusion. From Figure 6.12(b) and Figure 6.13 (b), film diffusion had greater R^2 values that intraparticle diffusion and in this way adsorption of MO and SY onto GT-cellulose was more favourable during transport of dye molecules to the adsorbent surface. Given that the plot do not pass through the origin, the intraparticle diffusion is not the only rate-controlling step (Wawrzkiewicz, 2011)(Lesaoana, 2018).

Table 6.6: Kinetic adsorption model parameters of MO and SY onto GT-cellulose.

	Kinetic parameters

Pseudo first-order	**C_0 (mg L^{-1})**	**K_1 (g (mg min)$^{-1}$)**	**q_e (mg g^{-1})**	**R^2**
Methyl orange	10	0.019	20.36	0.967
	20	0.024	40.52	0.979
	35	0.019	59.67	0.989
Sunset yellow	10	0.040	15.44	0.883
	20	0.015	32.74	0.956
	35	0.010	32.26	0.956
Pseudo second order	**C_0 (mg L^{-1})**	**K_2 (g (mg min)$^{-1}$)**	**q_e (mg g^{-1})**	**R^2**
Methyl orange	10	8.97×10^{-4}	23.45	0.927
	20	6.40×10^{-4}	45.48	0.940
	35	3.42×10^{-4}	67.96	0.984
Sunset yellow	10	2.97×10^{-3}	16.85	0.815
	20	4.26×10^{-4}	38.42	0.914
	35	3.06×10^{-4}	38.44	0.983
Intraparticle diffusion 1st line regression	**C_0 (mg L^{-1})**	**K_{Id} (g (mg min)$^{-1}$)**	**C_i (mg L^{-1})**	**R^2**
Methyl orange	10	2.47	-5.79	0.959
	20	4.42	-.5.20	0.928
	35	5.72	-6.32	0.969
Sunset yellow	10	2.29	-3.04	0.732
	20	3.63	-8.91	0.902
	35	2.56	-3.55	0.942

Intraparticle diffusion 2nd line regression	C_0 (mg L^{-1})	K_{Id} (g (mg min)$^{-1}$)	C_i (mg L^{-1})	R^2
Methyl orange	10	0.014	19.58	0.147
	20	0.014	38.11	0.459
	35	0.049	49.89	0.895
Sunset yellow	10	-0.005	15.24	0.164
	20	-0.060	30.31	-0.029
	35	1.063	10.11	0.972

6.5.3 Thermodynamic analysis

Calculated ΔG° values for MO and SY adsorption onto GT-cellulose were evaluated to be less than zero ($\Delta G^{\circ} < 0$), making them spontaneous in nature and thermodynamically feasible. It was further observed that ΔG° becomes less negative with an increase in temperature and favouring adsorption even at higher temperatures as shown in Figure 6.14 (Ilgin, Ozay and Ozay, 2020)(Haddadian *et al.*, 2013). Similar phenomenas were noted by Wang *et al*, on studies to use cellulose-based adsorbents for the adsorption of Congo-red anionic dye from aqueous solutions (Wang *et al.*, 2018).

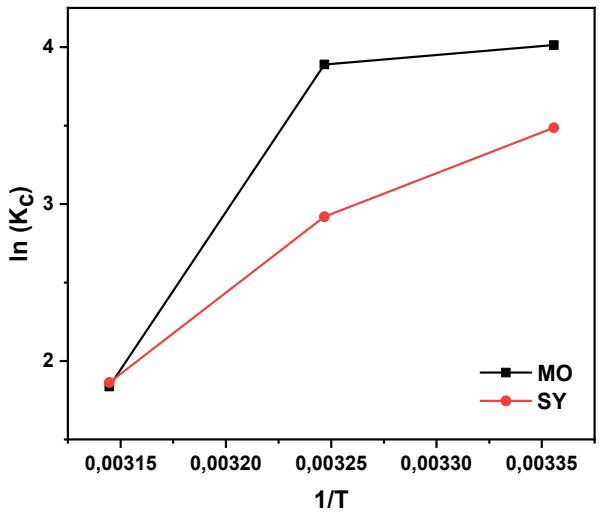

Figure 6.14: Vant' Hoff plot of MO and SY adsorption onto GT-cellulose

The enthalpy ΔH° of methyl orange and sunset yellow dyes were both greater zero ($\Delta H^{\circ} > 0$) making the adsorption processes, an endothermic process in nature. From Table 6.7, ΔH° = 84.86 kJmol^{-1} and ΔH° = 63.76 kJmol^{-1} for MO and SY adsorption, respectively. In the range ΔH° = 20-80 kJ mol^{-1}, physical adsorption mechanism is favoured, whereas ΔH° = 80-200 kJ mol^{-1}, chemisorption mechanism is favoured. Moreover, both dyes might be undergoing chemisorption and physisorption simultaneously. Corresponding results were recorded on the adsorption of cationic dyes onto sulfonic acid modified activated carbon (Goswami and Phukan, 2017). ΔS values illustrate a decreased randomness at the solid-solution interface during adsorption. The negative value of ΔS° suggested reduced randomness at adsorbent-adsorbate interface during the adsorption process of MO and SY onto GT-cellulose.

Table 6.1:Thermodynamic parameters for adsorption of MO and SY onto GT-cellulose.

	Thermodynamic parameters				
	ΔG° (kJ mol^{-1})			**ΔH° (kJ mol^{-1})**	**ΔS° (J mol^{-1}K^{-1})**
	298 K	**308 K**	**318 K**		
Methyl orange	-9.96	-9.94	-4.86	84.86	-248.73
Sunset yellow	-8.64	-7.48	-4.92	63.75	-184.24

6.6 Adsorption comparison studies between cellulose and GT-cellulose.

Comparison adsorption studies were examined using cellulose and GT-cellulose as adsorbents for the removal of MO and SY dyes from aqueous solutions as shown in Figure6.15. The adsorption capacity for the removal of MO dye from cellulose and GT-cellulose adsorbents were determined to be 8.0 mg g^{-1} and 37.6 mg g^{-1} respectively. Removal SY dye from cellulose and GT-cellulose adsorbents resulted in adsorption capacities of 4.0 mg g^{-1} and 35.6 mg g^{-1} respectively. From the trend observed in both dye molecules, it can be deduced that cationization resulted in an increase of surface area contributing to improved adsorption of dye contaminants onto GT-cellulose active sites through electrostatic attraction interactions, van der Waals interactions, and hydrogen bonding (Y. Gao *et al*., 2016)(Jiang and Hu, 2019).

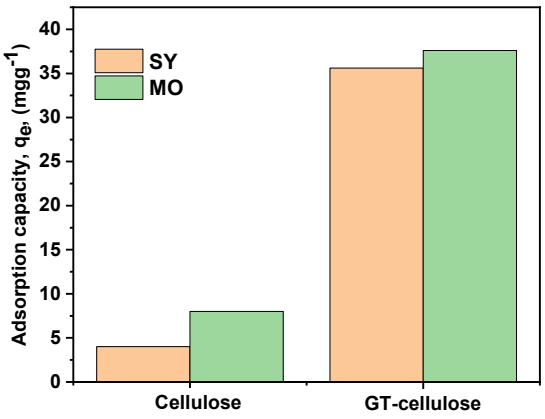

Figure 6.15: Adsorption of MO and SY onto cellulose and GT-cellulose.

6.7 Application of real water samples.

Real water samples were collected from tap water at wits university taps (Johannesburg, South Africa) and sea water at Mdhloti sea (Durban, South Africa). From the results, it was observed that tap water samples resulted in better adsorption capacity for both MO (5.2 mg g^{-1}) and SY (32.1 mg g^{-1}) due to less matrix effects present in tap water (see Figure 6.16). Dye spiked sea water resulted in lower adsorption capacities in both dyes due to the presence of salts, and other organic and inorganic substances including waste, sea salt, magnesium, calcium and many more (de Souza Ferreira *et al*., 2021). From the results, remediation of dye molecules from sea water samples, prior cleaning would be required.

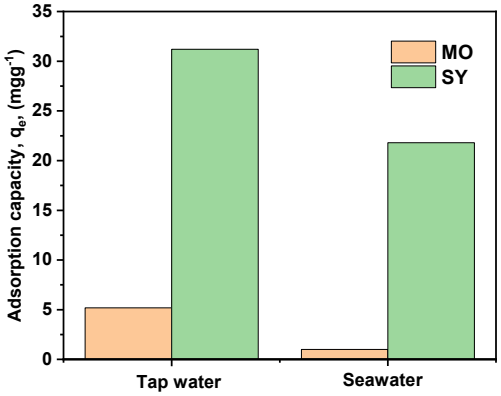

Figure 6.16: Application of GT-cellulose to tap water, and sea water spiked with MO and SY (Initial dye concentration = 20 mg g^{-1}, adsorbent mass = 10 mg, temperature 298.15 K, contact time for MO (120 min) and SY (270 min)).

6.8 Conclusion

This study investigated the use of a low-cost cationised cellulose material derived from hemp stem and branch fibres for the adsorption of methyl orange and sunset yellow dyes from aqueous solution. The FTIR spectrum of GT-cellulose adsorbent displayed the vital surface functional group required for adsorption at 1480 cm^{-1} attributed to epoxy moieties of GTMAC. XRD and TGA showed GT-cellulose with reduced crystallinity and reduced thermal stability. Effect of solution pH studies suggested that adsorption of MO and SY at pH 4 was not only due to electrostatic attraction interactions but also hydrogen bonding and van der Waals interactions. A lower adsorbent dosage (10 mg) was more favourable for dye uptake, due to the increased adsorption capacity, attributed to surface agglomeration at higher adsorbent dosage. Comparison studies for adsorption of dyes onto cellulose and GT-cellulose showed improved adsorption capacity when using GT-cellulose adsorbents for dye removal from aqueous solutions. The equilibrium adsorption isotherm data were best described by Langmuir model. The adsorption kinetics were best fit with pseudo first-order model for MO and SY adsorption. The thermodynamic study showed that the adsorption processes for MO and SY were both endothermic and spontaneous in nature. From the results, cationised cellulose adsorbents could be effectively applied for removal of anionic dye from wastewater.

6.9 References

Abd Malek, A. H., and Yasin. Y (2012) 'Use of Layered Double Hydroxides to Remove Sunset Yellow FCF Dye from Aqueous Solution', *Chemical Science Transactions*, 1(1), pp. 194–200. doi: 10.7598/cst2012.120.

Abdel-aziz, H. M. and Abdel-gawad, S. A. (2020) 'Removal of sunset yellow azo dye using activated carbon entrapped in alginate from aqueous solutions', *Journal of science*, 4(1), pp. 1–6. doi: 10.15406/oajs.2020.04.00142.

Abdel-Ghani, N. T., El-Chaghaby, G. A., Rawash, E. A., and Lima, E. C. (2017) 'Adsorption of Coomassie Brilliant Blue R-250 dye onto novel activated carbon prepared from Nigella sativa L. waste: Equilibrium, kinetics and thermodynamics', *Journal of the Chilean Chemical Society*, 62(2), pp. 3505–3511. doi: 10.4067/S0717-97072017000200016.

Abidi, N., Duplay, J., Jada, A., Errais, E., Ghazi, M., Semhi, K., and Trabelsi-Ayadi, M. (2019) 'Removal of anionic dye from textile industries' effluents by using Tunisian clays as adsorbents. Zeta potential and streaming-induced potential measurements', *Comptes Rendus Chimie*, 22(2–3), pp. 113–125. doi: 10.1016/j.crci.2018.10.006.

Alhogbi, B. G., Altayeb, S., Bahaidarah, E. A., and Zawrah, M. F. (2021) 'Removal of anionic and cationic dyes from wastewater using activated carbon from palm tree fiber waste', *Processes*, 9(3), pp. 1–21. doi: 10.3390/pr9030416.

Ayawei, N., Ebelegi, A. N. and Wankasi, D. (2017) 'Modelling and Interpretation of Adsorption Isotherms', *Journal of Chemistry*, 2017. doi: 10.1155/2017/3039817.

Chaker, A. and Boufi, S. (2015) 'Cationic nanofibrillar cellulose with high antibacterial properties', *Carbohydrate Polymers*, 131, pp. 224–232. doi: 10.1016/j.carbpol.2015.06.003.

Chen, H. and Zhao, J. (2009) 'Adsorption study for removal of Congo red anionic dye using organoattapulgite', *Adsorption*, 15(4), pp. 381–389. doi: 10.1007/s10450-009-9155-z.

Chukwuemeka-Okorie, H.O., Ekuma, F.K., Akpomie, K.G., Nnaji, J.C., and Okereafor, A.G. (2021) 'Adsorption of tartrazine and sunset yellow anionic dyes onto activated carbon derived from cassava sievate biomass', *Applied Water Science*, 11(2), pp. 1–8. doi: 10.1007/s13201-021-01357-w.

Dawood, S. and Sen, T. K. (2012) 'Removal of anionic dye Congo red from aqueous solution by raw pine and acid-treated pinecone powder as adsorbent: Equilibrium, thermodynamic, kinetics, mechanism and process design', *Water Research*, 46(6), pp. 1933–1946. doi: 10.1016/j.watres.2012.01.009.

Du, H., Liu, C., Mu, X., Gong, W., Lv, D., Hong, Y., Si, C., and Li, B. (2016) 'Preparation and characterization of thermally stable cellulose nanocrystals via a sustainable approach of FeCl3catalyzed formic acid hydrolysis', *Cellulose*, 23(4), pp. 2389–2407. doi: 10.1007/s10570-016-0963-5.

Ebelegi, A. N., Ayawei, N. and Wankasi, D. (2020) 'Interpretation of Adsorption Thermodynamics and Kinetics', *Open Journal of Physical Chemistry*, 10(03), pp. 166–182. doi: 10.4236/ojpc.2020.103010.

Eltaweil, A. S., Elgarhy, G. S., El-Subruiti, G. M., and Omer, A. M. (2020) 'Carboxymethyl cellulose/carboxylated graphene oxide composite microbeads for efficient adsorption of cationic methylene blue dye', *International Journal of Biological Macromolecules*, 154, pp. 307–318. doi: 10.1016/j.ijbiomac.2020.03.122.

Etale, A., Nhlane, D. S., Mosai, A. K., Mhlongo, J., Khan, A., Rumbold, K., Nuapia, Y. B. (2021) 'Synthesis and application of cationised cellulose for removal of Cr(VI) from acid mine-drainage contaminated water', *AAS Open Research*, 4, p. 4. doi: 10.12688/aasopenres.13182.1.

Fernandes, J. V., Rodrigues, A. M., Menezes, R. R., and de Araújo Neves, G. (2020) 'Adsorption of anionic dye on the acid-functionalized bentonite', *Materials*, 13(16), pp. 1–19. doi: 10.3390/MA13163600.

Fungaro, D. A., Borrely, S. I., and Carvalho, T. E. M.. (2013) 'Surfactant Modified Zeolite from Cyclone Ash as Adsorbent for Removal of Reactive Orange 16 from Aqueous Solution', *American Journal of Environmental Protection*, 1(1), pp. 1–9. doi: 10.12691/env-1-1-1.

Gandhi, N., Sirisha, D. and Chandra Sekhar, K. B. (2016) 'Adsorption of Fluoride (F-) from Aqueous Solution by Using Pineapple (Ananas comosus) Peel and Orange (Citrus sinensis) Peel Powders', *International Journal of Environmental Bioremediation and Biodegradation*, 4(2), pp. 55–67. doi: 10.12691/ijebb-4-2-4.

Gao, X., Chen, K., Zhang, H., and Yan, X. (2015) 'Characterization of cationic parenchyma cellulose derivative by rapid preparation of low microwave power', *Iranian Polymer Journal (English Edition)*, 24(9), pp. 747–758. doi: 10.1007/s13726-015-0363-y.

Gao, Y., Li, Q., Shi, Y., and Cha, R. (2016) 'Preparation and Application of Cationic Modified Cellulose Fibrils as a Papermaking Additive', *International Journal of Polymer Science*, 2016, pp. 1–8.

García-García, D., Balart, R., Lopez-Martinez, J., Ek, M., and Moriana, R. (2018) 'Optimizing the yield and physico-chemical properties of pine cone cellulose nanocrystals by different hydrolysis time', *Cellulose*, 25(5), pp. 2925–2938. doi: 10.1007/s10570-018-1760-0.

Ghaedi, M., Shokrollahi, A., Hossainian, H., and Kokhdan, S.N. (2011) 'Comparison of activated carbon and multiwalled carbon nanotubes for efficient removal of eriochrome cyanine R (ECR): Kinetic, isotherm, and thermodynamic study of the removal process', *Journal of Chemical and Engineering Data*, 56(7), pp. 3227–3235. doi: 10.1021/je200331u.

Ghaedi, M. (2012) 'Comparison of cadmium hydroxide nanowires and silver nanoparticles loaded on activated carbon as new adsorbents for efficient removal of Sunset yellow: Kinetics and equilibrium study', *Spectrochimica Acta - Part A: Molecular and Biomolecular Spectroscopy*, 94, pp. 346–351. doi: 10.1016/j.saa.2012.02.097.

Goswami, M. and Phukan, P. (2017) 'Enhanced adsorption of cationic dyes using sulfonic acid modified activated carbon', *Journal of Environmental Chemical Engineering*, 5(4), pp. 3508–3517. doi: 10.1016/j.jece.2017.07.016.

Gu, H., Gao, X., Zhang, H., Chen, K., and Peng, L. (2020) 'Fabrication and characterization of cellulose nanoparticles from maize stalk pith via ultrasonic-mediated cationic etherification', *Ultrasonics Sonochemistry*, 66, pp. 104932. doi: 10.1016/j.ultsonch.2019.104932.

Günay, A., Arslankaya, E. and Tosun, I. (2007) 'Lead removal from aqueous solution by natural and pretreated clinoptilolite: Adsorption equilibrium and kinetics', *Journal of Hazardous Materials*, 146(1–2), pp. 362–371. doi: 10.1016/j.jhazmat.2006.12.034.

Haddadian, Z., Shavandi, M. A., Zainal, Z., Halim, M., and Ismail, S. (2013) 'Removal Methyl Orange from Aqueous Solutions Using Dragon Fruit (Hylocereusundatus) Foliage', *Chemical Science Transactions*, 2(3), pp. 900–910. doi: 10.7598/cst2013.439.

Hasani, M., Cranston, E. D., Westman, G., and Gray, D. G. (2008) 'Cationic surface functionalization of cellulose nanocrystals', *Soft Matter*, 4, pp. 2238–2244. doi: 10.1039/b806789a.

Hashem, A. and El-Shishtawy, R. M. (2001) 'Preparation and characterization of cationized cellulose for the removal of anionic dyes', *Adsorption Science and Technology*, 19(3), pp. 197–210. doi: 10.1260/0263617011494088.

Hemmati, F., Jafari, S. M., Kashaninejad, M., Barani Motlagh, M. (2018) 'Synthesis and characterization of cellulose nanocrystals derived from walnut shell agricultural residues', *International Journal of Biological Macromolecules*, 120, pp. 1216–1224. doi: 10.1016/j.ijbiomac.2018.09.012.

Ho, Y. S. and McKay, G. (1998) 'A Comparison of chemisorption kinetic models applied to pollutant removal on various sorbents', *Process Safety and Environmental Protection*, 76(4), pp. 332–340. doi: 10.1205/095758298529696.

Huang, X., Dognani, G., Hadi, P., Yang, M., Job, A. E., and Hsiao, B.S. (2020) 'Cationic Dialdehyde Nanocellulose from Sugarcane Bagasse for Efficient Chromium(VI) Removal', *ACS Sustainable Chemistry and Engineering*, pp. 1–57. doi: 10.1021/acssuschemeng.9b06683.

Ibrahim, S., Ang, H. M. and Wang, S. (2009) 'Removal of emulsified food and mineral oils from wastewater using surfactant modified barley straw', *Bioresource Technology*, 100(23), pp. 5744–5749. doi: 10.1016/j.biortech.2009.06.070.

Ilgin, P., Ozay, H. and Ozay, O. (2020) 'The efficient removal of anionic and cationic dyes from aqueous media using hydroxyethyl starch-based hydrogels', *Cellulose*, 27(8), pp. 4787–4802. doi: 10.1007/s10570-020-03074-0.

Jarusiripot, C. (2014) 'Removal of Reactive Dye by Adsorption over Chemical Pretreatment Coal based Bottom Ash', *Procedia Chemistry*, 9, pp. 121–130. doi: 10.1016/j.proche.2014.05.015.

Jiang, Z. and Hu, D. (2019) 'Molecular mechanism of anionic dyes adsorption on cationized rice husk cellulose from agricultural wastes', *Journal of Molecular Liquids*, 276, pp. 105–114. doi: 10.1016/j.molliq.2018.11.153.

Kaboorani, A. and Riedl, B. (2015) 'Surface modification of cellulose nanocrystals (CNC) by a cationic surfactant', *Industrial Crops and Products*, 65, pp. 45–55. doi: 10.1016/j.indcrop.2014.11.027.

Kassab, Z., Abdellaoui, Y., Salim, M. H., Bouhfid, R., Qaiss, A. E., and El Achaby, M. (2020) 'Micro- and nano-celluloses derived from hemp stalks and their effect as polymer reinforcing materials', *Carbohydrate Polymers*, 245, pp. 1–12. doi: 10.1016/j.carbpol.2020.116506.

Katheresan, V., Kansedo, J. and Lau, S. Y. (2018) 'Efficiency of various recent wastewater dye removal methods: A review', *Journal of Environmental Chemical Engineering*, 6(4), pp. 4676–4697. doi: 10.1016/j.jece.2018.06.060.

Khumalo, N. P., Vilakati, G. D., Mhlanga, S. D., Kuvarega, A. T., Mamba, B. B., Li, J., and Dlamini, D. S. (2019) 'Dual-functional ultrafiltration nano-enabled PSf/PVA membrane for the removal of Congo red dye', *Journal of Water Process Engineering*, 31, pp. 1–8. doi: 10.1016/j.jwpe.2019.100878.

Konicki, W., Cendrowski, K., Bazarko, G., and Mijowska, E. (2015) 'Study on efficient removal of anionic, cationic and nonionic dyes from aqueous solutions by means of mesoporous carbon nanospheres with empty cavity', *Chemical Engineering Research and Design*, 94, pp. 242–253. doi: 10.1016/j.cherd.2014.08.006.

Lesaoana, M. (2018) 'Simultaneous sequestration of Cr(VI) and Cr(III) from aqueous solutions by activated carbon and ion-imprinted polymers', (Vi).

Li, K., Li, P., Cai, J., Xiao, S., Yang, H., and Li, A. (2016) 'Efficient adsorption of both methyl orange and chromium from their aqueous mixtures using a quaternary ammonium salt modified chitosan magnetic composite adsorbent', *Chemosphere*, 154, pp. 310–318. doi: 10.1016/j.chemosphere.2016.03.100.

Li, M., Wang, L. J., Li, D., Cheng, Y. L., and Adhikari, B. (2014) 'Preparation and characterization of cellulose nanofibers from de-pectinated sugar beet pulp', *Carbohydrate Polymers*, 102(1), pp. 136–143. doi: 10.1016/j.carbpol.2013.11.021.

Liu, C., Li, B., Du, H., Lv, D., Zhang, Y., Yu, G., Mu, X., and Peng, H. (2016) 'Properties of nanocellulose isolated from corncob residue using sulfuric acid, formic acid, oxidative and mechanical methods', *Carbohydrate Polymers*, 151, pp. 716–724. doi: 10.1016/j.carbpol.2016.06.025.

Ma, J., Cui, B., Dai, J., and Li, D. (2011) 'Mechanism of adsorption of anionic dye from aqueous solutions onto organobentonite', *Journal of Hazardous Materials*, 186(2–3), pp. 1758–1765. doi: 10.1016/j.jhazmat.2010.12.073.

Mahardika, M., Abral, H., Kasim, A., Arief, S., and Asrofi, M. (2018) 'Production of nanocellulose from pineapple leaf fibers via high-shear homogenization and ultrasonication', *Fibers*, 6(2), pp. 1–12. doi: 10.3390/fib6020028.

Mohammed, N., Grishkewich, N. and Tam, K. C. (2018) 'Cellulose nanomaterials: Promising sustainable nanomaterials for application in water/wastewater treatment processes', *Environmental Science: Nano*, 5(3), pp. 623–658. doi: 10.1039/c7en01029j.

Mosallanejad, N. and Arami, A. (2012) 'Kinetics and isotherm of sunset yellow dye adsorption on cadmium sulfide nanoparticle loaded on activated carbon', *Journal of Chemical Health Risks*, 2(2251–6719), pp. 31–40.

Muqeet, M., Malik, H., Mahar, R. B., Ahmed, F., Khatri, Z., and Carlson, K. (2017) 'Cationization of Cellulose Nanofibers for the Removal of Sulfate Ions from Aqueous Solutions', *Industrial and Engineering Chemistry Research*, 56(47), pp. 14078–14088. doi: 10.1021/acs.iecr.7b03739.

Nethaji, S., Sivasamy, A. and Mandal, A. B. (2013) 'Adsorption isotherms, kinetics and mechanism for the adsorption of cationic and anionic dyes onto carbonaceous particles prepared from Juglans regia shell biomass', *International Journal of Environmental Science and Technology*, 10(2), pp. 231–242. doi: 10.1007/s13762-012-0112-0.

Odabas, N., Amer, H., Bacher, M., Henniges, U., Potthast, A., and Rosenau, T. (2016) 'Properties of Cellulosic Material after Cationization in Different Solvents', *ACS Sustainable Chemistry and Engineering*, 4(4), pp. 2295–2301. doi: 10.1021/acssuschemeng.5b01752.

Rajesh, U. D. S. and Hemraz (2018) 'Synthetic Strategies for the Fabrication of Cationic SurfaceModified Cellulose Nanocrystals', *fibers*, 6(15), pp. 1–19. doi: 10.3390/fib6010015.

Rana, V., Malik, S., Joshi, G., Rajput, N. K., and Gupta, P. K. (2021) 'Preparation of alpha cellulose from sugarcane bagasse and its cationization: Synthesis, characterization, validation and application as wet-end additive', *International Journal of Biological Macromolecules*, 170, pp. 793–809. doi: 10.1016/j.ijbiomac.2020.12.165.

Rosli, N. A., Ahmad, I. and Abdullah, I. (2013) 'Isolation and characterization of cellulose nanocrystals from agave angustifolia fibre', *BioResources*, 8(2), pp. 1893–1908. doi: 10.15376/biores.8.2.18931908.

Sajjan, A. M., Premakshi, H. G. and Kariduraganavar, M. Y. (2015) 'Synthesis and characterization of GTMAC grafted chitosan membranes for the dehydration of low water content isopropanol by pervaporation', *Journal of Industrial and Engineering Chemistry*, 25, pp. 151–161. doi: 10.1016/j.jiec.2014.10.027.

Santos, R. M.M., Tronto, J., Briois, V., and Santilli, C. V. (2017) 'Thermal decomposition and recovery properties of ZnAl-CO3 layered double hydroxide for anionic dye adsorption: Insight into the aggregative nucleation and growth mechanism of the LDH memory effect.', *Journal of Materials Chemistry A*, 5(20), pp. 9998–10009. doi: 10.1039/c7ta00834a.

Silva, L. S., Lima, L. C. B., Ferreira, F. J. L., Silva, M. S., Osajima, J. A., Bezerra, R. D.S., and Silva Filho, E. C. (2015) 'Sorption of the anionic reactive red RB dye in cellulose: Assessment of kinetic, thermodynamic, and equilibrium data', *Open Chemistry*, 13(1), pp. 801–812. doi: 10.1515/chem-20150079.

de Souza Ferreira, I. L., de Medeiros, J. I., Steffens, F., and Oliveira, F. R. (2021) 'Seawater as an alternative to dye cotton fiber with reactive dyes', *Textile Research Journal*, 91(9–10), pp. 1184–1193. doi: 10.1177/0040517520972482.

Stanciu, M. C. and Nichifor, M. (2019) 'Adsorption of anionic dyes on a cationic amphiphilic dextran hydrogel: equilibrium, kinetic, and thermodynamic studies', *Colloid and Polymer Science*, 297(1), pp. 45–57. doi: 10.1007/s00396-018-4439-z.

Sujitha, R. and Ravindhranath, K. (2016) 'Removal of Coomassie brilliant blue dye from waste waters using active carbon derived from barks of Ficus racemosa plant', *Der Pharmacia Lettre*, 8(10), pp. 72–83.

Sun, D., Zhang, X., Wu, Y., and Liu, T. (2013) 'Kinetic mechanism of competitive adsorption of disperse dye and anionic dye on fly ash', *International Journal of Environmental Science and Technology*, 10(4), pp. 799–808. doi: 10.1007/s13762-012-0130-y.

Syafri, E., Kasim, A., Abral, H., Sudirman, Sulungbudi, G. T., Sanjay, M. R., and Sari, N. H. (2018) 'Synthesis and characterization of cellulose nanofibers (CNF) ramie reinforced cassava starch hybrid composites', *International Journal of Biological Macromolecules*, 120, pp. 578–586. doi: 10.1016/j.ijbiomac.2018.08.134.

Taha, N. D., Samaka, S. I. and Mohammed, L. A. (2013) 'Adsorptive removal of dye from industrial effluents using natural Iraqi palygors-kite clay as low-cost adsorbent', *Journal of Asian Scientific Research*, 3(9), pp. 945–955. Available at: http://www.aessweb.com/pdf-files/Jasr-3(9)-945-955.pdf.

Tejada-Tovar, C., Villabona-Ortíz, Á. and Gonzalez-Delgado, Á. D. (2021) 'Adsorption of azo-anionic dyes in a solution using modified coconut (Cocos nucifera) mesocarp: Kinetic and equilibrium study', *Water (Switzerland)*, 13(10). doi: 10.3390/w13101382.

An Tran, T.T., Duong, H. T. L., Pham, T. T. P., Nguyen, T., Nguyen, T.D., and An Tran B. (2021) 'Preparation of Magnetic Composite Polyaniline / Fe_3O_4 − Hydrotalcite and Performance in Removal of Methyl Orange', *Adsorption Science and Technology*, 2021, pp. 1–18.

Veni, V. K. and Brenda, T. H. (2021) 'Preparation of raw oyster shell for removal of coomassie brilliant blue R-250 dye from aqueous solution', in *IOP Conference Series: Earth and Environmental Science*, pp. 1–8. doi: 10.1088/1755-1315/765/1/012039.

Wang, Y., Zhao, L., Peng, H., Wu, J., Liu, Z., and Guo, X. (2016) 'Removal of Anionic Dyes from Aqueous Solutions by Cellulose-Based Adsorbents: Equilibrium, Kinetics, and Thermodynamics', *Journal of Chemical and Engineering Data*, 61(9), pp. 3266–3276. doi: 10.1021/acs.jced.6b00340.

Wang, Y., Zhao, L., Hou, J., Peng, H., Wu, J., Liu, Z., and Guo, X. (2018) 'Kinetic, isotherm, and thermodynamic studies of the adsorption of dyes from aqueous solution by cellulose-based adsorbents', *Water Science and Technology*, 77(11), pp. 2699–2708. doi: 10.2166/wst.2018.229.

Wawrzkiewicz, M. (2011) 'Sorption of Sunset Yellow dye by weak base anion exchanger-kinetic and equilibrium studies', *Environmental Technology*, 32(4), pp. 455–465. doi: 10.1080/09593330.2010.502188.

Willberg-Keyriläinen, P., Pitkänen, P., Hulkko, J., Asikainen, M., and Setälä, H. (2019) 'The effect of mixing and consistency on cellulose cationization', *Heliyon*, 5(3), pp. 1–15. doi: 10.1016/j.heliyon.2019.e01349.

Wong, S., Abd Ghafar, N., Ngadi, N., Razmi, F. A., Inuwa, I. M., Mat, R., and Amin, N. A. S. (2020)

‘Effective removal of anionic textile dyes using adsorbent synthesized from coffee waste’, *Scientific Reports*, 10(1), pp. 1–13. doi: 10.1038/s41598-020-60021-6.

Wu, F. C., Tseng, R. L. and Juang, R. S. (2009) ‘Initial behavior of intraparticle diffusion model used in the description of adsorption kinetics’, *Chemical Engineering Journal*, 153(1–3), pp. 1–8. doi: 10.1016/j.cej.2009.04.042.

Yin, Y., Hong, Z., Tian, X., Zhu, Q., Jiang, X., Wang, H., and Gao, W. (2017) ‘Cellulose nanocrystals modified with quaternary ammonium salts and its reinforcement of polystyrene’, *Polymer Bulletin*, pp. 1–17. doi: 10.1007/s00289-017-2131-y.

Yue, X., Huang, J., Jiang, F., Lin, H., and Chen, Y. (2019) ‘Synthesis and characterization of cellulosebased adsorbent for removal of anionic and cationic dyes’, *Journal of Engineered Fibers and Fabrics*, 14. doi: 10.1177/1558925019828194.

Zaman, M., Xiao, H., Chibante, F., and Ni, Y. (2012) ‘Synthesis and characterization of cationically modified nanocrystalline cellulose’, *Carbohydrate Polymers*, 89(1), pp. 163–170. doi: 10.1016/j.carbpol.2012.02.066.

Zhang, H., Luan, Q., Tang, H., Huang, F., Zheng, M., Deng, Q., Xiang, X., Yang, C., Shi, J., Zheng, C., and Zhou, Q. (2017) ‘Removal of methyl orange from aqueous solutions by adsorption on cellulose hydrogel assisted with Fe_2O_3 nanoparticles’, *Cellulose*, 24(2), pp. 903–914. doi: 10.1007/s10570-0161129-1.

Zhang, S. F., Yang, M. X., Qian, L. W., Hou, C., Tang, R. H., Yang, J. F., and Wang, X. C. (2018b) ‘Design and preparation of a cellulose-based adsorbent modified by imidazolium ionic liquid functional groups and their studies on anionic dye adsorption’, *Cellulose*, 25(6), pp. 3557–3569. doi: 10.1007/s10570-018-1815-2.

Zhu, M. X., Lee, L., Wang, H. H., and Wang, Z. (2007) ‘Removal of an anionic dye by adsorption/precipitation processes using alkaline white mud’, *Journal of Hazardous Materials*, 149(3), pp. 735–741. doi: 10.1016/j.jhazmat.2007.04.037.

CHAPTER 7: CONCLUSION AND RECOMMENDATIONS

7.1 General conclusion

This study set out to

(i) To investigate green approaches for the extraction of cellulose from hemp waste using organic and mineral acids using response surface methodology for the selection of reaction conditions i.e., acid type, acid concentration, reaction temperature and duration,

(ii) To characterise extracted cellulose for their physical and chemical properties using scanning electron microscope (SEM), X-ray diffraction (XRD). Thermogravimetric analysis (TGA), and Fourier-transform infrared spectroscopy (FTIR).

(iii) To modify the surface of extracted cellulose fibres by cationic moieties using GTMAC

(iv) To determine the removal efficiency of anionic dyes from water using cationised cellulose.

The extraction of CMFs has been successfully carried out from Hemp (*Cannabis Sativa* L.) bast fibres. Fibres were then acid hydrolysed using varies conditions (acid type, acid concentration, reaction time, and hydrolysis temperature) followed by homogenisation.

The surface morphology, chemical, crystalline, and thermal properties of the raw plant fibre, treated and acid hydrolysed fibres was determined using SEM, FTIR, XRD and TGA, respectively. From visual observations, alkaline treatment of raw plant fibre to remove of hemicellulose and other non-cellulosic content resulted in brown fibres, the bleaching process results showed white fibres as reported by other researchers depicting the formation of cellulose. Raw hemp fibres underwent alkali and bleaching treatments using 4wt% NaOH and 1.7wt% $NaClO_2$ in acetate buffer, respectively and it appears to be successful in removing lignin, hemicellulose, and other non-cellulosic components. SEM of CMFs confirmed that hydrolysis produced CMFs of average diameter between 7.06±1.86 μm and 11.27±2.01 μm and varying morphology. Raw plant fibre and bleached cellulose FTIR spectrum showed that some functional groups such as that of absorption band 1736 cm^{-1} were weakened in the bleached cellulose spectrum due to partial or complete removal of non-cellulose components after NaOH treatment, whereas the FTIR spectrum of CMFs showed that the main chemical structure of cellulose was not altered during the hydrolysis process. On the other hand, the XRD analysis showed that the crystallinity degree of the fibre increases after NaOH and bleaching treatments. The crystallinity degree of the raw hemp fibre was 60% and treatment, the crystallinity degree of the cellulose increased to 73% following removal of lignin and hemicellulose components. CMFs showed a range of crystallinity from 40% to 75% that was depended on type of acid used. Sulfuric acid hydrolysed CMFs showed a more varying crystallinity due to the harshness of the conditions applied. Based on the results of the TG and DG curves, the main thermal decomposition step for the raw hemp fibre and cellulose fibre occurs at 386°C

and 359°C, respectively, whereas CMFs showed increased thermal decomposition temperatures suggesting improved thermal stability from cellulose which is a favourable property for high temperature applications particularly as flame-retardant material.

To optimise the experimental conditions of acid hydrolysis for production of highly crystalline CMFs, using a RSM-CCD model. For acid hydrolysis processes using sulfuric acid, formic acid and maleic acid, the acid concentration, hydrolysis temperatures, and hydrolysis time within the ranges 45–64 wt%, 45–65°C, and 30–90 min, respectively. Therefore, this study allows the following conclusions, for sulfuric acid hydrolysis the model showed that the crystallinity strongly depended on the acid concentration even at low hydrolysis time and hydrolysis temperature. Whereas, for formic acid hydrolysis, interaction between acid concentration and hydrolysis temperature was more favourable to obtain maximized crystallinity degree. For maleic acid hydrolysis, crystallinity was highly influenced by an increase in temperature and in acid concentration 50-61%. Under the optimum hydrolysis conditions, the predicted crystallinity degree of 82% predicted by the model agreed with the experimental results of ~84% of crystallinity and validated by the model generated by CCD-RSM. This optimum crystallinity degree was obtained by applying the following hydrolysis conditions, using formic acid at 62% acid concentration, 47 °C hydrolysis temperature and 36 minutes of reaction time. This study established that the wide available bast fibre can be regarded as a greener and sustainable waste for the preparation of CMFs and RSM-CCD can be used to optimise extraction conditions.

This study investigated the use of a low-cost cationised cellulose material derived from hemp stem and branch fibres for the adsorption of methyl orange and sunset yellow dyes from aqueous solution. The FTIR spectrum of GT-cellulose adsorbent displayed the vital surface functional group required for adsorption at 1480 cm^{-1} attributed to epoxy moieties of GTMAC. XRD and TGA showed GT-cellulose with reduced crystallinity and reduced thermal stability. Effect of solution pH studies suggested that adsorption of MO and SY at pH 4 was not only due to electrostatic attraction interactions but also hydrogen bonding and van der Waals interactions. A lower adsorbent dosage (10 mg) was more favourable for dye uptake, due to the increased adsorption capacity, attributed to surface agglomeration at higher adsorbent dosage. The maximum adsorption capacity for MO and SY onto GT-cellulose were found to be 71.65 mgg^{-1} and 41.19 mgg^{-1}, respectively. Comparison studies for adsorption of dyes onto cellulose and GT-cellulose showed improved adsorption capacity when using GT-cellulose adsorbents for dye removal from aqueous solutions. The equilibrium adsorption isotherm data were best described by Langmuir model. The adsorption kinetics were best fit with pseudo first-order model for MO and SY adsorption. The thermodynamic study showed that the adsorption processes for MO and SY were both endothermic and spontaneous in nature. From the results, cationised cellulose adsorbents could be effectively applied for removal of anionic dye from wastewater

7.2 Recommendations and future work

- Hemicellulose, lignin, and cellulose yields at each stage of alkali, bleaching and acid hydrolysis treatment could be evaluated to determine the changes in cellulose yield as we may be losing valuable material with each step.
- Following extraction of cellulose microfibres, characterisation such as Atomic Force Microscopy (AFM) could be explored to further evaluate the surface roughness to narrow down suitable application.
- Comparison studies of fibres extracted with acid hydrolysis only and those with acid hydrolysis - assisted ultrasonic treatment.
- For the cationised cellulose fibres used for dye uptake, reusability studies to evaluate the performance of the adsorbent after multiple uses and from a matrix of competing ions studies could also be investigated to determine the affinity between dyes and GT-cellulose
- Application of GT-cellulose for the removal of inorganic anionic pollutants e.g., arsenate could be investigated.